San Joaquin Valley Drainage Authority

San Joaquin River
Up-Stream DO TMDL Project
ERP - 02D - P63

Task 7: BOD Isotope Study

A Multi-Isotope Tracer Approach to Understanding Organic Matter and Nutrient Source Dynamics in the San Joaquin River

Final Task Report

May 14, 2008

Carol Kendall, Megan B. Young, Steven R. Silva,
and Daniel H. Doctor

U.S. Geological Survey
Isotope Tracers Project
345 Middlefield Rd, MS 434
Menlo Park, CA 94025

Abstract

Water and particulate organic matter (POM) samples were collected bi-weekly to monthly from March 2005 through December 2007 from sites along the San Joaquin River (SJR) and from tributary, drainage, and spill sites that provide water to the San Joaquin. All of the samples were analyzed for $\delta^{13}C$, $\delta^{15}N$, and C:N ratio of particulate organic matter (POM), $\delta^{18}O$ and $\delta^{2}H$ of water, and $\delta^{15}N$ and $\delta^{18}O$ of nitrate (NO_3). Subsets of the samples were also analyzed for $\delta^{13}C$ of dissolved organic carbon (DOC), $\delta^{18}O$ of phosphate, and $\delta^{34}S$ and $\delta^{18}O$ of sulfate (SO_4). This study employs a multi-isotope approach in order to identify the primary sources and composition of the POM throughout the San Joaquin River during different seasons and to identify spatial and temporal patterns in water and nutrient sources to the SJR. Transport of oxygen-consuming materials, particularly algae, from the San Joaquin River into the Stockton Deep Water Ship Channel (DWSC) has been identified as a major factor in the occurrence of low dissolved oxygen conditions in the DWSC. Isotope analysis can provide unique insights into the sources and biogeochemical cycling of various biological oxygen-demanding substances throughout the San Joaquin River basin.

The low C:N ratios of POM, combined with algal pigment data, indicate that most of the POM in the mainstem of the San Joaquin River was of algal origin. The major east-side tributaries had both a wider range and higher average C:N ratios, as well as lower concentrations of algal pigments, suggesting that POM from these tributaries contained more terrestrial material. C:N ratios were generally higher during high flow periods than during the low flow summer, reflecting more input of terrestrial POM during storm runoff. POM samples from different wetlands and drain sites often have distinctive isotopic signatures that allow determination of relative contributions of these different sources to the SJR.

The $\delta^{15}N$ and $\delta^{18}O$ of nitrate in the San Joaquin River and tributaries showed large spatial and temporal variability. However, there were distinct differences in nitrate isotopic composition between different sites, particularly in the relationship between $\delta^{15}N$ and $\delta^{18}O$. At the downstream SJR mainstem sites, $\delta^{15}N$ and $\delta^{18}O$ followed very similar patterns, suggesting mixing with multiple nitrate sources was the dominant process controlling the isotopic composition. At some upstream sites (e.g., Lander Avenue, Mud Slough, San Luis Drain), the parallel increases in $\delta^{15}N$ and $\delta^{18}O$ with decreasing nitrate concentration suggested that algal uptake was the dominant process affecting nitrate isotopes. In contrast, the decoupling of the $\delta^{15}N$ and $\delta^{18}O$ values at some of the minor tributaries (e.g., Orestimba, Del Puerto, and Ingram Creeks) indicated that nitrification, not mixing, was the main process controlling the isotopic composition.

Water isotopes can be useful for distinguishing water inputs from different sources. The three major east-side tributaries had generally lower $\delta^{18}O$ and $\delta^{2}H$ than the upstream and west-side tributaries, and water inputs from these rivers were reflected in downstream trends of decreasing water isotope values in the mainstem SJR, particularly during higher flow periods. Upstream and west-side tributaries usually had higher $\delta^{18}O$ and $\delta^{2}H$ than the east-side tributaries and mainstem SJR, most likely reflecting a combination of precipitation with higher $\delta^{18}O$ and $\delta^{2}H$ values in those watersheds and increased evaporation in irrigation return waters, mostly during

the summer and fall.

The temporal and spatial variation in isotopic composition is signal, not noise, and provides unique insights into sources of organic matter, nutrients, salt, and water that could not have been gained with standard chemical and hydrological measurements. In a sense, the mainstem sites are the recipients of frequent, system-wide, natural tracer tests, in that the natural perturbations in isotopic composition at upstream sites provide strong, often unambiguous signals that can be traced from the source to the river, incorporated into mass balance models, and used to identify the likely sources of nitrate and organic matter that cannot be accounted for in these models. One of the most effective uses of these isotope data will be for use in testing hypotheses developed with other datasets. The isotopic "fingerprints" of different sources of nitrate and organic matter provides considerable information about the substances, and models developed with other data must be able to account for the isotopic compositions.

The report contains a wealth of observations about sources of nitrate and POM, the biogeochemical processes that produce them, and mixing relations at different sites. Some of the more noteworthy observations are listed below:

- Mainstem SJR sites showed decreasing relative contributions of fresh and older algae downstream, while the relative contributions of an unknown source of POM with low BOD derived mainly from the major east-side tributaries increases but also from some of the minor east-side tributaries (e.g., MID 5 and Westport) increased downstream.
- POM from the upstream wetlands sites (e.g., Los Banos, San Luis Drain, Mud Slough) is dominated (~80%) by fresh and old algae, whereas POM from Salt Slough, like Del Puerto Creek, is dominated by old algae and more refractory sources of POM.
- The average POM in the minor east and west-side tributaries show a wide range of average compositions, with sites ranging from fresh algae-dominated (e.g., Ramona Lake) to ones dominated by refractory and terrestrial POM sources similar to the POM in the major tributaries (e.g., MID Lat 5).
- The POM "signatures" from the minor east and west-side tributaries are not distinctive except that Harding Drain and MID Lat 5 have unusually high $\delta^{13}C$ values, probably because of intense photosynthetic activity but perhaps because of large contributions of organic matter derived from C4 plants.
- West-side tributaries are characterized by different nitrate isotope signatures than east-side tributaries. In specific, frequent pulses of high-nitrate water in many west-side tributaries show that nitrification, not mixing of sources, is the main control on nitrate isotopes during these periods.
- Algal growth appears to be the main process controlling nitrate isotopic compositions in upstream wetlands sites like Mud Slough and San Luis Drain. However, nitrate isotopes in Salt Slough, like west-side tributaries, shows that nitrification is a dominant process.
- During low flow conditions in the mainstem SJR in summer and fall 2007, the $\delta^{15}N$ of the SJR increased downstream, in contrast to the normal pattern of a downstream decrease in $\delta^{15}N$ associated with input of low-$\delta^{15}N$ water from the major tributaries. The high $\delta^{15}N$ values cannot be explained by known inputs and strongly suggests that there

was addition of nitrate with a high $\delta^{15}N$ (probably from human or animal waste) from an unidentified and unsampled source or sources along this reach, especially downstream of Vernalis.

Introduction

General Background of Study

The San Joaquin River (SJR) receives elevated concentrations of nitrate, dissolved organic carbon (DOC), and particulate organic matter (POM) from non-point sources. These discharges are associated with agriculture, dairy, and wetlands land uses and have led to compromised water quality and water supply conflicts among stakeholders. High organic matter concentrations can cause increases in aquatic biological oxygen demand (BOD) when the organic matter decays. Moreover, high concentrations of nitrate (NO_3^-) and ammonium can cause undesirable algal blooms, which increase both particulate and dissolved organic matter concentrations and further reduce water quality (including taste and color). As a consequence, the Ecosystem Restoration Program of the CALFED Drinking Water Quality Program has been designated to specifically address the sources of nutrients and organic matter that contribute to low dissolved oxygen levels.

Task 7 uses a combined isotope and chemical mass balance approach to characterize and differentiate various sources of organic matter and nutrients from different land uses to the SJR. Characterization of oxygen-demanding substances in the SJR is complicated due to numerous factors including the wide variety of land uses within the watershed, changing seasonal water inputs, and algal growth and decay dynamics. This study uses a multi-isotope approach to identify "characteristic fingerprints" of different biomass and nutrient sources, providing information that cannot be obtained through concentration measurements alone.

Objectives

The objective of Task 7 is to resolve the relative importance of different BOD fractions in various areas of the SJR to loads transported to Channel Point. Four main goals for Task 7 were developed from peer review recommendations:

(1) Provide a useful and cost-effective adjunct to routine monitoring efforts by improving the identification of sources of biomass and nutrients.

(2) Link algal sources and loads in the upper watersheds with algal loads downstream.

(3) Provide better quantification of specific sources of biomass which will be useful for improving river modeling efforts

(4) Improve the characterization of various types of BOD sources and sinks in the SJR.

The Task 7 study utilizes many different isotopic techniques to gain a better understanding of the spatial and temporal variations in source inputs and river dynamics over the course of the study period. These results will also be compared to results from preliminary isotope investigations conducted in the SJR in 2000 and 2001 (Kratzer et al., 2004) and integrated into the ongoing

CALFED PIN700 Study "Determination of Sources of Organic Matter and Nutrients in the San Joaquin River" in order to assess long-term changes related to BOD sources and sinks in the SJR.

Funding for Task 7 of the SJR Up-Stream DO TMDL Project covered the analysis of a limited set of isotope samples collected during just the first two years of the DO TMDL project, the preparation of quarterly and annual reports, plus some time spent on a preliminary interpretation of the data for the final report. The analysis of a similar limited set of isotope samples collected during the third year of the study was partially covered by the ongoing CALFED-funded PIN700 study. The PIN700 project also partially covered the analysis of a more complete set of isotope samples collected during all 3 years of the DO TMDL project. The additional samples covered by PIN700 are directly relevant to the objectives of Task 7 and the major goals of the SJR Up-Stream DO TMDL Project. For this reason, all currently available isotope data for samples collected as part of the DO TMDL project have been included in this report. However, some of the analyses covered only by PIN700 have not been completed, and therefore the PIN700 Final Report (due August 2008) will include a considerable amount of additional information related to the SJR and DWSC. Furthermore, a more extensive interpretation of the data will be included as part of the PIN700 report.

Background about the Use of Isotopes

Potential sources of organic material within the SJR include primary production by phytoplankton and periphyton in the mainstem SJR and its larger tributary streams, and runoff from adjacent agricultural land. Potential losses of organic matter include microbial and photochemical degradation of organic material. Both degradation and production of organic matter are evident in SJR water. Aerobic degradation of organic matter causes an oxygen deficit in the SJR -- most notably at the Stockton Deep Water Ship Channel (DWSC) -- and oxygen supersaturation is observed in association with algal blooms.

In order to investigate these biogeochemical processes occurring in the SJR, stable isotope analyses of particulate organic matter ($\delta^{13}C$ and $\delta^{15}N$ of POM), nitrate ($\delta^{15}N$ and $\delta^{18}O$ of NO_3^-), dissolved organic carbon ($\delta^{13}C$ of total DOC), and water ($\delta^{18}O$ and $\delta^{2}H$ of H_2O) were performed. These measurements offer qualitative – and sometimes quantitative -- insight into the sources and cycling of nutrients and organic matter that control changes in water quality and quantity in aquatic systems. Other isotope analyses were also performed on selected archived splits of these samples at a later date (e.g., POM-$\delta^{34}S$, sulfate-$\delta^{34}S$ and $\delta^{18}O$, phosphate-$\delta^{18}O$).

Isotope tracers have been extremely useful in providing new insights into hydrologic processes because they integrate small-scale variability to give an effective indication of catchment-scale processes. The isotopic composition of water, biomass, and dissolved nutrients can provide a wide range of information about sources entering the river, as well as biogeochemical processes occurring within the river itself. Because the ratio of a heavier to lighter isotope of an element (e.g., for carbon $^{13}C/^{12}C$) changes with biological and chemical processes, these isotope ratios provide a powerful tool for tracing sources and processes in many environments (see Kendall and McDonnell, 1998, for a more detailed discussion).

Isotope jargon can be a bit confusing and off-putting at first; the novice reader is advised to view

the odd terminology as merely "isotope concentration units". The negative signs of the $\delta^{13}C$, $\delta^{18}O$, and $\delta^{2}H$ values are also a source of confusion. These were caused by picking international standards (e.g., VPDB and VSMOW, which are defined as 0‰) based on marine samples that have higher $\delta^{13}C$, $\delta^{18}O$, and $\delta^{2}H$ values than most freshwater samples, with the result that the freshwater samples have lower values than 0‰ – or negative numbers. Despite the negative numbers, δ values can be used in calculations just as you would use ppm and other more conventional concentration units.

POM isotopes. The biological reactivity of POM is largely related to its source. The $\delta^{13}C$, $\delta^{15}N$, and C:N (atomic) ratio of particulate organic matter (POM) can be used to assess both changes in nutrient sources and changes in organic matter sources. In freshwater aquatic systems, the sources of POM may be categorized into five groups (Figure 1): algae, heterotrophic bacteria, macrophytes, soil organic matter, and terrestrial plant material (Kendall et al., 2001; Finlay and Kendall, 2007). Trends in $\delta^{13}C$ and $\delta^{15}N$ of POM are most useful in assessing changes in nutrient sources over time and location, while C:N ratio is the most diagnostic factor for discriminating between plankton and the other 3 sources. The C:N ratio is especially useful for discriminating between plankton (algae and/or bacteria) and the other sources because the C:N ratio of plankton falls between 5 and 8, while the C:N ratio of terrestrial plants is generally greater than 15. The C:N ratios of macrophytes and soil organic matter fall between those of terrestrial plant material and phytoplankton, and therefore isotope data and algal pigment data are useful for further distinguishing the different sources. The $\delta^{13}C$ values from all sources may overlap; however, the $\delta^{13}C$ of soil organic matter and terrestrial vegetation from C4 plants (e.g., corn, sugar cane, many grasses) is distinctly higher (about -16 and -9 ‰) than material derived from C3 plants (most other types of plants).

Commonly observed ranges of $\delta^{13}C$, $\delta^{15}N$, and C:N values for different sources of organic matter, based on a literature survey, are shown in Figure 2. The large range of $\delta^{13}C$ values for terrestrial soil and leaves reflects the possible range for a mixture of C3 and C4 plants. However, in most ecosystems, terrestrial organic matter has a $\delta^{13}C$ value in the range of -25‰ ± 1‰, indicating that contributions from C4 plants are usually extremely minor. Figure 3 shows the much smaller "normal" $\delta^{13}C$ and $\delta^{15}N$ ranges of organic matter in large US rivers. The $\delta^{13}C$ range for terrestrial organic matter in most rivers is much smaller than shown in Figure 2 because of the minimal contributions of C3 plant material. The $\delta^{15}N$ range of aquatic plants in most rivers is also much smaller (but usually with higher) than the theoretical range because of the minimal contributions of wetlands-derived plants (with very low $\delta^{15}N$ values) to most large rivers. The ranges of C:N values are approximately the same on both plots.

The $\delta^{13}C$, $\delta^{15}N$ and $\delta^{34}S$ of aquatic plants (including algae, bacteria, and macrophytes) is controlled by the $\delta^{13}C$, $\delta^{15}N$, and $\delta^{34}S$ of the dissolved inorganic C (DIC), N (DIN), and S (DIS) in the water column that is assimilated by the plants. The isotopic compositions of the dissolved species reflect both the isotopic compositions of the sources of the DIC (primarily bicarbonate), DIN (primarily nitrate and ammonium), and DIS (primarily sulfate) to the water column but also processes that alter (fractionate, or change) the isotopic compositions (see Finlay and Kendall (2007) for a more detailed discussion).

Biological processes preferentially utilize molecules with "light isotopes" – the ones with lower

masses and consequently weaker bonds between atoms – because these require less energy expenditures. This biological preference of isotope species – called "isotope fractionation" -- causes the byproducts of biological processes to have slightly lower δ values and the residual (leftover) materials to have slightly higher δ values. Typical fractionating processes in aquatic systems include: (1) assimilation (uptake) of DIC, DIN, or DIS (which results in increases in the $\delta^{13}C$, $\delta^{15}N$, and $\delta^{34}S$ of the residual solutes); (2) nitrification (which usually results in decreases in the $\delta^{15}N$ and sometimes the $\delta^{18}O$ of nitrate); (3) denitrification (which results in increases in the $\delta^{15}N$ and $\delta^{18}O$ of the residual nitrate, along slopes in the range of 1:1 to 1:2); (4) photosynthesis (which also results in increases in the $\delta^{15}N$ and $\delta^{18}O$ of the residual nitrate, along slopes in the range of 1:1 to 1:2), and (5) respiration of organics (which produces DIC with about the same $\delta^{13}C$ as the oxidized organic matter, usually resulting in a decrease in the $\delta^{13}C$ of the total DIC).

The effects of these and other processes on the $\delta^{13}C$ of DIC and the $\delta^{15}N$ of DIN are shown in Figure 4. The $\delta^{13}C$ values of plankton are often lower than the values from other sources, and are directly related to the $\delta^{13}C$ values of the dissolved organic carbon (DIC). The $\delta^{15}N$ of POM reflects both N-nutrients (ammonium or nitrate) to algae as well as organic N from other sources. The $\delta^{15}N$ values of terrestrial sources usually fall between +2 and +7 ‰, while the $\delta^{15}N$ values of aquatic sources may range between -15 and +20 ‰.

DOC isotopes. The bulk $\delta^{13}C$ isotopic composition of dissolved organic carbon (DOC) is a potentially useful tracer of DOC source, and may also provide information about carbon cycling, particularly when combined with other analyses such as DOC concentration and $\delta^{13}C$ of POM. In general, lower $\delta^{13}C$ values often indicate relatively higher aromaticity and more labile organic carbon, while higher $\delta^{13}C$ values are associated with older, more recalcitrant organic carbon. In other words, the $\delta^{13}C$ of stream DOC can serve to distinguish between terrigenous-derived DOC and that derived in-situ in streams in cases where decomposition of phytoplankton is a major DOC source (Wang et al., 1998). However, both carbon cycling dynamics as well as the $\delta^{13}C$ of DOC sources can vary significantly across ecosystems. Hence, it is necessary to characterize the isotope signatures of sources within a particular area in order to best interpret spatial and temporal variation in $\delta^{13}C$ of DOC.

Two dominant pools tend to contribute to DOC in surface waters: (1) a younger, more labile pool derived from recent organic matter (e.g., from soils or from primarily productivity in streams), and (2) an older, more refractory pool derived from groundwater, deeper soil horizons, lake bottoms, etc. DOC that is mobilized into streams during storm events is generally young compared to that of groundwater feeding the stream during baseflow, indicating that extensive cycling of the labile DOC takes place in catchment soils. In general, the DOC of streams in forested catchments is formed in soil organic horizons (Schiff et al., 1990). Riparian flowpaths can account for the greatest proportion of DOC exported to headwaters streams (Hinton et al., 1998). While there is a lot less known about variations in the $\delta^{13}C$ of DOC than POM, the $\delta^{13}C$ values for different sources of DOC are probably similar to the ranges for POM sources (Figure 2).

DOC is a primary drinking water constituent of concern. Contained within the total pool of natural and anthropogenic DOC are precursors of harmful disinfection by-products (DBPs) that

form during chlorination of drinking water. In addition, DOC fuels a component of the heterotrophic biological production in aquatic systems, and therefore fuels a component of in-stream biological oxygen demand (BOD). One of the parameters potentially useful for tracing sources of DOC is the bulk $\delta^{13}C$ isotopic composition of DOC. Like DOC concentration, this parameter is relatively easy to measure on a large number of samples without requiring laborious sample preparation or chemical fractionation. Thus, correlations between $\delta^{13}C$-DOC values and other characteristics (such as $\delta^{13}C$ of POM, DOC concentration, and Specific Ultraviolet Absorbance (SUVA)) could reveal changes in DOC source and/or quality that may be important indicators of sources of the DOC (e.g., terrestrial vs algal) and DPB formation potential.

Nitrate isotopes. The dual-isotope approach, using both the $\delta^{15}N$ and $\delta^{18}O$ values of nitrate, provides a considerable amount of information about nitrate sources and cycling (Figure 5) (Kendall, 1998). $\delta^{15}N$ values of nitrate can be very useful in distinguishing between soil or fertilizer nitrate sources (0 to +5 ‰) and animal waste or sewage sources (+10 to +20 ‰). $\delta^{18}O$ values of nitrate are useful for distinguishing between atmospheric sources (+50 to +90 ‰) and terrestrial sources (generally -15 to +15 ‰). Additionally, the combined use of $\delta^{15}N$ and $\delta^{18}O$ of nitrate can be used to identify environments in which nitrate consumptive processes like denitrification or uptake are occurring. The isotopic compositions of both nitrogen and oxygen increase during denitrification and uptake in a ratio of about 2:1 (e.g., slope 0.5) in non-marine environments. Therefore, an observed decrease in nitrate concentrations coupled to a shift in isotopic composition along this line strongly suggests that denitrification or uptake are an important process in that particular system.

Phosphate isotopes. The oxygen isotopic composition of phosphate (referred to as $\delta^{18}O\text{-}PO_4$ or $\delta^{18}Op$) may reflect inputs and mixing of different phosphate sources, in-situ biological cycling of phosphate (in which oxygen molecules are exchanged with the surrounding water), or a combination of both. Complete biological cycling of phosphate will bring the $\delta^{18}O$ of phosphate into isotopic equilibrium with the surrounding water, and this equilibrium value is controlled by the temperature and isotopic composition of the surrounding water. The expected equilibrium value of $\delta^{18}O\text{-}PO_4$ can be calculated using experimentally and empirically derived equations (Longinelli and Nuti, 1973; Blake et al., 1997). Therefore, it is possible to determine whether or not a source signature is present in the $\delta^{18}O\text{-}PO_4$ at any given location by using temperature and $\delta^{18}O$-water to calculate if the $\delta^{18}O\text{-}PO_4$ is out of isotopic equilibrium with the surrounding water (indicating biological cycling has not erased the isotopic source signature). The previous use of $\delta^{18}O$ of phosphate in aquatic ecosystems has been quite limited compared to other isotope tracers such as $\delta^{15}N$ and $\delta^{13}C$. However, recent studies are showing that $\delta^{18}O$ of phosphate has considerable promise for identifying and distinguishing sources of phosphate in diverse aquatic ecosystems (McLaughlin et al., 2006a, b).

Water isotopes. The isotopic composition of water provides information about water source, flowpath, and mixing. All samples from this study are analyzed for $\delta^{18}O$ and $\delta^{2}H$. In streams and rivers, variability in the isotopic composition of water arises primarily from the latitude and altitude of the recharge areas, mixing between waters of different compositions, and possible

isotopic fractionation due to evaporation in stagnant water areas (Kendall and Coplen, 2001). Proportions of end-member source waters of known composition can be quantitatively assessed within mixed samples. Water isotope signatures can also be used to determine if changes in nutrient and/or organic matter concentrations and compositions are associated with changes in water source or with biogeochemical processes occurring within a water parcel.

In most low-temperature, near-surface environments, stable hydrogen and oxygen isotopes behave conservatively. This means that as water molecules move through the subsurface, chemical exchange between the water and oxygen and hydrogen in the organic and inorganic materials through which flow occurs will have a negligible effect on the overall isotope ratios of the water (an exception is within certain geothermal systems, especially in carbonates where large amounts of oxygen exchange between the water and rock can occur).

Craig (1961) observed that the $\delta^{18}O$ and $\delta^{2}H$ (or δD) values of precipitation that has not been evaporated are linearly related by: $\delta^{2}H = 8*\delta^{18}O + 10$. This equation, known as the "Global Meteoric Water Line" (GMWL), is based on precipitation data from locations around the globe. The slope and intercept of the "Local Meteoric Water Line" (LMWL) for rain from a specific catchment or basin can be different from the GMWL. On $\delta^{18}O$ vs. $\delta^{2}H$ plots (Figure 6), water that has evaporated from open surfaces (e.g., ponds and lakes), or mixed with evaporated water, plots below the meteoric water line along a trajectory typically with a slope of between 2 and 5. This trajectory, which starts at the initial composition of the water on the LMWL, is called the "evaporation line" (Figure 6).

The $\delta^{18}O$ and $\delta^{2}H$ values of rivers reflect a seasonally variable mixture of water from different sources including local precipitation, agricultural drains and tributaries, discharge from upstream reservoirs, groundwater discharge, and evaporation. Precipitation during the summer and fall tends to have higher $\delta^{18}O$ and $\delta^{2}H$ values than precipitation during colder seasons. Also, precipitation from higher elevations (e.g., the Sierras) tends to have higher $\delta^{18}O$ and $\delta^{2}H$ values than precipitation in the warmer valleys (e.g., the San Joaquin Valley). Seasonal variations will be larger in small streams or drains where recent precipitation is the main source of flow, and smaller in large rivers where groundwater or reservoir releases are the dominant sources. As the basin size increases, the isotopic compositions of river waters are also increasingly affected by evaporation.

Sulfate isotopes. The main hydrological application of $\delta^{34}S$ and $\delta^{18}O$ of sulfate has been to quantify the effects of atmospheric deposition on sulfur cycling in the natural environment, particularly in forest ecosystems. This is in response to increased sulfur loadings to terrestrial ecosystems from anthropogenic sulfur emissions, as sulfur is a dominant component of "acid rain". These tracers can also be used to identify sulfur sources and transformations along flow pathways in groundwater. In specific, bacterially mediated sulfate reduction causes isotope fractionation, resulting in increases in the $\delta^{34}S$ and $\delta^{18}O$ of residual sulfate, and low $\delta^{34}S$ values of new sulfate formed from oxidation of the H_2S. Hence, sulfate derived from marshes typically has low $\delta^{34}S$ values because of the extent of sulfate reduction in reducing environments. Soil and rock sources of sulfur include sulfide minerals, chemically precipitated sulfate minerals, and oxidation of S in organics. Sulfate isotopes can also be used to identify sources of salts in rivers and groundwater, and anthropogenic pollutants. The general ranges of sulfate $\delta^{34}S$ and $\delta^{18}O$

from different sources are shown in Figure 7.

Methods

All samples used for Task 7 were collected as part of the existing monitoring program described in Task 4. The field collection and laboratory analytical procedures and QA/QC data are described in Appendix A.

Results

This report contains 5 appendices (A-F). Figures and tables in the appendices have the appendix letter in front of the number (e.g., Figure B3 is the third figure in Appendix B).

Table 1 lists the site names, ID numbers, and abbreviations used in the figures for all of the core sites and selected intermittent (e.g., infrequently samples) sites. Table 2 shows the average, standard deviations, minimum, and maximum values, and numbers of samples analyzed for the different mainstem SJR sites, and Table 3 shows these statistics for all other frequently-sampled sites. Many of the figures in this report have top and bottom panels, which are referred to as "a" and "b" in the text, respectively, even though they are not so-labeled on the figures.

The distributions of isotope and elemental values are shown in a series of box-and-whisker plots (Figures 8-10, 13, 17-18, 28-29, 32-33). Each figure has 2 panels; the top panel (panel a) contains values for the mainstem sites and the bottom panel (panel b) contains values for major east-side tributaries, east-side drains, west-side creeks, and upstream wetlands sites. In each panel and each site group (e.g., east-side drains), the sites are listed in order from upstream (right) to downstream (left). Note that the top and bottom panels have different scales.

BOD Sources to the SJR: POM and DOC

General spatial patterns in POM isotopes. The isotopic compositions of POM measured in this study are similar to values previously observed in 2000-2001 in this system (Kratzer et al., 2004). POM showed a wide range of $\delta^{13}C$ values (-37 to -20 ‰), $\delta^{15}N$ values (-1 to +22 ‰), and C:N values (4 to 26), with mean values of -27.2 ‰, +6.8 ‰, and 8.4, respectively. The distributions of values are shown in Figures 8-10.

Mainstem San Joaquin River (SJR) sites have similar means (~ -28 ‰) and distribution of $\delta^{13}C$ values except for the site at Lander, which has a much wider range of $\delta^{13}C$ values and a mean value about 2‰ lower than other sites (Figure 8). The distribution of $\delta^{13}C$ values for the entire dataset is approximately normal, with a skewness value of -0.16. As with the water and nitrate isotopes, the POM isotopes from SJR at Lander Avenue were different from both the other mainstem SJR sites and the upstream wetland sites (Salt Slough, Mud Slough, Los Banos Creek). In general, the $\delta^{13}C$ values of the drains, creeks, and wetlands sites are more variable than the mainstem sites (except for Lander), and have higher $\delta^{13}C$ values. The highest $\delta^{13}C$ values observed in this study were from minor west-side drains (e.g., Harding) and wetlands

sites (e.g., San Luis Drain). In general, POM from mainstem sites had $\delta^{13}C$ values about 1‰ lower than in the three major tributaries (the Merced, the Tuolumne, and the Stanislaus Rivers), and showed a slight increase in $\delta^{13}C$ downstream. The mean $\delta^{13}C$ values of three of the upstream wetlands sites (Salt Slough, Mud Slough, Los Banos Creek) are similar to the mainstem SJR, but have more variability, whereas the San Luis Drain site has a lower mean $\delta^{13}C$ value like the Lander site. The $\delta^{13}C$ values fall in the typical range of $\delta^{13}C$ values expected for plankton and C3 terrestrial plants (Figure 2).

Mainstem SJR sites have similar means (~ +7‰) and distribution of $\delta^{15}N$ values (Figure 9). The distribution of $\delta^{15}N$ values for the entire dataset is approximately normal, with a skewness value of +0.64. The sites at Patterson and Lander both have slightly higher mean values (~+8‰) than other mainstem sites. In general, the tributaries and drains have lower mean $\delta^{15}N$ values (~+6‰) than mainstem sites, except for Mud Slough, Los Banos Creek, and San Luis Drain which have higher mean $\delta^{15}N$ values (~+8‰) than mainstem sites. The tributary, drain, and wetlands sites also have larger ranges of $\delta^{15}N$ values than mainstem sites. The highest $\delta^{15}N$ values observed in this study were from upstream wetland sites Salt Slough, Mud Slough, and Los Banos Creek.

Mainstem SJR sites have similar means (~ 8) and distribution of C:N values (Figure 10), with slightly lower values at the Lander site. The other sites have mean C:N values in the range of 7 to 9 except for the three tributaries (the Merced, the Tuolumne, and the Stanislaus Rivers), which have an average mean of 10.1, with values as high as 26. Hospital Creek, Mud Slough, and San Luis Drain all have slightly lower C:N values than other minor sites. The C:N distributions for the entire dataset and for most sites, are significantly skewed (+2.28), with many more outliers with high C:N values. This is because few sources of organic matter have C:N values lower than 5 whereas old and refractory terrestrial organic matter can have C:N values of >100. The San Luis Drain site had slightly lower C:N values than the other wetlands sites, with occasional values in the unusual range of 5-6. In general, the wetland sites had lower C:N values (average = 7.9) than the creek and drain sites (8.7), suggesting a greater dominance of algae in POM from the wetlands sites.

Plots showing the $\delta^{13}C$ vs. $\delta^{15}N$ and $\delta^{13}C$ vs C:N of different types of sites and of selected individual sites are shown in Appendix B (Figures B1-B5). Figure 3 showed that different sources of POM have relatively distinctive compositions, with the combination of C:N and $\delta^{13}C$ providing good separation of plankton and terrestrial sources of POM. Hence, by plotting the data on expanded versions of Figure 3, we can identify the dominant source of POM at different groups of sites. There is little variation among sites in the mainstem SJR (Figures 8-10, and Figure B2a), with overlapping $\delta^{13}C$, $\delta^{15}N$, and C:N values for all sites except Lander, where POM samples often have lower $\delta^{13}C$ values than at the other sites. The major tributary sites also show overlapping $\delta^{15}N$ and $\delta^{13}C$ values (Figures 8-10, and Figure B2b), but generally have higher $\delta^{13}C$ and lower $\delta^{15}N$ than the mainstem sites. Hence, the values for mainstem sites (except for Landers) can be grouped together, and the values for the tributary sites can also be grouped together.

Figure 11 compares the $\delta^{13}C$ vs. $\delta^{15}N$ and $\delta^{13}C$ vs C:N relations for mainstem sites, with the Lander Avenue site plotted separately, and for the major east-side tributaries. The distributions of the values for mainstem sites, Landers, and tributary sites are distinctively different. POM

from the Landers site appears to be more dominated by planktonic algae than other mainstem sites. POM from the mainstem sites is much more dominated by algae than the major tributaries, where the POM is clearly dominated by organic matter derived from soils, terrestrial plants, and perhaps other aquatic plants.

Figure 12 compares the $\delta^{13}C$ vs. $\delta^{15}N$ and $\delta^{13}C$ vs C:N relations for mainstem sites, selected minor east and west-side tributaries, and upstream wetlands sites. The values for individual sites are shown in Figures B3-B5. The $\delta^{13}C$-C:N data clusters for drain and creek sites are mostly indistinguishable except that Harding Drain has a band of samples with higher $\delta^{13}C$ and C:N values than usually seen at other sites (Figure B5b). The $\delta^{13}C$-C:N data clusters for the Mud Slough, Salt Slough, and Los Banos wetlands sites are indistinguishable; however, the San Luis Drain samples are moderately distinguishable from the other wetlands sites because of the lower $\delta^{13}C$ and higher $\delta^{15}N$ values (Figure B3b). The values for the upstream wetlands sites (Mud and Salt Slough, San Luis Drain, and Los Banos Creek) are very similar to the values shown by mainstem sites. Hence, the POM at wetlands sites, like the mainstem sites, is mostly derived from algae.

At first glance (and especially when looking at a black & white version of Figures 11 and 12, it appears that the values for minor tributaries (e.g., east-side drains and west-side creeks) are very similar to the values shown in Figure 11 for the major tributaries. However, closer inspection of colored versions of the plots (and Figures 8-10) shows that while the ranges of values (especially $\delta^{13}C$ and $\delta^{15}N$) are similar, the major tributaries have considerably higher C:N values than the minor tributaries. Hence, while the POM from all the major and minor tributaries contains a lot more terrestrial organic matter than the algae-dominated mainstem and wetlands sites, the POM from the minor tributaries contains a higher proportion of algae than the major tributaries.

Figure 12 clearly shows that the $\delta^{13}C$, $\delta^{15}N$, and C:N values of POM from wetlands sites overlap almost the entire range of values for mainstem sites. If we exclude the Landers site, the mainstem sites show a more limited range of values. Samples from small creeks and drains (e.g., west-side drains like Harding and Westport Drains; east-side creeks like Orestimba, Del Puerto, and Ingram Creeks) have relatively narrow ranges of compositions, with lower $\delta^{15}N$ and higher $\delta^{13}C$ than mainstem or wetlands sites (Figures B3, B5). Hence, the mainstem isotope values "could" be explained simply as wetlands-derived POM but could not be explained simply as drain, creek, or tributary-derived POM. However, the $\delta^{15}N$ and $\delta^{13}C$ values at mainstem sites "could" also be explained by various mixtures of wetlands-derived POM and POM derived from the other sites. None of these sites have statistically distinctive $\delta^{13}C$-$\delta^{15}N$ isotopic compositions.

Temporal variation in POM isotopes. Most sites showed considerable temporal variation in $\delta^{15}N$, $\delta^{13}C$, and C:N, with much of the variability apparently caused by changes in flow. Not surprisingly, during high discharge periods, larger amounts of terrestrial-derived POM are transported into the river. This POM is "isotopically" and "elementally" labeled -- with higher $\delta^{13}C$ values, lower $\delta^{15}N$ values, and most importantly, higher C:N values than algal-derived POM (Figure 3). This section will summarize the main observations regarding the temporal variation in sources of POM to the different sites. Note that many of the figures showing temporal variations in POM composition have been included in the appendices.

Appendix C contains a large number of plots showing the temporal variation of POM at different

sites, and a more detailed discussion of the temporal variation in POM. Two major types of plots are given here. The first type emphasizes comparison of $\delta^{15}N$, $\delta^{13}C$, and C:N between sites by plotting temporal variations in $\delta^{15}N$ (Figures C1-C3), $\delta^{13}C$ (Figures C4-C6), or C:N (Figures C7-C9) data from several sites, or groups of sites, on separate plots. The second type emphasizes the correspondence of temporal changes in $\delta^{13}C$, $\delta^{15}N$, and C:N at individual sites by plotting the data for each site on a separate plot (Figures C10-C21).

The most important point to be taken from an inspection of all these plots is that the $\delta^{15}N$, $\delta^{13}C$, and C:N values are not showing random noise but instead represent a "signal" of changes in POM sources. Comparison of these patterns (and those of other parameters) provides information about whether the temporal oscillations can best be explained by inputs of terrestrial organic material, perhaps releases of irrigation waters containing algae, or other processes (such as algal uptake or nitrification) in the water column (Figure 4).

Temporal variation in POM-$\delta^{15}N$. The POM of mainstem and major tributaries show larger temporal oscillations in $\delta^{15}N$ during high flow periods than during low flow periods. The sudden increases and decreases in composition reflect sudden storm-based changes in flow, which wash surface soil and other terrestrial materials into the river. In general, the mainstem sites (except for Landers, which shows more oscillations, and with a wider range of $\delta^{15}N$ values, than other sites) show less temporal variability in $\delta^{15}N$ than the major tributaries. In many instances, the tributaries show similar oscillations to each other and to mainstem sites. For example, all three tributaries show increases in $\delta^{15}N$ as flow increases in March 2005, then remain relatively constant during the summer and fall of 2005 until all show a decrease in $\delta^{15}N$ as flow increases in early January 2006, and then they oscillate up and down during 2007. The $\delta^{15}N$ values of POM at mainstem and major tributaries during the dry season in 2005 are significantly lower than for summer of 2007, with gradually decreasing values as flow declined. There does not seem to be a comparable dry season/low flow pattern in 2006, perhaps because this was an unusually wet year. Upstream wetlands sites, except for Mud Slough, show considerably more temporal variation in $\delta^{15}N$ values than seen in the creek and drain sites. As was seen in mainstem and major tributary sites, oscillations are greater during high flow periods (seasons with successive storms) than during low flow periods.

Temporal variation in POM-$\delta^{13}C$. The POM at most sites shows considerably less variation in $\delta^{13}C$ than was seen with $\delta^{15}N$. While temporal patterns in the $\delta^{13}C$ and $\delta^{15}N$ were not tightly coupled and showed considerable variation between sites, the $\delta^{13}C$ values at mainstem sites generally dropped when $\delta^{15}N$ values increased. The change probably reflects the higher $\delta^{15}N$ and lower $\delta^{13}C$ of algae, and the generally lower $\delta^{15}N$ and higher $\delta^{13}C$ of terrestrial-derived organic matter. There is good correspondence between the oscillations in $\delta^{13}C$ for the different tributaries -- and good correspondence between the oscillations in $\delta^{13}C$ for the different mainstem sites (except for Landers, where the temporal changes in $\delta^{13}C$ seem almost totally unrelated to changes at other sites) -- especially during high flow periods where the $\delta^{13}C$ values usually decrease and then increase a week or so later. During dry spells, the $\delta^{13}C$ values slowly increase. There is generally very little correspondence of oscillations in the wetlands, creek, and

drain sites. One notable exception is the close match of $\delta^{13}C$ values at the Mud Slough and Los Banos Creek sites in late summer and fall 2007, probably related to the management of the wetlands sites. All tributaries and most mainstem sites show a general trend of decreasing $\delta^{13}C$, with changes of about 1.5‰ in 2.7 years; however, the r^2 values are unimpressive (~0.1); some minor tributaries also show a slight trend of decreasing $\delta^{13}C$ over time (e.g., Los Banos Creek, Salt Slough, Del Puerto Creek).

Temporal variation in POM-C:N. The POM at virtually all sites shows tremendous seasonal variability in C:N, with higher values generally occurring during high flow periods and slowly decreasing C:N values as flows slowly decline during the late summer and fall. As with $\delta^{13}C$, there is good correspondence between the oscillations in C:N for the major tributary and mainstem sites (except for Landers, where the temporal changes in C:N seem almost totally unrelated to changes at other sites) -- especially during high flow periods. While the trends are difficult to see amidst the oscillations, C:N values of major tributary sites increase by >1 during the 2.7 years of this study.

Surprisingly, Mossdale shows more variation in C:N than upstream sites. This could be interpreted as additional inputs between Mossdale and Vernalis, but could also reflect problems with the sampling site. USGS protocols for large river sampling require depth and width-integrated samples. This type of expensive sampling is more critical for constituents that can settle out of solution or are particle-attractive, like suspended sediments. The spatial and temporal patterns of C:N may be useful for improving the interpretation of other water quality data collected at these sites.

DOC. A selected number of DOC samples collected March-December 2005 were analyzed for $\delta^{13}C$; later samples are archived but have not been analyzed. These samples showed a wide range of $\delta^{13}C$ values (-33.8 to -22.4 ‰), with mean values (n = 325) of -26.4‰. The distributions of values are shown in Figure 13. $\delta^{13}C$ values at mainstem sites are very similar, except for Landers which shows slightly lower $\delta^{13}C$ values and a much wider range of values.

The mainstem DOC-$\delta^{13}C$ boxplots closely resemble the boxplots for POM-$\delta^{13}C$ (Figure 8), except that the average DOC-$\delta^{13}C$ values are about 1‰ higher than for POM. As was seen with POM-$\delta^{13}C$, the major tributaries, drains, creeks, and wetlands sites show more variability in DOC-$\delta^{13}C$ than the mainstem sites. However, in this case the minor sites appear to have, in general, lower $\delta^{13}C$ values than the mainstem sites, instead of higher $\delta^{13}C$ values as was seem with POM. Like POM, higher $\delta^{13}C$ values of DOC are observed in the larger tributary streams (Merced, Tuolumne, and Stanislaus) and in the smaller west-side tributaries (Turlock and Modesto irrigation district drains) than in the mainstem SJR. The Stanislaus showed the widest range of DOC-$\delta^{13}C$ values, ranging from -30 to -23‰ (Table 3). This wide range of $\delta^{13}C$ values clearly indicates that the DOC is derived from both algal and terrestrial sources. This is interesting because we had expected that the DOC would be largely derived from respiration of terrestrial organic matter.

The $\delta^{13}C$ data suggest that more of the DOC in the major and minor tributaries is of terrestrial origin, whereas more of the DOC in the mainstem SJR is derived from algal. Whether the algal-

derived DOC is a byproduct of algal productivity (e.g., "leaked" from algae) or respiration of algae or algal sediments is currently unknown. However, this question could be evaluated by measuring the BOD of the DOC, and/or by making additional isotopic measurements such as analyzing the DOM for $\delta^{15}N$ and $\delta^{34}S$, measuring the $\delta^{13}C$ of DIC in the water column, etc. These methods have been evaluated as part of our PIN700 project and other CALFED-funded studies.

Values of $\delta^{13}C$ of total dissolved organic carbon (DOC) and of POM were compared in order to shed light on the contribution of terrestrial DOC versus the contribution from in-stream phytoplankton productivity to the total DOC load. There is a rough correspondence between the $\delta^{13}C$ values of DOC and $\delta^{13}C$ values of POM, with the data for most sites clustering around the 1:1 line on a plot of POM-$\delta^{13}C$ vs. DOC-$\delta^{13}C$ (Figure 14). This correspondence is consistent with the POM being a major source of the co-existing DOC. Samples from the Modesto ID sites did not cluster along the 1:1 line, and the POM generally had higher $\delta^{13}C$ values than the DOC. The high $\delta^{13}C$ values of the DOC (-24 to -21‰) suggest that it is not of terrestrial origin; such high values are probably the result of intensive photosynthesis (Figure 4).

The DOC dataset show no obvious correlation of $\delta^{13}C$ with DOC or algal pigments (Figure 15). DOC derived from respiration (oxidation) of terrestrial C3 organic matter would be expected to have a similar range of $\delta^{13}C$ values (e.g., -27 to -24‰; Figure 3). DOC resulting from planktonic algae effluents or respiration would be expected to show $\delta^{13}C$ values similar to the algae (-35 to -25‰; Figure 3). Hence, contributions from planktonic algae can explain the DOC-$\delta^{13}C$ values in the range of -31 to -27‰. The $\delta^{13}C$ values > -24‰ might be derived from benthic algal effluents or respiration (Figure 2). Alternatively, they could result from such intensive photosynthesis in a semi-confined location that the pool of DIC was highly fractionated, resulting in very high $\delta^{13}C$ values (Figure 4). We have seen DOC-$\delta^{13}C$ values as high as -20‰ during an intense algal bloom in Willow Slough. At that site, $\delta^{13}C$ was inversely correlated with DOC concentration and positively correlated with nitrate concentration. Therefore, it is likely that large number of samples with DOC-$\delta^{13}C$ values outside the normal C3 plant range reflect DOC derived from photosynthetic activity, even though there is no correlation of $\delta^{13}C$ and algal pigments.

Nutrient Sources

Nitrate. Nitrate in the mainstem SJR and major and minor tributaries shows a wide range of $\delta^{15}N$ and $\delta^{18}O$ values (Figures 16-18). The $\delta^{15}N$ values ranged from +1.8 to +20.8‰, and the $\delta^{18}O$ values ranged from -12.5 to +18.4‰. With the exception of the Lander Avenue site, the mainstem sites generally had intermediate $\delta^{15}N$ and $\delta^{18}O$ values, and showed less variability than many of the tributary sites. In the Merced, Tuolumne, and mainstem SJR, higher NO_3 concentrations generally occurred at the same time as higher $\delta^{15}N$ values (Figure 19). However, no such pattern was observed in either the Stanislaus or many of the minor drains, creeks, and wetlands sites (Figure 19b and 20). The $\delta^{18}O$ values in the mainstem SJR and tributaries did not show any clear relationship with nitrate concentration.

Nitrate concentrations and $\delta^{15}N$ in the SJR mainstem (except Lander Avenue) and the major east-side tributaries followed similar patterns, which appear to be related to mean daily flow. In general, lower nitrate concentrations and lower $\delta^{15}N$ values occurred during periods of high flow

(Figure 21). Nitrate in the Stanislaus, Merced, and Tuolumne Rivers showed a similar pattern to that seen in the SJR mainstem. During periods of low flow, $\delta^{15}N$ in the Merced River was close to or higher than $\delta^{15}N$ in the mainstem SJR (Figure 22), while during periods of high flow the Merced $\delta^{15}N$ tended to be much lower than that observed in the mainstem SJR.

Samples collected at the SJR at Lander Avenue site showed a different pattern, with high nitrate concentrations sometimes occurring at the same time as low $\delta^{15}N$ values (Figure 23). However, it was not possible to analyze all of the SJR at Lander Avenue samples for nitrate isotopes due to periods of extremely low nitrate concentrations. Although flows were much lower at Lander Avenue in comparison to the rest of the SJR (Lander Avenue is upstream of all the confluences with major tributaries), the general pattern of higher flows corresponding to lower nitrate concentrations was evident.

Several of the upstream mixed agricultural and wetlands sites (Mud Slough, San Luis Drain, and Los Banos) had $\delta^{15}N$ values that were usually higher than the $\delta^{15}N$ in the mainstem SJR, regardless of flow conditions (Figure 24). Figure 25 shows the average nitrate $\delta^{15}N$ and $\delta^{18}O$ values for all of the SJR and core tributary sites. Due to high temporal variability at all of the sites, there is considerable overlap. However, some sites tend to have distinct nitrate isotope signatures, such as SJR at Lander Avenue, Mud Slough and San Luis Drain, which both tend to have high $\delta^{18}O$ values, and Ingram Creek, which tends to have lower $\delta^{15}N$ values than the other sites.

Phosphate. Significant variation was observed in the $\delta^{18}Op$ measured in the mainstem SJR sites and various tributaries (much larger than analytical error), indicating that this relatively new isotopic tool may be useful in the San Joaquin River area for identifying phosphate sources. $\delta^{18}O_p$ ranged from +9.2 to +16.4 ‰, with the lowest values measured in the Merced River and Harding Drain, and the highest values measured in Salt Slough Mud Slough, and Los Banos Creek (Figure 26). A larger range of $\delta^{18}Op$ values was observed in the tributaries and drains in comparison to the mainstem SJR

Other Tracers

Water isotopes. Mainstem SJR sites showed a wide range of $\delta^{18}O$ and $\delta^{2}H$ values (Figure 27). $\delta^{18}O$ values ranged from -13.6 to -4.4 ‰, and $\delta^{2}H$ ranged from -99.3 to -47.3 ‰. A wider range of both $\delta^{18}O$ and $\delta^{2}H$ values was measured at Lander Avenue than at any of the other mainstem SJR sites. The range of $\delta^{18}O$ measured in all samples, including tributaries and drains, was -13.6 to -4.2 ‰, and the range for $\delta^{2}H$ was -99.3 to -43.5 ‰ (Figures 27-29). The major east-side tributaries had relatively low $\delta^{18}O$ and $\delta^{2}H$ values throughout the study period, while the highest values for $\delta^{18}O$ and $\delta^{2}H$ were found in many of the smaller tributaries (Figure 27).

The upstream tributaries (Salt Slough, Mud Slough, San Luis Drain, Los Banos) usually had higher $\delta^{18}O$ and $\delta^{2}H$ values than the mainstem SJR while the major east-side tributaries had lower values (Figure 30). The influence of the lower water isotope values in the major east-side tributaries can be seen in the changing water isotope values of the mainstem SJR going downstream (Figure 31). Seasonal changes in the $\delta^{18}O$ and $\delta^{2}H$ in the mainstem SJR did not follow the typical sinusoidal pattern seen in precipitation and small streams, namely low values

in the winter and during major storms, and high values in the summer. Instead, during major increases in flow in the SJR, $\delta^{18}O$ and $\delta^{2}H$ generally showed sharp increases on the rising limb of the hydrograph, reaching values that were sometimes higher than observed during the late summer and fall, followed by sharp decreases on the falling limb.

Sulfate isotopes. A selected number of samples for 2005 and 2006 were analyzed for sulfate $\delta^{34}S$ and $\delta^{18}O$. The highest $\delta^{34}S$ values were consistently measured at Lander Avenue, while the lowest values were found in the San Luis Drain and Mud Slough (Figure 32- 34). Sulfate in the mainstem SJR (except for Lander) showed a distinct downstream increase in $\delta^{34}S$ (Figure 35), with little seasonal variation in the trends at different sites. This is a bit surprising, given the flow-related changes in nitrate, water, and POM isotopes. $\delta^{34}S$ values at Lander Avenue were very different from the rest of the mainstem SJR sites, and followed a totally different pattern. $\delta^{34}S$ at all the mainstem sites between Lander Avenue and Laird Park were almost indistinguishable from each other. The $\delta^{34}S$ at downstream sites (Maze, Vernalis, and Mossdale) were generally significantly higher than the upstream sites (excluding Lander Avenue), and had similar values.

Sulfate isotope data can be used to determine the source of the sulfate and to check salt budget calculations. These preliminary data suggest that there is enough variation in sulfate $\delta^{34}S$ and $\delta^{18}O$ in the San Joaquin River basin for sulfate isotopes (and $\delta^{34}S$ of POM and DOM) to be useful tracers here. This is being pursued as part of the PIN700 project. The $\delta^{34}S$ values at Mossdale were similar to the values for Salt Slough (Figure 36), which is believed to be a major source of sulfate to the SJR. The high $\delta^{34}S$ values at Landers suggest contributions from some unknown source of S. The generally low $\delta^{34}S$ values of sulfate from Mud Slough and San Luis Drain are consistent with sulfate produced by surface water oxidation of sulfate released by sulfate reduction in anoxic environments in the wetlands.

No relationship between sulfate $\delta^{34}S$ and $\delta^{18}O$ was evident for any of the sites (Figure 34). The SO_4-$\delta^{18}O$ values were much more variable and did not show clear downstream or site-to-site patterns (Figure 36). The two sites with the highest electrical conductivity (San Luis Drain and Mud Slough) tended to have the lowest $\delta^{34}S$ values, while sites with low to moderate electrical conductivity spanned a wide range of $\delta^{34}S$ values (Figure 37). No relationship between $\delta^{18}O$ and electrical conductivity was observed.

Discussion

What is the Dominant Source of POM in the SJR?

The River Continuum Concept (Figure 38) predicts that the relative contribution of the five main sources of organic matter (Figure 1) to total organic carbon in rivers varies with stream size (Vannote et al., 1980). In this model, terrestrial carbon is expected to be the dominant source of organic matter in small forest streams because overhanging trees block sunlight, greatly reducing algal productivity, and add large amounts of detritus to streams. Canopy shading decreases with increasing stream size for medium-size rivers, with the result that algal productivity becomes a more important source of carbon. Finally, in large or disturbed rivers, decreases in light

penetration because of increases in turbidity limits in-situ production again. Hence, terrestrial sources of carbon are expected to dominate in large rivers as well as in headwater streams. However, several recent studies have shown that some large rivers in the USA (e.g. the Mississippi River) have appreciable amounts of algal productivity (Kendall et al., 2001; Wissel and Fry, 2005; Delong and Thorp 2006).

When our USGS group first started looking at POM in the San Joaquin River in 1998, the prevailing theory was that this river was too turbid to support much phytoplankton growth, and consequently that terrestrial sources of organic matter from the major tributaries and from agricultural activities near the river were responsible for most of the upstream loads of POM. However, chlorophyll and POM isotopic data generated in 2000-2001 during a CALFED and USGS-funded project led by Charlie Kratzer soon showed that most of the POM was algal in origin (Kratzer et al., 2004). Subsequent publications have confirmed these findings and have provided a great deal of information on spatial changes in loads and algal dynamics (e.g., Volkmar and Dahlgren, 2006; Ohte et al., 2007). So it is no longer a surprise that the dominant source of POM to the SJR is algae. What is less certain is where it comes from. In particular: (1) how much grows in the mainstem itself versus what is derived from upstream wetlands and various drains and creeks, and (2) how do these source contributions change with season.

Since the small set of POM isotope data gathered as part of the Kratzer study in 2000-2001 proved so useful, we proposed as part of Task 7 of the Up-Stream DO TMDL project to use isotopes to resolve the relative importance of different BOD fractions in various areas of the SJR to the loads transported to Channel Point. To do so, we have characterized the POM in the SJR, its main tributaries, and main sub-watersheds, with the intent that isotopic characterization methods will be integrated to provide a fingerprint comparison among sites in the watersheds and in the mainstem SJR. Towards this goal, we will now compare the C:N, $\delta^{15}N$, and $\delta^{13}C$ values for POM, and the $\delta^{13}C$ values of DOC, with algal pigment, BOD, and other chemical and hydrological data generated by Will Stringfellow and his team as part of Task 4.

Relations between Algal Pigments, BOD, and the C:N, $\delta^{15}N$, and $\delta^{13}C$ of POM

The measurement of algal pigments (chlorophyll-A plus pheophytin) provides a means for identifying "relatively" fresh organic matter produced by phytoplankton. There is a very close correlation of chlorophyll with algal pigments, with an r^2 of 0.96 for the set of samples analyzed for POM isotopes. One way to determine the "freshness" or bioavailability of algal and other organic matter is to analyze the samples for Biological Oxygen Demand (BOD). BOD can also be further separated into nitrogenous BOD (NBOD) and carbonaceous BOD (CBOD), depending on how much nitrate and carbon dioxide, respectively, are produced by microbial respiration (oxidation) during laboratory incubations. Hence, the measurement of BOD provides an independent measure of the bioavailability of organic matter. There is a good positive correlation of BOD and algal pigments (r^2 of 0.57 for the samples analyzed for POM isotopes) because most of the bioavailable organic matter is of algal origin. The higher C:N values and chemical composition of terrestrial organic matter make it generally less useful for bacterial respiration than algal material with an average C:N of 6.7 (the so-called Redfield Ratio).

We will now compare algal pigment and BOD concentrations and C:N ratios and carbon and nitrogen isotopic compositions, to explore how the elemental and isotope data allow enhanced

discrimination among sources of POM. This discussion will be divided into 3 sections, each aimed at discussing the usefulness of one of the new parameters measured.

Correlation of POM-C:N with algal pigment and BOD concentrations. The isotopic compositions of POM measured in this study are similar to values previously observed in this system (Kratzer et al., 2004). The majority of the POM from the mainstem SJR and the upstream wetlands sites exhibit C:N ratios between 6 and 8. This indicates the dominance of phytoplankton in the organic matter of these samples (Figure 3). A comparison of C:N ratios with the concentration of algal pigments (data from Sharon Borglin) shows that virtually all the samples with high algal pigment (AP) concentrations (> 25 μg/L) fall within the C:N range typical of phytoplankton (Figure 39a). For samples with AP <25 μg/L (Figure 39b), which comprise ~65% of the total AP measurements, ~60% have C:N < 9, indicating a dominantly algal origin, with an average BOD = 3.3 mg/L. The ~40% of POM samples with AP<25 but C:N >9 have a slightly lower BOD = 2.4 mg/L. Hence, there is little difference in bioavailability of the algal-dominated and non-algal-dominated POM samples with low pigment concentrations (<25 μg/L).

The sites with the highest AP concentrations were wetlands sites and the SJR at Lander Avenue. All of these sites are located in the upstream region of the study area, and represent drainage from wetlands as well as agricultural tile drainage and return flows. Major tributaries and minor creeks and drains generally have much lower pigment concentrations. The other mainstem SJR samples usually have higher algal pigment concentrations than the major tributary samples (4.0 vs 1.3), reflecting the higher contributions of algae to mainstem sites, and perhaps the younger age of the mainstem algae.

Although a large percent of mainstem samples with very high pigment concentrations (>100 μg/L) are from the Lander site (Figure 40a), examination of the lower concentration samples (Figure 40b), shows that all mainstem sites show a wide range of pigment concentrations, with a large percent of samples with relative low pigment levels suggestive of either terrestrial material or old algal material. About half of the mainstem samples (excluding Landers) have algal pigment concentrations <25; of these samples, about 30% of C:N ratios are >9, indicating significant quantities of terrestrial material.

Only about 3% of these mainstem samples with AP >25 have C:N ratios >9.0. These statistics suggest that C:N <9 and AP >25 are not unreasonable cut-off values for distinguishing fresh algal material, old algal material (C:N <9, AP <25), fresh (new) non-algal or mixed-source material (C:N >9, AP >25), older, more terrestrial-dominated, mixed-source, material (C:N >9, AP <25), and definitely terrestrial-dominated material (C:N >9, AP <5). Below we will use this simple proposed metric to evaluate differences in the sources of POM from different sites. These results from this POM characterization scheme could also be used to assess seasonal changes in POM at the different sites.

Figure 41 shows the correlation of C:N ratios and AP values for upstream wetlands sites, drains, and creeks; the values of mainstem sites are included for reference. Samples with low C:N values show a range of pigment concentrations, but samples with high C:N only have low AP values. Mud Slough, Los Banos Creek, and San Luis Drain have much higher pigment concentrations than Salt Slough. Salt Slough has low AP values, similar to the creek and drain

sites. For wetlands sites, about 40% of the samples have AP<25; of these samples, about 75% have C:N values <9. For samples with AP>25, only about 5% have C:N>9. Hence, while a lot of the wetlands POM is fresh algae, there is also a large proportion of non-fresh algae and terrestrial organic matter. Most of the samples on Figure 41 with low AP values are from drains and creeks; these have a range of C:N values but little of it appears fresh.

A comparison of C:N ratios with BOD concentration (data from Will Stringfellow) shows a wide range of BOD concentrations for samples with C:N values that suggest that POM is predominately derived from phytoplankton (Figure 42a). This plot also shows a distinctive increase in C:N for samples with BOD <5 mg/L, suggesting that a large percentage of the POM in these samples is of terrestrial origin. Virtually all the samples with high BOD concentrations (>5 mg/L) fall within the C:N range typical of phytoplankton (Figure 42a). For samples with BOD < 5 mg/L (Figure 42b), which comprises ~70% of the total BOD measurements, 60% of these samples have C:N <9, indicating a dominantly algal origin. These low C:N samples have an average AP = 15 μg/L, in contrast to average AP = 7 μg/L for samples with C:N >9.

Figure 43 shows the correlation of C:N ratios with BOD concentrations for mainstem and tributary sites. Most of the samples with high BOD (and C:N <9) are from the Lander site. Oddly, Mossdale also has a high proportion of the high-BOD samples, more so than Vernalis, the closest upstream site. Hence, there must be some significant source (or production) of fresh algae along this section of the river.

About 75% of the POM samples from the tributary sites have C:N values >9, suggestive of a high proportion of terrestrial organic matter. Examination of Figure 44b shows that there is a distinct cluster of mainly-tributary POM samples with BOD values < ~2 and a wide range of C:N values. Few (<20%) mainstem samples have BOD values < ~2. It is curious that there seems to be little correlation of BOD and C:N for this set of tributary samples, suggesting a lack of correlation of easy-to-oxidize low-C:N material with amount of oxidizable products.

In an attempt to determine the origin of this low-BOD material, separate plots were made of CBOD and NBOD for different sites (see Appendix D). It is important to point out that CBOD can be caused by respiration of DOC as well as POC. Approximately 30% of the BOD at mainstem and major tributary sites is NBOD (Figure 44), with some samples (especially ones with low BOD) showing that >50 of the BOD is NBOD. Assessment of temporal variations in NBOD – and their causes -- using the isotope and other data from this project is a topic for future investigation as part of the PIN700 project.

Mainstem samples with low C:N tend to have higher NBOD than samples with high C:N (Figure 45), but most of the data fall in a cluster of C:N values in the algal range of 6-9 and CBOD values in the range of 1-5 mg/L. A higher percent of the BOD is NBOD at drain/creek sites (40%) that at wetlands sites (30%), but otherwise the distributions of NBOD concentrations for the different site types are rather similar (Figure 46). Figure 46b shows that much of the BOD with values < ~2, showing a wide range of C:N values, is NBOD. Hence, it is perhaps not unreasonable to use a cut-off value of BOD = 2 mg/L to characterize this unknown source of BOD which is strongly associated with much of the NBOD in these samples.

POM classification scheme. Using the C:N, AP, and BOD relations discussed above, and natural clustering of the data, we have developed a simple preliminary scheme for estimating the

relative contributions of several different types of POM to each site. This classification scheme was intended to take advantage of the usefulness of C:N in distinguishing between algae and terrestrial sources of POM (Figures 11-12), use AP data to distinguish between new and old algae (Figure 39), and then use BOD to provide a mechanism for distinguishing relatively refractory organic matter (Figure 42).

According to this scheme, the POM in each sample is classified as 1 of 6 categories of POM, with a 7th category reserved for samples that lack BOD measurements (~10% of the samples for the frequently sampled sites (Figure 47), and 10-50% of the samples at the less-frequently sampled sites (Figure 48)). In most cases, we could have estimated the BOD well enough using the AP data to correctly bin the data into the BOD<2 and BOD>2 categories, but chose not to do so on this first attempt at characterizing the POM sources. It is important to keep in mind that this kind of classification scheme assigns all POM collected at each sampling period to a single "average" category, whereas the sample actually contains various proportions of POM from many sources. Since the POM from each sampling time is assigned a single "average" composition by this scheme, the resulting data could be used to assess temporal differences in "average" POM source/type.

Classification scheme:

fresh algal POM (BOD >2, C:N <9, AP >25),
older algal POM (BOD >2, C:N <9, AP <25),
fresh mixed-source POM (BOD >2, C:N >9, AP >25),
older mixed-source POM (BOD >2, C:N >9, AP 5-25),
terrestrial-dominated POM (BOD >2, C:N >9, AP <5)
unknown refractory POM associated with NBOD (BOD < 2)
unclassified POM (samples missing BOD measurements)

The data for the frequently sampled sites are shown in Figure 47, with the sites divided into 5 different "site" groups; within each group, the sites are listed in order upstream to downstream (right to left, respectively). The data for the less-frequently sampled sites are shown in Figure 48, with the sites divided into 6 different groups based on the degree of connection to the SJR sampling sites. See Table 1 for the list of site names for the various DO#. Primary sites (1°) are ones that drain directly into the SJR (e.g., French Camp Slough, DO-11). The 2°, 3°, and 4° level sites have increasingly indirect drainage into the SJR, passing through 2-4 other sampling points.

The most striking feature of Figure 47 is the clear indication of decreasing relative contributions of fresh algae downstream, which is not the general perception of the composition of POM in the river. The percentages of older algae (AP<25) and mixed-source algae (C:N > 9, AP= 5-25) also decreased downstream, although the trend is less clear because Laird Park (a mainstem sampling site where the water is apparently not well mixed) had more of this older/mixed POM than the adjacent sites. Keeping in mind that ~10% of the samples could not be classified because of they had not been analyzed for BOD, >70% of the POM at Lander was algae (fresh plus older), which decreased to about 50% at Mossdale.

While the percentages of algal-derived materials decreased downstream, the amount of an unknown source of POM with low BOD -- which is typical of POM from the major tributaries

and some of the minor east-side tributaries (e.g., MID 5 and Westport) -- increased downstream. At first glance, this would seem inconsistent with the findings of Volkmar and Dahlgren (2006) and Ohte et al. (2007), who documented increases in algal productivity downstream. However, it is important to keep in mind that Figure 47 shows the relative proportions of different POM sources at the different sites, not the absolute amounts. Hence, the decreasing percent of fresh algae and old/mixed algae downstream could be largely explained by mixing with and dilution by the low-BOD, apparently refractory, and probably terrestrial-dominated POM from the major tributaries. Still, this downstream decreasing trend in fresh and old algae is unexpected. It is important to keep in mind that this trend reflects **average** compositions of POM, and the trends may be very different during low and high flow periods (see other discussions of the temporal variability in POM compositions and sources).

Another surprising aspect of Figure 47 is that the major east-side tributaries are not dominated simply by young terrestrial sources of POM. These sites have higher proportions of terrestrial and mixed-source POM than mainstem sites, but this high C:N material is only a significant source of POM to the major tributaries during high flow periods. The low-BOD material, while certainly dominated by POM with C:N values consistent with a terrestrial source, has a wide range of C:N values and no simple relations with algal pigments. A relatively high proportion of BOD of this source is NBOD. It would be interesting to analyze this POM source for ^{14}C. It is possible that this material reflects old, highly altered, organic matter derived from reservoirs on the Sierran tributaries.

The POM at the upstream wetlands sites is dominated by algae. For 3 of the sites (Los Banos, San Luis Drain, and Mud Slough), fresh plus old algae comprises ~80% of the POM. POM from Salt Slough has a different composition, with little fresh algae (<10%), a large portion of older algae (~50%), and a much larger component of mixed and refractory sources of POM than the other wetlands sites. The POM from Salt Slough is very similar to the POM from Del Puerto Creek, whereas the POM from the other wetlands sites is very similar to the algal-dominated POM from Ramona Lake. Salt Slough is the only wetlands site containing the low-BOD endmember (< 10%).

Figure 47 divides the minor tributaries into "east-side" and "west-side" groups to investigate whether the POM derived from the small creeks and drains draining east vs west soil types and land uses was different. While we have not performed any statistical evaluations of the data in Figure 47, the POM from the minor tributaries on the east and west-sides are not distinctively different. Instead, the different sites show a wide range of POM "signatures", ranging from MID 5 which has proportions of low-BOD POM very similar to those in the major tributaries, to Ramona Lake where the algal-dominated POM is similar to POM from upstream sites, to sites like Harding Drain where ~25% of the POM is of mixed/terrestrial sources. Except for Ramona Lake, the minor tributaries generally have significantly higher proportions of terrestrial and mixed-source POM than any other site group.

Harding Drain shows the highest proportions of terrestrial and older-mixed sources of POM of any of the core sites (Figure 47), plus a moderate amount of old algae-derived POM. There has been some controversy over the extent to which the water and organic matter in Harding Drain represents municipal waste water vs agricultural runoff. This is difficult to assess without analyzing the composition of the suspected waste water source. However, it is worth noting that the characteristics of Harding Drain POM (as described in Figure 47) seem similar to what you

would get if you combined the terrestrial and older-mixed sources of POM from the west-side Orestimba and Del Puerto Creeks, and then added the old algal component from Hospital Creek. Harding has a slightly lower percentage of the refractory POM endmember than other sites, but it is not very much larger than the contribution to Del Puerto Creek.

What is different about the POM from Harding Drain is its $\delta^{13}C$ value (-24.8‰), the highest **average** $\delta^{13}C$ of any of the core sites (Figure 8). Even higher $\delta^{13}C$ values are occasionally observed at the SRJ mainstem site at Lander, Hospital Creek, and Westport Drain, but these have lower average $\delta^{13}C$ values (Figure 8). These high $\delta^{13}C$ values could reflect contributions of organic matter derived from (1) C4 plants in the agricultural basin drained by Harding Drain, C4 plants (e.g., corn and sugar cane) in the diet of the people whose waste is processed in the municipal WWTP, (3) cannery or other agricultural waste from C4 plants that either is processed in the WWTP or flows into Harding Drain, (4) significant contributions of benthic algae and other aquatic plants known to often have high $\delta^{13}C$ values (see Figure 3), or (5) intense photosynthesis in either WWTP reactors, the drain itself, or in waters contributing to Harding Drain. One of the less frequently sampled east-side sites, MID Lat 5 (DO-23), has an even higher $\delta^{13}C$ value, -22.4‰ (Table 3); hence, this kind of POM in a minor tributary is not unusual. These different hypotheses about the source/cause of the high $\delta^{13}C$ values can all be tested with isotopic data, perhaps even the data the group has already generated.

Figure 48 shows the classification of POM samples from the infrequently sampled sites. Since the average number of sampling points was 3, the data are unlikely to be representative of the average compositions of POM from many sites. These minor sampling locations show a wide range of POM types, with old algal material comprising a large percent of the POM. POM from several of the east-side 1° sites is dominated by the low-BOD refractory source. POM from the SJR and 4° sites are similar in that both site groups are dominated by fresh algae, except for site DO-88 (Ramona drain @ Apricot Ave.).

We were very pleased at the success of this first attempt at using part of the wealth of data available from this study to characterize site-specific differences in the source and quality of the POM, success being defined as finding that the different geographic groupings of sites often showed different – and meaningful -- mixtures of POM. In the future, we will test a range of other schemes for characterizing spatial and temporal changes in POM source and quality, including ranking methods (e.g., Stringfellow, 2008) and PCA. Advantages of our simple preliminary approach include (1) the divisions came directly from inspection of the data, (2) several of these divisions seem intuitive, and (3) the C:N and BOD, and to a lesser extent the AP, reflect a bulk, integrative property of the POM This is in contrast to PCA approaches where it is often difficult to find a physical basis for the categories.

Appendix D contains a discussion of plots showing correlations of algal pigment and BOD concentrations with $\delta^{15}N$ (Figures D1, D2-D3) and $\delta^{13}C$ (Figures D4-D8) of POM. The intent of the appendix was to explore whether the isotopic values provide any additional insights into the source of the BOD beyond what could be determined using C:N. The distributions of AP and BOD values with $\delta^{15}N$ and $\delta^{13}C$ are different from each other and from the distributions with C:N. High AP and BOD values are skewed towards low C:N values (e.g., Figures 39 and 42, respectively), whereas high AP and BOD values are skewed towards high $\delta^{15}N$ values and low $\delta^{13}C$ values because fresh algal material generally higher $\delta^{15}N$ and lower $\delta^{13}C$ than terrestrial sources of POM. This means that incorporation of the $\delta^{13}C$ and $\delta^{15}N$ values into the source

characterization scheme described above will likely provide enhanced ability to distinguish sources.

What is the Relationship between POM and NO_3 in the River?

During "pseudo-Lagrangian" downstream sampling trips in 2002-2003 (Silva et al., 2003; Kratzer et al., 2004), an offset was observed between the $\delta^{15}N$ values of algal-dominated POM and the NO_3, with the $\delta^{15}N$-POM being approximately 4 ‰ lower than the $\delta^{15}N$-NO_3. This offset is consistent with isotope fractionation during uptake as algae preferentially utilize NO_3 with low $\delta^{15}N$ values as a primary nutrient source. Other studies of nitrate and POM isotope isotopes in big rivers have also reported 4-6‰ fractionations (Battaglin et al., 2001). Similar offsets between the $\delta^{15}N$ values of nitrate and POM were observed at mainstem SJR sites during certain periods of time in 2005 through 2007, particularly during times of low flow. However, this offset disappeared during high flow events, with the $\delta^{15}N$-POM reaching equal or even lower values than the $\delta^{15}N$-NO_3. Nitrate concentrations decrease due to dilution during the high flow events, and the disappearance of the offset may be due to a combination of decreased nitrate availability and input of additional POM with different $\delta^{15}N$ values.

Lower offsets have been observed when the nitrate concentrations were low, which can be explained by the common observation that biological systems show less of an isotope preference when there is a limited supply of a required substance (Finlay and Kendall, 2007). Hence, when the $\delta^{15}N$ of fresh algae is less than 2-4‰ lower than the $\delta^{15}N$ of the co-existing nitrate, this lower fractionation is consistent with nutrient limitation. Comparison of the $\delta^{15}N$ values of POM and nitrate of algae-dominated samples shows a wide range of values (-4 to +10‰) at different sites and times, when +4‰ is a typical value for a non-nutrient limited system. Hence, these data need a lot more evaluation before we can attempt to tease out the actual isotope fractionations under different conditions.

Temporal trends in the isotopic composition of POM are greatly influenced by the flow in the river. The $\delta^{15}N$ values of POM tend to be higher during higher flow periods, and show a steady decline as the SJR enters its lowest flow regime (Figures C1-C3). Nitrate also shows flow-related changes in $\delta^{15}N$ (Figures 21-23).

In Figures 49-51, downstream changes in nitrate concentration, POM-$\delta^{15}N$, and NO_3-$\delta^{15}N$ for mainstem sites are shown for selected dates. These plots also show the nitrate concentrations and $\delta^{15}N$ values of POM and NO_3 of selected other sites, to provide information about potential significant inputs to the SJR that might provide alternative explanations for the downstream changes in composition of the mainstem sites than that they are caused primarily by in-situ algal productivity. Detailed discussions of these plots is beyond the scope (and resources) of this report. They are included mainly to provide a more concrete visualization of how the seasonal changes in $\delta^{15}N$ are produced and what they mean for interpretation of downstream changes in the compositions of POM and nitrate at mainstem sites.

Figure 49 presents the downstream changes for two high flow periods in 2005: March 31 and April 21. These are both times when the $\delta^{15}N$ values are in the range of 0-5‰, within the normal range expected for situations where algal uptake of nitrate in the river results in POM-$\delta^{15}N$ values that reflect the $\delta^{15}N$ of the nitrate source. Alternative explanations include: (1) the

algae may have been transported into the stream, carrying the isotopic signatures of that different environment; (2) the in-stream algae may be utilizing ammonium (derived from minor drains) not in-stream nitrate at this time; (3) the POM could be largely terrestrial instead of algal (these are high flow periods, when this is not unlikely); or (4) the nitrate dynamics could reflect intermittent contributions of different downstream sources during a period when the algae is not actively growing. These hypotheses can be evaluated with data generated by the combined DO TMDL and PIN700 project teams.

But let's concentrate on a simple interpretation – that the $\delta^{15}N$ of the nitrate and POM mainly reflect mixing of sources. For March 31, the nitrate-$\delta^{15}N$ at Lander is very similar to the $\delta^{15}N$ of nitrate from the upstream San Luis Drain and Mud Slough sites, and the $\delta^{15}N$ of POM is very similar to that from Salt Slough; hence, these are plausible sources of the nitrate and POM at Lander. The increase in the $\delta^{15}N$ of the POM could be explained by input of the POM from the Merced, which has an appropriate composition (but one would have to check the relative loads).

But why does the nitrate in the SJR continue to increase in concentration and $\delta^{15}N$ from Lander to Patterson? If the measured $\delta^{15}N$ values of known drains are inconsistent with this increase in $\delta^{15}N$, then it is time to look for another mechanism; the changes in the various isotope tracers and other data will constrain the possible explanations. Additional inputs of water from other upstream wetlands sites could explain the trends. The decrease in the $\delta^{15}N$ of POM between Patterson and Maze could be explained by the $\delta^{15}N$ of POM from the Tuolumne (assuming the loads are high), but the $\delta^{15}N$ of nitrate is low and cannot explain why the $\delta^{15}N$ of the SJR at Maze is so high. A local algal bloom at between Patterson and Maze could explain the decreasing $\delta^{15}N$ of the POM and increasing $\delta^{15}N$ of the "residual" nitrate. Inputs of nitrate and POM from the Stanislaus could explain the changes downstream of Maze.

At first glance, the parallel changes in the $\delta^{15}N$ of POM and nitrate from April 21 (Figure 49b) seem consistent with in-situ algal production resulting in $\delta^{15}N$ of algal that reflects the changing $\delta^{15}N$ of the nitrate. However, note that the POM from both upstream wetlands and the Merced have lower $\delta^{15}N$ values than at Landers, and inputs of material from these sources could explain the downstream decreases in $\delta^{15}N$. The compositions of the inputs from the Tuolumne and Stanislaus could explain other downstream changes in $\delta^{15}N$. Hence, the parallel downstream changes in $\delta^{15}N$ of POM and nitrate could reflect simple mixing.

Figure 50 presents the downstream changes for two high flow periods in 2005: May 5 and May 18. These are both times when the $\delta^{15}N$-POM is 2-4‰ lower than $\delta^{15}N$- NO_3, within the normal range expected for situations where algal uptake of nitrate in the river results in POM-$\delta^{15}N$ values that reflect the $\delta^{15}N$ of the nitrate source. The $\delta^{15}N$ of nitrate at mainstem sites decreased downstream at both times, whereas the $\delta^{15}N$ of POM decreased downstream on May 5 but increased downstream on May 18. The compositions observed at Lander can be explained by nitrate and POM loads from Los Banos being equivalent to the combined loads from the other 3 wetlands sites. The downstream patterns are then consistent with downstream loads from the major tributaries. Upstream wetlands inputs combined with downstream inputs from the major tributaries can explain the data for May 18 also. That does not mean that these are the correct interpretations -- just that a preliminary evaluation of a partial dataset can be used to formulate a reasonable and easily tested hypothesis.

Downstream changes for two low flow periods with relatively high nitrate concentrations are shown in Figure 51, for August 25, 2006 and February 1, 2007. In August, nitrate concentrations and $\delta^{15}N$ values at the upstream wetlands sites were very high. While the $\delta^{15}N$ of POM at Lander is consistent with a wetlands source, the $\delta^{15}N$ of the nitrate at Lander is too low to be derived mainly from the wetlands. There must be some other major source of nitrate with a $\delta^{15}N$ even lower than what was observed at Lander that mixes with wetlands-derived nitrate. The low $\delta^{15}N$ of the nitrate at Lander cannot be explained by massive algal uptake because that would have increased the $\delta^{15}N$. The decrease in $\delta^{15}N$ is, however, consistent with nitrification; hence an examination of ammonium concentrations and NBOD might prove useful in testing this hypothesis. Subsequent downstream changes in the $\delta^{15}N$ of POM and nitrate are consistent with the compositions of inputs from the major tributaries.

Mixtures of inputs from upstream wetlands and tributaries can explain the trends in $\delta^{15}N$ of POM and nitrate downstream to Patterson on Feb 1 (Figure 51b), and then the trends in $\delta^{15}N$ of nitrate downstream to Mossdale. However, the $\delta^{15}N$ values of POM from the tributaries are lower than at mainstem sites and hence cannot explain the downstream increase in $\delta^{15}N$ of POM from Patterson to Lander. Hence, there must be some additional source or sources of POM. The increase in $\delta^{15}N$ cannot be explained by in-situ productivity (utilizing nitrate) because the $\delta^{15}N$ of the POM is higher than the $\delta^{15}N$ of the nitrate.

These brief discussions of the patterns observed on Figures 49-51 were not intended to be definitive. They were simply to demonstrate an approach – how to use the isotopic "fingerprints" of POM and nitrate to develop and then test plausible interpretations about downstream sources of nitrate and organic matter. These discussions have largely omitted consideration of inputs from the drains and creeks because addition of data from these sites would have made the figures too complex. Of course these data, and the wealth of other data available at over 20 sites in this study, would need to be evaluated before arriving at tentative conclusions about any particular sampling date.

Sources of Nutrients to the SJR

The majority of samples collected from the San Joaquin River, drains, and tributaries have nitrate $\delta^{15}N$ and $\delta^{18}O$ values which fall in the expected ranges for soil nitrate and nitrate from manure and sewage (Figure 52). The relatively high $\delta^{15}N$ values seen in many of the sites can either be the result of nitrate inputs from sewage and animal waste, or may also be the result of various different nitrogen cycling processes such as denitrification and assimilation. It is likely that both nitrogen cycling and waste inputs contribute to the nitrate isotope signature in the San Joaquin, and that different sites are affected by different processes.

In the mainstem SJR, the highest $\delta^{15}N_3$ values were observed at Mossdale, and the highest $\delta^{18}O$ values were observed at Lander Avenue (Figure 53). The unusually high $\delta^{15}N$ values at Mossdale occurred between May and September of 2007 during a period of low flow (Figure 54), and at this time $\delta^{15}N$ values were increasing downstream, rather than the usual pattern of a downstream decrease in $\delta^{15}N$ associated with inputs of low $\delta^{15}N$ water from the Tuolumne and Stanislaus Rivers. At the time of the $\delta^{15}N$ increase, NO_3 concentrations were very low in the Stanislaus River, and the samples that contained enough NO_3 for isotope analysis showed low $\delta^{15}N_3$ values. The nitrate isotope measurements demonstrate that during this time period, the

source of nitrate in the SJR at Mossdale was not primarily from the east-side tributaries, but was instead from another source with high $\delta^{15}N$. This source appears to be some type of human or animal waste, rather than in-stream denitrification, because the nitrate isotopes do not show a denitrification trend.

Between June and September 2007, the mainstem SJR contained nitrate with high $\delta^{15}N$ values that could not easily be explained by nitrate from the sampled tributaries. At this time, the Merced River also generally had high $\delta^{15}N$, but the $\delta^{15}N$ in the upstream sites was either equal or lower than the $\delta^{15}N$ in the mainstem SJR (Figures 55-57). Additionally, none of the nitrate in the downstream tributaries had $\delta^{15}N$ values higher than the mainstem SJR, suggesting that the downstream increase in $\delta^{15}N$ during this low flow period was either a result of biological processes within the river, or addition of nitrate with high $\delta^{15}N$ values from an unidentified and unsampled source.

In order to test if the high $\delta^{15}N$ values were being produced in-stream through either denitrification or mixing, plots were made to examine how the $\delta^{15}N$ changed downstream with nitrate concentration (Figure 58). For each date, the $\delta^{15}N$ values of all the downstream SJR sites were plotted against both $1/[NO_3]$ and $\ln NO_3$ (Figure 59). If the $\delta^{15}N$ in the mainstem SJR is driven primarily by mixing of two nitrate sources with distinct isotopic compositions, plotting $1/[NO_3]$ vs $\delta^{15}N$ should produce a linear trend. If the $\delta^{15}N$ in the SJR mainstem is controlled mainly by either denitrification or nitrate assimilation (uptake), this will result in a negative linear trend for $\ln NO_3$ vs $\delta^{15}N$. Since no linear trends are apparent, this suggests that the high $\delta^{15}N$ values in the SJR mainstem at this time was caused either by input of more than one water source with high $\delta^{15}N$, or was a product of nitrification (conversion of organic nitrogen compounds into nitrate) within the river. It is unlikely that nitrification alone could produce the observed increase in $\delta^{15}N$, therefore it is highly likely that additional sources of nitrate with high $\delta^{15}N$ are entering the SJR. Likely nitrate sources include groundwater discharge, sewage infiltration, and unmeasured agricultural return flows.

Differences in Nitrate Isotope Signatures Between Sites

The relationship between nitrate $\delta^{15}N$ and $\delta^{18}O$ followed very different patterns at some of the tributary sites, and may be a useful tool for "fingerprinting" nitrate when used in conjunction with nitrate mass balance calculations. At the downstream SJR mainstem sites, $\delta^{15}N$ and $\delta^{18}O_3$ followed very similar temporal patterns, indicating that the nitrate isotopic composition at these sites is controlled primarily by mixing (Figure 49). Some biological processes, such as denitrification and uptake, may also cause $\delta^{15}N$ and $\delta^{18}O$ to change in the same proportions. However, as discussed in the previous paragraph, the changes in $\delta^{15}N$ and $\delta^{18}O$ in relation to NO_3 concentration do not support either denitrification or two end-member mixing as the primary factors in determining the nitrate isotope signatures at these sites. The relationship between $\delta^{15}N$ and $\delta^{18}O$ shows more decoupling in the further upstream SJR sites (Crows Landing and Lander Avenue) (Figure 61. Biological processes, particularly nitrification of organic nitrogen, result in decoupling of the $\delta^{15}N$ and $\delta^{18}O$ because the $\delta^{15}N$ signature comes from the organic nitrogen, while the $\delta^{18}O$ comes from some combination of oxygen in water molecules and dissolved oxygen (Kendall et al., 2007).

Interestingly, nitrate samples from Mud Slough and San Luis Drain show similar trends,

including a very tight coupling between $\delta^{15}N$ and $\delta^{18}O$; this pattern is not seen in nitrate in Salt Slough (Figures 62-63). The nitrate isotope data in both San Luis Drain and Mud Slough show evidence of either denitrification or uptake (assimilation) of nitrate, processes which both cause the $\delta^{15}N$ and $\delta^{18}O$ to shift along approximately a 1:1 line (Figure 65). The lower concentrations of nitrate measured in Mud Slough compared to those in San Luis Drain, combined with the similar nitrate isotope patterns, strongly suggest that although the nitrate in San Luis drain is diluted with lower-nitrate water as it enters Mud Slough, very little biological cycling of nitrate takes place between the end of San Luis Drain and the sampling site at Mud Slough.

In contrast, nitrate isotopes in Salt Slough do not fall along the 1:1 line, and the changes in $\delta^{15}N$ appear to be decoupled from changes in $\delta^{18}O$. Additionally, the $\delta^{15}N$ in Salt Slough is generally lower than that measured in San Luis Drain and Mud Slough and. The decoupling of the $\delta^{15}N$ and $\delta^{18}O$ suggests that more nitrification of organic matter may be occurring in Salt Slough in comparison to San Luis Drain and Mud Slough. It is unclear if this hypothesis is supported by the NBOD data; Salt Slough has a much higher % NBOD than the other sites (40% vs 16-25%), but the actual NBOD is lower (1.5 vs 1.8-2.0). The average $\delta^{15}N$ values measured in the upstream mixed wetland sites are similar to those measured in the mainstem SJR and the minor east-side tributaries (Figure 17).

All three minor east-side tributaries (Harding Drain, Westport Drain, and TID Lat 6&7) have very similar $\delta^{15}N$ and $\delta^{18}O$ values. From March 2005 through approximately the spring of 2007, $\delta^{15}N$ in all of the minor east-side tributaries was higher than that in the SJR mainstem. Around March 2007, $\delta^{15}N$ in the SJR mainstem increased, while the $\delta^{15}N$ in the minor east-side tributaries either remained about the same (Westport and TID Lat 6&7), or decreased slightly (Harding). All three of these sites appear to have a human waste/manure nitrate isotope signature, and do not show clear evidence of either denitrification of nitrate assimilation. Harding Drain receives wastewater treatment plant discharges, while it is not well known if human waste infiltrates into Westport Drain. TID Lat 6&7 contains primarily agricultural discharge, although there are significant amounts of dairy and other animal husbandry in the area. In this case it will be necessary to use additional tracers in order to separate the influence of animal and human waste-derived nitrate.

$\delta^{15}N$ in the Merced and Tuolumne followed very similar temporal patterns, but the Merced River nitrate generally had higher $\delta^{15}N$ values than the Tuolumne River throughout each year. In both rivers, $\delta^{15}N$ was higher during the summer and lower during the winter and spring. High $\delta^{15}N$ values in both rivers corresponded to periods of increased nitrate concentrations. The shift in both concentration and isotope values suggests that the nitrate in the rivers during the winter is most likely contains more soil nitrate (characterized by lower $\delta^{15}N$), while agricultural and/or waste nitrate sources become more prominent in the late spring through fall. Nitrate isotopes in the Stanislaus River showed more variability than either of the other major east-side tributaries. $\delta^{15}N$ in the Stanislaus ranged from values typical for soil nitrate up to values consistent with waste sources, and unlike the Tuolumne and Merced Rivers, did not show a discernable seasonal pattern. Nitrate concentrations are very low in the Stanislaus, and therefore even small changes in nitrate inputs with distinct isotope signatures will be reflected in the nitrate isotope composition of the Stanislaus River water.

Nitrate isotope patterns in the west-side tributaries are quite different from those observed in the east-side tributaries, particularly with respect to $\delta^{18}O$. In three of the west-side tributaries,

Orestimba Creek, Del Puerto Creek, and Ingram Creek, the $\delta^{15}N$ and $\delta^{18}O$ appear to be decoupled. At each of these sites, large increases in $\delta^{18}O$ occur in conjunction with some of the increases in nitrate concentration, while the $\delta^{15}N$ doesn't change. These spikes in $\delta^{18}O$ are only observed in the west-side tributaries. The high $\delta^{18}O$ (coupled with level $\delta^{15}N$) suggests that this nitrate has formed through nitrification of ammonia or organic N compounds. This hypothesis is supported by the very high NBOD values associated with algal-derived POM at both Del Puerto and Orestimba (Figure 46).

Nitrate in Hospital Creek shows different patterns than those seen in the other west-side tributaries, although this data set spans a shorter length of time. In Hospital Creek, changes in $\delta^{15}N$ are coupled with similar changes in $\delta^{18}O$, suggesting that either mixing of different nitrate sources or nitrate uptake processes (denitrification and/or assimilation) are the controlling factors in Hospital Creek.

Phosphate

Since biological cycling can overprint the original $\delta^{18}O$ (sometimes referred to as $\delta^{18}O_p$) of DIP through equilibration with the $\delta^{18}O$ of the surrounding water, it is necessary to first determine whether or not the $\delta^{18}O_p$ in a given area has reached equilibrium with the local water. Almost none of the samples from the SJR and tributaries had reached isotopic equilibrium with the surrounding water (Figure 62), indicating that complete biological cycling (multiple breaking and reforming of the P-O bond) had not taken place, and that some degree of isotopic source signature remained. These results are promising for future studies, since it indicates that there are measurable differences between the sites, and that source signatures are not entirely overprinted by biological cycling.

Unlike nitrate isotopes, there is not enough published data available for us to determine whether or not a given $\delta^{18}O_p$ value is indicative of a specific type of phosphate source. Our current studies suggest that the phosphate isotope signature of various sources such as waste water treatment plant effluent, fertilizers, and natural sources may vary depending upon geographical region, and therefore source signatures most likely must be determined for each individual area.

Sources of Water and Salt to the SJR

Water sources. Water isotopes from samples collected in the SJR mainstem and the major and minor tributaries did not fall along the national meteoric water line ($\delta^2H = 7.95\ \delta^{18}O + 6.03$; from Yurtsever and Gat, 1981). This is expected, since global, national, and local meteoric water lines are developed from precipitation data, while water in rivers, drains and tributaries can mix from many different areas and can also undergo evaporation. The slopes for all SJR mainstem and tributary sites were between 3.7 and 5.6; these values are low but not abnormal for warm and/or arid regions (Tables F1 and F2). There was considerable scatter away from the local meteoric water line for most sites, and it appears that evaporation often played a major role in setting the isotopic composition of the water.

A comparison of water isotopes between the sites (Figures F1-F4) shows that the upstream SJR sites have a larger isotopic range than the downstream sites, and the upstream sites often have higher isotopic values. The major east-side tributaries drain Sierran water, which has

significantly lower $\delta^{18}O$ and $\delta^{2}H$ than the other tributaries during most of the year. Increased precipitation at high latitudes results in rainfall with lower $\delta^{18}O$ and $\delta^{2}H$ compared to lower latitudes in the same geographical area. The sites draining the upstream wetlands area had $\delta^{18}O$ and $\delta^{2}H$ values that were noticeably higher than the SJR mainstem and other tributary sites. Also, the $\delta^{18}O$ and $\delta^{2}H$ of west-side tributaries were generally higher than the east-side major and minor tributaries. All of the west-side tributaries and drains discharge from relatively low elevation watersheds, which will result in higher $\delta^{18}O$ and $\delta^{2}H$. Furthermore, evaporation during the long residence times, particularly during periods of little to no precipitation, will result in the upstream wetland sites having even higher $\delta^{18}O$ and $\delta^{2}H$ than the other west-side sites.

The r^2 values for all of the sampling sites are lower than those typically found for local meteoric water lines based on precipitation samples (Tables F1-F2). This is not surprising for river and tributary samples, particularly in an arid area, since evaporation can move the isotopic composition of a sample away from the local meteoric water line. The exact isotopic change from evaporation depends upon the relative humidity, and therefore will be different depending upon the location of each site, season, and local weather conditions. Agricultural return flow may also introduce isotopically distinct evaporated water into tributaries and the SJR mainstem, and the form of return flow (i.e., open surface drainage vs underground tile return flow) will also affect the final isotopic composition of the water.

Sulfate sources. Although measurement of sulfate and chloride concentrations was not part of the original nutrient-oriented suite of measurements authorized by stakeholders and included in Task 4, samples were archived by two investigators who figured that these normal water quality measurements would later be wanted. Sure enough, halfway through the study, some of the modelers commented that they wished they had more conservative tracer data to use in their models. At this point, Dahlgren began analyzing his archived samples for sulfate and chloride concentrations. And our Isotope Tracers group, once the sulfate measurements were available, began selecting archived water samples to analyze for sulfate $\delta^{34}S$ and $\delta^{18}O$ to investigate whether these data might be useful for identifying sources of water, salt, and processes in the system. A detailed interpretation of the small set of data is beyond the scope of this report but will be included in the PIN700 report.

Conclusions

Based upon the $\delta^{13}C$ and $\delta^{15}N$ of POM, the C:N ratio of the POM, and algal pigment concentrations in the river water, the POM in the mainstem SJR throughout 2005 and 2007 was primarily of algal origin. The $\delta^{13}C$, $\delta^{15}N$, C:N, and algal pigment concentration of most samples from upstream wetlands sites are consistent with a young algal origin of most of the POM. For much of the year, the compositions of POM at mainstem sites could be explained by large inputs of wetlands-derived POM; however, the loads in wetlands waters are not high enough to explain the POM loads at mainstem sites. The $\delta^{13}C$, $\delta^{15}N$, and C:N ratio of POM in the mainstem SJR sites suggest that the source of the POM is a combination of in-situ algal growth, inputs of algal material from upstream wetlands sources, and smaller inputs of mixed algal and terrestrial material from the east-side tributaries.

The major east-side tributaries generally had lower δ^{13}C-POM and δ^{15}N-POM, higher C:N ratios, and lower algal pigment concentrations than the mainstem SJR sites. This suggests that although these tributaries account for the majority of water in the downstream SJR, they do not exert major controls over the composition of the POM in the SJR. The POM in the east-side tributaries is usually dominated by terrestrial C3 plant material as indicated by the higher δ^{13}C-POM values and the higher C:N ratios, especially during high flow periods.

Preliminary efforts to combine the information gained by δ^{15}N, δ^{13}C, and C:N of POM with BOD, algal pigments, and POM concentration have demonstrated that this approach should be pursued further. The combination of C:N and POM concentration may provide a cheaper estimate for BOD than algal pigments. It appears likely that this multi-tracer approach will result in identifying diagnostic signatures of POM from different sites that would permit testing time and site specific hypotheses about sources of organic matter in the SJR.

Nitrate in the mainstem of the San Joaquin River has an isotopic composition that suggests animal or human waste as the primary source of nitrate. Three of the minor east-side tributaries (Harding Drain, Westport Drain, and TID Lat 6/7) all have consistently high δ^{15}N-NO_3 values that also fall in the expected range of human and/or animal waste. In contrast, the isotopic composition of nitrate in two of the major east-side tributaries, the Tuolumne and the Merced Rivers, shows a seasonally variable composition consistent with soil-derived nitrate during the winter and of human and/or animal waste during the late spring through early fall. The Stanislaus River has low nitrate concentrations and highly variable nitrate isotope compositions, although the δ^{15}N-NO_3 in the Stanislaus River is usually lower than that of the mainstem SJR.

Nitrate isotopes also provide information about the dominant nitrate cycling processes occurring in the San Joaquin River and tributaries. There is no isotopic evidence of significant denitrification taking place within the mainstem of the San Joaquin River, and the nitrate isotope composition of nitrate in the mainstem appears to be controlled by mixing of multiple nitrate sources. Temporal nitrate isotope patterns in both the San Luis Drain and Mud Slough indicate either active denitrification or nitrate assimilation, probably mainly the latter. The nitrate isotope patterns observed in Salt Slough are distinct from the patterns seen in Mud Slough and San Luis Drain. The decoupling of δ^{15}N-NO_3 and δ^{18}O-NO_3 and large increases in δ^{18}O-NO_3 observed in Salt Slough and in several of the west-side tributaries, provides evidence that nitrification (conversion of ammonia or organic N compounds to nitrate), not mixing of sources, is the main process controlling the nitrate isotopic composition at these sites.

During periods of high flow, the nitrate isotope signature of nitrate in the SJR mainstem appears to be primarily controlled by mixing with nitrate sources with elevated δ^{15}N-NO_3 including the Merced River, and dilution from mixing with low nitrate concentration water from the Tuolumne and Stanislaus Rivers, which also tend to have lower δ^{15}N-NO_3 signatures. However, during periods of low flow, particularly in the summer and fall of 2007, the nitrate in the SJR mainstem showed increasing δ^{15}N-NO_3 downstream, yet none of the measured water sources could account for this trend. Relationships between nitrate concentration and nitrate isotope composition did not point to a single dominant biological process as the source for this high δ^{15}N nitrate. The most likely explanation for the increases in δ^{15}N downstream is unmeasured water inputs such as groundwater or agricultural return flows during low flow periods. Nitrate isotope patterns suggest that mixing of multiple nitrate sources is the primary control on nitrate isotopic composition in the downstream SJR, while biological processes, particularly nitrification of

organic N may play a much larger role in the upstream sites and some of the upstream wetland drainages.

Differences between sites were also observed in the water isotopic compositions. Upstream and west-side tributaries generally had higher $\delta^{18}O$ and $\delta^{2}H$, probably due to a combination of lower altitude precipitation and evaporation, particularly in upstream areas with high water residence times. Water in the three major east-side tributaries which drain from higher elevations had distinctly lower isotopic values. During high flow periods, large inputs of water with low $\delta^{18}O$ and $\delta^{2}H$ values from the major west-side tributaries were observed, creating a pattern of decreasing $\delta^{18}O$ and $\delta^{2}H$ downstream in the SJR. The distinct differences between the water from the major tributaries, wetlands, and minor west-side tributaries indicate that these data can be used for water mass balance budgets.

Our hypothesis that isotope data would prove useful for resolving the relative importance of different BOD fractions in various areas of the SJR to the loads transported to Channel Point has been clearly demonstrated by the wealth of interpretable temporal and spatial patterns in isotopic composition shown for samples from different sites and dates during this 2.7 year study. We hope that the brief discussions of the results and data, and the rich variety of interesting figures, makes the simple point that the isotope variation is signal, not noise, and provides considerable insight into sources of organic matter, nutrients, salt, and water that could not have been gained with standard chemical and hydrological measurements. Hence, the isotope data (1) provide enhanced identification and quantification of specific sources of biomass and nutrients to the SJR, which will be useful for improving river modeling efforts, and (2) are useful complements to traditional measurements like BOD.

In a sense, the mainstem sites are the recipients of frequent, system-wide, natural tracer tests, in that the natural perturbations in isotopic composition at upstream sites provide strong, sometimes unambiguous signals that can be traced from the source to the river, and used in mass balance models. One of the most effective uses of these isotope data will be for use in testing hypotheses developed with other datasets. The isotopic "fingerprints" of different sources of nitrate and organic matter provides considerable information about the substances, and models developed with other data must be able to account for the isotopic compositions.

Recommendations for Future Action

Given the wealth of data available from this study, there are a number of approaches for characterizing site-specific differences in the source of nitrate, and the source and quality of the POM and DOM that should be explored. We were very pleased at the success of our first simple scheme for classifying POM, success being defined as finding that the different geographic groupings of sites often showed different – and meaningful -- mixtures of POM. In the future, we will test a range of other schemes for characterizing spatial and temporal changes in POM, DOM, and nitrate source and quality, including ranking methods (e.g., Stringfellow, 2008) and PCA.

Our preliminary set of sulfur isotope analyses suggests that $\delta^{34}S$ might be a useful adjunct to the study of organic matter transport through the system. In the entire estuary system, there is a

35‰ range in $\delta^{34}S$, from about -15‰ for organic matter derived from the anoxic wetlands to +20‰ in the fully marine parts of the Bay. Hence, the $\delta^{34}S$ of POM and DOM might be the best isotope tracer of organics along the river-estuary continuum. Sulfate $\delta^{34}S$ and $\delta^{18}O$ also show promise in that they show several locations where different sources of sulfate are entering the river part of the system.

A large portion of the DOC at mainstem sites, and some tributary sites, appears to be algal in origin. Improved characterization of this DOM might allow a better evaluation of the contribution of this DOM to BOD in the DWSC and to food webs in the Delta and Bay. Hence, analysis of the DOM for $\delta^{15}N$, $\delta^{13}C$, and ^{14}C is likely to provide useful information.

An important next step is to try to incorporate the isotope data into mass balance models. For example, water isotopes are the ideal conservative tracers of water sources and, along with chloride and sulfate budgets, have a high likelihood for producing useful insights into fine-scale temporal and spatial resolution of the contributions from different sources of water, including groundwater and undocumented inputs, to the SJR. Nitrate and sulfate isotopes can help with salt load estimates, in part by providing additional geochemical constraints on the models. While the isotopic compositions of POM, nitrate, sulfate, and DOC are sometimes not sufficiently conservative to be considered "simple" conservative tracers (like water isotopes and chloride), these tracers do provide a great deal of information about various kinds of non-conservative processes in the stream, and, with a little care, the non-conservative changes in compositions can be factored out and the tracers used for mass balance calculations. POM isotopes provide unique information about sources of organic matter, and for algal productivity, detailed information about sources of DIN and DIC to the water column but also biogeochemical processes that are affecting nutrient cycling.

Many of these objectives are beyond the scope of this report. However, the Task 7 isotope study is a part of the larger-scope PIN700 project, and we still have a few more months to interpret these data before the final PIN700 report is due. Hence, we will be able to take advantage of the final conclusions of the Up-stream DO TMDL project in our interpretation of the PIN700 data, and integrate these combined findings into the ongoing CALFED PIN700 Study "Determination of Sources of Organic Matter and Nutrients in the San Joaquin River" in order to assess long-term changes related to BOD sources and sinks in the SJR.

References

Battaglin, W.A., Kendall, C., Chang, C.C.Y., Silva, S.R., and Campbell, D.H. (2001) Chemical and isotopic evidence of nitrogen transformation in the Mississippi River, 1997-98, Hydrological Processes 15,1285-1300.

Blake, R.E., O'Neil, J.R., and Garcia, G.A. (1997) Oxygen isotope systematics of biologically mediated reactions of phosphate: I. Microbial degradation of organophosphorus compounds. Geochimica et Cosmochimica Acta 61, 4411-4422.

Casciotti, K.L., Sigman, D.M., Galanter Hastings, M., Bohlke, J.K., and Hilkert, A. (2002)

Measurement of the oxygen isotopic composition of nitrate in seawater and freshwater using the denitrifier method. Analytical Chemistry 74, 4905-4912.

Craig, H. (1961) Isotopic variations in meteoric waters. Science 133, 1702-1703.

Delong, M.D., and Thorp, J.H. (2006) Significance of instream autotrophs in trophic dynamics of the Upper Mississippi River. Oecologia 147, 76-85.

Esptein, S. and Mayeda, T. (1953) Variation of O^{18} content of waters from natural sources. Geochim. Cosmochim. Acta 4, 213-224.

Finlay, J.C., and Kendall, C. (2007) Stable isotope tracing of temporal and spatial variability in organic matter sources to freshwater ecosystems, Chapter 10, In: R.H. Michener and K. Lajtha (Eds.), **Stable Isotopes in Ecology and Environmental Science**, 2nd edition, Blackwell Publishing, p. 283-333.

Fry, B, Silva, S., Kendall, C., and Anderson, R.K. (2002) Oxygen isotope corrections for online $\delta^{34}S$ analysis. Rapid Communication in Mass Spectrometry 16, 854-858.

Hinton M.J., Schiff S.L., and English M.C. (1998) Sources and flowpaths of dissolved organic carbon in two forested watersheds of the Precambrian Shield. Biogeochemistry 41, 175-197.

Karl, D. M., and Tien, G. (1992), MAGIC: A sensitive and precise method for measuring dissolved phosphorus in aquatic environments. Limnology and Oceanography *37*, 105-116.

Kendall, C. (1998) Tracing nitrogen sources and cycling in catchments. In Kendall, C. and McDonnell J.J., eds., **Isotope Tracers in Catchment Hydrology**, Elsevier Science, p. 519-576.

Kendall, C. and Coplen, T.B. (2001) Distribution of oxygen-18 and deuterium in river waters across the United States: Hydrological Processes 15, 1363-1393.

Kendall, C., Silva, S.R., and Kelly, V.K. (2001) Carbon and nitrogen isotopic compositions of particulate organic matter in four large river systems across the United States. Hydrological Processes 15, 1301-1346.

Kendall, C., Elliott, E.M., and Wankel, S.D. (2007) Tracing anthropogenic inputs of nitrogen to ecosystems, Chapter 12, In: R.H. Michener and K. Lajtha (Eds.), **Stable Isotopes in Ecology and Environmental Science**, 2nd edition, Blackwell Publishing, p. 375-449.

Krabbenhoft, D.P., Bowser, C.J., Kendall, C., and Gat, J.R. (1994) Use of oxygen-18 and deuterium to assess the hydrology of ground-water/lake systems, in: Baker, L.A. (ed.) **Environmental Chemistry of Lakes and Reservoirs**, American Chemical Society, Monograph #237, p. 67-90.

Kratzer, C.R., Dileanis, P.D., Zamora, C., Silva, S.R., Kendall, C., Bergamaschi, B.A., and Dahlgren, R.A. (2004) Sources and transport of nutrients, organic carbon and chlorophyll-a in the San Joaquin River upstream of Vernalis, California during Summer and Fall, 2000 and 2001. U.S. Geological Survey, Water-Resources Investigation Report 03-4127, 113pp.

Lis, G., Wassenaar, L.I., and Hendry, M.J. (2008) High precision laser spectroscopy D/H and

18O/16O measurements of microliter natural water samples. Analytical Chemistry 80, 287-293 10.1021/ac701716q S0003-2700(70)01716-X.

Longinelli, A. and Nuti, S. (1973) Revised phosphate-water isotopic temperature scale. Earth and Planetary Science Letters 19, 373-376.

McLaughlin, K., Silva, S., Kendall, C., Stuart-Williams, H., Paytan, A. (2004) A precise method for the analysis of d18O of dissolved inorganic phosphate in seawater. Limnology and Oceanography Methods 2, 202-212.

McLaughlin, K., Kendall, C., Silva, S., Young, M., Paytan, A. (2006a) Phosphate oxygen isotope ratios as a tracer for sources of phosphate in North San Francisco Bay, California. Journal of Geophysical Research 11, G03003.

McLaughlin, K., Chavez, F., Pennington, T., Paytan, A. (2006b) A time series investigation of the oxygen isotopic composition of dissolved inorganic phosphate in Monterey Bay, California. Limnology and Oceanography 51, 2370-2379.

Ohte N., Dahlgren R. A., Silva S. R., Kendall C., Kratzer C. R. and Doctor, D. H. (2007) Sources and transport of algae and nutrients in a Californian river in a semi-arid climate. Freshwater Biology 52, 2476-2493, doi:10.1111/j.1365-2427.2007.01849.x.

Schiff S.L., Aravena R., Trumbore S.E., and Dillon P.J. (1990) Dissolved organic carbon cycling in forested watersheds: A carbon isotope approach. Water Resources Research. 26, 2949-2957.

Shanley, J.B., Mayer, B., Mitchell, M.J., Michel, R.L., Bailey, S.W., and Kendall, C. (2005) Tracing sources of streamwater sulfate during snowmelt using S and O isotope ratios of sulfate and 35S activity. Biogeochemistry 76, 161–185.

Sigman, D.M., Casciotti, K.L., Andreani, M., Barford, C. Galanter, M., and Bohlke, J.K. (2001) A bacterial method for the nitrogen isotopic analysis of nitrate in seawater and freshwater. Analytical Chemistry 73, 4145-4153.

Silva, S., Kendall, C., Wankel, S., Bemis, B., Kratzer, C., Bergamasch,i B., and Fram, M. (2003) Isotopic study of the sources and cycling of nitrate and algae associated with low dissolved oxygen concentrations in the San Joaquin River, California. EOS Trans. AGU, 84(46), Fall Meet. Suppl., Abstract H52C-01.

St. Jean G. (2003) Automated quantitative and isotopic (^{13}C) analysis of dissolved inorganic carbon and dissolved organic carbon in continuous-flow using a total organic carbon analyzer. Rapid Communications in Mass Spectrometry 17(5), 419-428.

Stringfellow, W.T. (2008) Ranking tributaries for setting remediation priorities in a TMDL context. Chemosphere 71, 1895-1908.

Vannote, R.L., Minshall, G.W., Cummins, K.W., Sedell, J.R. et al. (1980) The river continuum concept. Canadian Journal of Fisheries and Aquatic Sciences, 37, 130-137.

Volkmar, Emily C., and Dahlgren, Randy A. (2006) Biological oxygen demand dynamics in the Lower San Joaquin River**,** California**,** Environmental Science and Technology 40, 5653-5660.

Wang Y., Huntington T.G., Osher L.J., Wassenaar L.I., Trumbore S.E., Amundson R.G., Harden

J.G., McKnight D.M., Schiff S.L., Aiken G.R., Lyons W.B., Aravena R. O., and Baron J.S. (1998) Carbon cycling in terrestrial environments. In *Isotope Tracers in Catchment Hydrology* (eds. C. Kendall and J.J. McDonnell), pp. 577-610. Elsevier Science Publishers.

Wissel, B., and Fry, B. (2005) Sources of particulate matter in the Mississippi River, USA. Large Rivers 15 (1-4), Arch. Hydrobiol. Suppl. 155/1-4, 105-118.

Yurtsever, Y and Gat, J.R. (1981). Chapter 6, Atmospheric Waters. In: J.R. Gat and R. Gonfiantini (eds) **Stable Isotope Hydrology, Deuterium and oxygen-18 in the Water Cycle**. IAEA Technical Report Series No. 210, Vienna.

Tables

Table 1. Summary of sites used in figures and site abbreviations for box plots.

Site Number	Site ID	Site Name (short)	Box Plot Abbreviation
4	DO-04	SJR at Mossdale	MS
5	DO-05	SJR at Vernalis	VN
6	DO-06	SJR at Maze	MZ
59	DO-59	SJR at Laird Park	LP
7	DO-07	SJR at Patterson	PT
8	DO-08	SJR at Crows Landing	CL
10	DO-10	SJR at Lander Avenue	LR
12	DO-12	Stanislaus River at Caswell Park	STAN
14	DO-14	Tuolumne River at Shiloh Bridge	TUOL
16	DO-16	Merced River at River Road	MER
18	DO-18	Mud Slough near Gustine	MUD
19	DO-19	Salt Slough at Lander Avenue	SALT
20	DO-20	Los Banos Creek Flow Station	LB
21	DO-21	Orestimba Creek at River Road	ORT
22	DO-22	Modesto ID Lateral 4 to SJR	
23	DO-23	Modesto ID Lateral 5	
24	DO-24	Modesto ID Lateral 6	
25	DO-25	Modesto ID Main Drain Miller Lake	
28	DO-28	Turlock ID Westport Drain	WST
29	DO-29	Turlock ID Harding Drain	HRD
30	DO-30	Turlock ID Lateral 6&7 at Levee	TID 6/7
31	DO-31	BCID- New Jerusalem Drain	
33	DO-33	Hospital Creek	HOS
34	DO-34	Ingram Creek	ING
36	DO-36	Del Puerto Creek Flow Station	DEL
44	DO-44	San Luis Drain End	SLD
57	DO-57	Ramona Lake Drain	

Table 2. Summary statistics for samples from the main stem SJR sites, March 2005 to December 2007.

Site		$\delta^{13}C$-POM	$\delta^{15}N$-POM	C:N-POM	$\delta^{13}C$-DOC	$\delta^{15}N$-NO_3	$\delta^{18}O$-NO_3	$\delta^{18}O$-H_2O	$\delta^{2}H$-H_2O	$\delta^{34}S$-SO_4	$\delta^{18}O$-SO_4
All Mainstem SJR	**n**	**418**	**418**	**418**	**110**	**390**	**390**	**409**	**420**	**61**	**53**
	mean	-28.3	7.4	7.8	-26.7	10.8	5.2	-10.2	-77.2	-4.6	4.7
	stdev	1.5	2.0	1.4	1.2	2.2	2.9	1.6	8.1	3.5	2.5
	min	-35.9	-0.3	4.2	-33.8	2.0	-1.1	-13.6	-99.3	-10.6	-1.3
	max	-21.2	13.2	14.7	-24.4	17.0	18.4	-2.0	-34.7	4.4	9.5
DO-4 Mossdale	**n**	**65**	**65**	**65**	**16**	**62**	**62**	**63**	**65**	**3**	**3**
	mean	-27.7	7.2	7.8	-26.6	11.3	4.1	-10.7	-79.6	-3.7	5.4
	stdev	1.0	2.2	1.4	0.9	2.5	2.4	1.2	5.4	0.5	1.7
	min	-30.0	-0.3	4.2	-27.8	6.7	-0.9	-12.5	-91.8	-4.2	3.6
	max	-25.3	13.2	11.8	-24.8	16.9	10.9	-5.4	-62.0	-3.3	7.1
DO-5 Vernalis	**n**	**67**	**67**	**67**	**18**	**66**	**66**	**65**	**67**	**3**	**3**
	mean	-27.9	7.2	8.2	-26.6	10.7	4.2	-10.9	-80.3	-4.8	6.4
	stdev	0.9	1.7	1.4	1.0	1.9	1.8	0.9	4.7	1.1	2.7
	min	-29.9	4.1	6.1	-28.3	5.5	-0.6	-12.6	-90.2	-5.6	4.2
	max	-25.5	12.1	14.0	-24.5	14.7	9.3	-6.4	-66.6	-3.5	9.5
DO-6 Maze	**n**	**65**	**65**	**65**	**16**	**65**	**65**	**64**	**66**	**3**	**3**
	mean	-28.1	7.4	7.9	-26.5	10.8	4.6	-10.4	-78.3	-4.7	4.9
	stdev	1.2	2.0	1.4	1.4	1.9	1.8	1.5	7.0	1.0	0.4
	min	-30.9	3.4	5.3	-29.8	4.5	0.6	-12.5	-91.8	-5.8	4.6
	max	-24.6	12.9	13.2	-24.4	16.1	9.7	-2.5	-52.9	-3.8	5.3
DO-7 Patterson	**n**	**68**	**68**	**68**	**15**	**65**	**65**	**66**	**68**	**15**	**15**
	mean	-28.3	7.6	8.0	-26.4	11.4	4.7	-10.2	-77.0	-6.5	4.9
	stdev	1.0	1.9	1.7	0.6	1.6	1.9	1.5	6.9	0.9	2.1
	min	-30.0	4.3	4.5	-27.5	7.0	-0.6	-13.0	-96.9	-8.6	1.1
	max	-25.0	12.2	14.7	-24.8	16.5	11.9	-5.1	-59.6	-5.0	9.4
DO-8 Crows L	**n**	**64**	**64**	**64**	**17**	**60**	**60**	**63**	**65**	**15**	**15**

Site		$\delta^{13}C$-POM	$\delta^{15}N$-POM	C:N-POM	$\delta^{13}C$-DOC	$\delta^{15}N$-NO_3	$\delta^{18}O$-NO_3	$\delta^{18}O$-H_2O	$\delta^{2}H$-H_2O	$\delta^{34}S$-SO_4	$\delta^{18}O$-SO_4
	mean	-28.4	7.2	7.7	-26.8	11.3	5.4	-10.1	-77.1	-6.6	5.1
	stdev	1.0	1.9	1.1	1.1	1.8	2.1	1.6	7.6	0.9	2.7
	min	-30.7	3.0	5.8	-29.1	4.6	-1.1	-13.1	-96.7	-8.4	0.6
	max	-25.5	11.7	11.7	-24.4	13.8	13.8	-2.0	-49.5	-5.1	9.2
DO-10 Lander	**n**	**67**	**67**	**67**	**15**	**50**	**50**	**66**	**67**	**12**	**12**
	mean	-29.5	7.7	7.3	-27.7	9.0	9.2	-9.0	-70.5	1.8	3.0
	stdev	2.4	2.1	1.0	2.1	2.9	4.4	2.1	12.0	2.1	2.6
	min	-35.9	3.7	4.4	-33.8	2.0	-0.3	-13.6	-99.3	-3.2	-1.3
	max	-21.2	12.9	10.0	-25.7	17.0	18.4	-3.8	-47.3	4.4	7.7
DO-59 Laird P	**n**	**22**	**22**	**22**	**13**	**22**	**22**	**22**	**22**	**10**	**2**
	mean	-27.7	6.9	8.1	-26.5	11.2	4.6	-10.9	-79.6	-6.7	6.6
	stdev	1.2	1.7	1.5	0.9	1.5	1.4	0.6	3.9	1.4	2.7
	min	-29.9	3.4	6.0	-27.7	6.9	1.8	-12.1	-86.8	-10.6	4.7
	max	-24.4	9.4	12.7	-25.1	13.2	7.1	-9.8	-70.3	-5.8	8.6

Table 3. Summary statistics for samples from selected tributary and drain sites, March 2005 to December 2007

.

Site		$\delta^{13}C$-POM	$\delta^{15}N$-POM	C:N-POM	$\delta^{13}C$-DOC	$\delta^{15}N$-NO_3	$\delta^{18}O$-NO_3	$\delta^{18}O$-H_2O	$\delta^{2}H$-H_2O	$\delta^{34}S$-SO_4	$\delta^{18}O$-SO_4
DO-12 Stanislaus	**n**	**67**	**66**	**67**	**19**	**37**	**37**	**65**	**66**	**0**	**0**
	mean	-26.6	5.7	10.0	-26.3	8.0	1.5	-11.2	-81.6		
	stdev	1.1	1.7	1.9	1.5	3.1	3.2	0.9	5.0		
	min	-29.8	-0.3	6.7	-29.7	1.8	-6.0	-12.4	-86.7		
	max	-23.8	8.9	15.9	-23.4	14.8	7.6	-7.4	-63.1		
DO-14 Tuolumne	**n**	**68**	**68**	**68**	**19**	**62**	**62**	**66**	**68**	**0**	**0**
	mean	-26.4	6.5	10.1	-26.0	9.1	3.0	-11.5	-83.2		
	stdev	1.1	2.0	2.8	0.7	2.8	1.7	0.8	7.6		
	min	-29.4	1.2	5.6	-26.9	2.2	-1.8	-12.6	-91.7		
	max	-23.8	12.0	24.0	-24.9	12.5	8.6	-8.9	-44.6		
DO-16 Merced	**n**	**67**	**67**	**67**	**17**	**57**	**56**	**64**	**67**	**0**	**0**
	mean	-26.4	5.9	10.2	-26.4	11.3	4.1	-11.7	-86.3		
	stdev	0.8	1.8	2.5	1.1	2.6	1.5	1.0	5.5		
	min	-28.6	1.5	5.8	-29.2	2.5	-1.1	-13.0	-93.6		
	max	-24.2	10.9	23.8	-24.6	14.9	7.7	-6.1	-61.2		
DO-18 Mud Sl.	**n**	**63**	**62**	**63**	**2**	**60**	**60**	**63**	**65**	**14**	**14**
	mean	-27.5	8.1	7.7	-25.9	11.0	7.9	-7.4	-62.9	-8.7	3.7
	stdev	1.6	2.3	1.0	0.6	2.0	2.0	1.3	7.9	1.2	2.3
	min	-33.1	4.6	6.0	-26.4	5.2	1.8	-11.8	-82.0	-10.7	-2.4
	max	-23.0	16.0	12.3	-25.5	15.6	12.2	-4.8	-46.1	-7.0	6.9
DO-19 Salt Sl.	**n**	**68**	**68**	**68**	**12**	**56**	**56**	**67**	**69**	**15**	**15**
	mean	-27.7	6.5	8.4	-27.4	8.5	4.8	-8.9	-70.7	-4.6	5.4
	stdev	0.8	2.0	1.2	1.0	1.9	3.4	1.2	6.9	0.5	1.9
	min	-29.4	3.8	6.1	-28.8	4.9	-4.6	-11.6	-88.0	-5.1	0.9
	max	-25.4	14.2	12.8	-26.0	15.1	12.2	-4.5	-53.6	-3.1	8.1

Site		$\delta^{13}C$-POM	$\delta^{15}N$-POM	C:N-POM	$\delta^{13}C$-DOC	$\delta^{15}N$-NO_3	$\delta^{18}O$-NO_3	$\delta^{18}O$-H_2O	$\delta^{2}H$-H_2O	$\delta^{34}S$-SO_4	$\delta^{18}O$-SO_4
DO-20 Los Banos	**n**	**57**	**57**	**57**	**8**	**41**	**41**	**55**	**56**	**14**	**14**
	mean	-27.7	8.6	7.8	-27.1	12.7	4.2	-7.9	-64.9	-2.8	5.4
	stdev	1.4	2.7	1.2	2.7	3.2	4.4	1.6	9.1	2.0	2.0
	min	-30.6	4.4	5.5	-31.4	5.6	-11.1	-11.1	-91.0	-7.4	2.2
	max	-24.7	14.9	13.3	-24.2	20.8	14.6	-3.1	-43.5	0.2	8.9
DO-21 Orestimba	**n**	**58**	**58**	**58**	**15**	**58**	**58**	**56**	**59**	**0**	**0**
	mean	-26.4	5.4	8.8	-26.5	6.6	3.7	-9.1	-69.0		
	stdev	0.8	1.4	1.3	1.3	1.7	3.4	1.4	7.5		
	min	-29.2	2.3	6.0	-29.3	2.7	-1.1	-12.4	-91.1		
	max	-24.4	9.9	12.0	-24.6	10.4	17.3	-4.2	-48.0		
DO-23 MID Lat 5	**n**	**28**	**28**	**28**	**15**	**18**	**17**	**28**	**28**	**0**	**0**
	mean	-22.4	4.3	8.3	-25.2	7.1	1.9	-11.2	-82.7		
	stdev	1.5	1.4	1.9	1.6	2.5	3.1	0.8	6.2		
	min	-25.2	0.1	5.6	-27.6	2.7	-0.8	-12.3	-91.2		
	max	-19.8	6.3	15.9	-22.4	12.5	11.5	-8.2	-61.7		
DO-25 Miller L	**n**	**34**	**34**	**34**	**6**	**33**	**33**	**33**	**35**	**0**	**0**
	mean	-28.6	7.8	7.8	-26.6	9.9	1.6	-10.2	-77.7		
	stdev	2.7	2.1	1.5	0.5	3.5	4.2	1.2	5.8		
	min	-34.4	3.7	5.8	-27.5	2.1	-12.5	-12.7	-91.3		
	max	-21.8	12.5	12.8	-26.1	20.8	5.1	-6.5	-60.0		
DO-28 Westport	**n**	**49**	**48**	**48**	**12**	**48**	**48**	**50**	**50**	**0**	**0**
	mean	-26.2	5.8	9.0	-25.0	11.2	3.9	-10.8	-80.8		
	stdev	1.6	1.9	1.7	1.1	1.8	1.4	0.7	4.2		
	min	-32.3	-0.5	5.2	-27.2	8.0	0.2	-11.8	-86.3		
	max	-21.9	8.9	14.0	-23.5	14.7	7.2	-8.7	-62.3		
DO-29 Harding D	**n**	**64**	**64**	**64**	**14**	**63**	**63**	**63**	**65**	**0**	**0**
	mean	-24.8	5.8	8.6	-25.3	11.9	3.3	-10.7	-79.9		
	stdev	0.8	1.1	1.0	1.8	1.5	1.6	0.7	5.2		

Site		$\delta^{13}C$-POM	$\delta^{15}N$-POM	C:N-POM	$\delta^{13}C$-DOC	$\delta^{15}N$-NO_3	$\delta^{18}O$-NO_3	$\delta^{18}O$-H_2O	$\delta^{2}H$-H_2O	$\delta^{34}S$-SO_4	$\delta^{18}O$-SO_4
	min	-26.7	2.4	6.8	-30.2	9.3	-1.2	-12.1	-92.6		
	max	-22.7	9.7	11.1	-23.4	15.9	6.7	-8.8	-59.4		
DO-30 TID 6/7	**n**	**35**	**35**	**35**	**1**	**35**	**35**	**35**	**35**	**0**	**0**
	mean	-25.3	5.4	8.8	-26.2	12.9	4.2	-10.8	-80.9		
	stdev	1.0	1.1	1.6		1.3	1.3	0.7	3.5		
	min	-27.6	3.1	6.2		10.7	2.3	-11.8	-85.6		
	max	-22.6	7.9	13.8		18.5	7.5	-8.7	-71.8		
DO-33 Hospital C	**n**	**15**	**15**	**15**	**4**	**15**	**15**	**15**	**15**	**0**	**0**
	mean	-25.3	5.6	7.4	-26.1	10.0	2.0	-10.8	-79.3		
	stdev	1.4	1.3	1.4	0.5	2.8	3.5	0.8	4.2		
	min	-26.9	4.1	5.3	-26.7	6.0	-4.0	-12.5	-88.4		
	max	-21.3	7.9	9.7	-25.5	15.6	10.0	-9.6	-75.5		
DO-34 Ingram	**n**	**43**	**43**	**43**	**4**	**44**	**44**	**43**	**44**	**0**	**0**
	mean	-26.4	5.5	8.4	-27.2	5.4	4.4	-9.6	-72.8		
	stdev	1.0	1.7	1.1	1.8	1.8	5.0	1.3	6.8		
	min	-28.5	2.8	5.6	-29.5	2.7	-2.1	-12.1	-88.0		
	max	-23.7	10.7	11.3	-25.7	11.6	17.3	-6.7	-48.9		
DO-36 Del Puerto	**n**	**57**	**57**	**57**	**16**	**55**	**55**	**57**	**58**	**0**	**0**
	mean	-26.0	5.7	8.5	-27.2	7.2	4.7	-9.4	-71.9		
	stdev	1.1	1.7	1.5	1.6	2.5	3.6	1.5	7.6		
	min	-29.1	2.9	5.8	-31.4	3.2	-0.1	-11.6	-85.7		
	max	-23.7	13.6	14.4	-25.5	13.4	14.9	-4.8	-51.3		
DO-44 SLD	**n**	**56**	**56**	**56**	**3**	**56**	**56**	**57**	**59**	**12**	**12**
	mean	-28.9	9.1	7.4	-25.9	11.3	8.4	-7.6	-62.9	-9.6	2.3
	stdev	2.8	2.3	0.9	1.9	1.9	2.0	0.9	4.3	2.7	1.6
	min	-34.6	2.4	5.3	-27.7	6.2	2.9	-10.9	-82.0	-11.5	-1.8
	max	-22.8	14.1	9.3	-24.0	15.9	14.4	-5.9	-55.4	-1.4	4.7
DO-57 Ramona L	**n**	**22**	**22**	**22**	**0**	**20**	**20**	**21**	**22**	**0**	**0**

Site		$\delta^{13}C$-POM	$\delta^{15}N$-POM	C:N-POM	$\delta^{13}C$-DOC	$\delta^{15}N$-NO_3	$\delta^{18}O$-NO_3	$\delta^{18}O$-H_2O	$\delta^{2}H$-H_2O	$\delta^{34}S$-SO_4	$\delta^{18}O$-SO_4
	mean	-28.6	8.0	6.8		9.2	5.6	-9.1	-70.2		
	stdev	2.8	3.5	0.7		1.7	1.6	1.7	10.6		
	min	-33.9	2.5	5.7		6.1	3.4	-12.6	-93.2		
	max	-21.7	14.6	8.1		13.3	9.8	-5.2	-48.4		

Figure 1. The five main sources of organic matter to stream ecosystems. "Bacteria" = both benthic and planktonic heterotrophs", and "algae" = benthic and planktonic algae and cyanobacteria. From Finlay and Kendall (2007).

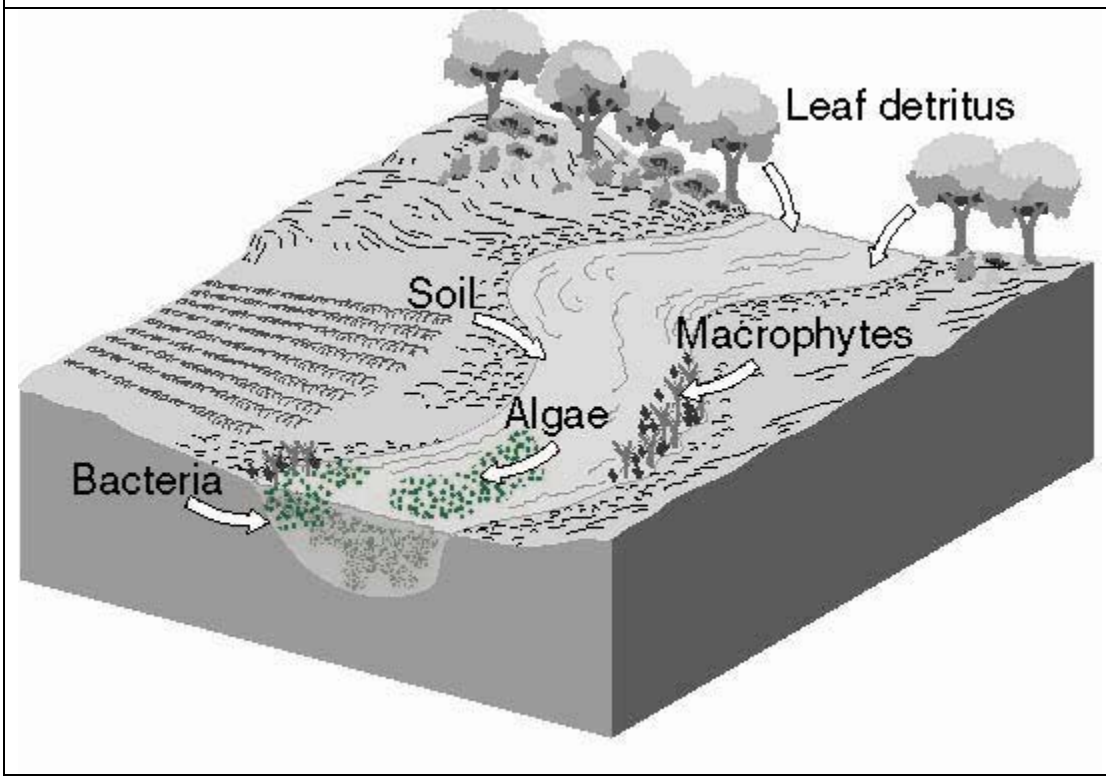

Figure 2. Typical ranges in $\delta^{15}N$, $\delta^{13}C$, and C:N (atomic) values of different particulate organic matter sources to rivers, based on a literature survey. From Finlay and Kendall (2007).

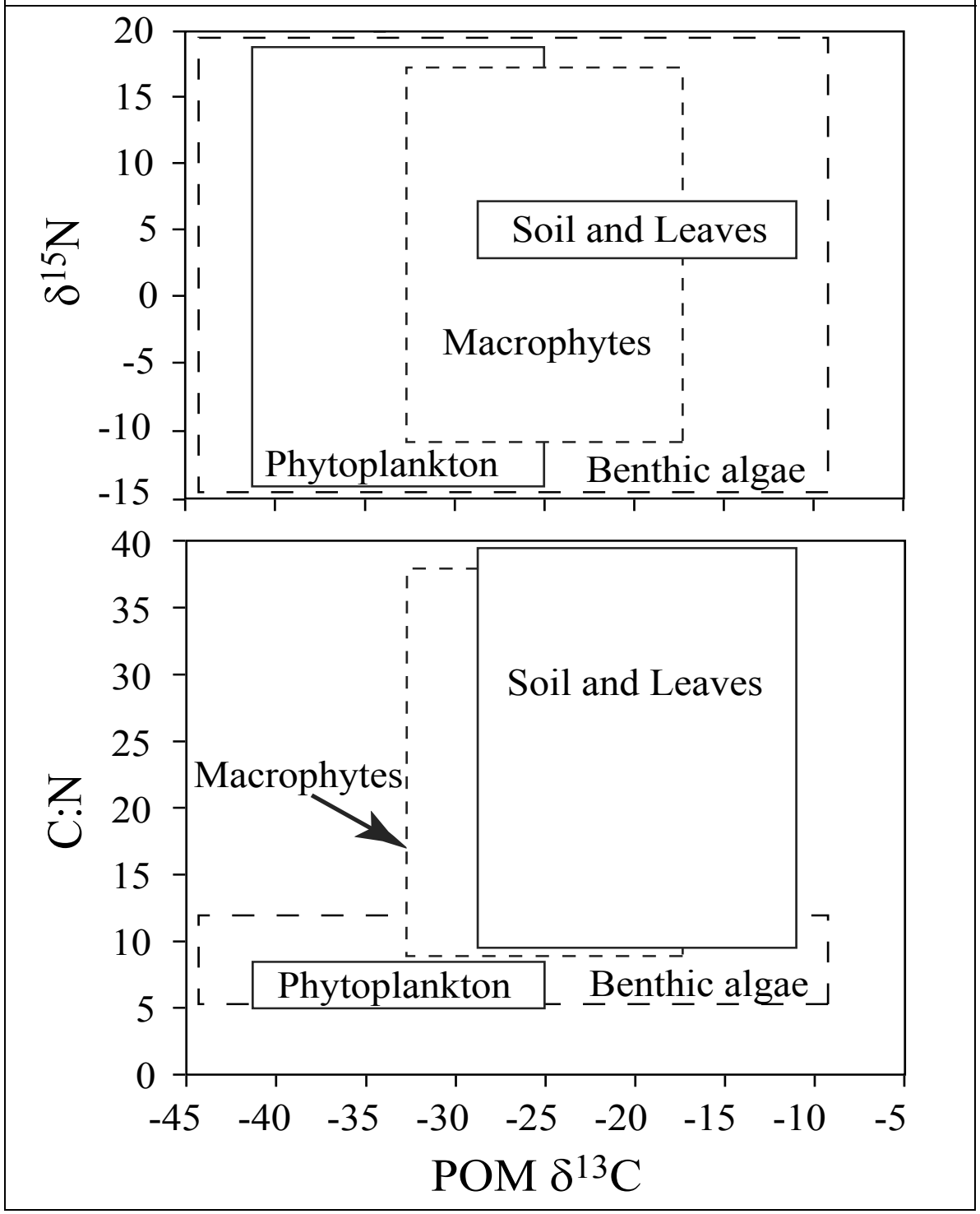

Figure 3. Typical compositions of different POM (seston) sources to the US rivers. Note that the ranges for different organic matter sources are usually much less than shown in Figure 2. From Finlay and Kendall (2007).

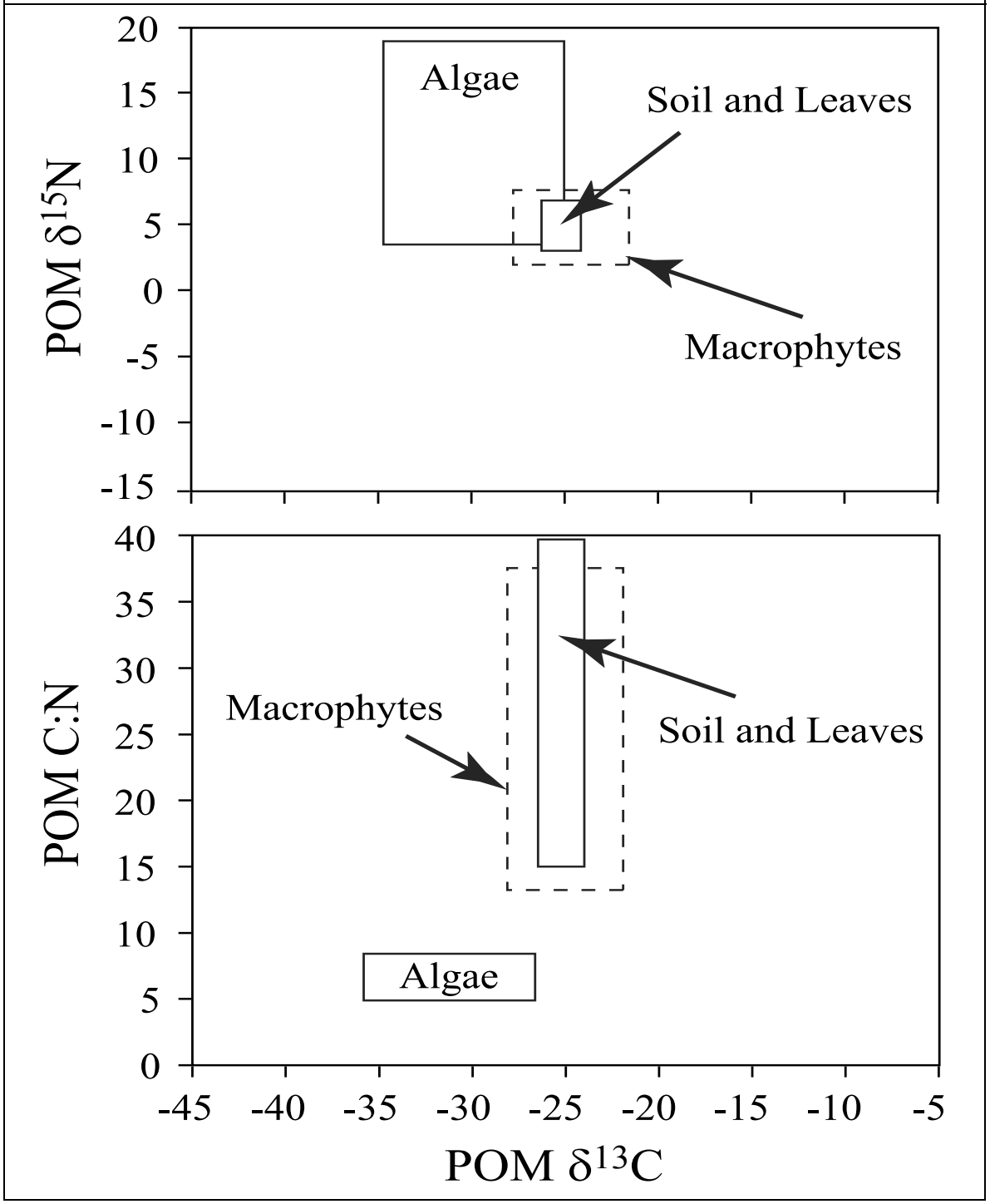

Figure 4. Conceptual model showing the main biogeochemical processes that control the $\delta^{13}C$ of DIC and the $\delta^{15}N$ of nitrate, and consequently the $\delta^{13}C$ and $\delta^{15}N$ of aquatic plants and POM. The arrows indicate the usual effect of an increased amount of the specified process on the $\delta^{13}C_{DIC}$ and/or $\delta^{15}N_{NO3}$, the $\delta^{13}C$ and/or $\delta^{15}N$ of the aquatic plants growing in the ecosystem, and ultimately the food webs based on these plants.

For example, increased amounts of NO_3^- formed by nitrification of NH_4^+ probably causes decreases in $\delta^{15}N$ of nitrate (but usually minimal affect on $\delta^{13}C$-DIC), and assimilation causes significant increases in both $\delta^{13}C$-DIC and $\delta^{15}N$-NO3. The approximate $\delta^{13}C$ and $\delta^{15}N$ values of important C and N sources are also shown (e.g., C3 plants and nitrate from manure, respectively). From Finlay and Kendall (2007).

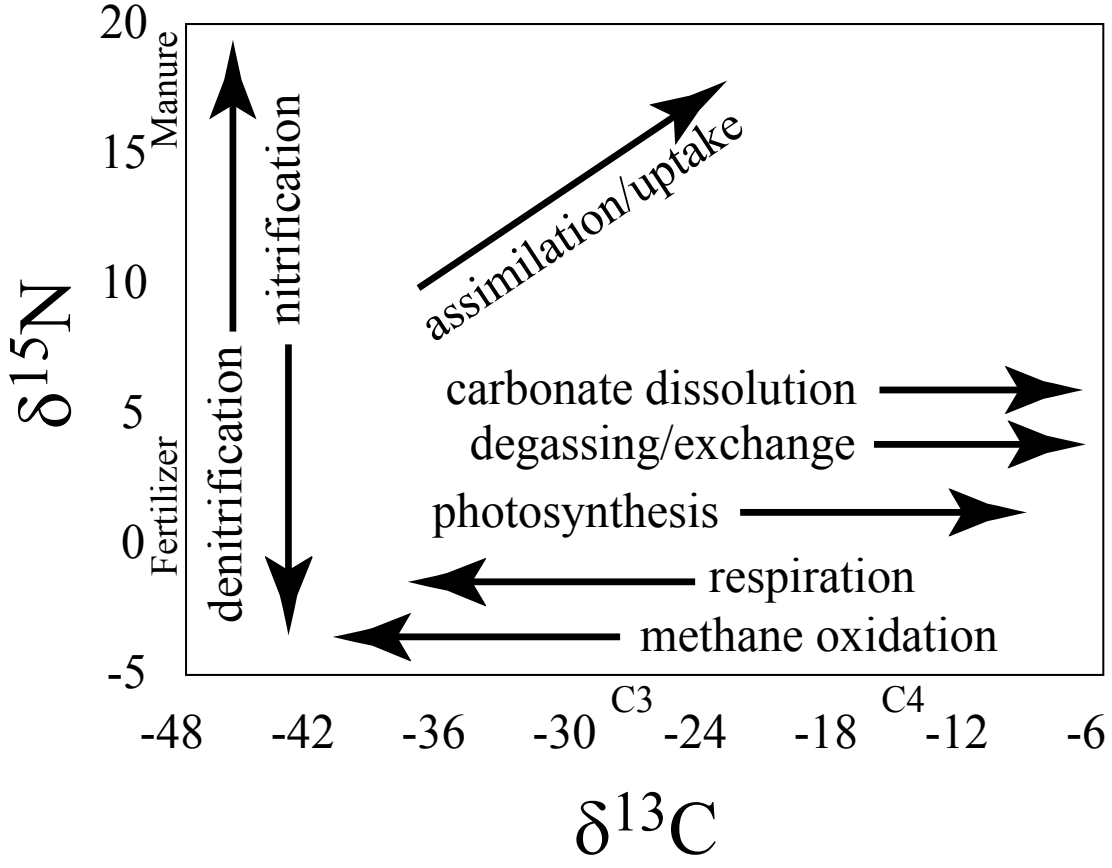

Figure 5. Typical $\delta^{15}N$ and $\delta^{18}O$ values of NO_3 derived from various sources and/or processes. The two arrows show the relationships that are typical for nitrate derived from these processes- if a set of samples follows either a 2:1 or 1:1 $\delta^{15}N$ vs $\delta^{18}O$ slope, this strongly suggests that one of these processes is controlling the nitrate isotope values.

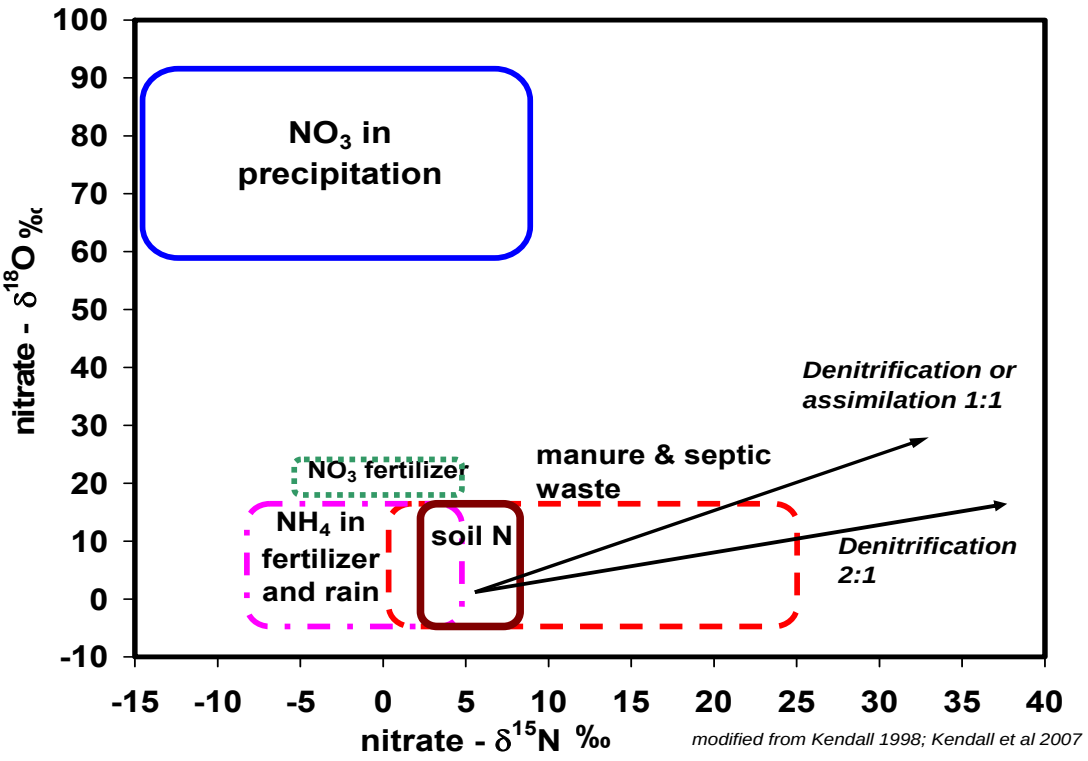

Figure 6. Schematic showing the $\delta^{18}O$ and $\delta^{2}H$ of precipitation and evaporated waters.

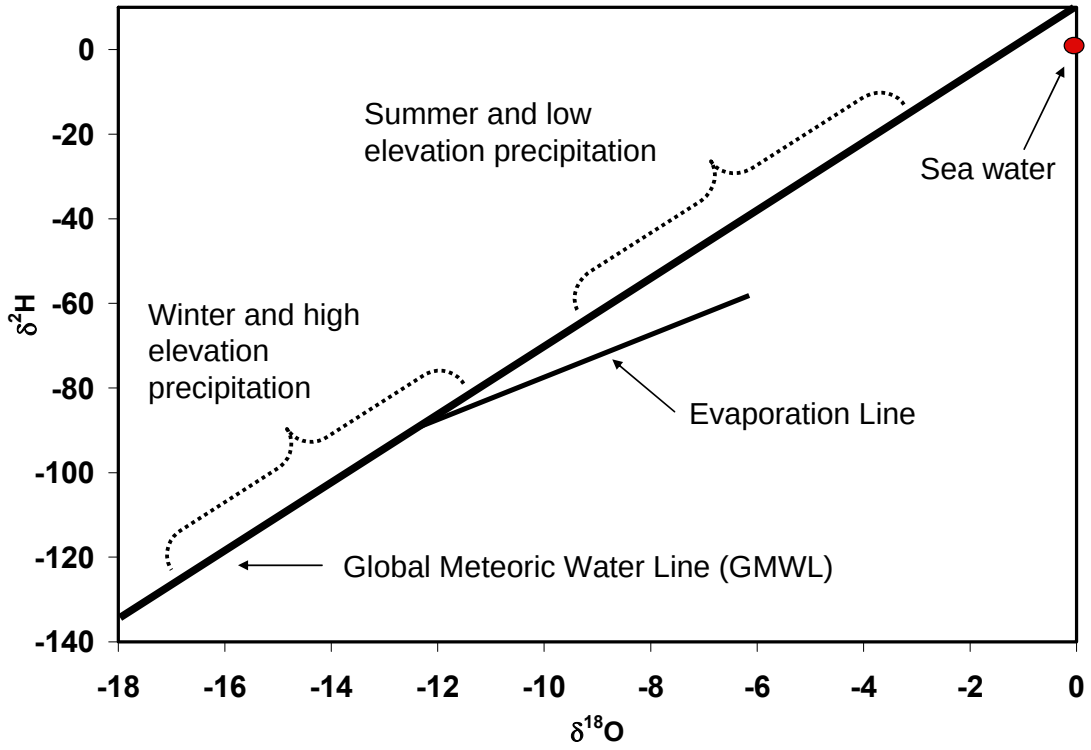

Figure 7. Typical $\delta^{34}S$ and $\delta^{18}O$ SO_4 values for various potential sulfate sources. The values shown are for unaltered dissolved SO_4 from each source. Biological sulfate cycling processes such as sulfate reduction will alter the isotopic composition of the sulfate.

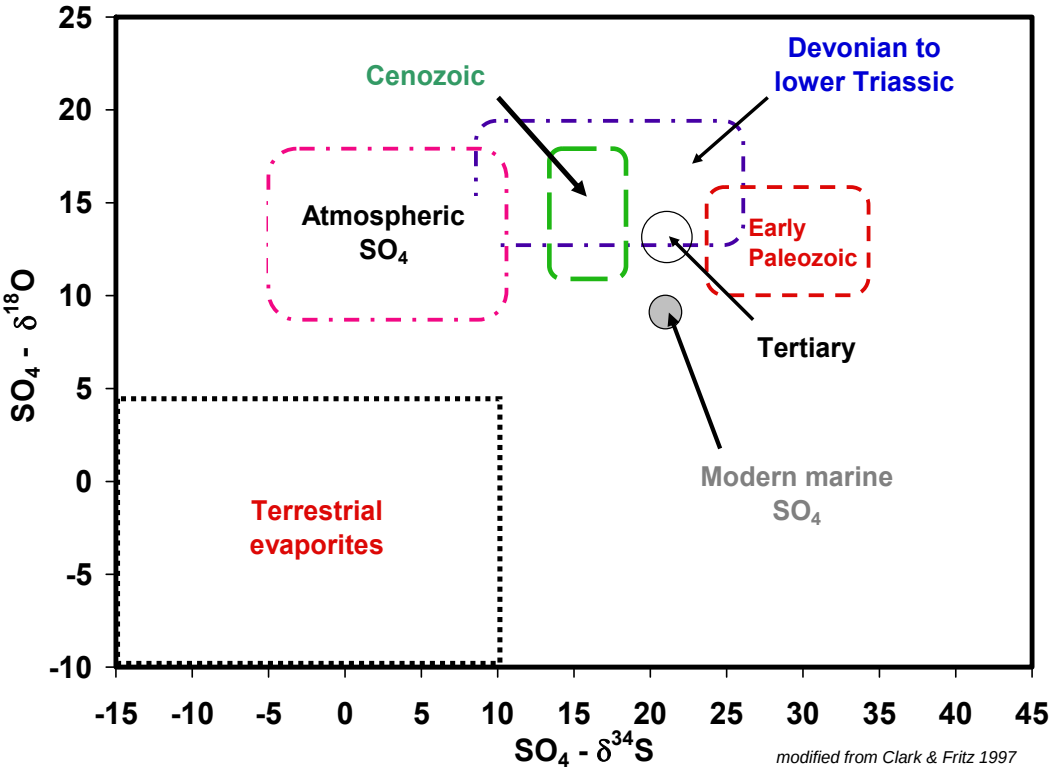

Figure 8. Distribution of POM $\delta^{13}C$ values for San Joaquin River mainstem sites (top) and major tributaries and drains (bottom) from March 2005 through December 2007. The median (line), 25th and 75th percentile (box), 10th and 90th percentile (whisker), and outlier points (circles) are shown.

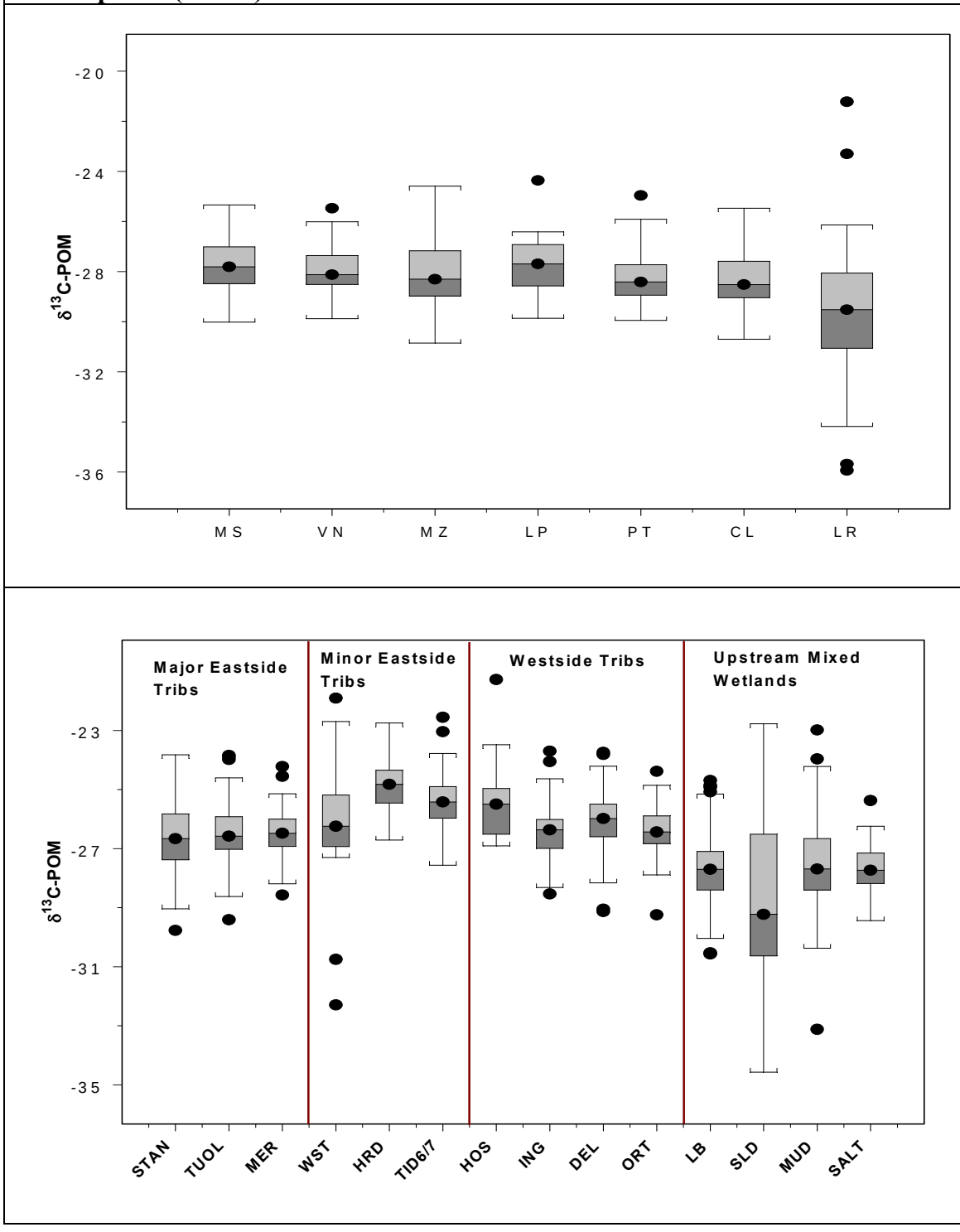

Figure 9. Distribution of POM $\delta^{15}N$ values for San Joaquin River mainstem sites (top) and major tributaries and drains (bottom) from March 2005 through December 2007.

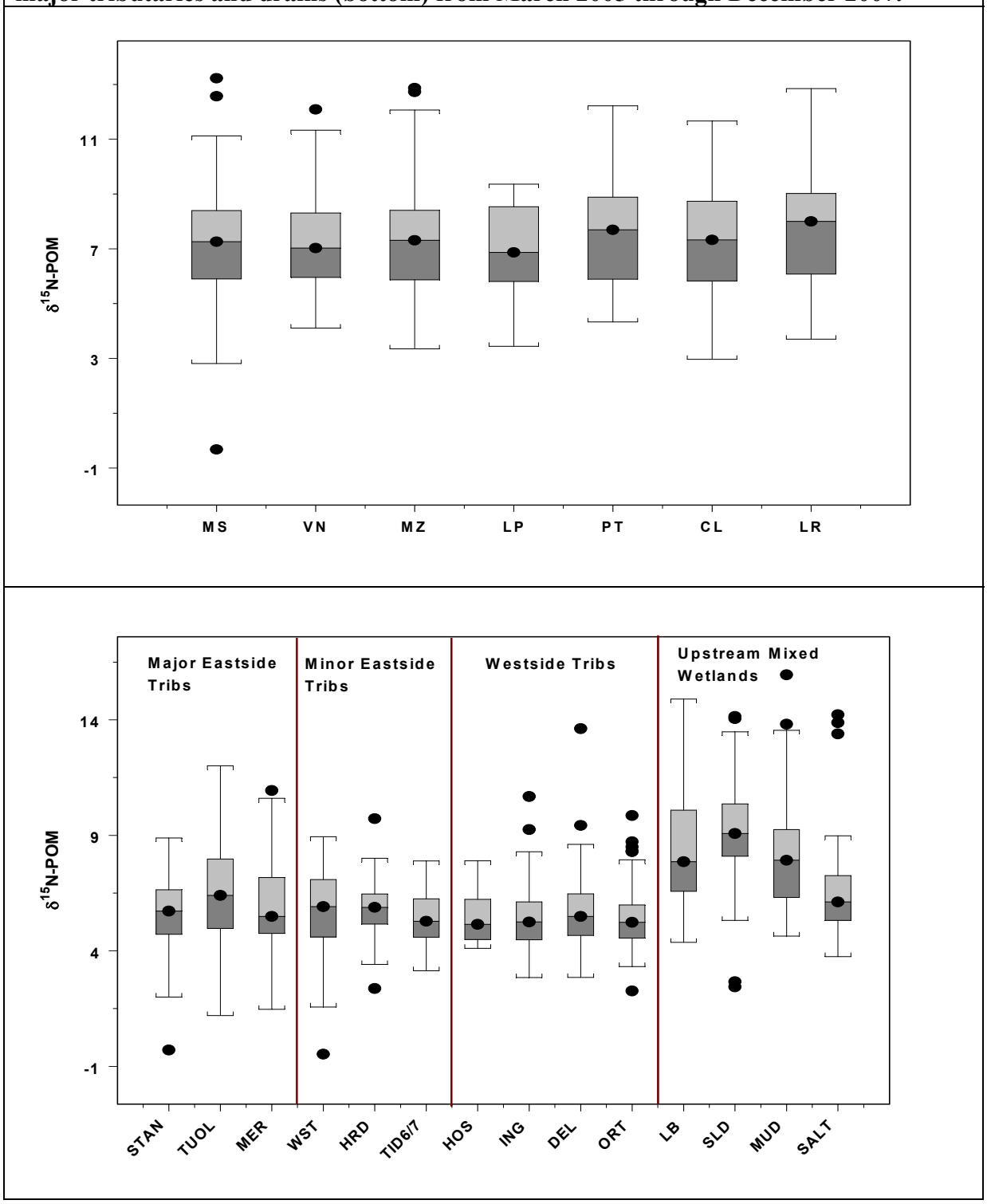

Figure 10. Distribution of POM C:N atomic ratios for San Joaquin River mainstem sites (top) and major tributaries and drains (bottom) from March 2005 through December 2007.

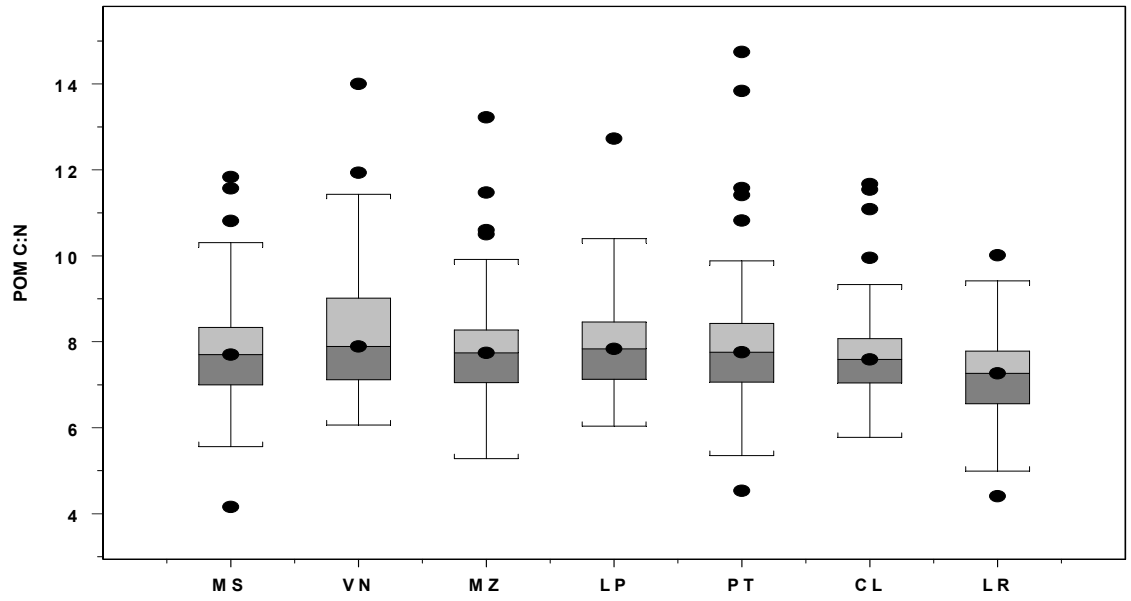

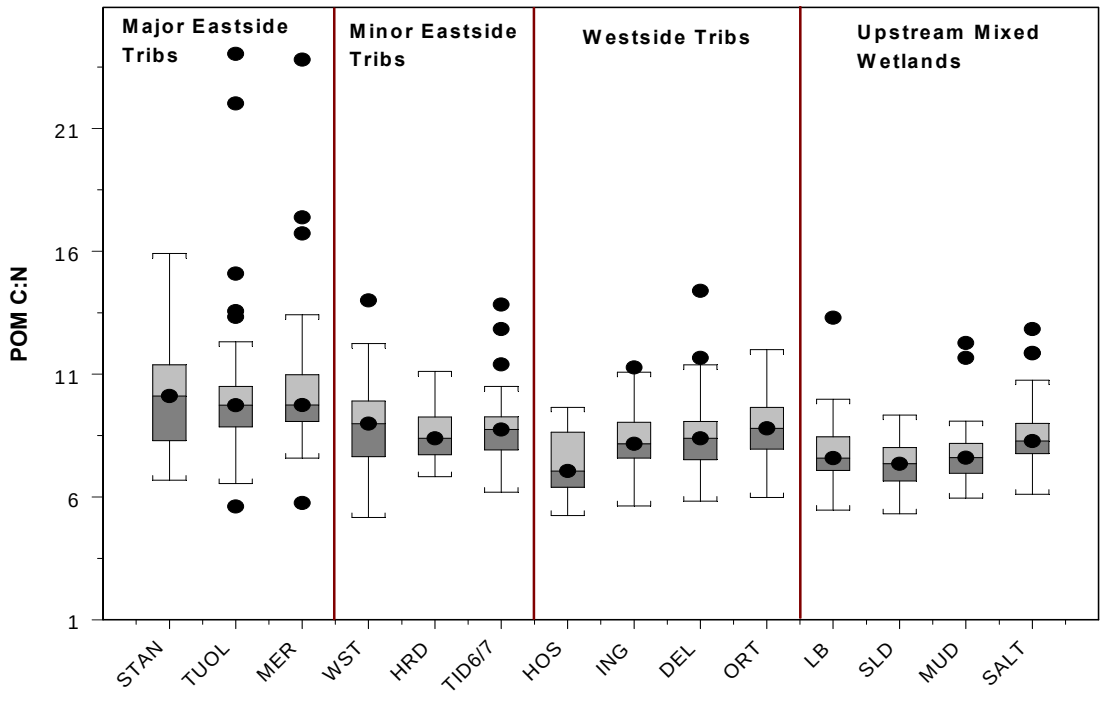

Figure 11. Distribution of $\delta^{15}N$ vs $\delta^{13}C$ (top) and C:N vs $\delta^{13}C$ (bottom) values of POM from mainstem SJR and major tributary sites, with the expected ranges of values for major sources of POM.

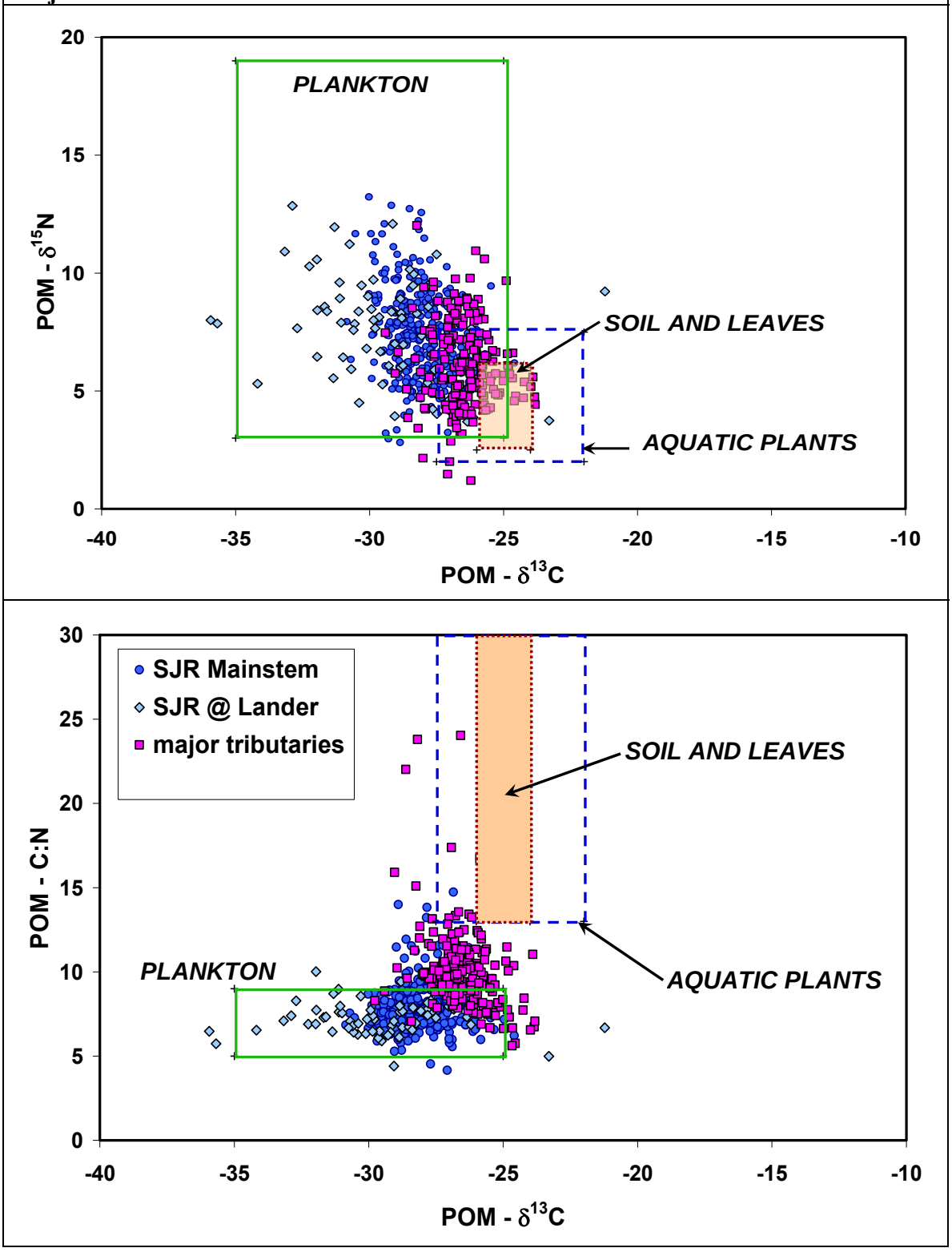

Figure 12. Distribution of $\delta^{15}N$ vs $\delta^{13}C$ (top) and C:N vs $\delta^{13}C$ (bottom) values of POM from mainstem SJR, minor tributaries, and upstream wetlands sites, with the expected ranges of values for major sources of POM.

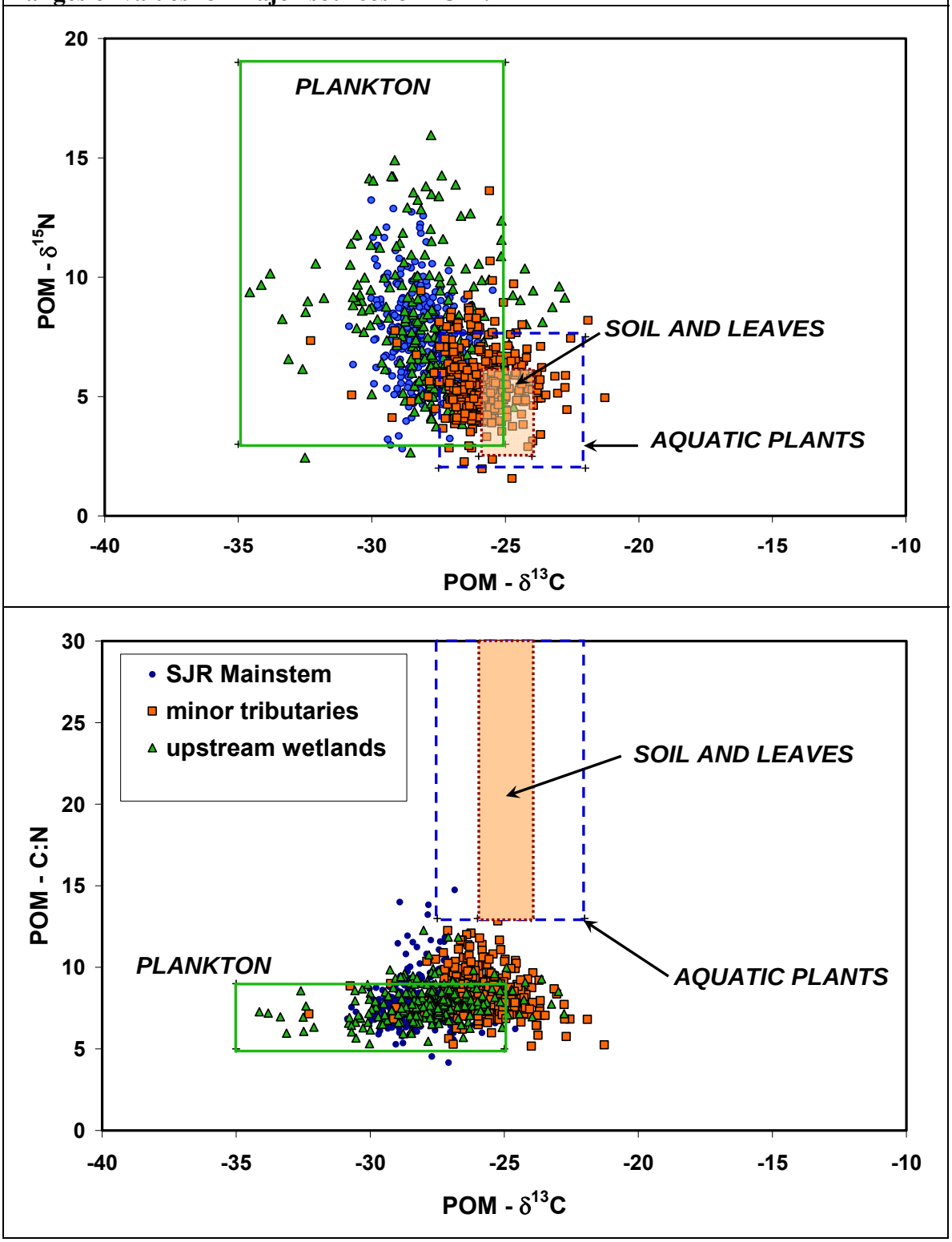

Figure 13. Distribution of DOC $\delta^{13}C$ values for San Joaquin River mainstem sites (top) and major tributaries and drains (bottom) from March 2005 through December 2006.

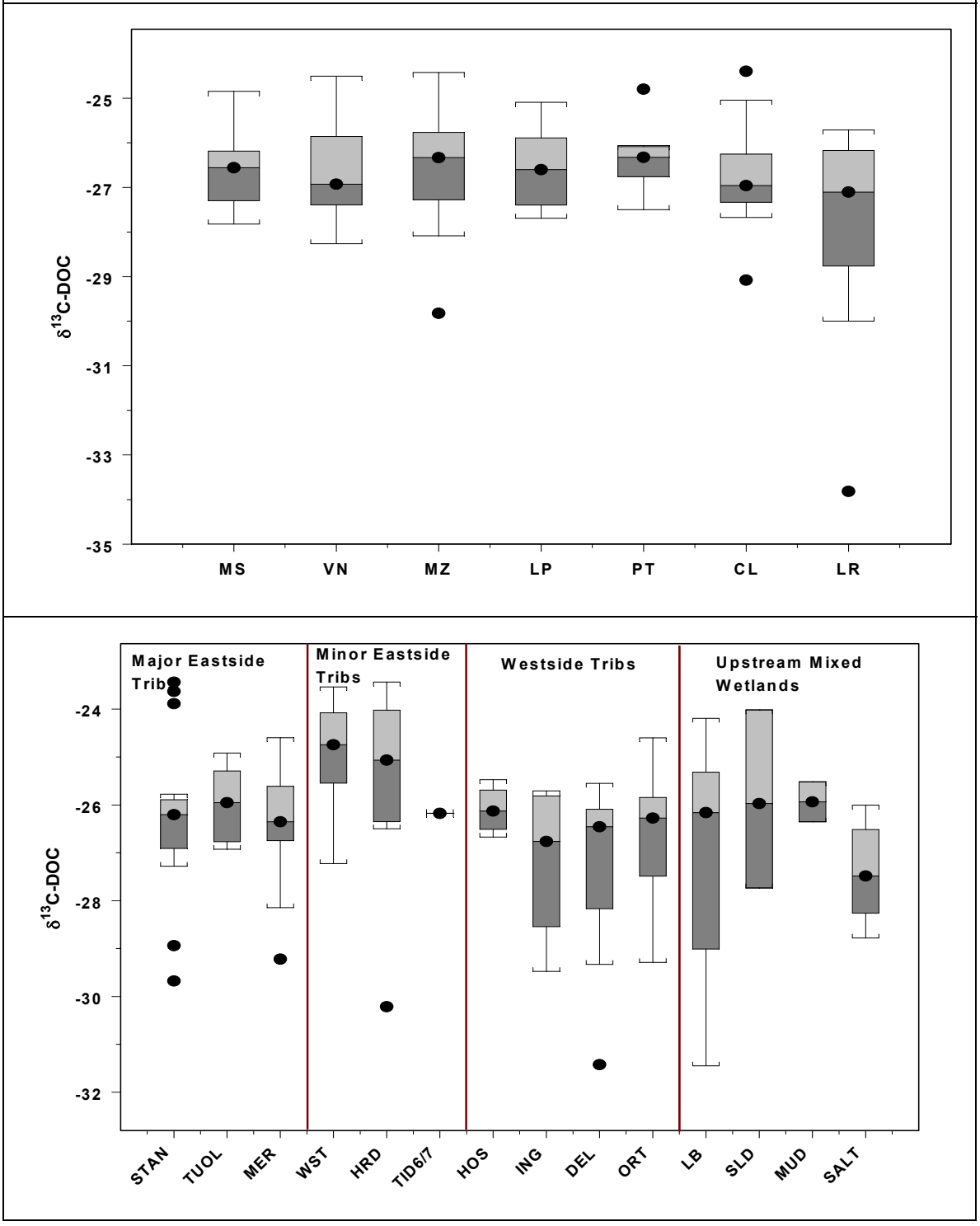

Figure 14. Comparison of $\delta^{13}C$ values of DOC and POM for all samples collected 2005-2006. A diagonal 1:1 line is provided for reference.

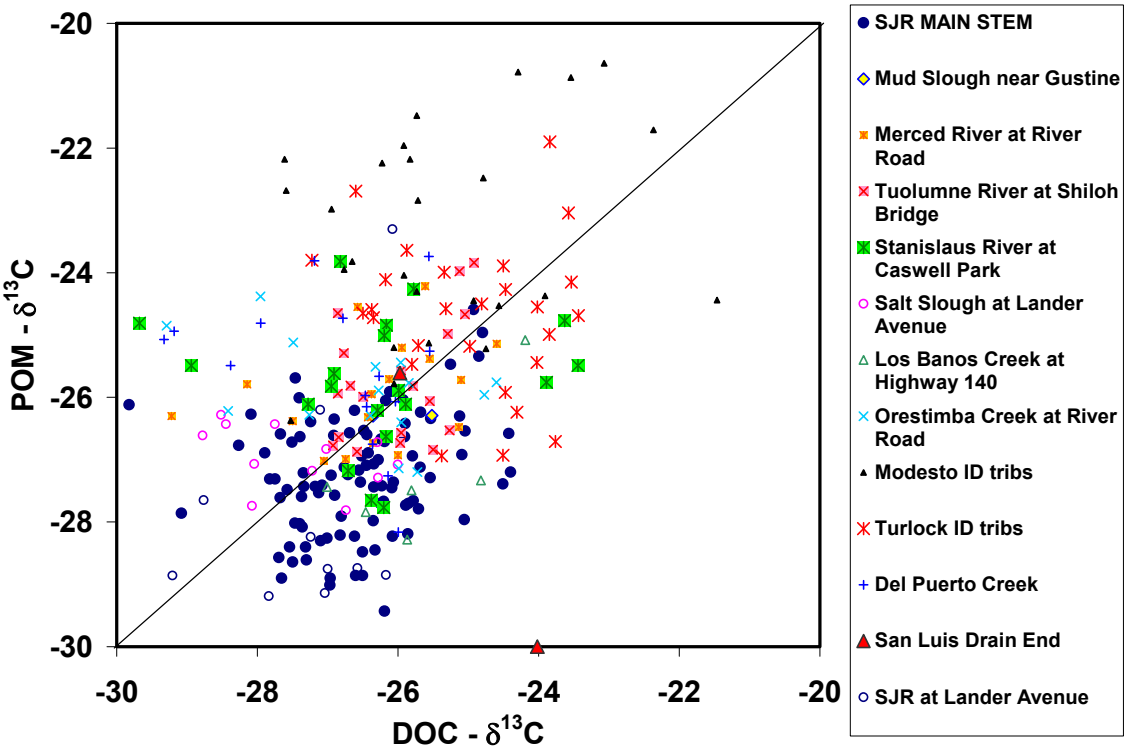

Figure 15. Correlation of DOC-$\delta^{13}C$ with DOC concentration (top) and algal pigments concentration (bottom) for different site types.

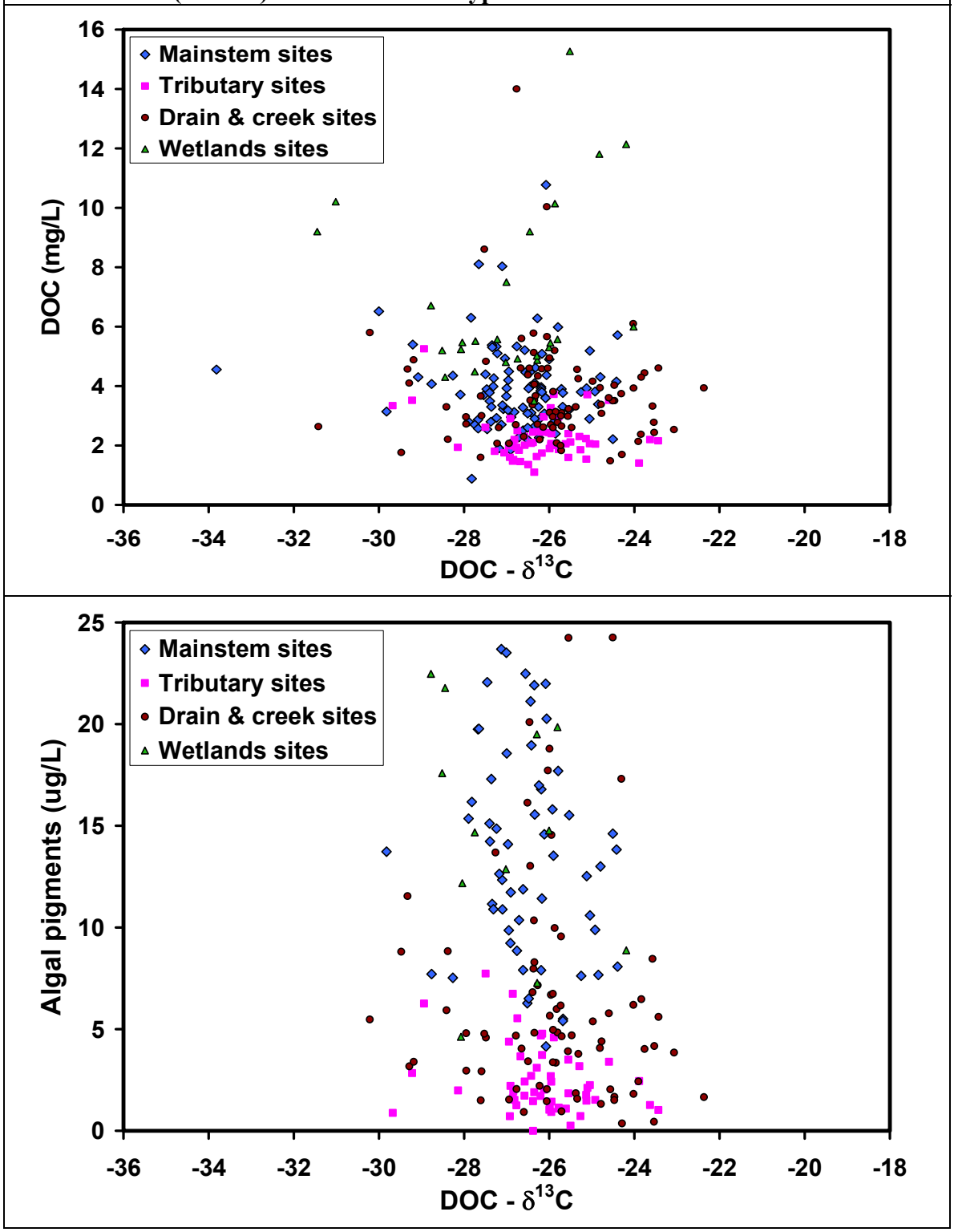

Figure 16. Nitrate $\delta^{15}N$ and $\delta^{18}O$ values for all core sampling sites from March 2005 to December 2007.

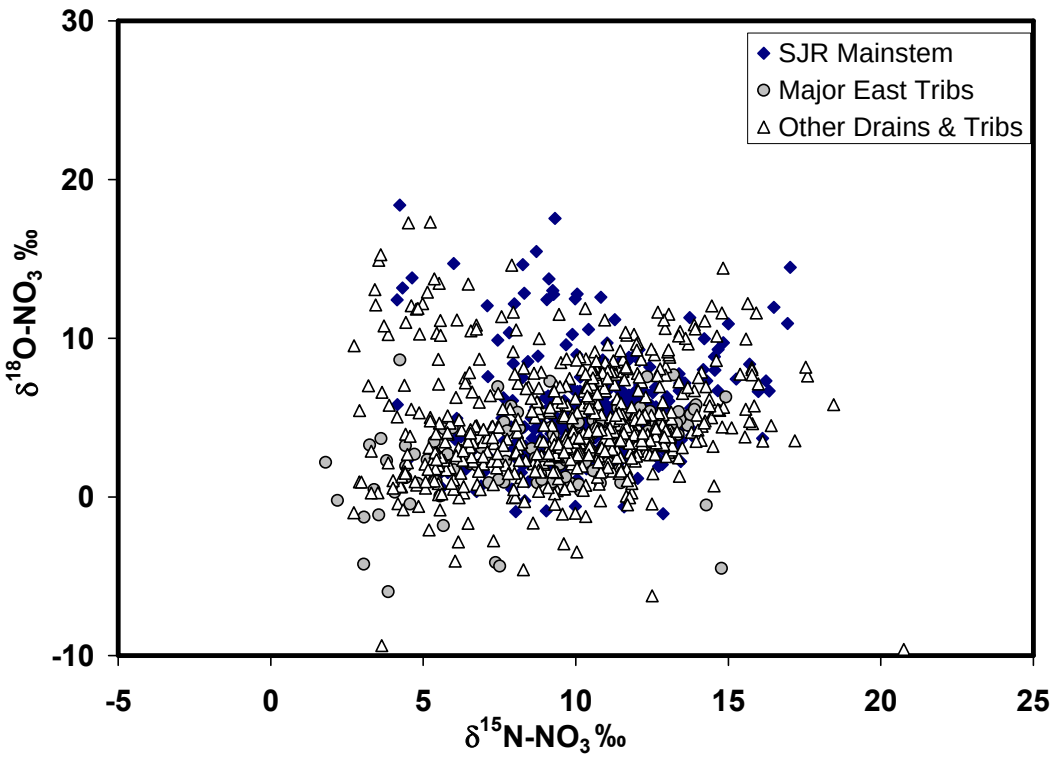

Figure 17. Distribution of nitrate $\delta^{15}N$ values for San Joaquin River mainstem sites (top) and major tributaries and drains (bottom) from March 2005 through December 2007.

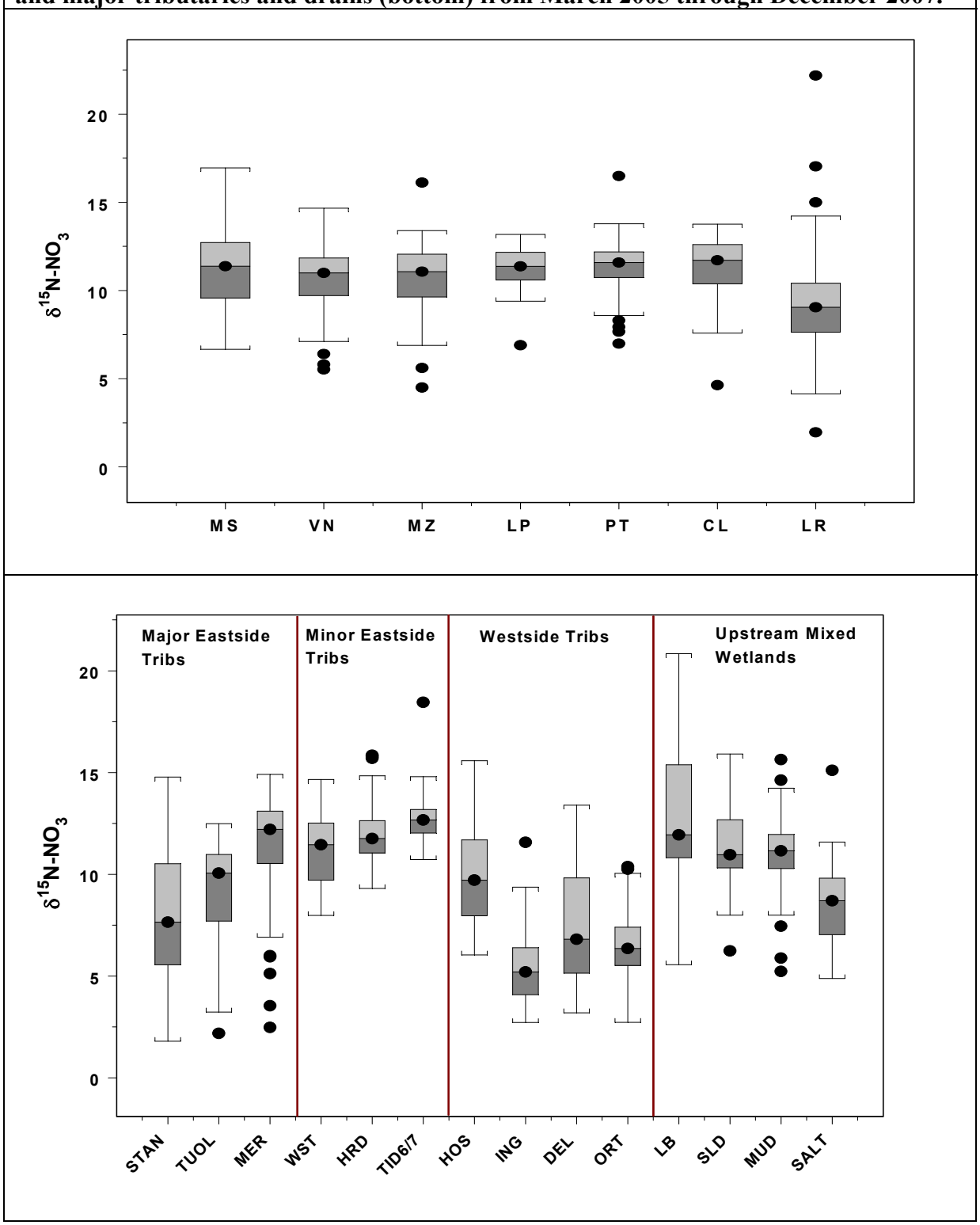

Figure 18. Distribution of nitrate $\delta^{18}O$ values for San Joaquin River mainstem sites (top) and major tributaries and drains (bottom) from March 2005 through December 2007.

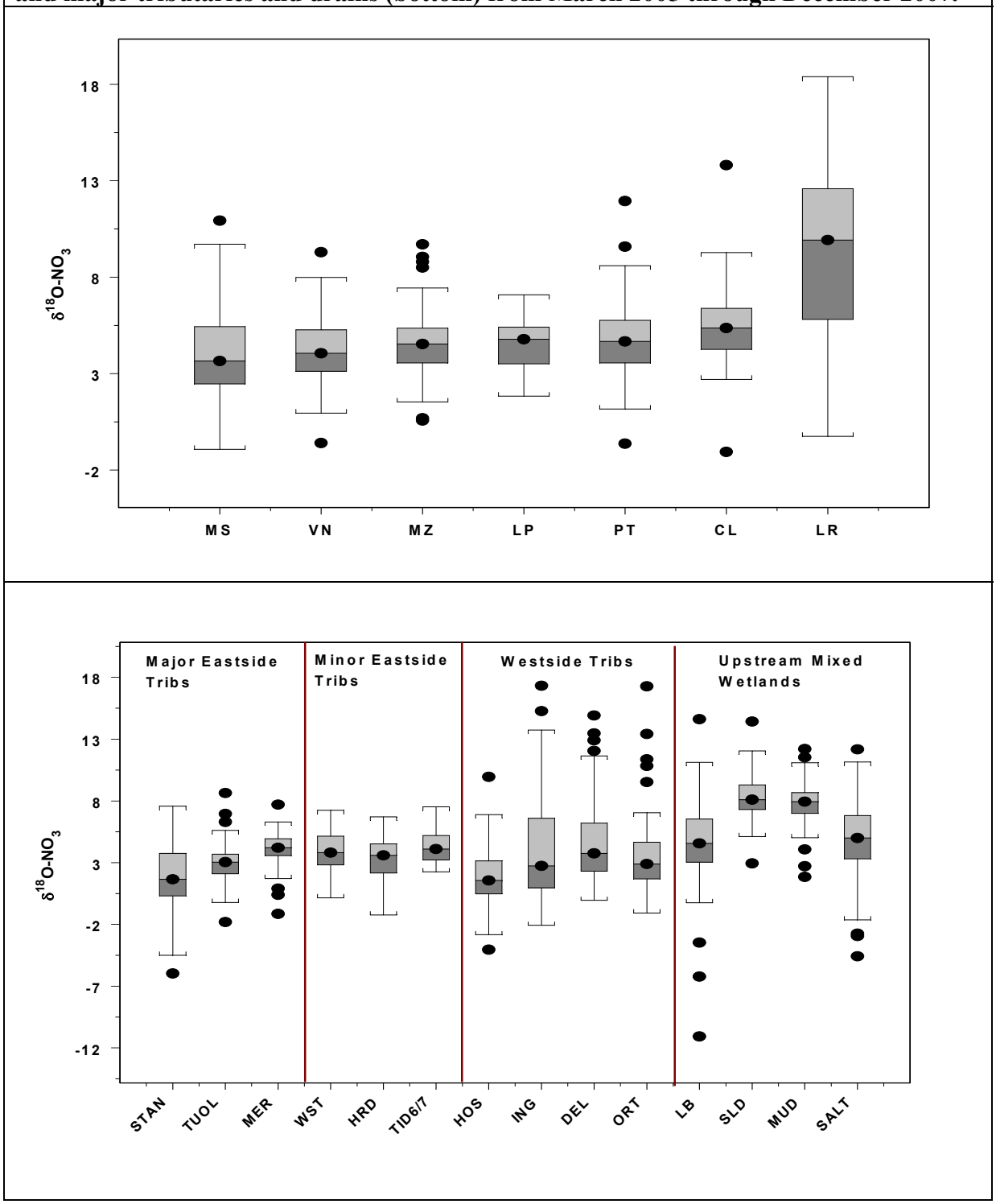

Figure 19. Nitrate concentration vs $\delta^{15}N$ for the SJR mainstem and Merced, Tuolumne, and Stanislaus Rivers. The top panel shows all of the data, while the bottom panel shows the distribution of samples from the three major tributaries, with one mainstem SJR site for reference.

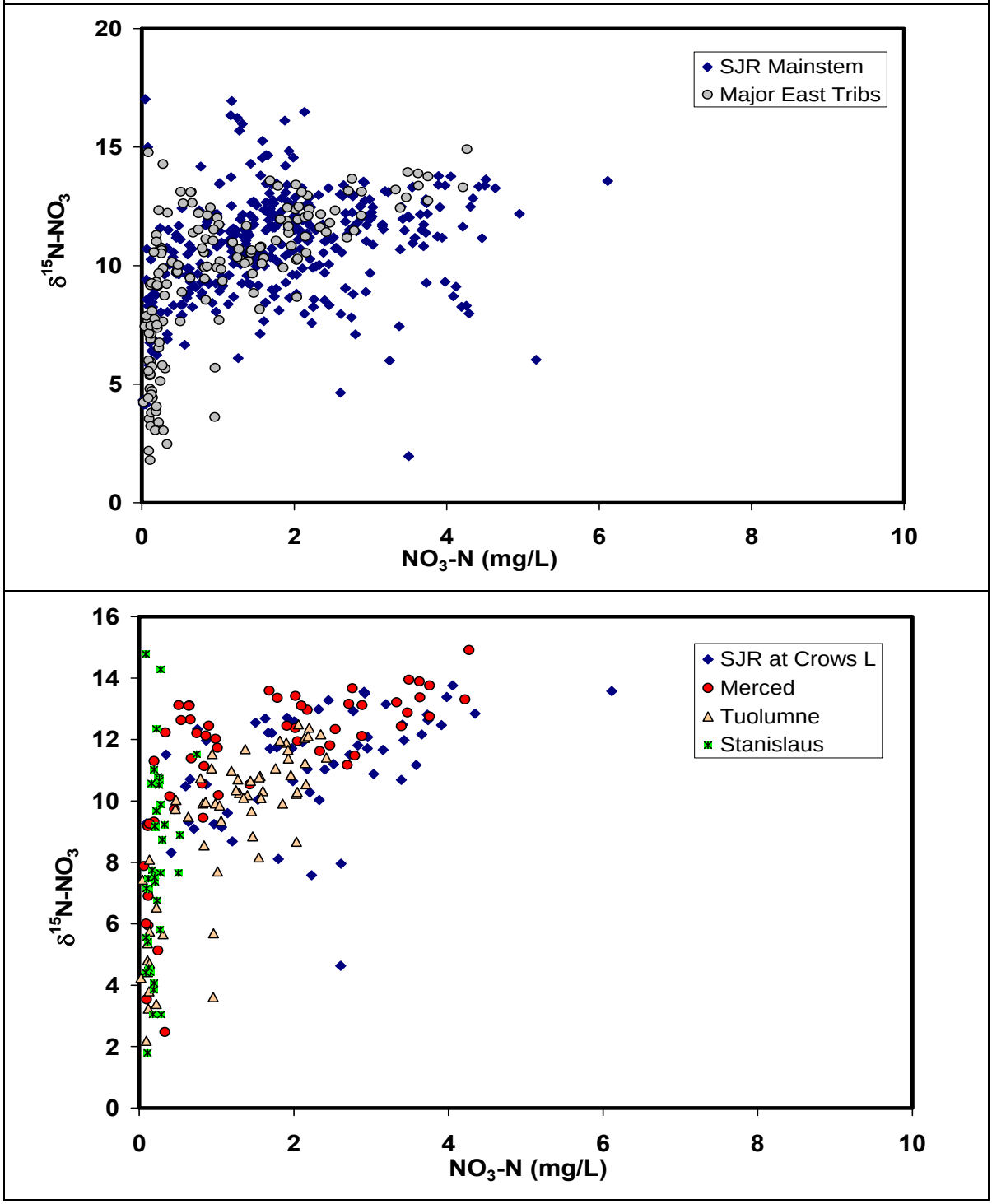

Figure 20. Nitrate concentration vs $\delta^{15}N$ for all of the core sampling sites (including drains & tributaries) from March 2005- December 2007.

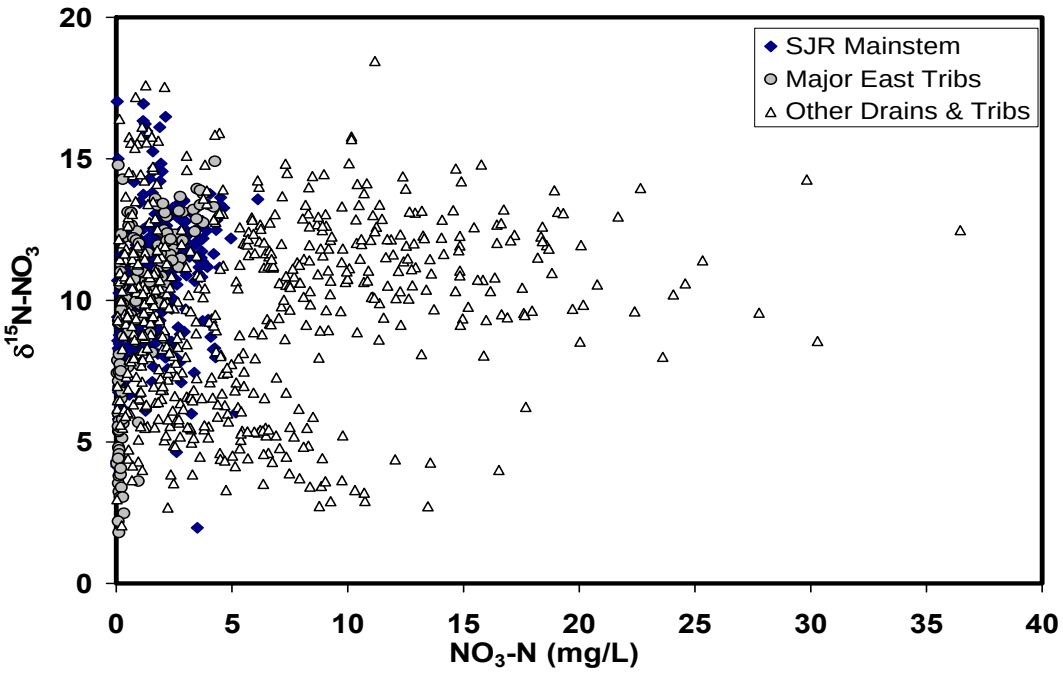

Figure 21. Nitrate concentration, $\delta^{15}N$, and flow data (from SJR Vernalis) for the entire study period at one upstream (Crows Landing) and one downstream (Vernalis site).

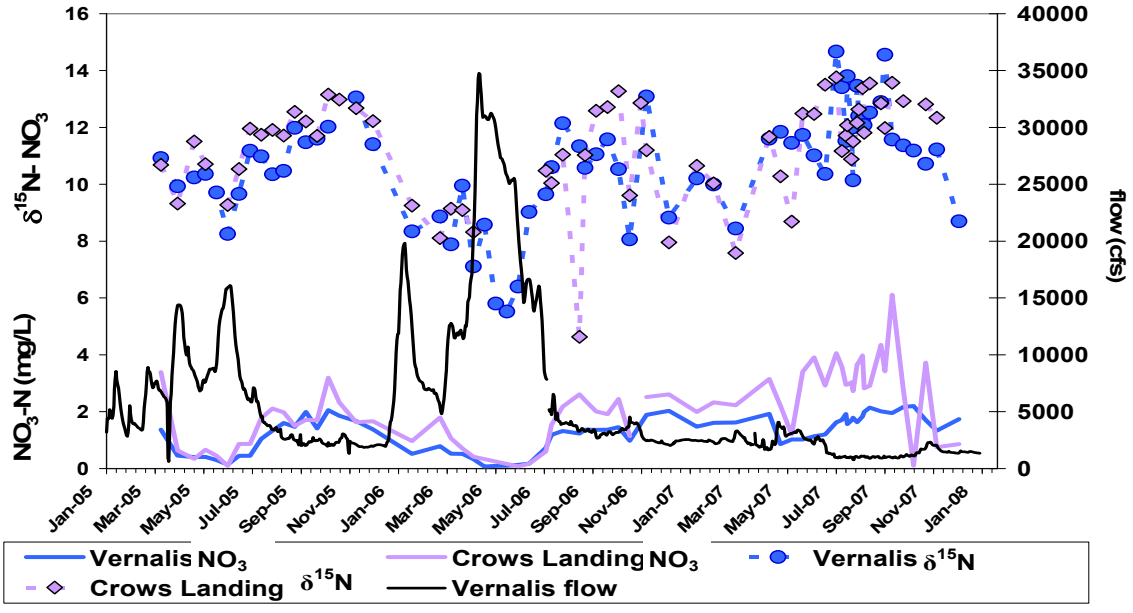

Figure 22. $\delta^{15}N$ in the Merced River and the SJR at Crows Landing (downstream of the confluence with the Merced). During low flow periods, the Merced River tends to carry nitrate with a high $\delta^{15}N$ signature.

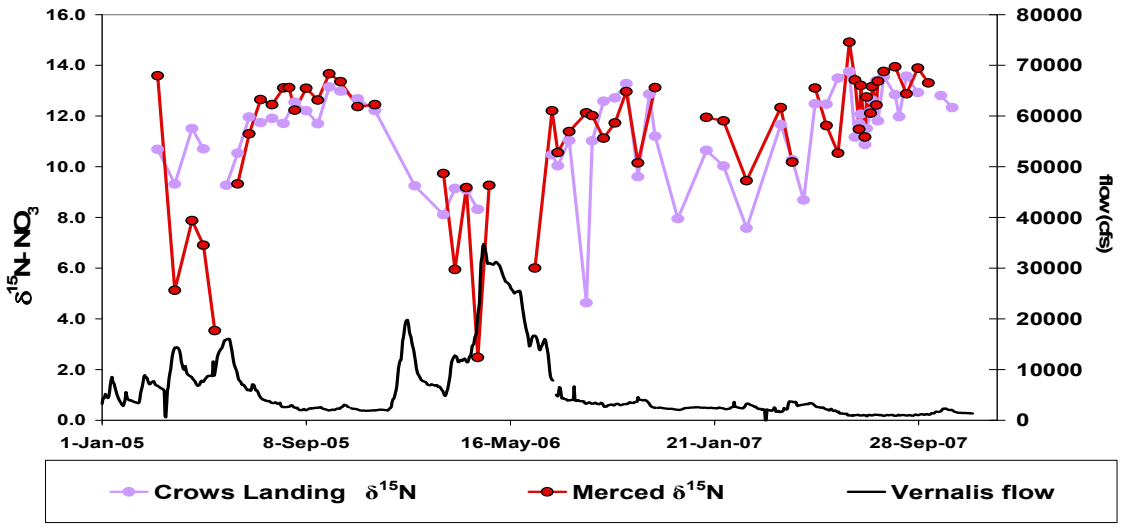

Figure 23. Nitrate concentration and $\delta^{15}N$ in the SJR at Lander Avenue, upstream of the confluence with the Merced River.

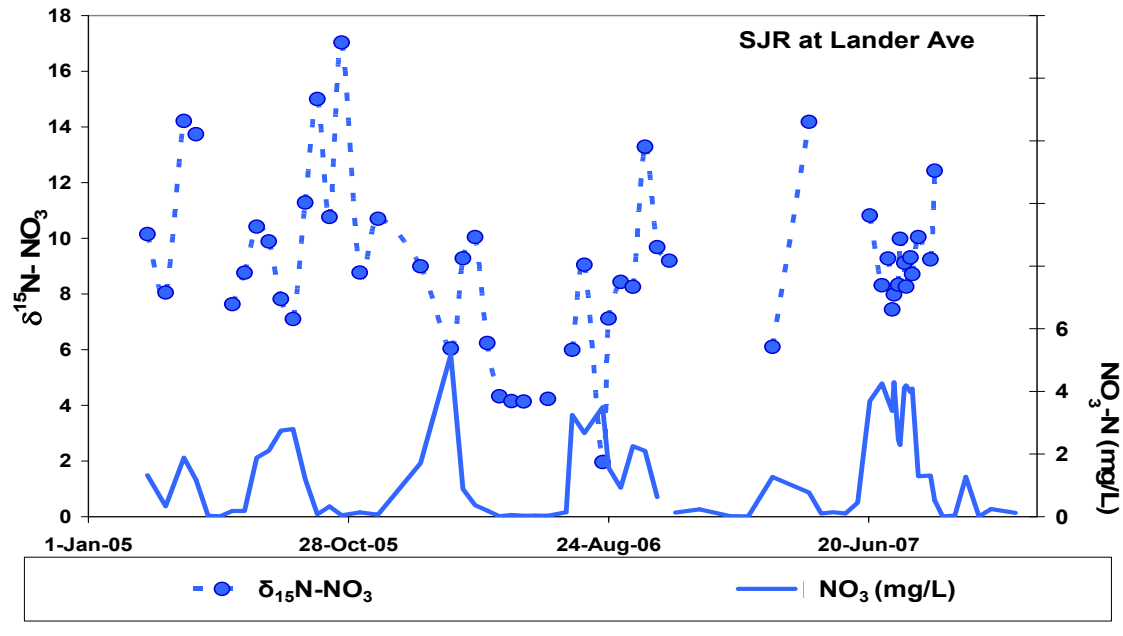

Figure 24. Comparison of nitrate concentration, $\delta^{15}N$, and $\delta^{18}O$ of the mainstem SJR sites, upstream tributaries, and major east-sideside tributaries under high flow (top panel) and low flow (bottom panel) conditions.

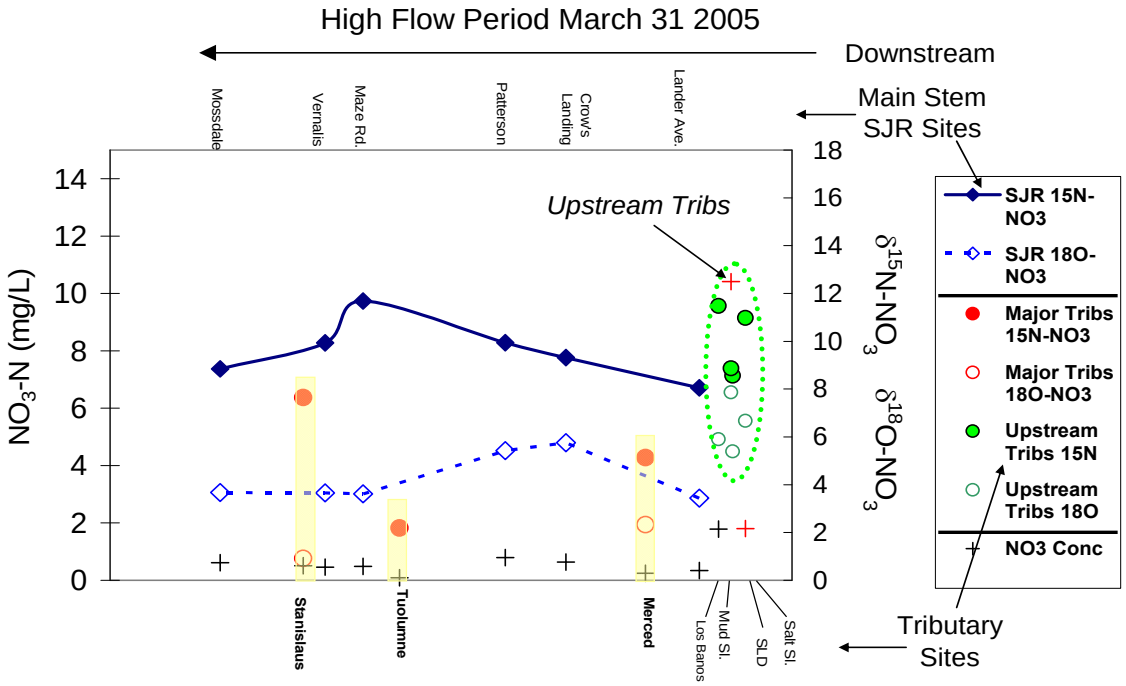

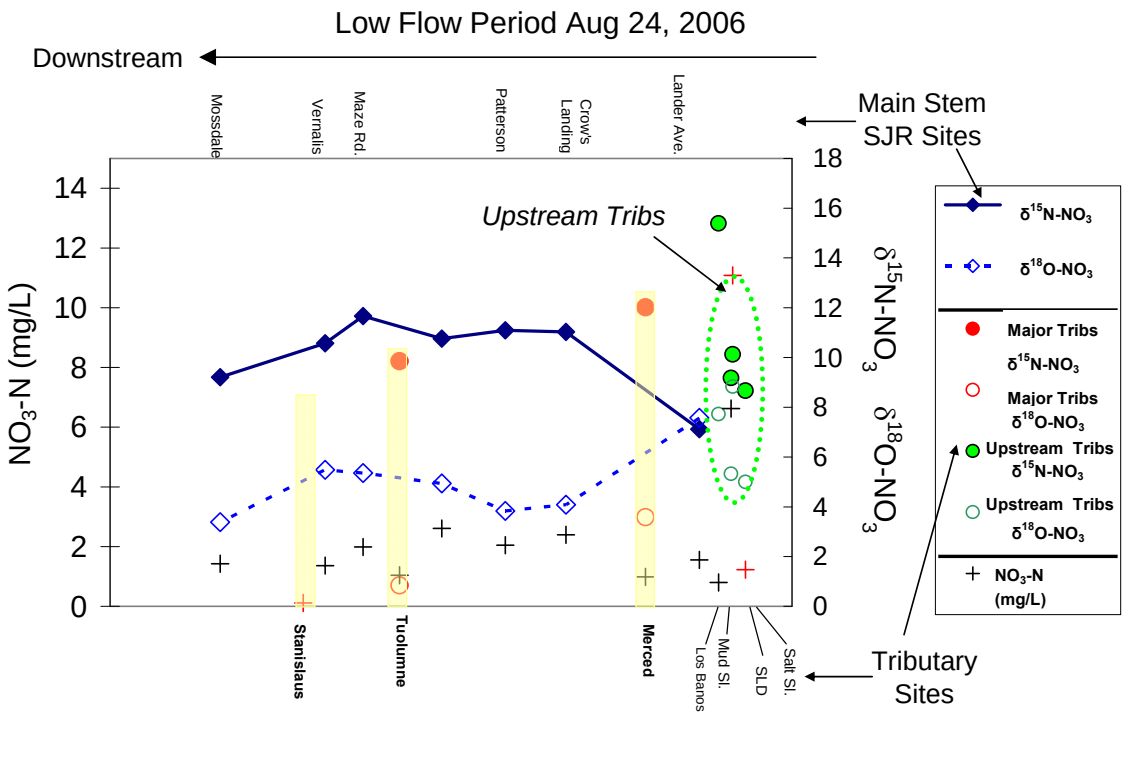

Figure 25. Mean nitrate $\delta^{15}N$ and $\delta^{18}O$ for all core sampling sites between March 2005 and December 2007. Error bars show one standard deviation.

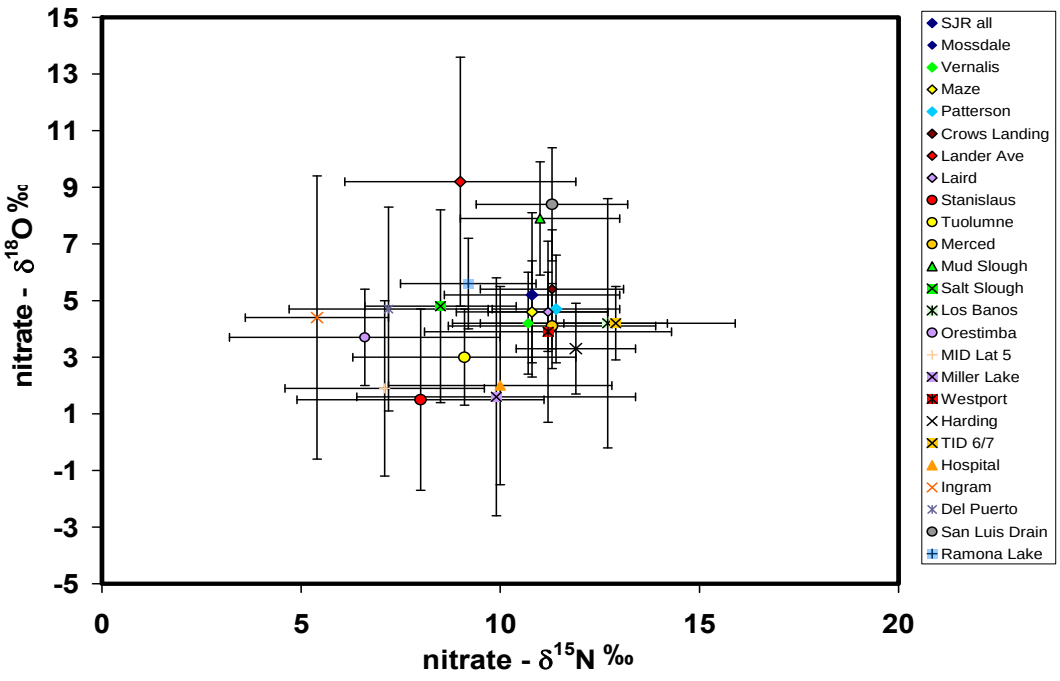

Figure 26. The □^{18}O of dissolved inorganic phosphate in the San Joaquin River and tributaries. The differences between sites are much larger than analytical error. Error bars represent replicate analyses.

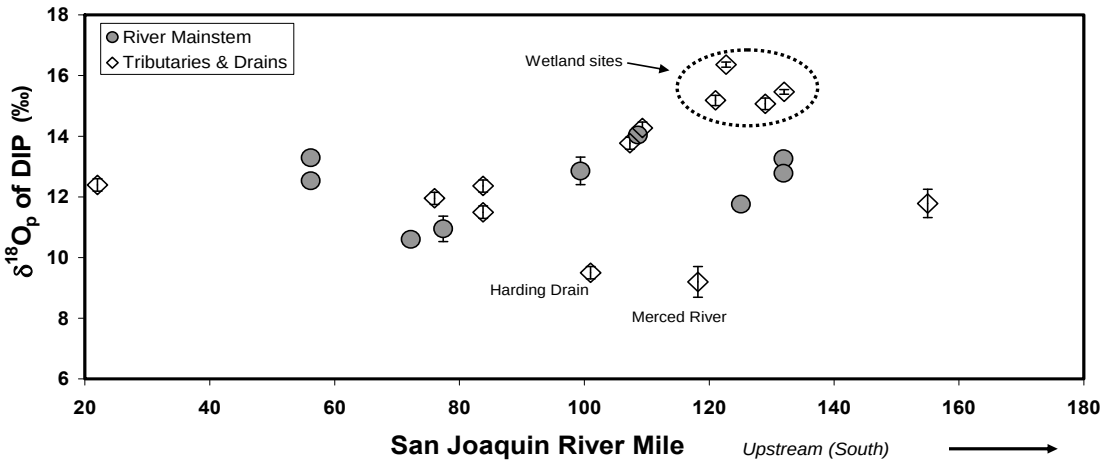

Figure 27. $\delta^{18}O$ and $\delta^{2}H$ of water for all of the mainstem SJR sites (top) and all core sites (bottom) sampled between March 2005 and December 2007.

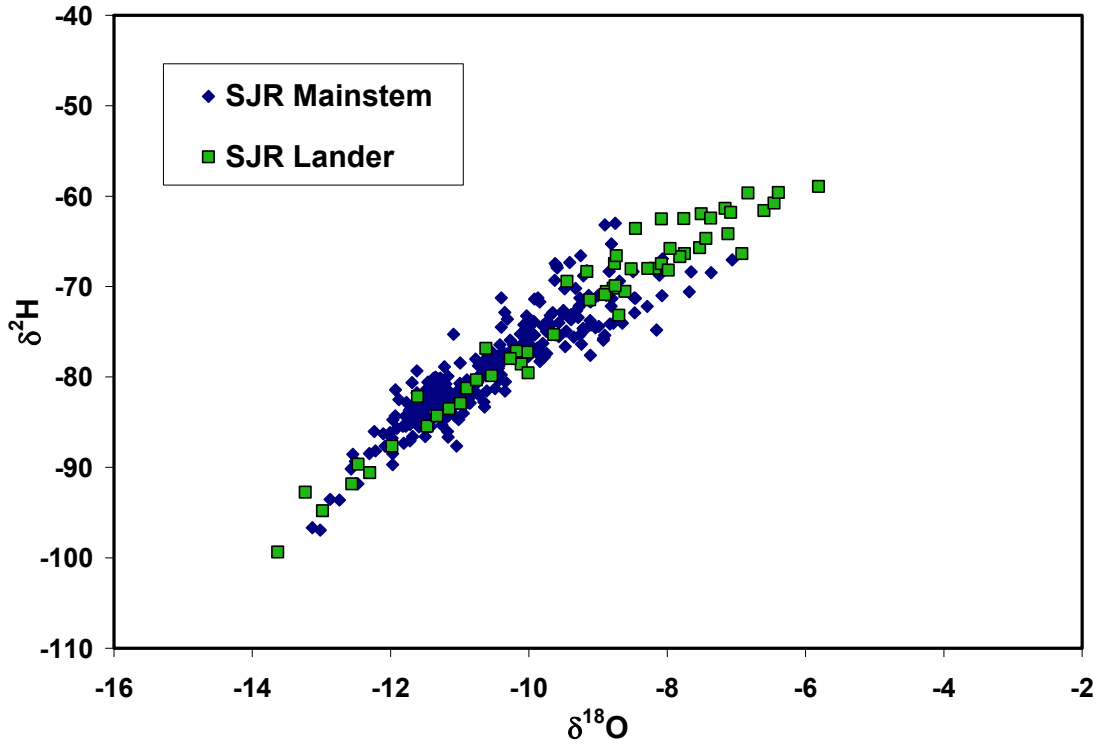

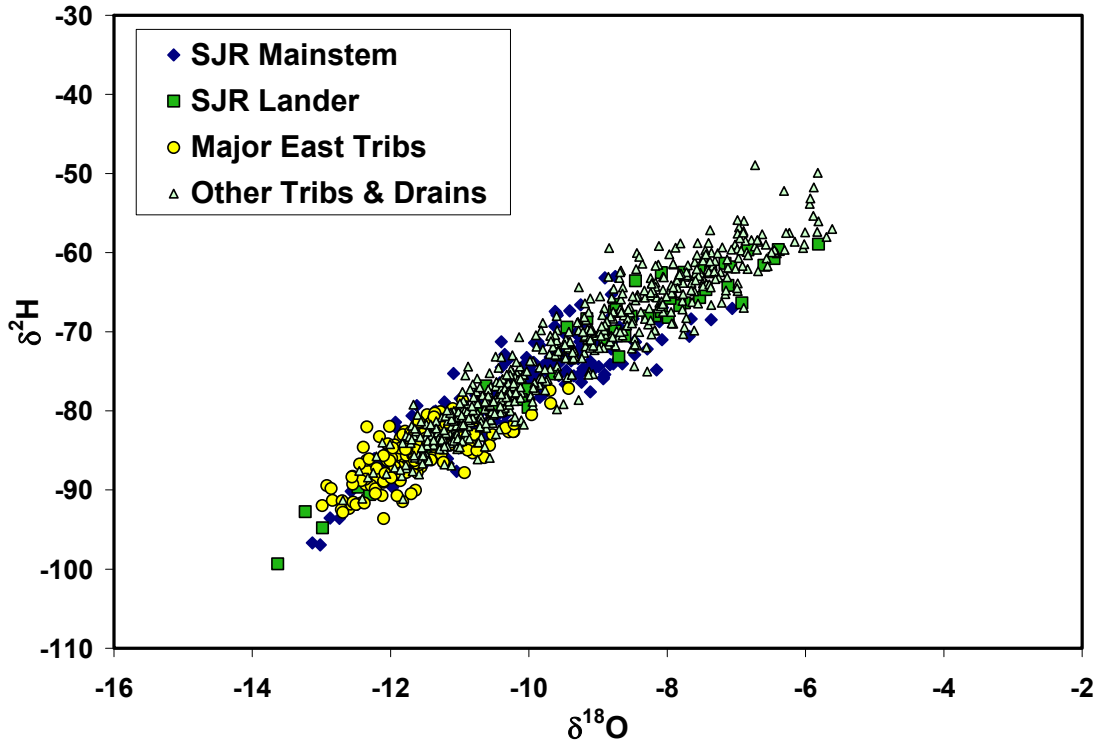

Figure 28. Distribution of water $\delta^{18}O$ values for San Joaquin River mainstem sites (top) and major tributaries and drains (bottom) from March 2005 through December 2007.

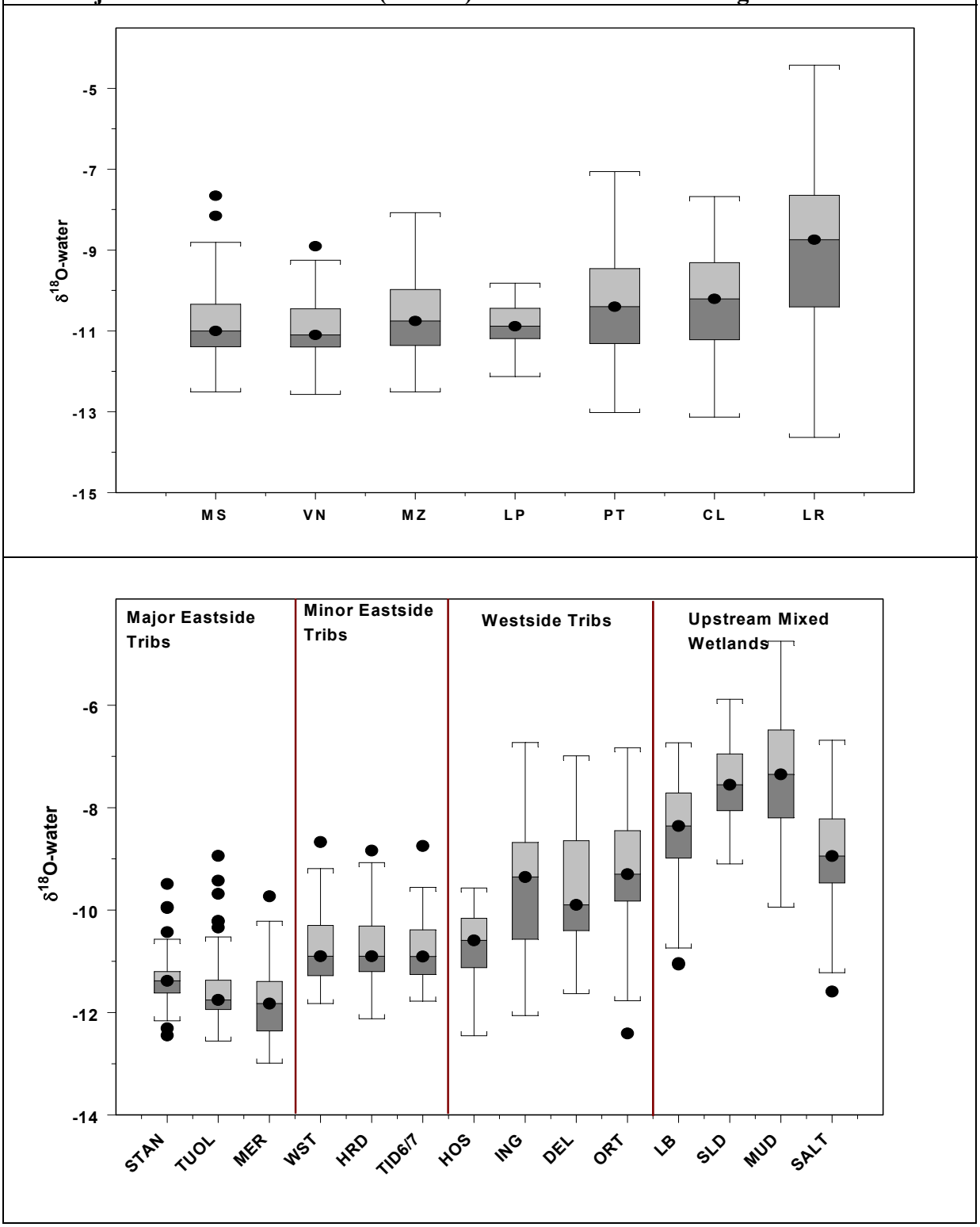

Figure 29. Distribution of water δ^2H values for San Joaquin River mainstem sites (top) and major tributaries and drains (bottom) from March 2005 through December 2007.

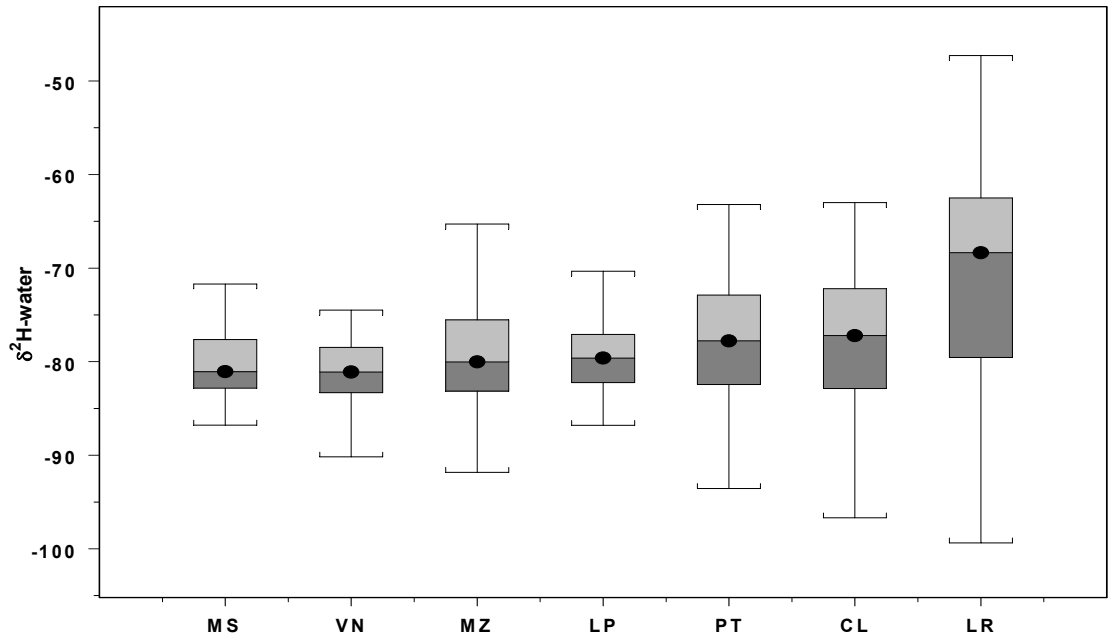

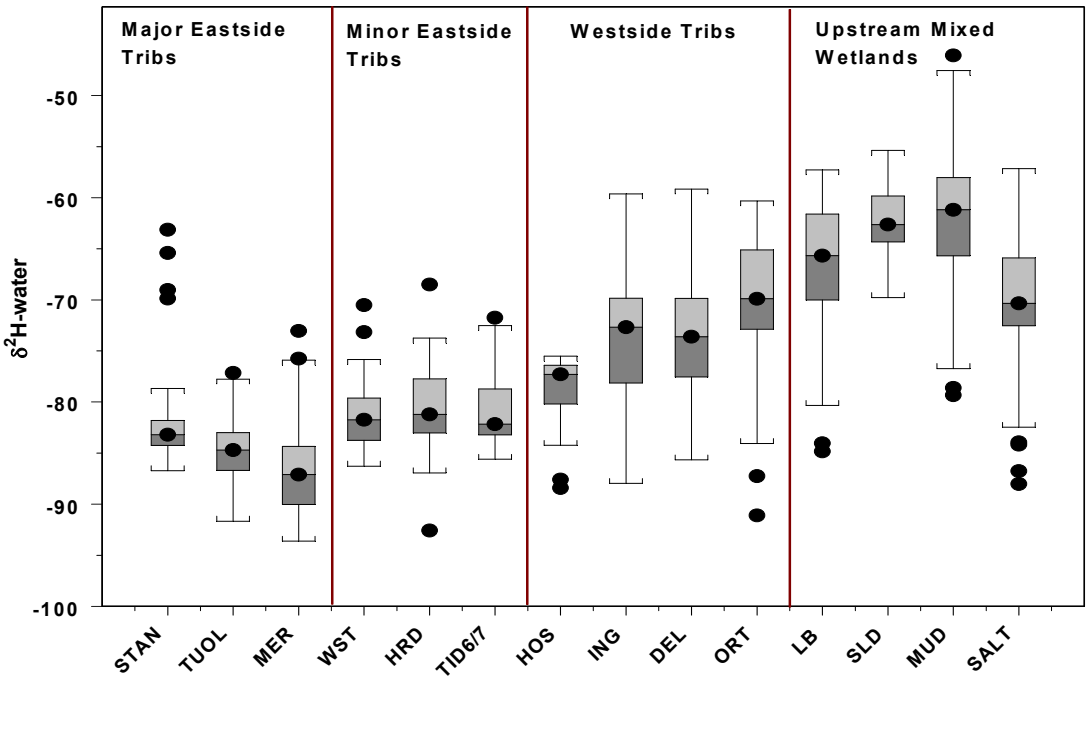

Figure 30. Temporal variability in the $\delta^{18}O$ of water for the major east-sideside tributaries and Salt Slough. SJR at Crows Landing is included for reference.

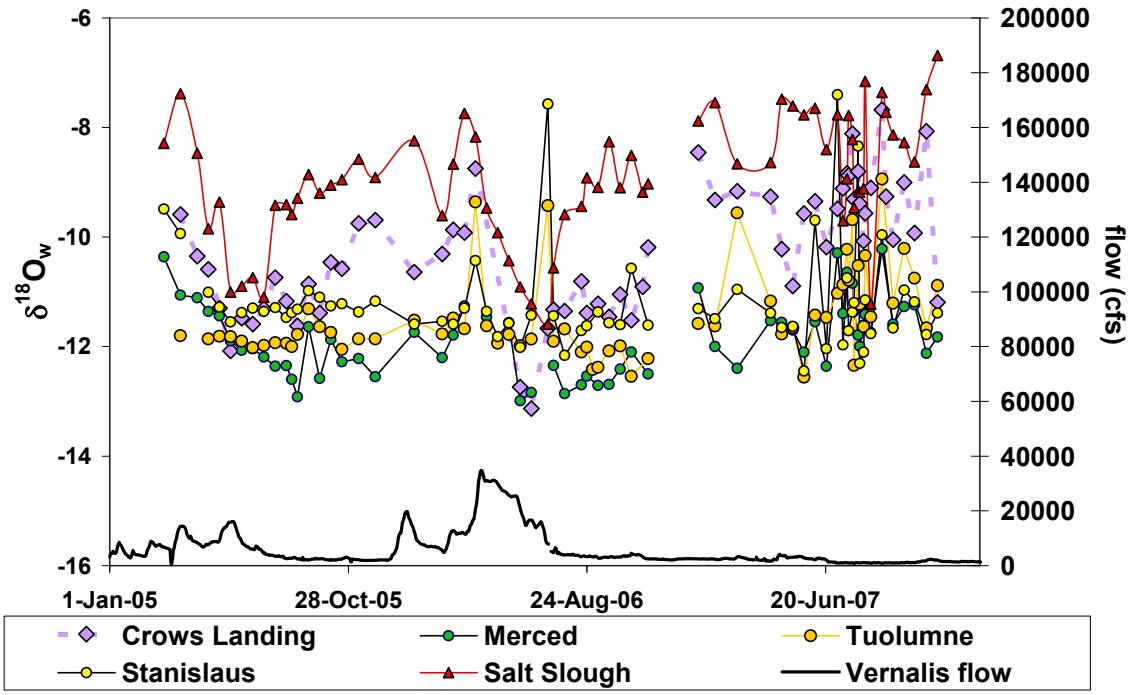

Figure 31. Spatial variability in $\delta^{18}O$ of water in the mainstem SJR, major east-sideside tributaries, and upstream wetlands sites during a high flow period (top) and a low flow period (bottom).

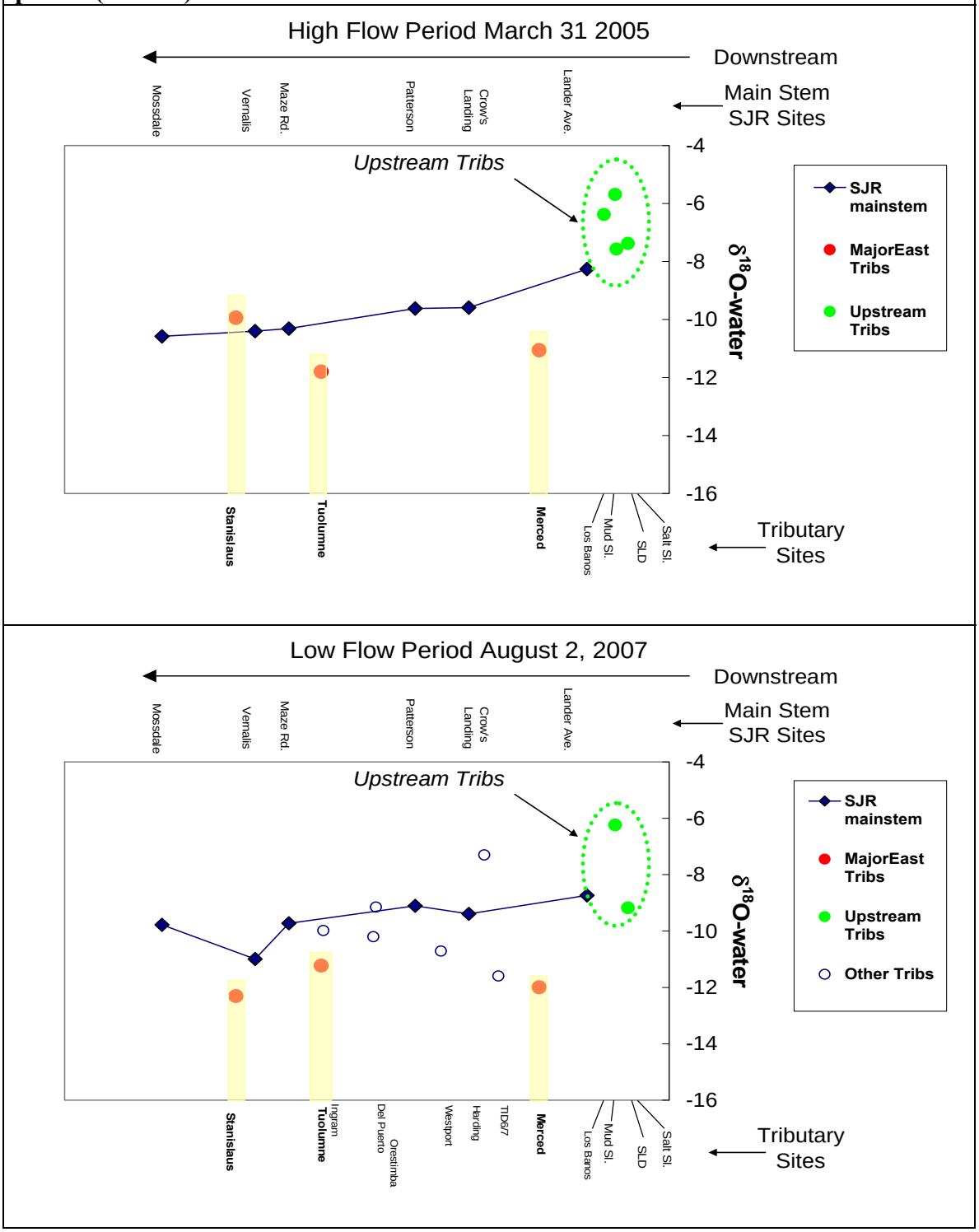

Figure 32. Distribution of sulfate $\delta^{34}S$ values for San Joaquin River mainstem sites (top) and major tributaries and drains (bottom) from March 2005 through December 2007.

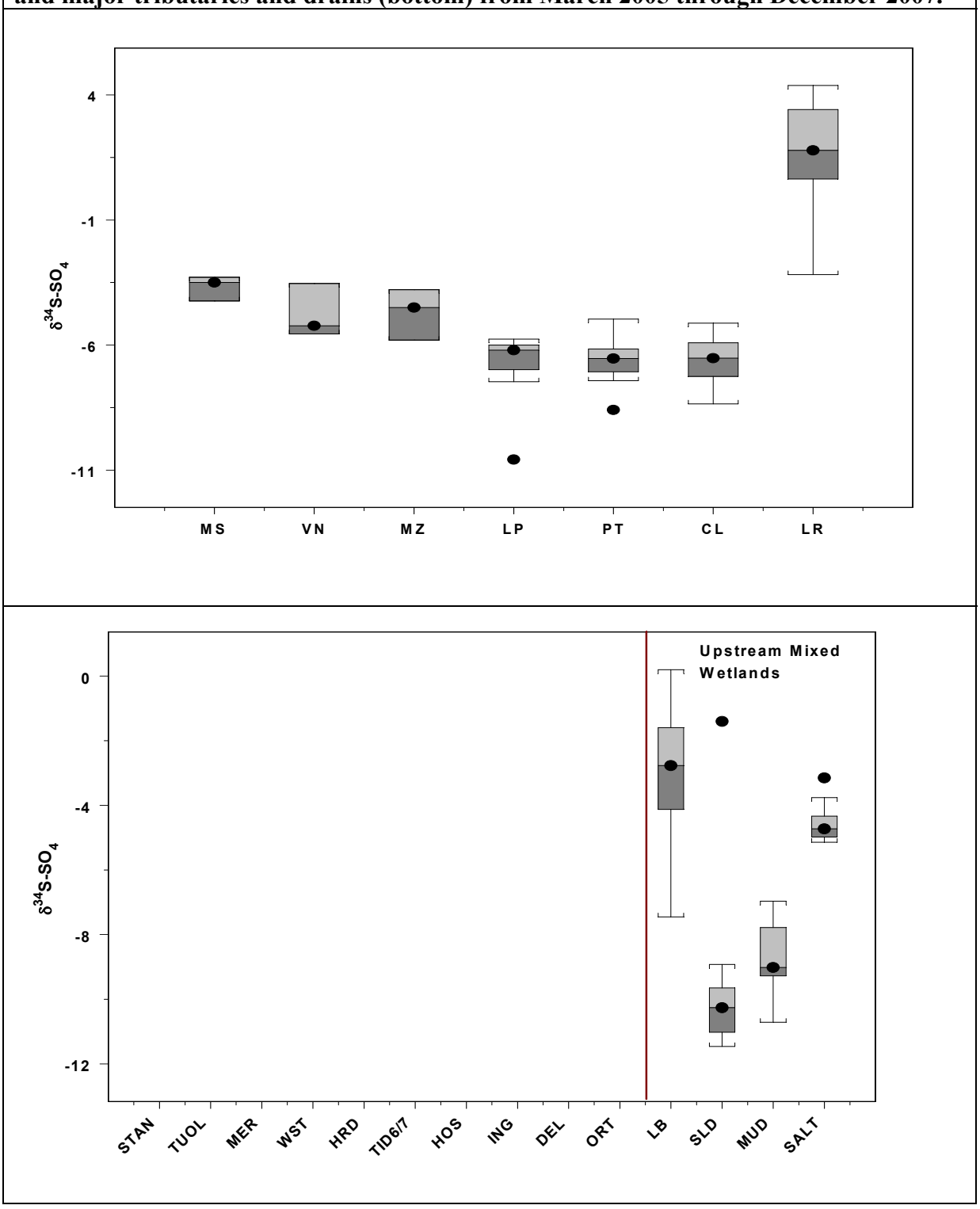

Figure 33. Distribution of sulfate $\delta^{18}O$ values for San Joaquin River mainstem sites (top) and major tributaries and drains (bottom) from March 2005 through December 2007.

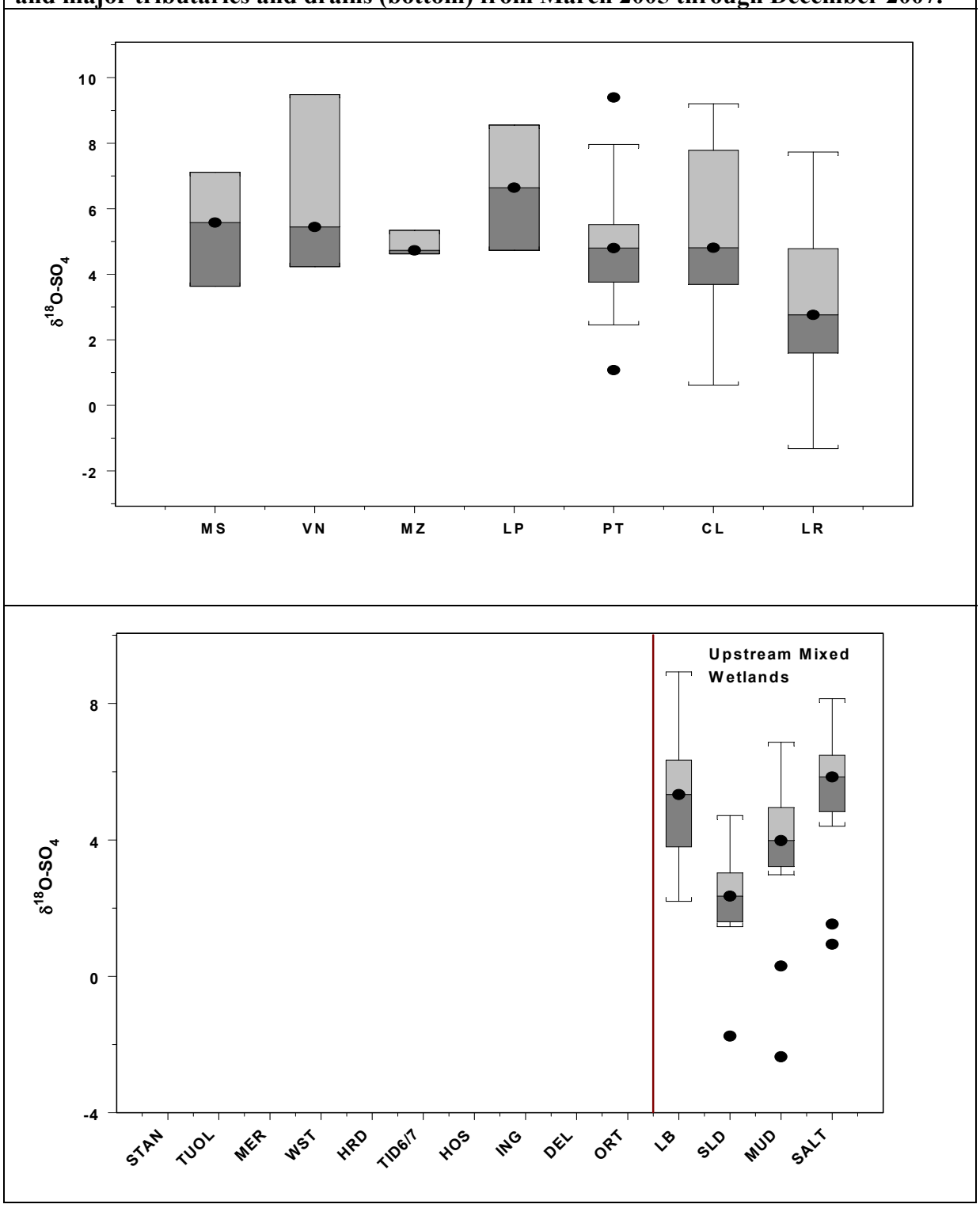

Figure 34. Sulfate $\delta^{34}S$ and $\delta^{18}O$ for all SJR mainstem, tributary, and drain sites, with expected ranges shown for major potential sulfate sources.

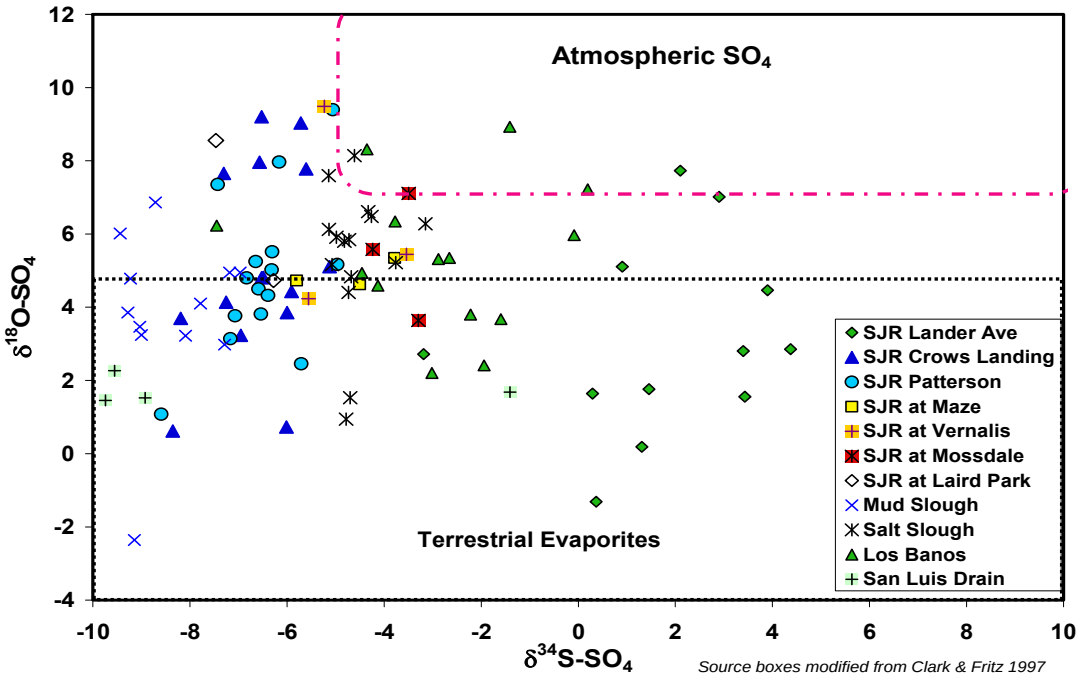

Figure 35. Sulfate $\delta^{34}S$ values over time for mainstem SJR sites. The three sites upstream of the confluence with the Tuolumne River have $\delta^{34}S$ values that are distinct from the downstream sites.

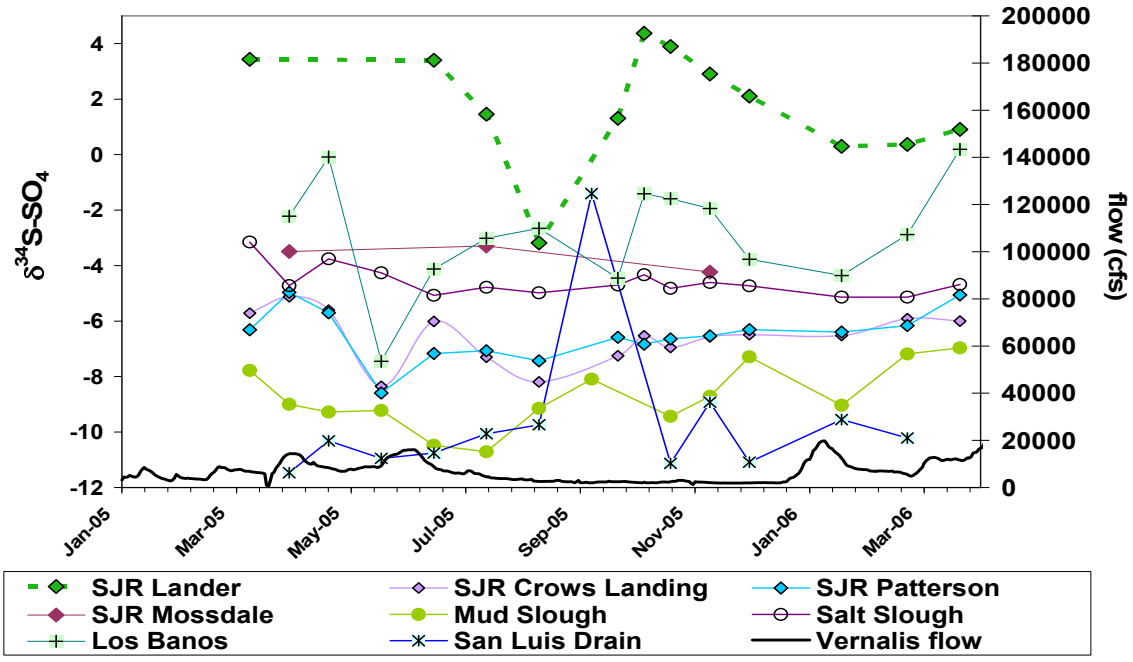

Figure 36. Sulfate $\delta^{34}S$ values over time for selected mainstem SJR and tributary sites (top), and $\delta^{18}O$ values for mainstem SJR sites (bottom).

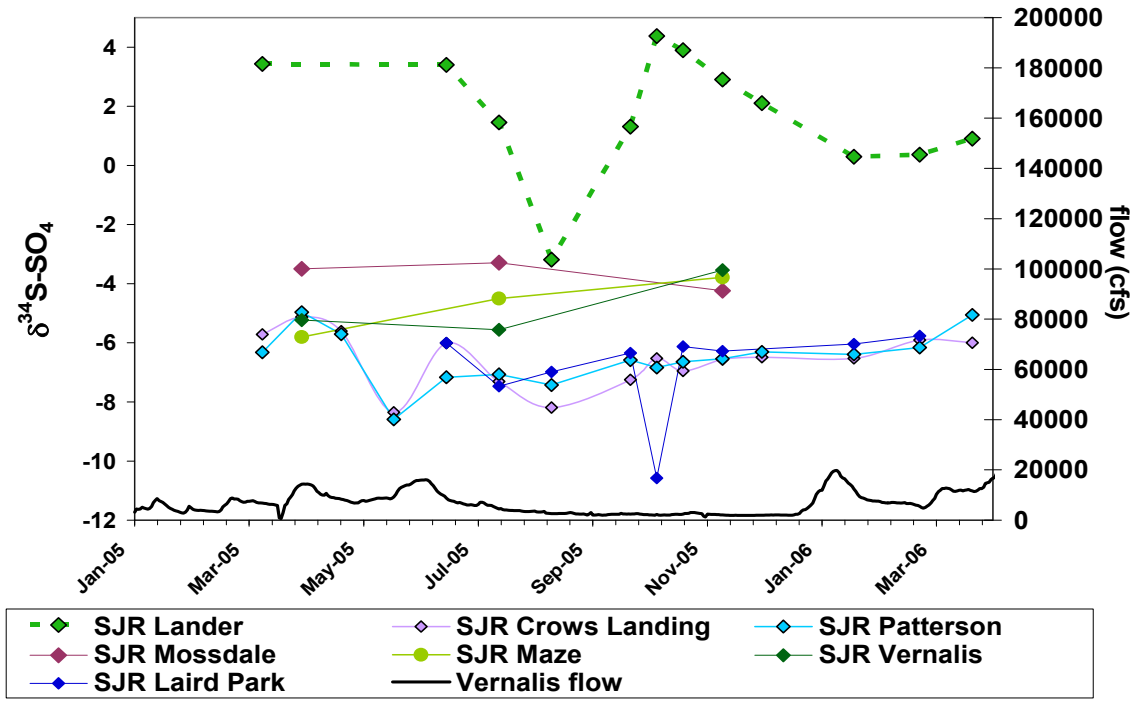

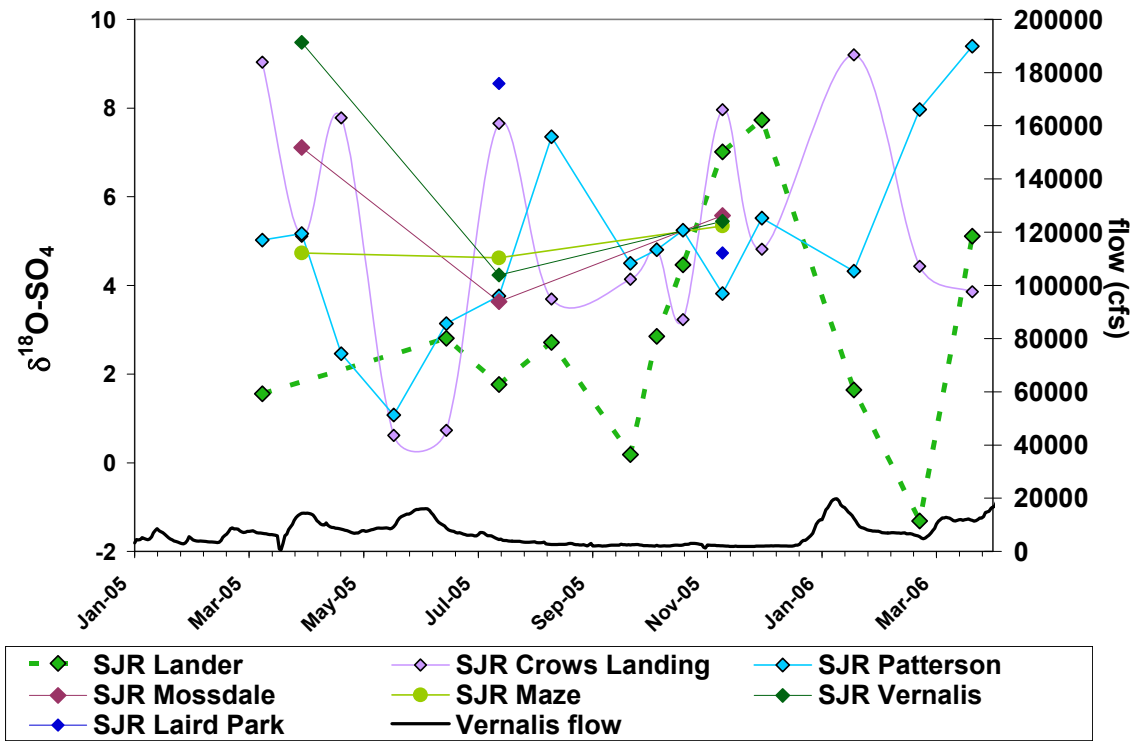

Figure 37. Relationship between sulfate $\delta^{34}S$ and electrical conductivity for selected mainstem SJR, tributary, and drain sites.

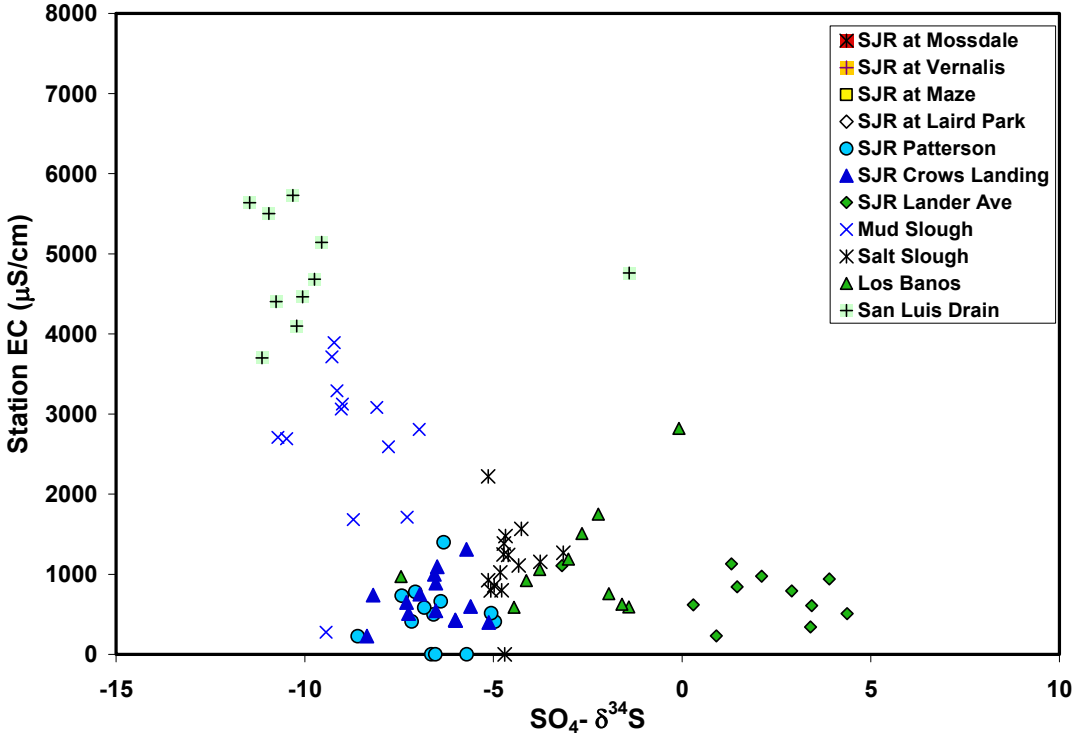

Figure 38. General predictions of relative contribution of terrestrial and autotrophic organic matter to rivers, as inferred from the River Continuum Model of Vannote et al. (1980).

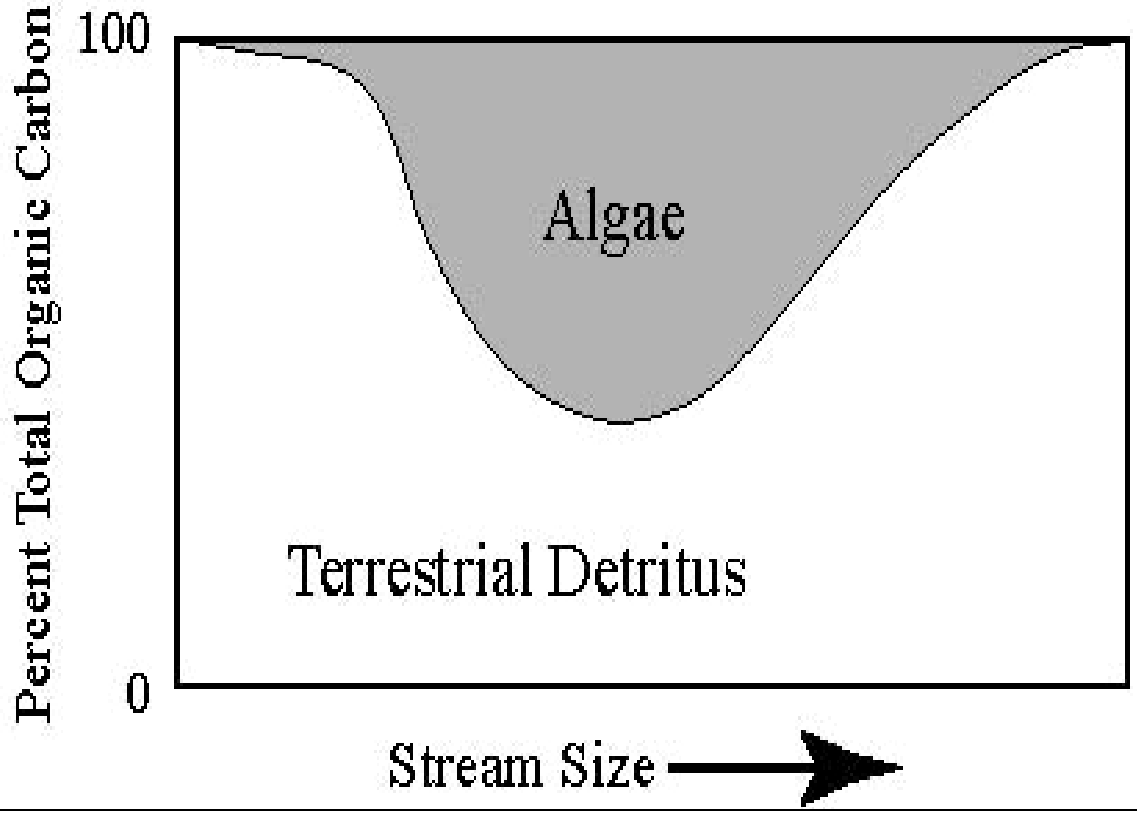

Figure 39. Correlation of algal pigments (the sum of chlorophyll-*A* and pheophytin) with C:N of POM samples from various groups of sites (top) with an expanded pigments scale (bottom).

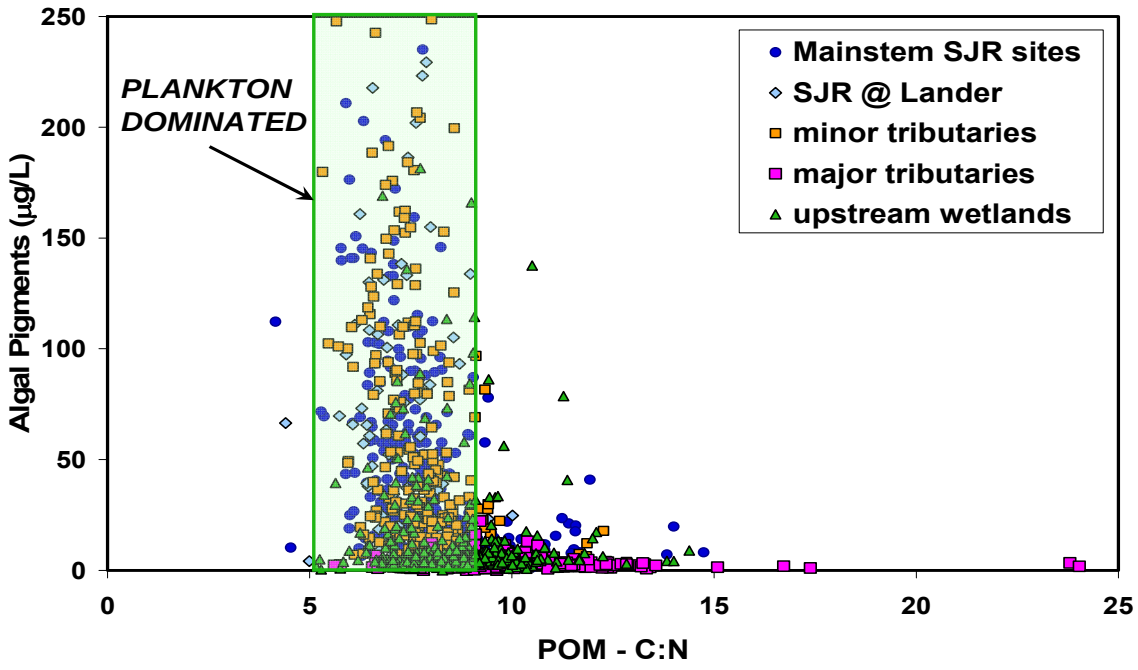

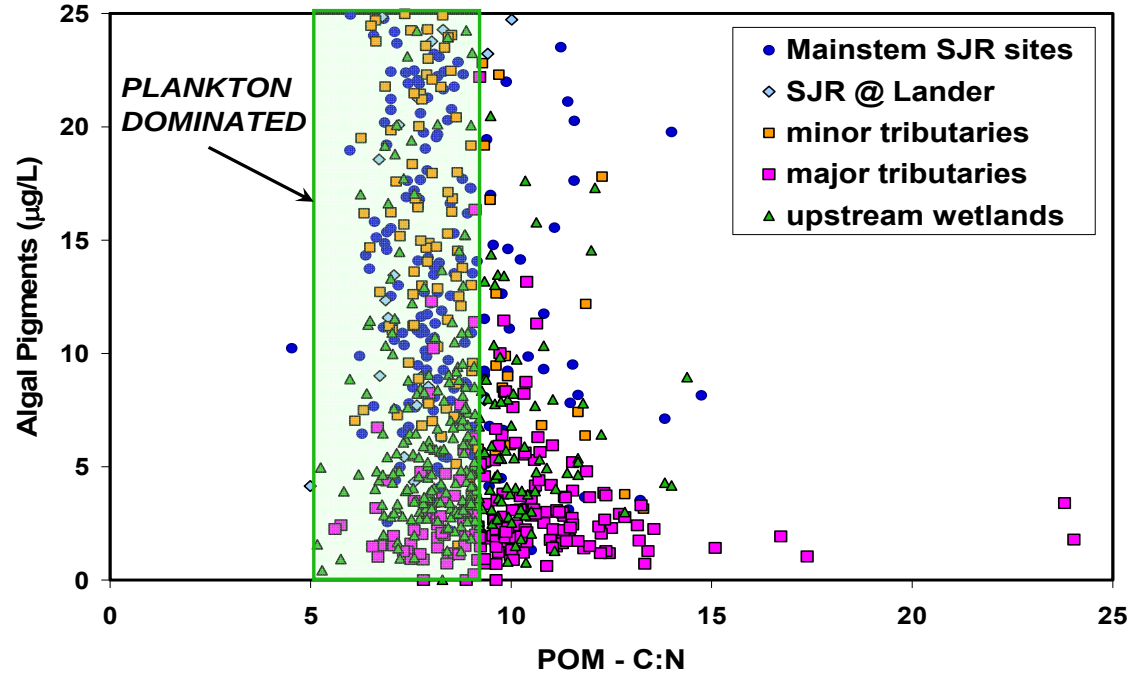

Figure 40. Correlation of C:N values of POM and algal pigment concentrations for mainstem SJR sites (top), with the data presented with an expanded algal pigment scale below (bottom).

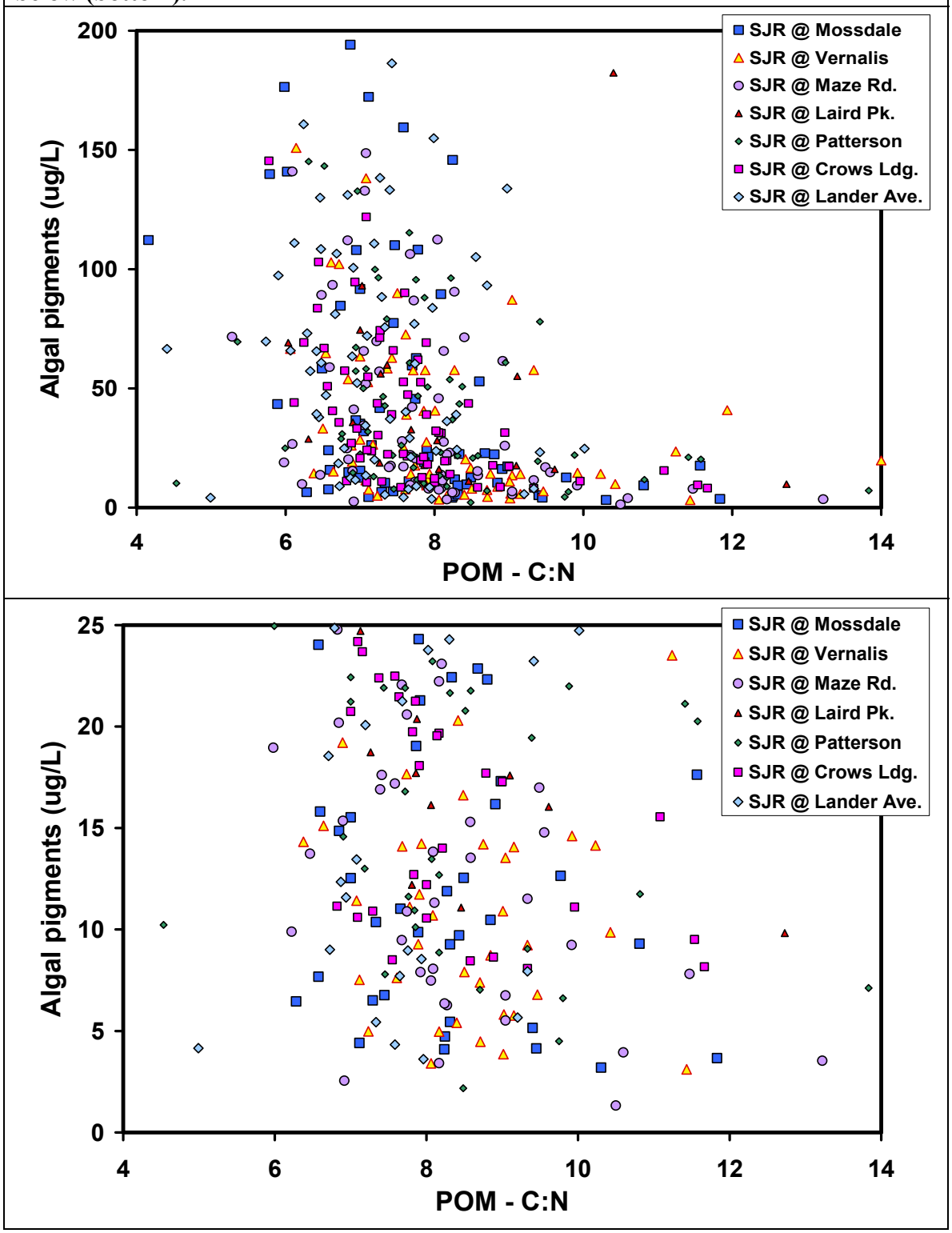

Figure 41. Correlation of C:N values of POM and algal pigment concentrations for selected drain, creek, and wetlands sites (top), with the data presented with an expanded algal pigment scale below (bottom). Wetlands sites generally have lower C:N values than other sites. Different site types all show wide ranges of pigment values; however, average wetlands pigments values are generally higher than for other sites. At low pigment concentrations (bottom) there is little correlation of pigments and C:N whereas at higher pigment concentrations, the C:N values are significantly lower.

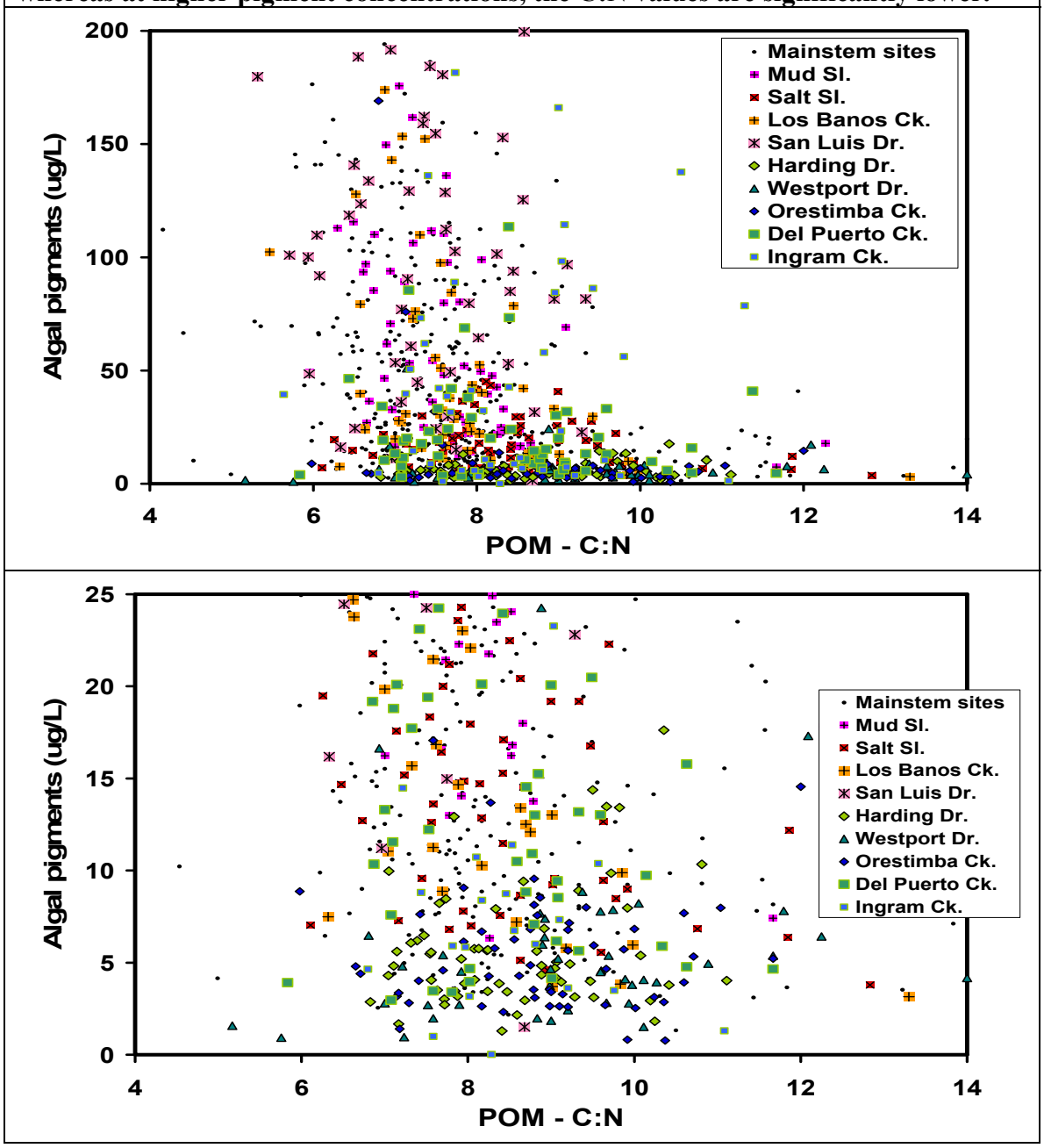

Figure 42. Distribution of BOD vs C:N from various groups of sites (top) with an expanded scales (bottom) so the symbols are more readable.

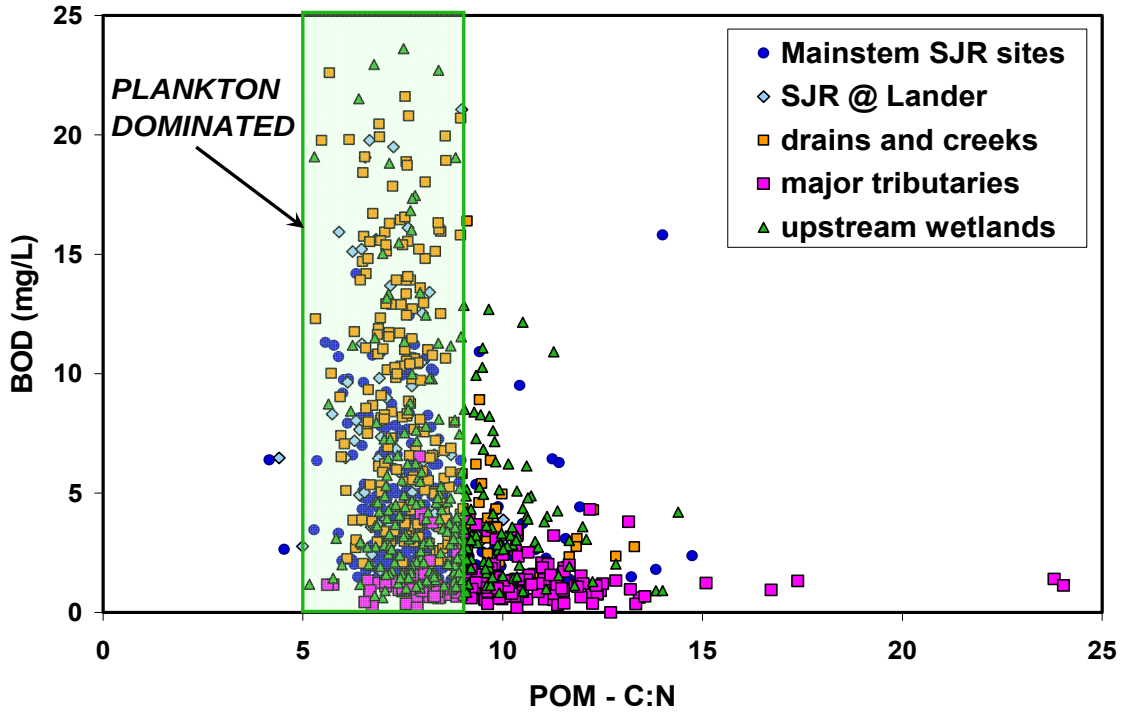

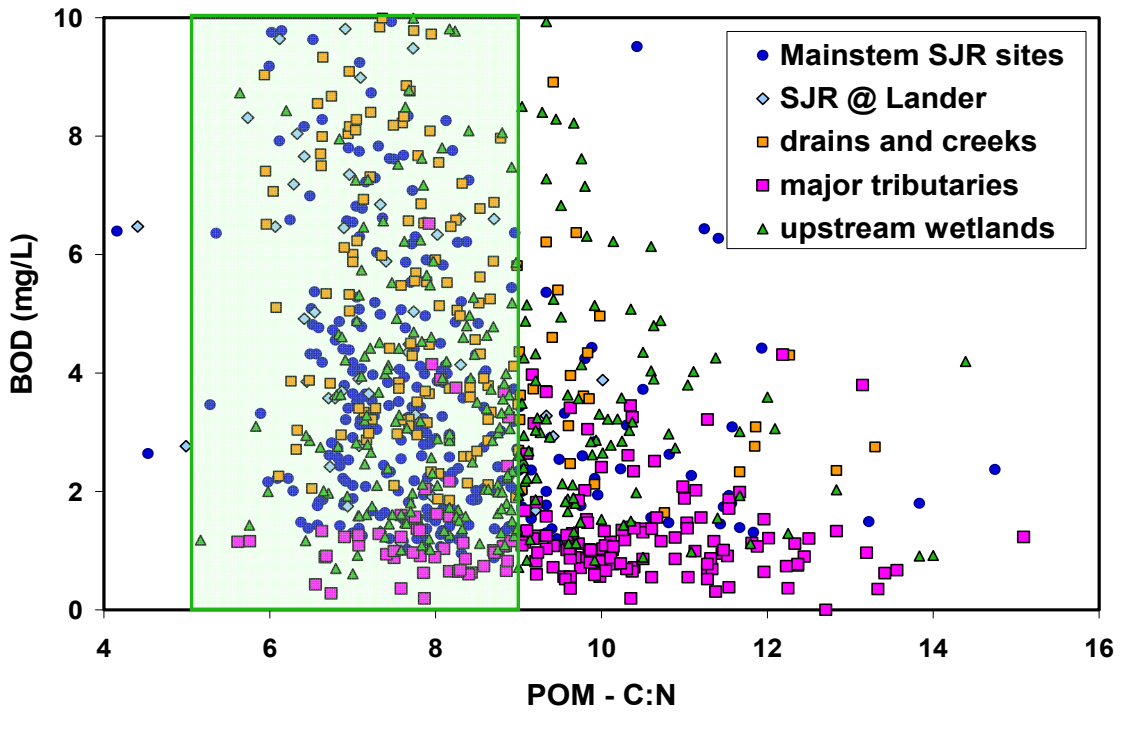

Figure 43. Correlation of C:N of POM and BOD for mainstem SJR sites (top) and major tributaries (bottom). Tributary sites have much lower BOD concentrations than mainstem sites. Samples with low C:N values have a wide range of BOD values, whereas samples with high C:N have low BOD values.

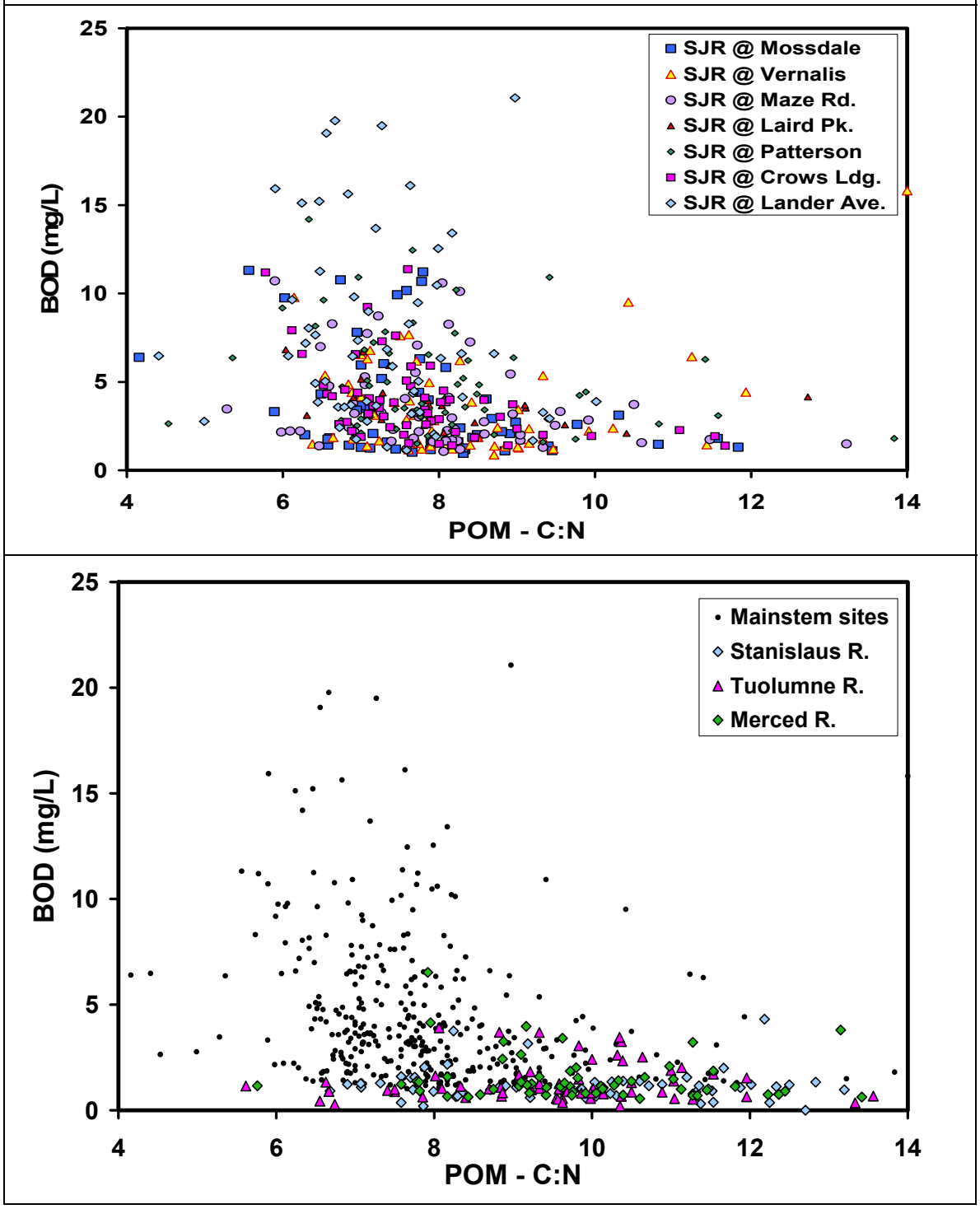

Figure 44. Correlation of C:N values of POM and CBOD (top) and NBOD (bottom) for major tributaries and mainstem SJR sites. Mainstem sites have a larger range of CBOD and NBOD values than tributaries. A higher proportion of the BOD is NBOD in the tributaries than the mainstem sites.

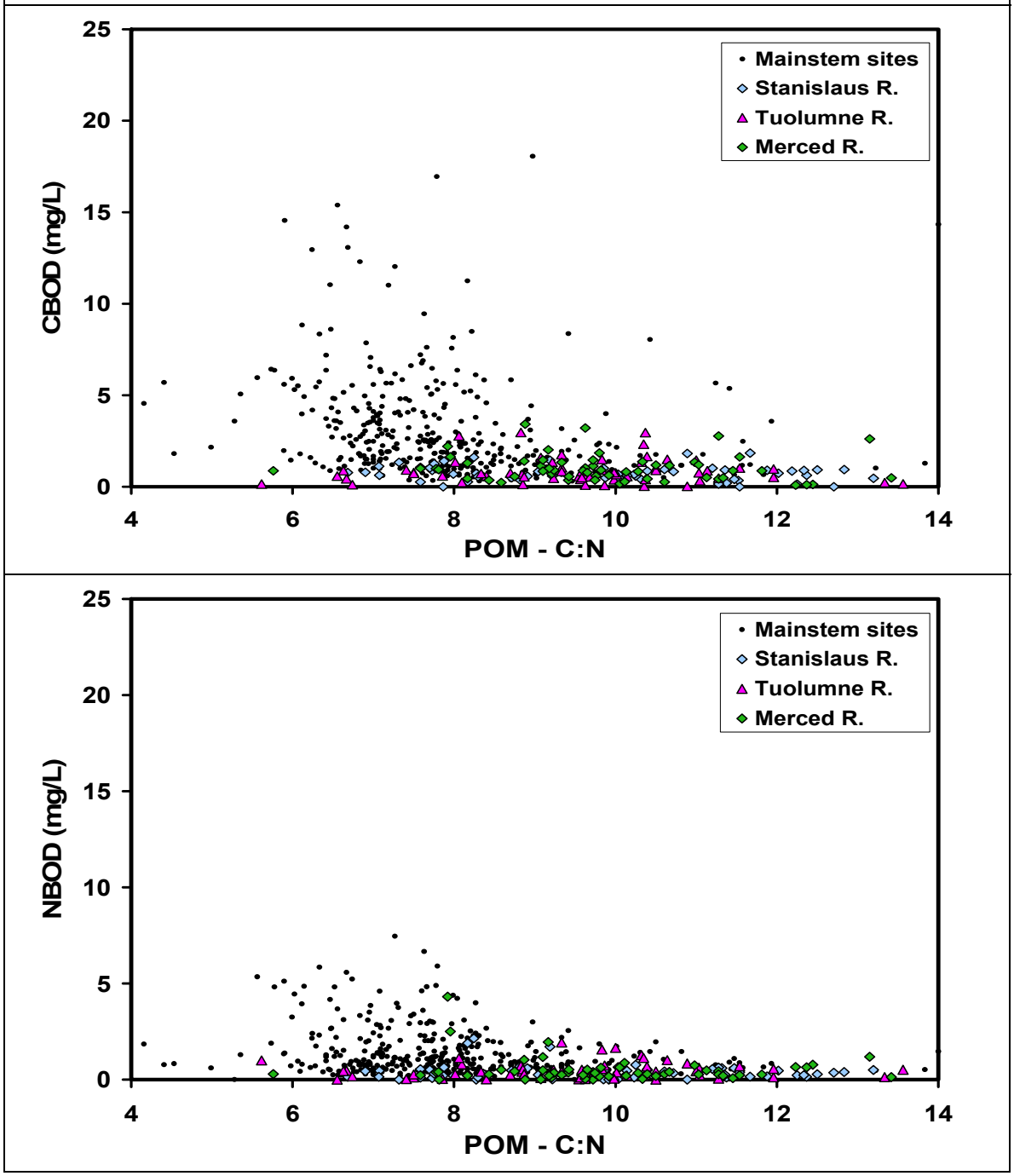

Figure 45. Correlation of C:N values of POM and CBOD (top) and NBOD (bottom) for the different mainstem SJR sites.

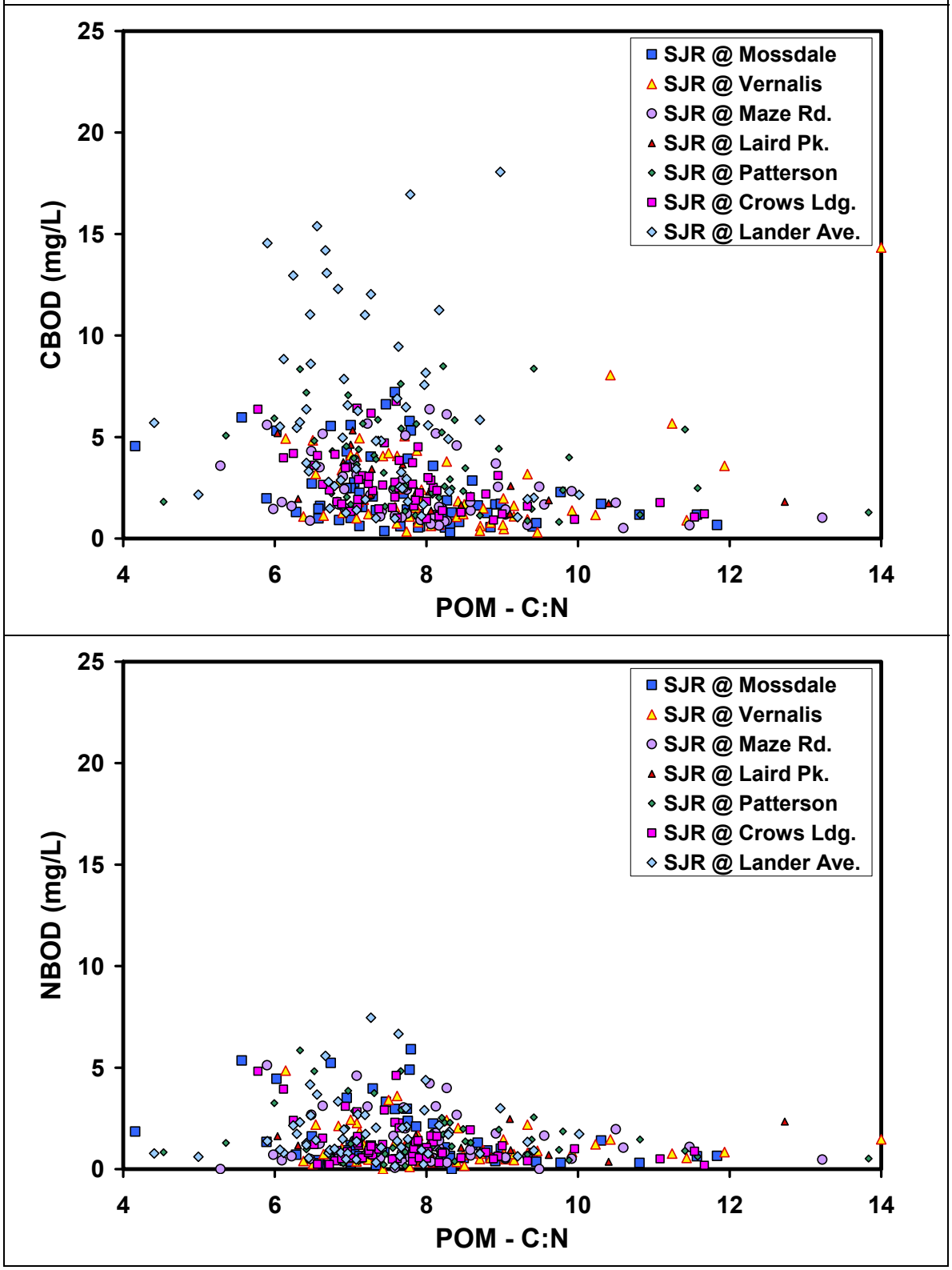

Figure 46. Correlation of C:N of POM and BOD for selected drain, creek, and wetlands sites. Different site types have similar ranges of BOD values. However, samples with high C:N have lower BOD values than samples with low C:N. Mud Slough, Los Banos Creek, and San Luis Drain have higher BOD concentrations than Salt Slough.

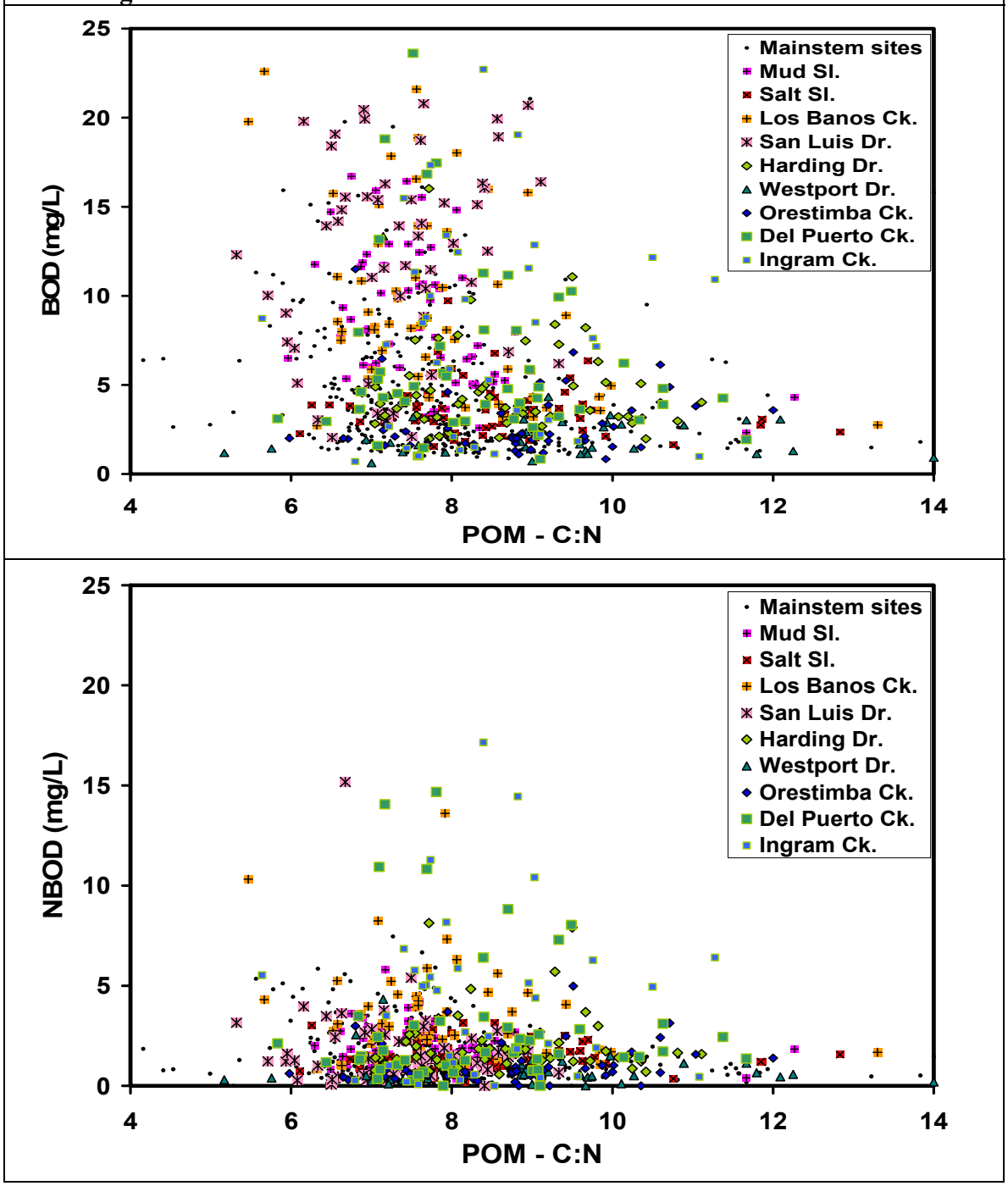

Figure 47. Relative contributions of different kinds of POM to the different sites, based on the criteria listed in the legend. Within each group of sites, sites are listed in order of upstream (right) to downstream (left). Each bar reflects an average of 53 samples, with a range of 14 to 69 samples for each site. Note that about 10% of the samples did not have BOD measurements, resulting in "unclassified" POM samples.

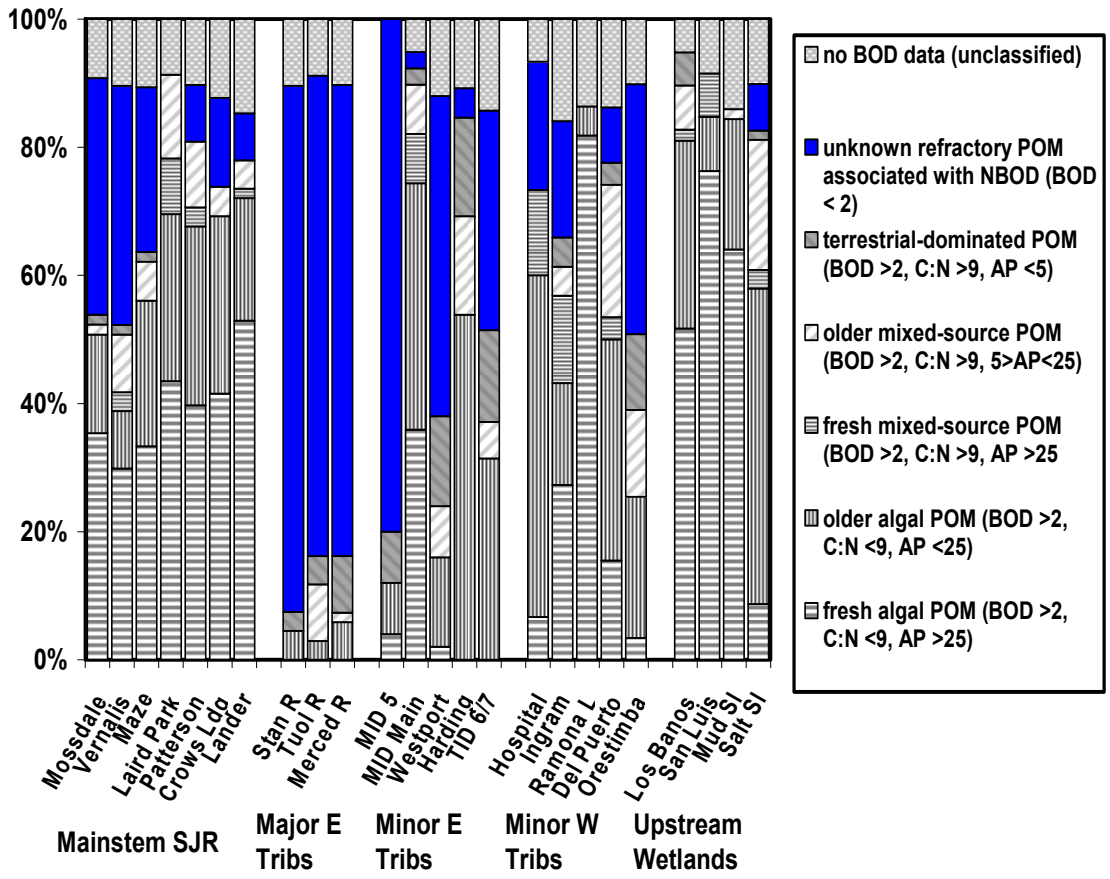

Figure 48. Relative contributions of different kinds of POM to various infrequently sampled sites, based on the criteria listed in the legend. Each bar reflects an average of 3 samples, with a range of 1-9 samples for each site. Within each group of sites, sites are listed in order of DO#. Note that 10-50% of the samples did not have BOD measurements, resulting in "unclassified" POM samples.

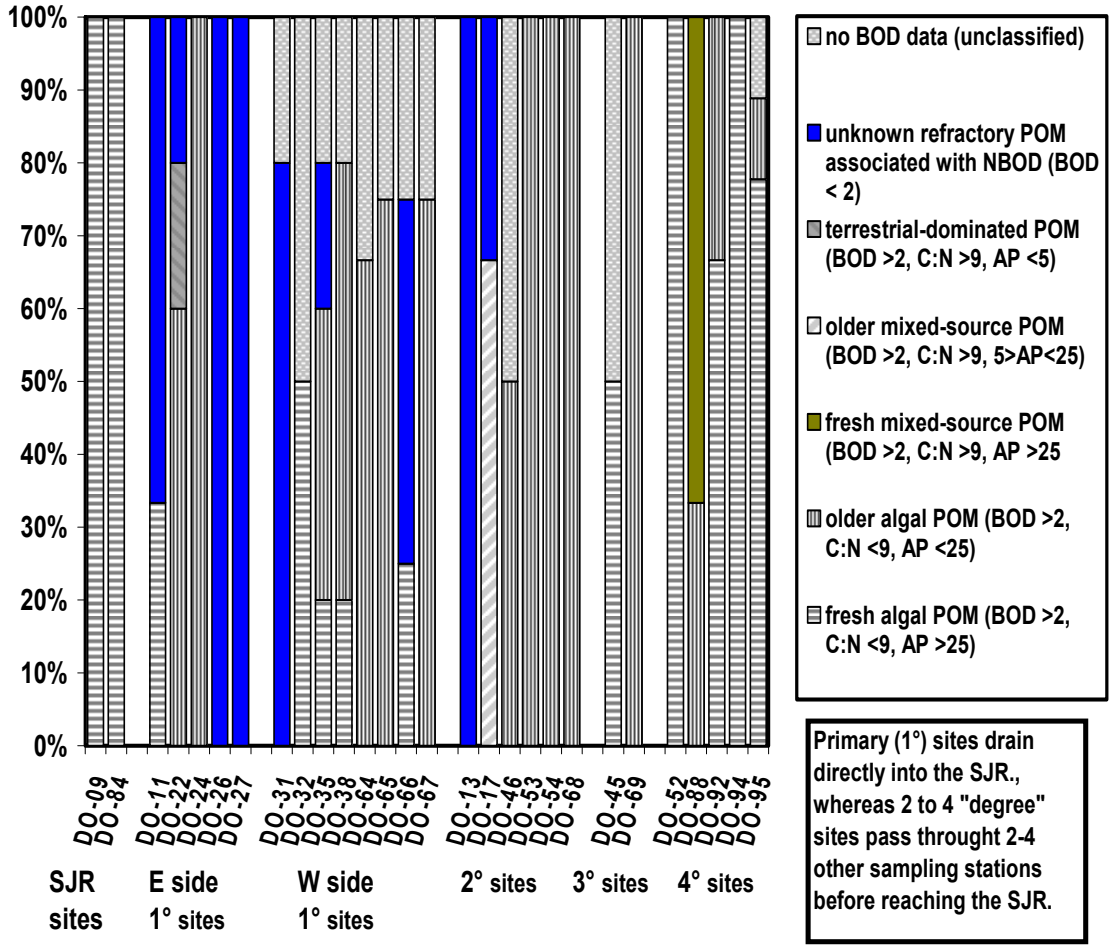

Figure 49. Downstream changes in nitrate concentration and $\delta^{15}N$ of NO3 and POM for mainstem, major tributary, and wetlands sites for high flow periods in March 31, 2005 (top) and April 21, 2005 (bottom). $\delta^{15}N$ values for wetlands sites are circled in green, and $\delta^{15}N$ values of POM and NO3 for tributary sites are connected with yellow vertical bands. The X axis is latitude of the site.

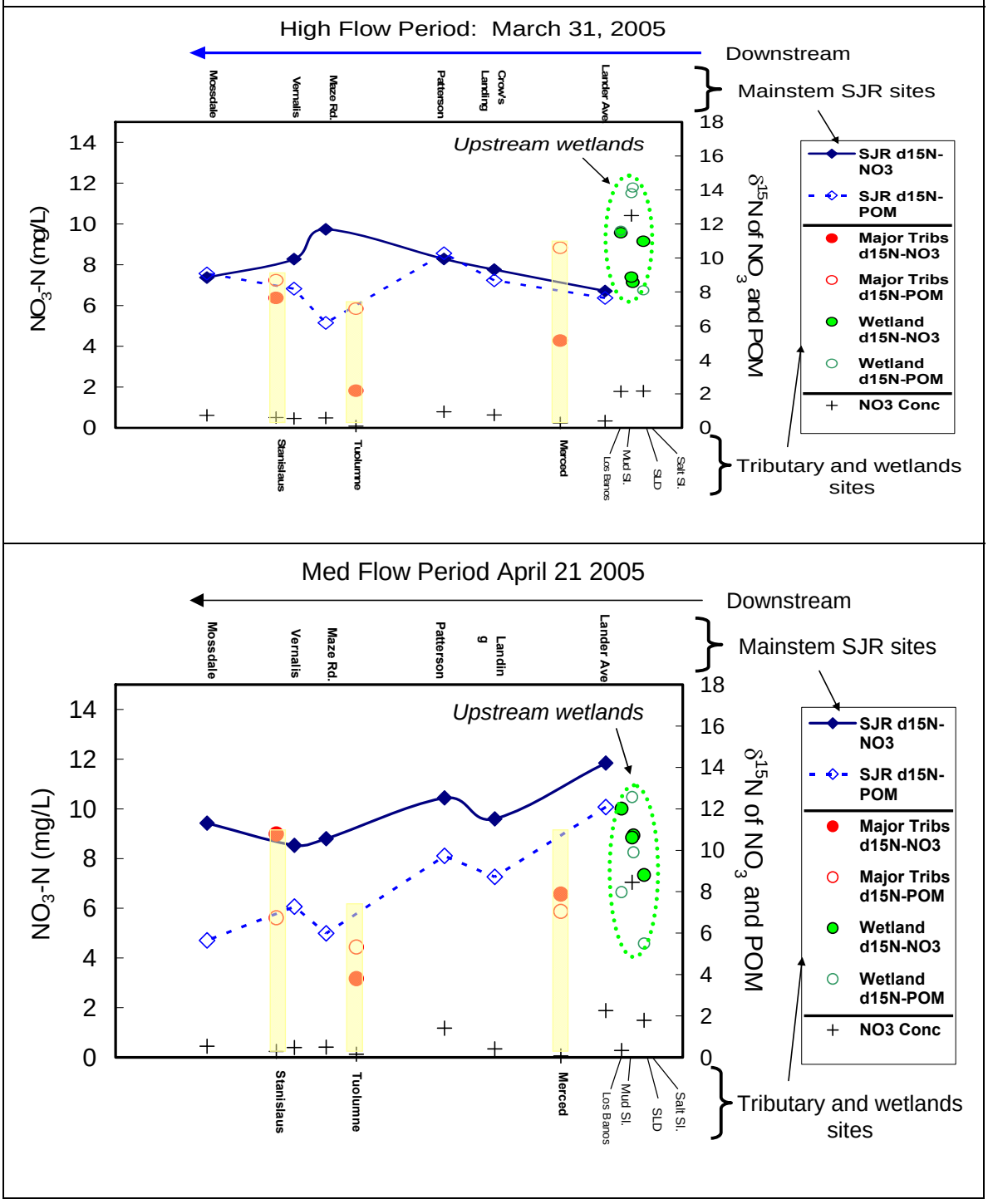

Figure 50. Downstream changes in nitrate concentration and $\delta^{15}N$ of NO3 and POM for mainstem, major tributary, and wetlands sites for high flow periods in May 5, 2005 (top) and May 18, 2005 (bottom). $\delta^{15}N$ values for wetlands sites are circled in green, and $\delta^{15}N$ values of POM and NO3 for tributary sites are connected with yellow vertical bands. The X axis is latitude of the site.

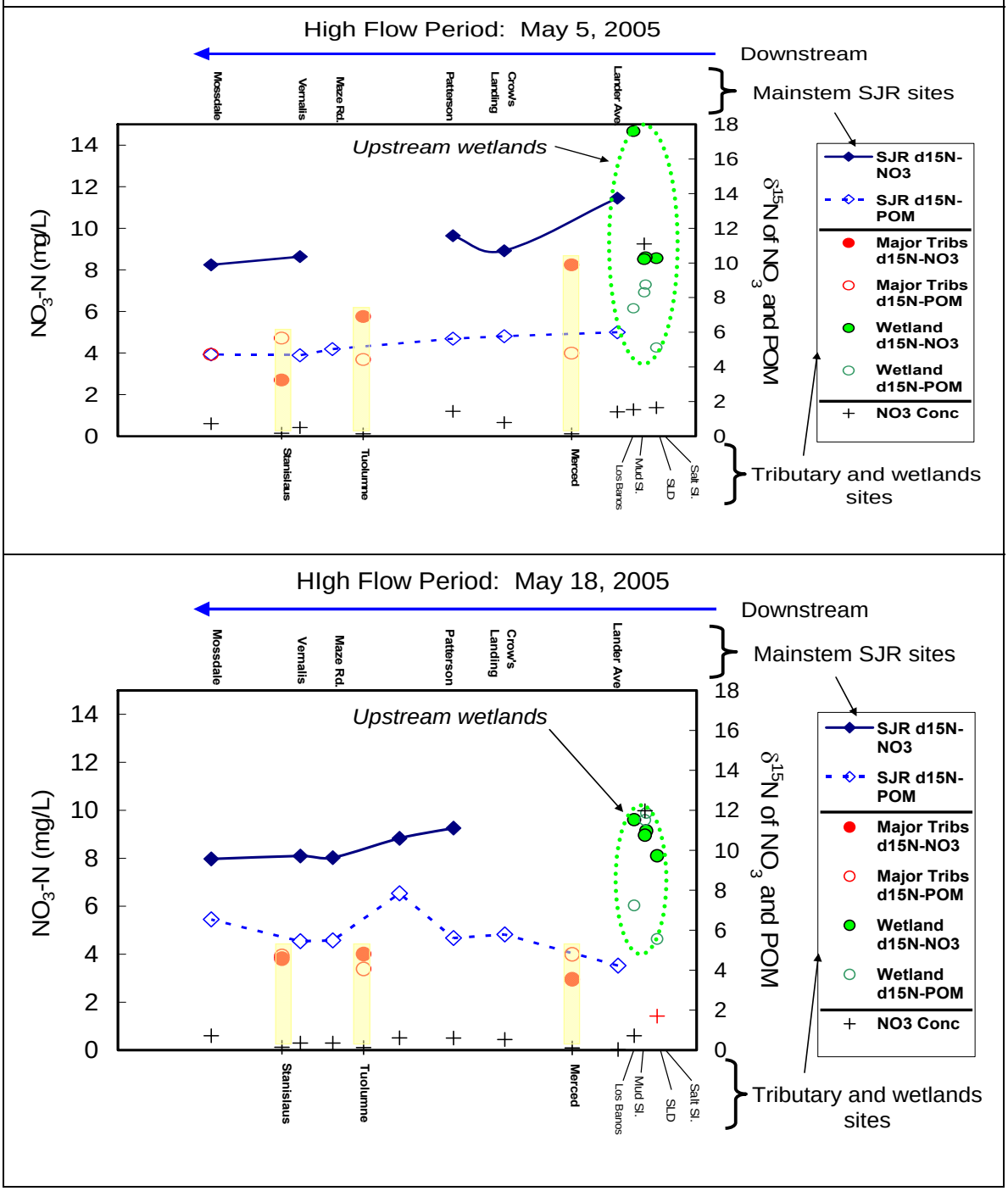

Figure 51. Downstream changes in nitrate concentration and $\delta^{15}N$ of NO3 and POM for mainstem, major tributary, and wetlands sites for low flow periods in August 25, 2006 (top) and February 1, 2007 (bottom). $\delta^{15}N$ values for wetlands sites are circled in green, and $\delta^{15}N$ values of POM and NO3 for tributary sites are connected with yellow vertical bands. The X axis is latitude of the site.

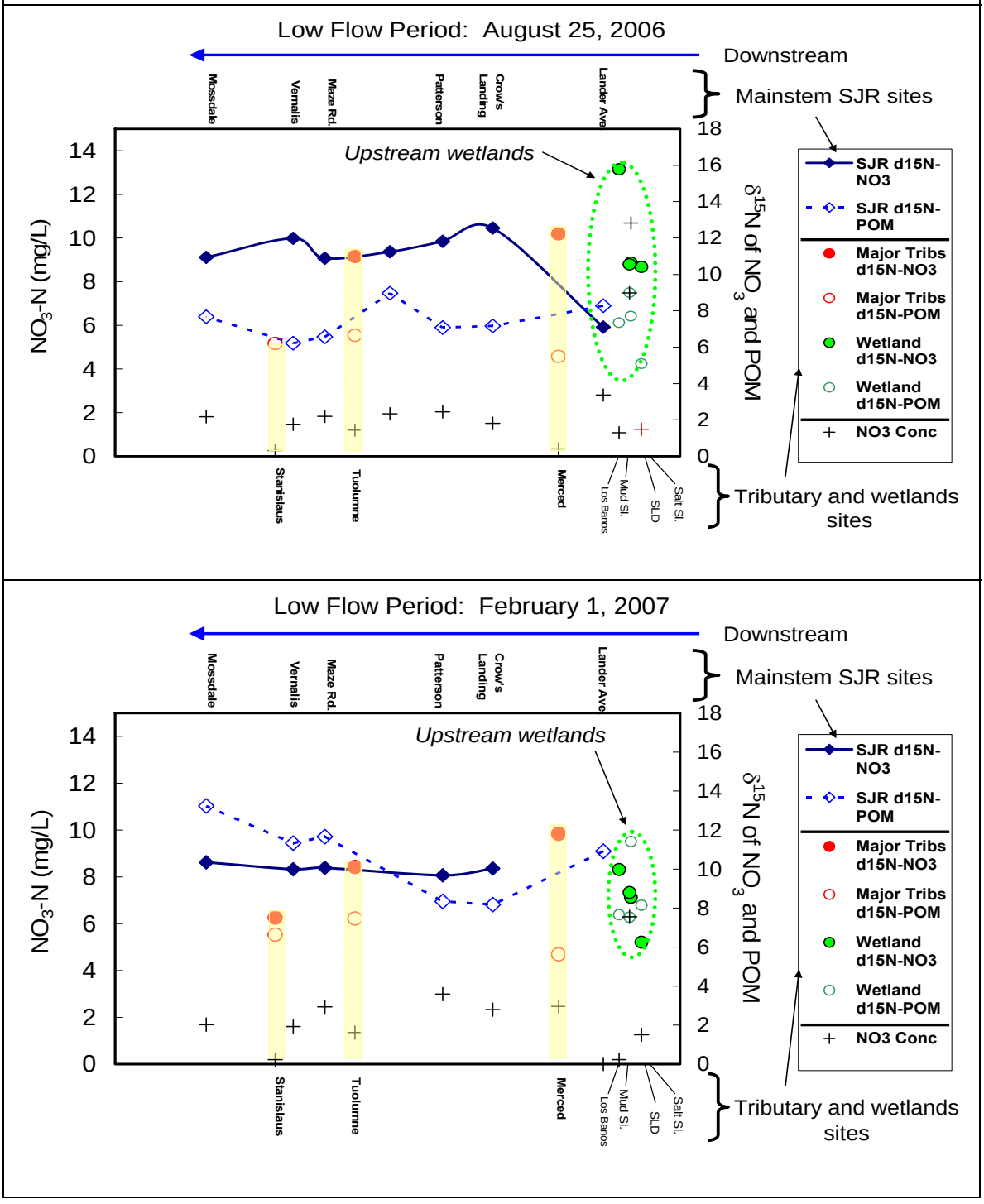

Figure 52. Distribution of nitrate isotope values for selected sites, with expected ranges shown for various potential nitrate sources.

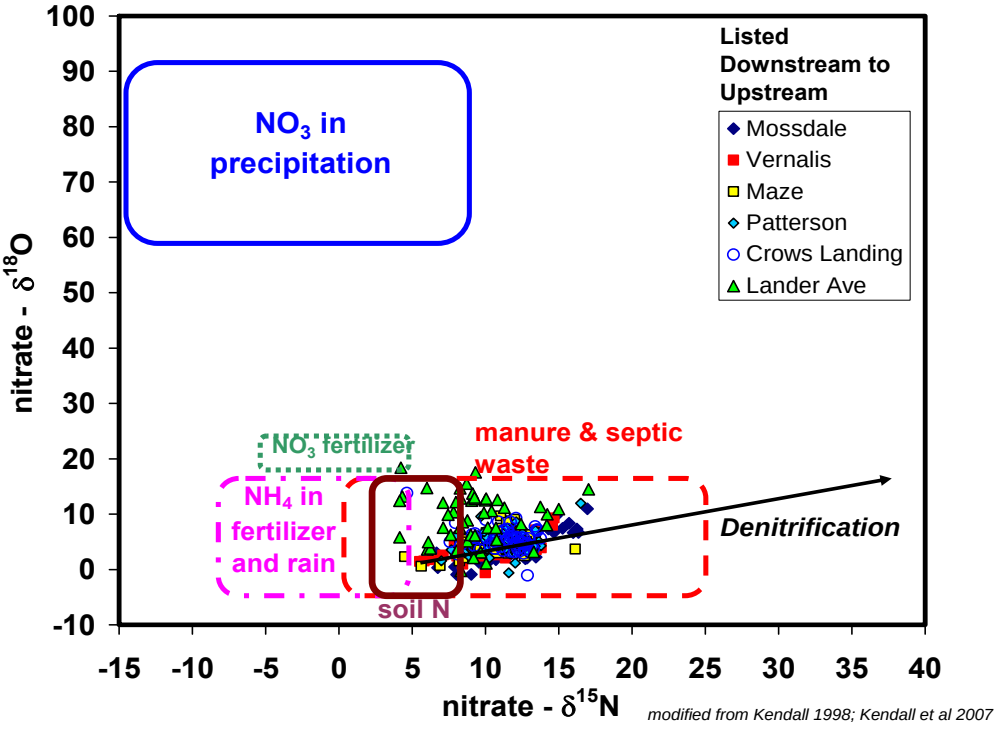

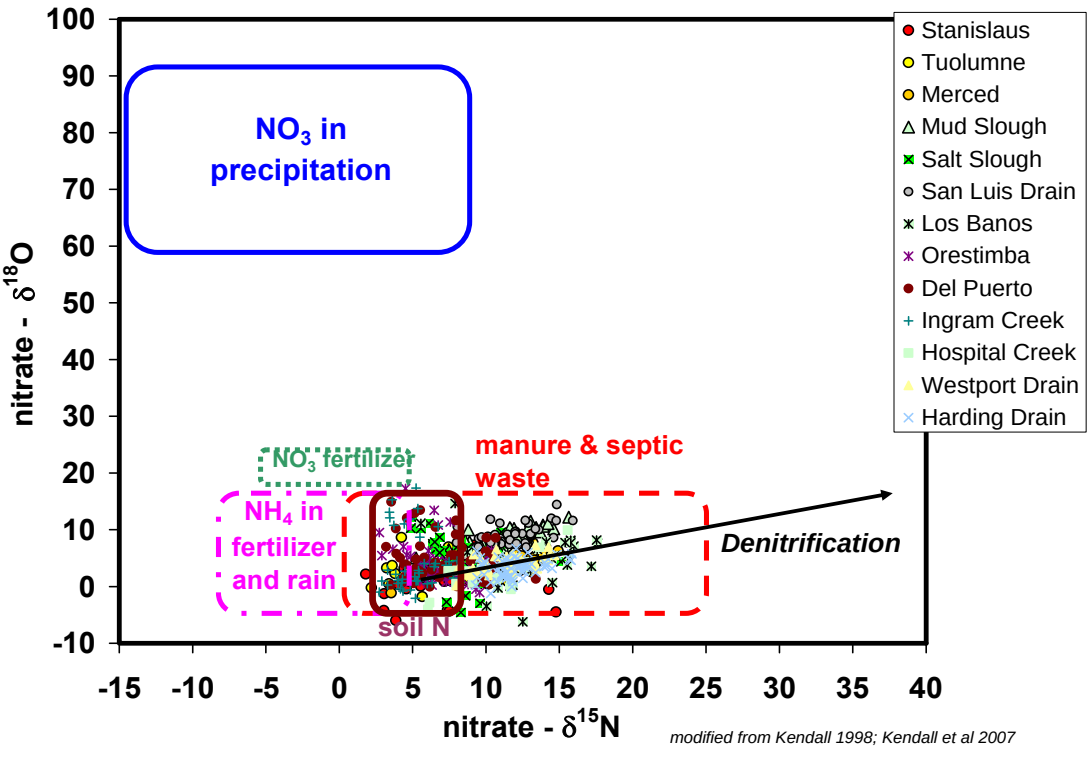

Figure 53. Detail of the nitrate isotope composition of samples from the mainstem SJR.

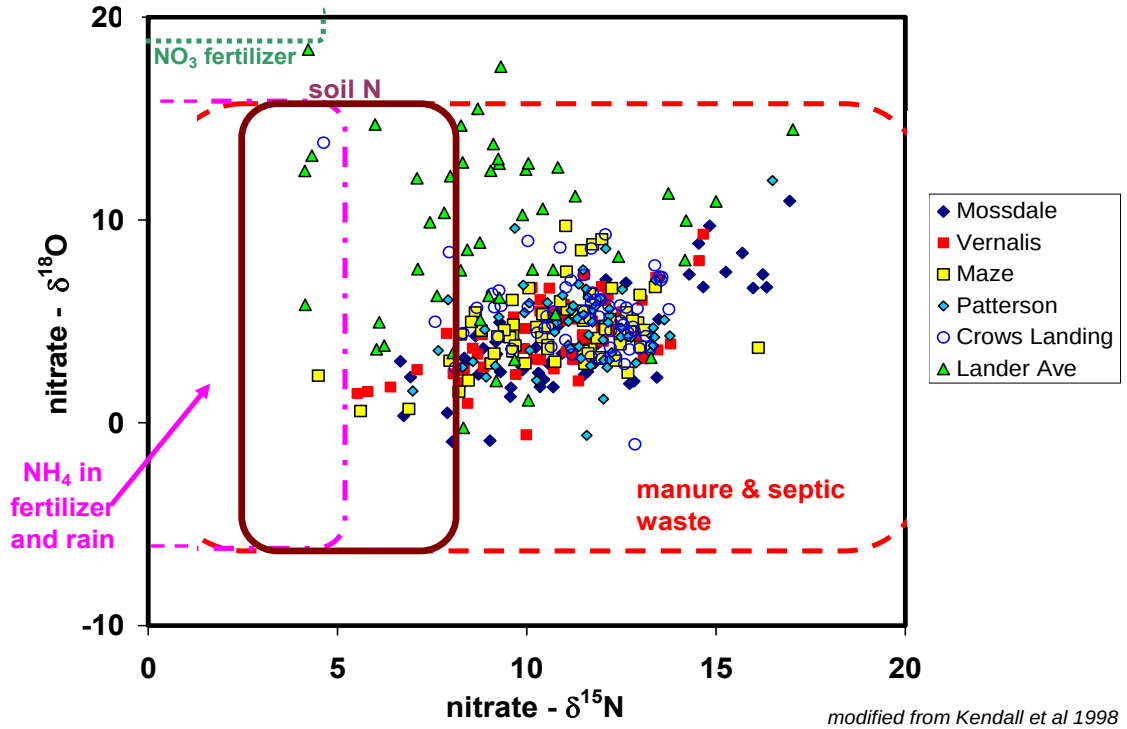

Figure 54. $\delta^{15}N\text{-}NO_3$ upstream (Crows Landing) and downstream (Mossdale) in the SJR. Values for the Stanislaus River are also shown, since this is a major water source upstream of Mossdale and Vernalis.

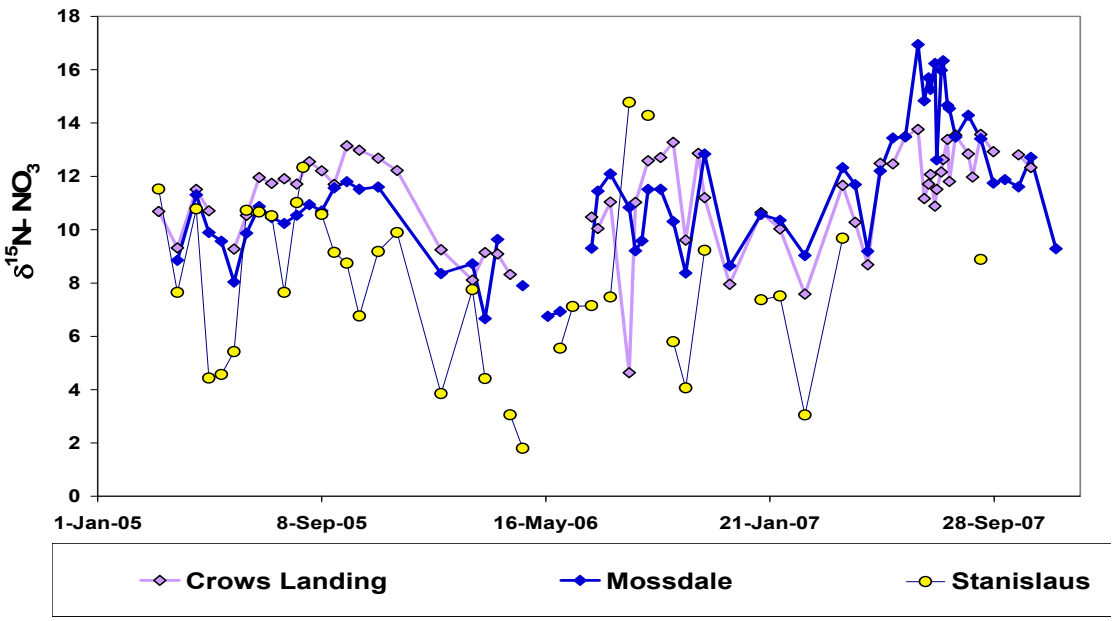

Figure 55. Downstream nitrate isotope dynamics in the SJR mainstem and tributaries between June 7 and September 27. During this period, $\delta^{15}N\text{-}NO_3$ values at the downstream SJR sites increase in relation to the upstream sites, and none of the measured tributaries have high $\delta^{15}N\text{-}NO_3$ values that could account for the increase.

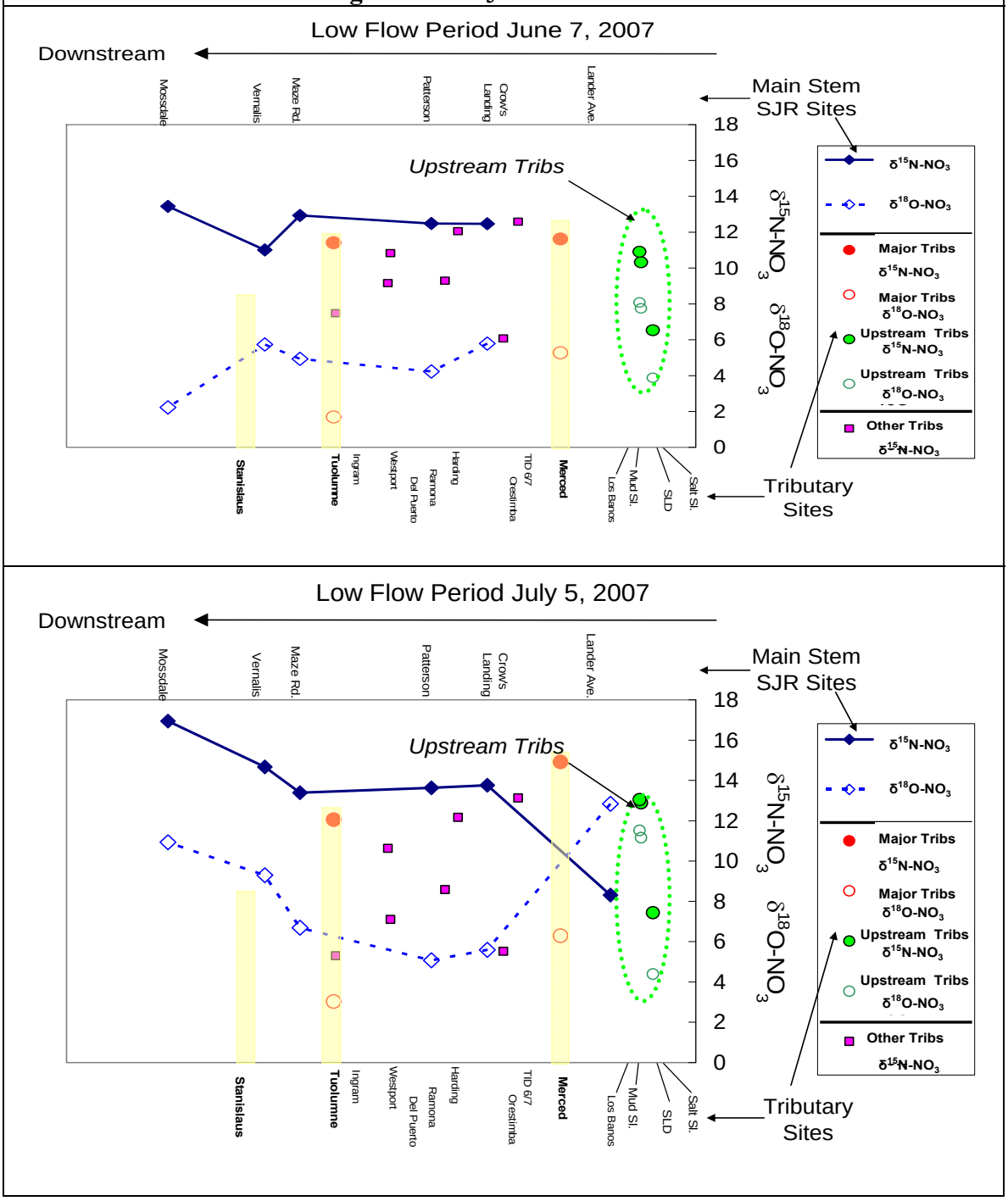

Figure 56. Downstream nitrate isotope dynamics in the SJR mainstem and tributaries between June 7 and September 27. During this period, $\delta^{15}N$ values at the downstream SJR sites increase in relation to the upstream sites, and none of the measured tributaries have high $\delta^{15}N$ values that could account for the increase.

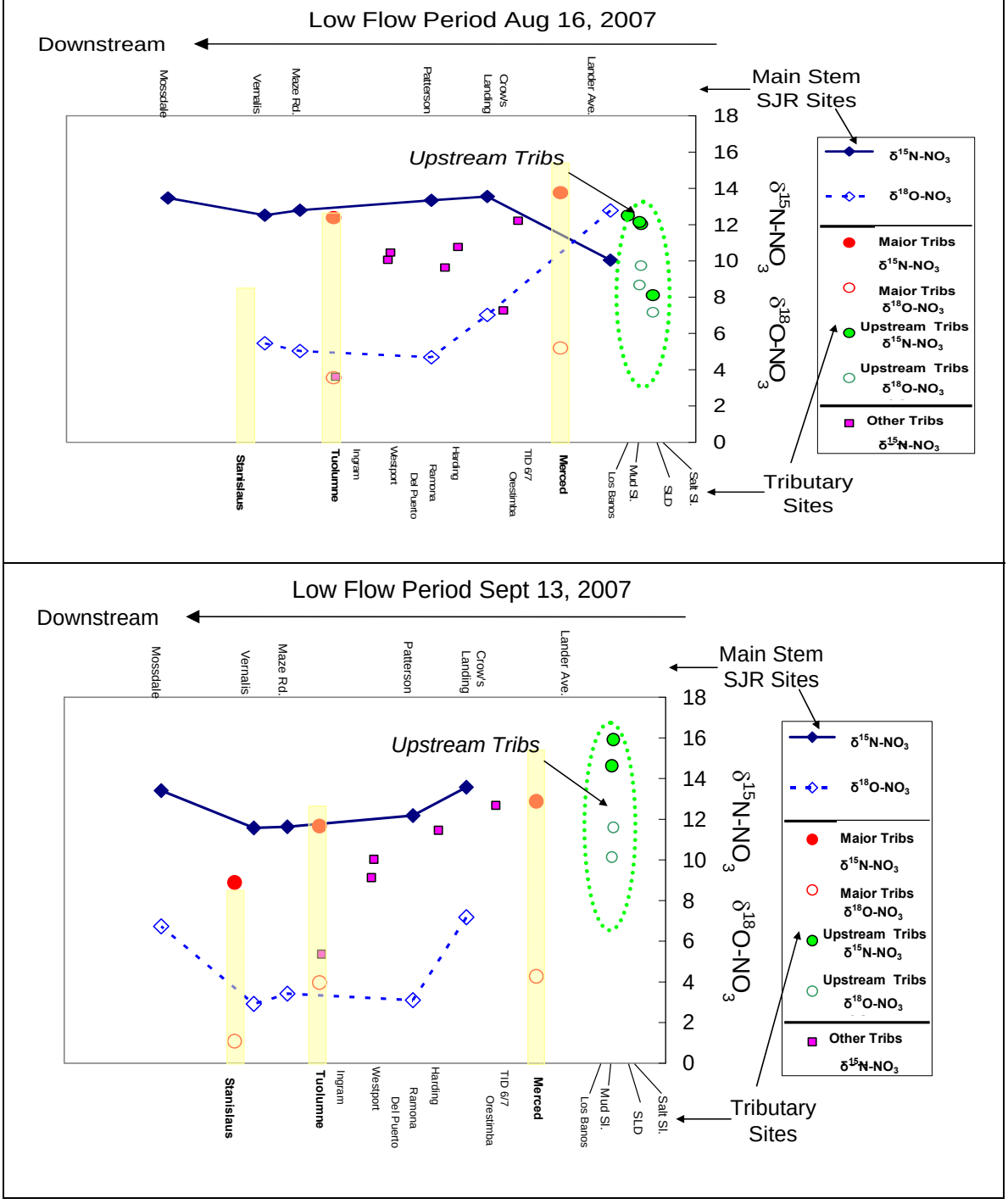

Figure 57. Downstream nitrate isotope dynamics in the SJR mainstem and tributaries between June 7 and September 27. During this period, $\delta^{15}N$ values at the downstream SJR sites increase in relation to the upstream sites, and none of the measured tributaries have high $\delta^{15}N$ values that could account for the increase.

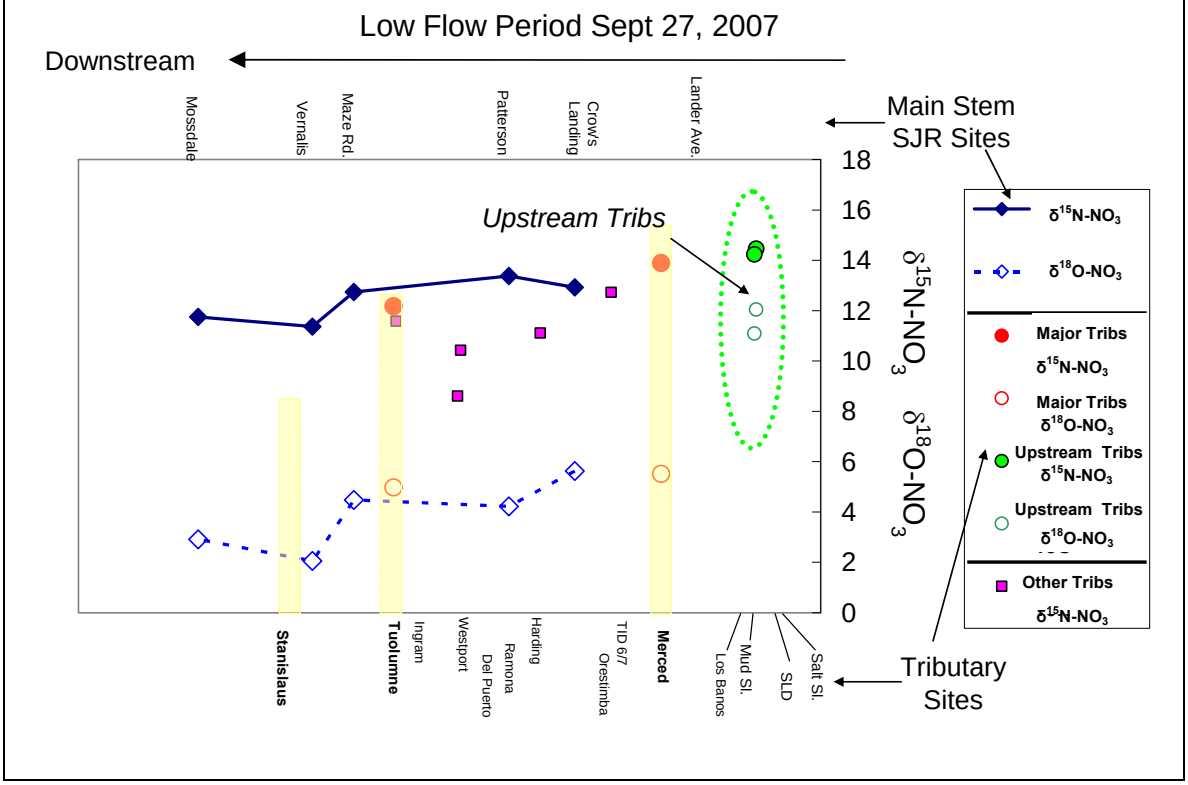

Figure 58. The curves on a plot of $\delta^{15}N$ vs NO_3 (a), resulting from mixing of two sources of nitrate with different concentrations can be distinguished from the curves resulting from denitrification with two different fractionations by plotting $\delta^{15}N$ vs ln NO_3 (b) where different denitrification fractionations yield straight lines whereas mixing yields a curve, and by plotting $\delta^{15}N$ vs $1/NO_3$ (c) where different denitrification fractionations yield curves whereas mixing yields a straight line. From Kendall et al. (2007).

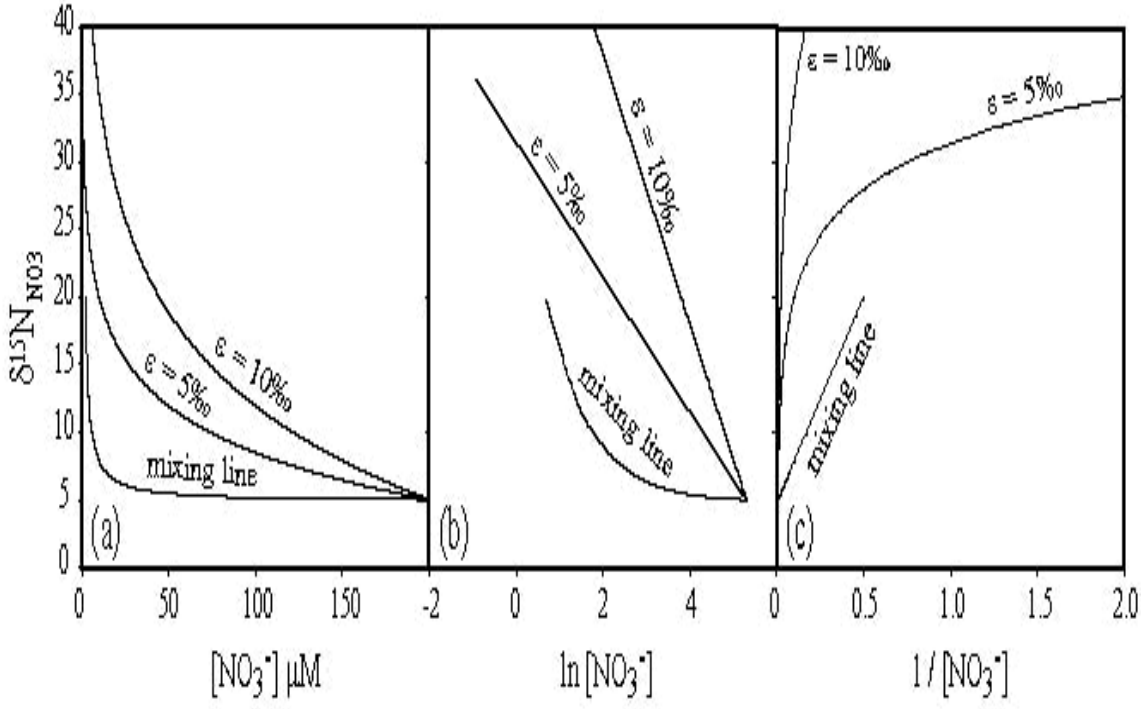

Figure 59. Relationship between $\delta^{15}N\text{-}NO_3$ and the inverse of nitrate concentration (top). The lack of linear trends suggest that the observed $\delta^{15}N\text{-}NO_3$ in the SJR mainstem cannot be explained by simple mixing between two nitrate sources. Relationship between $\delta^{15}N\text{-}NO_3$ and ln $[NO_3]$ (bottom). The lack of linear trends indicates that the $\delta^{15}N\text{-}NO_3$ in the SJR mainstem cannot be explained only by uptake or denitrification, but the data do not rule out nitrification or input of multiple nitrate sources with high $\delta^{15}N$ values.

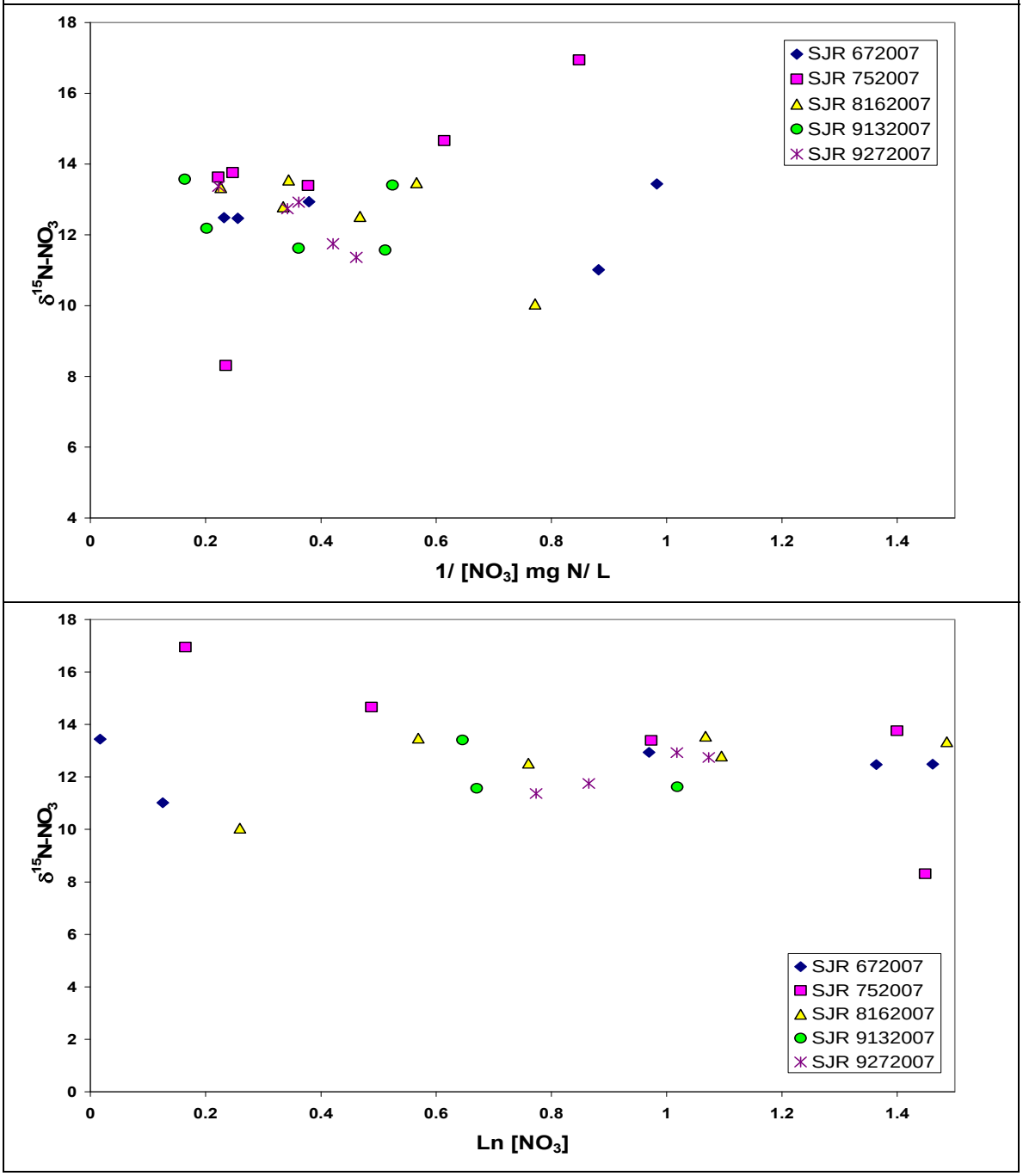

Figure 60. Temporal patterns in the $\delta^{15}N$, $\delta^{13}C$, and C:N of POM for the mainstem SJR at Mossdale (top) and Vernalis (bottom).

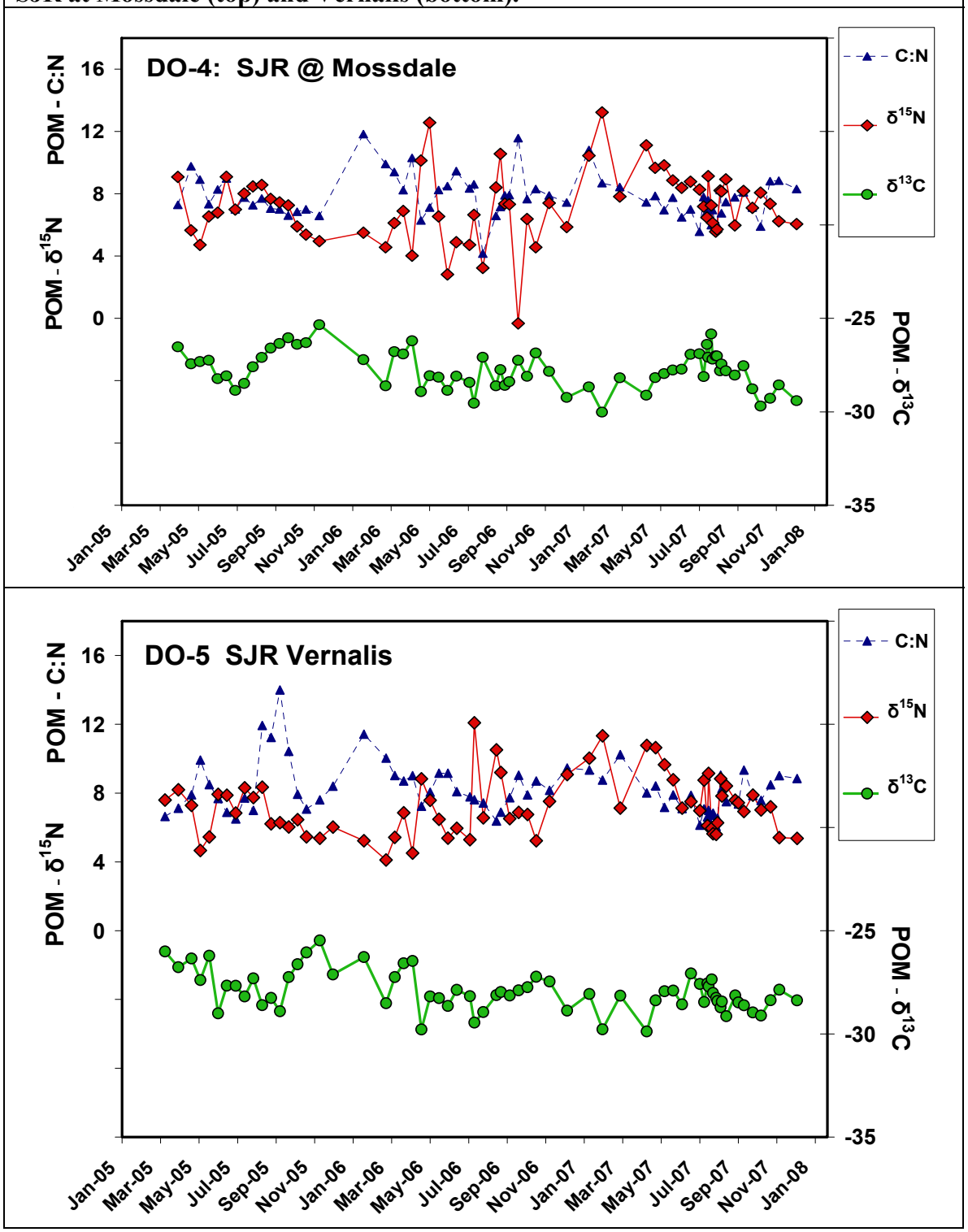

Figure 61. Temporal patterns in the $\delta^{15}N$, $\delta^{13}C$, and C:N of POM for the mainstem SJR at Crows Landing (top) and Lander (bottom).

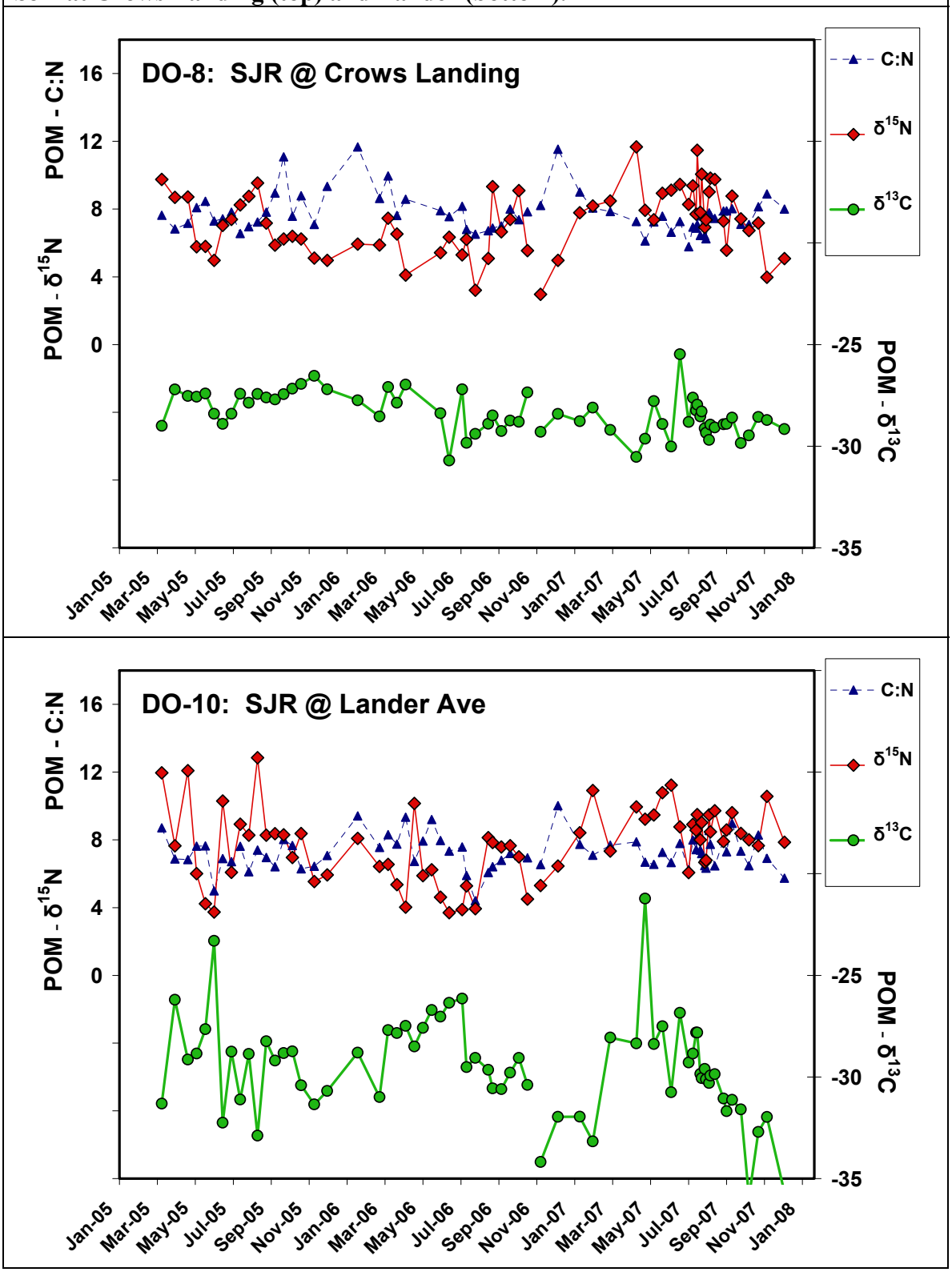

Figure 62. Temporal patterns in the $\delta^{15}N$, $\delta^{13}C$, and C:N of POM for upstream wetlands sites at Mud Slough (top) and Salt Slough (bottom).

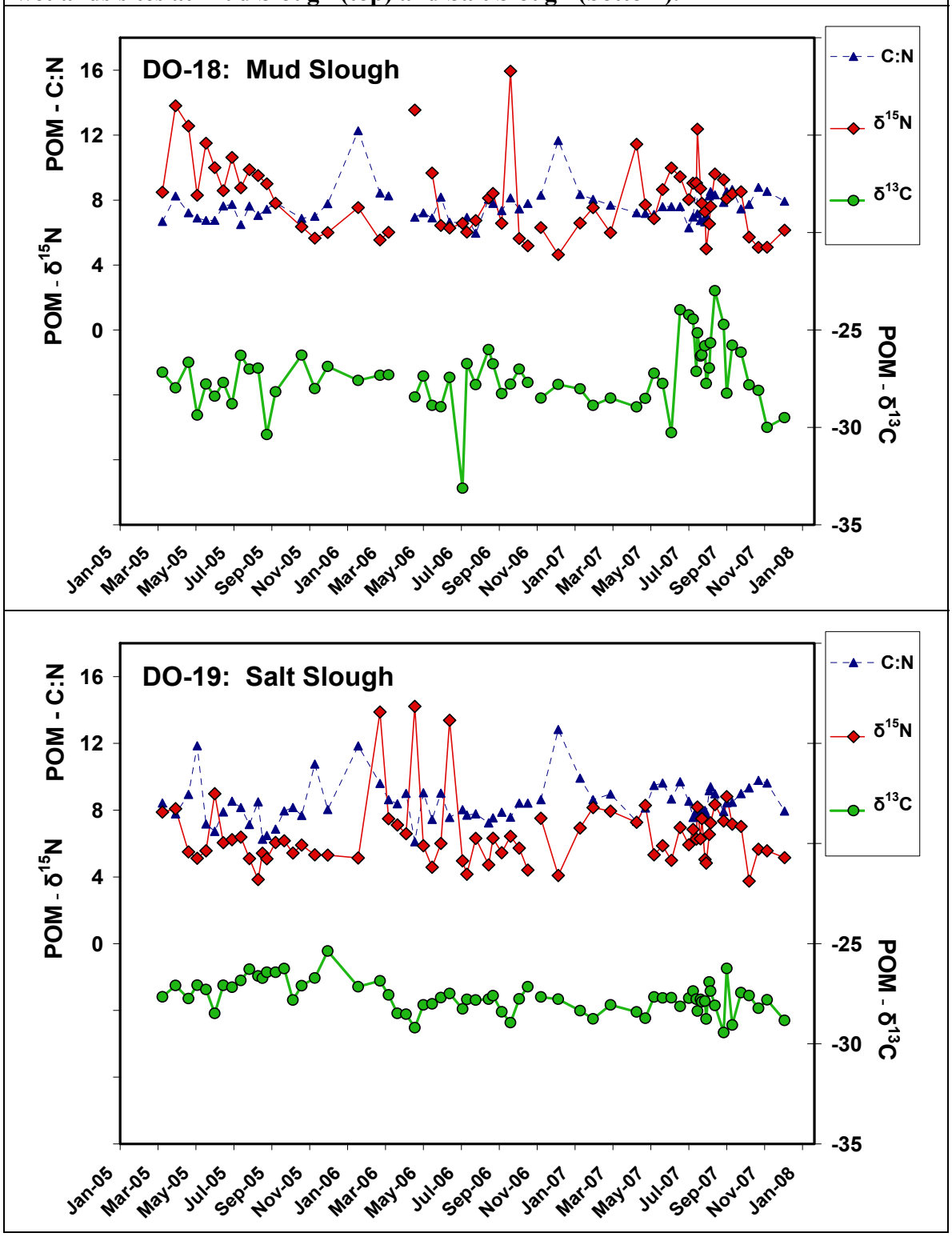

Figure 63. Temporal patterns in the $\delta^{15}N$, $\delta^{13}C$, and C:N of POM for the San Luis Drain.

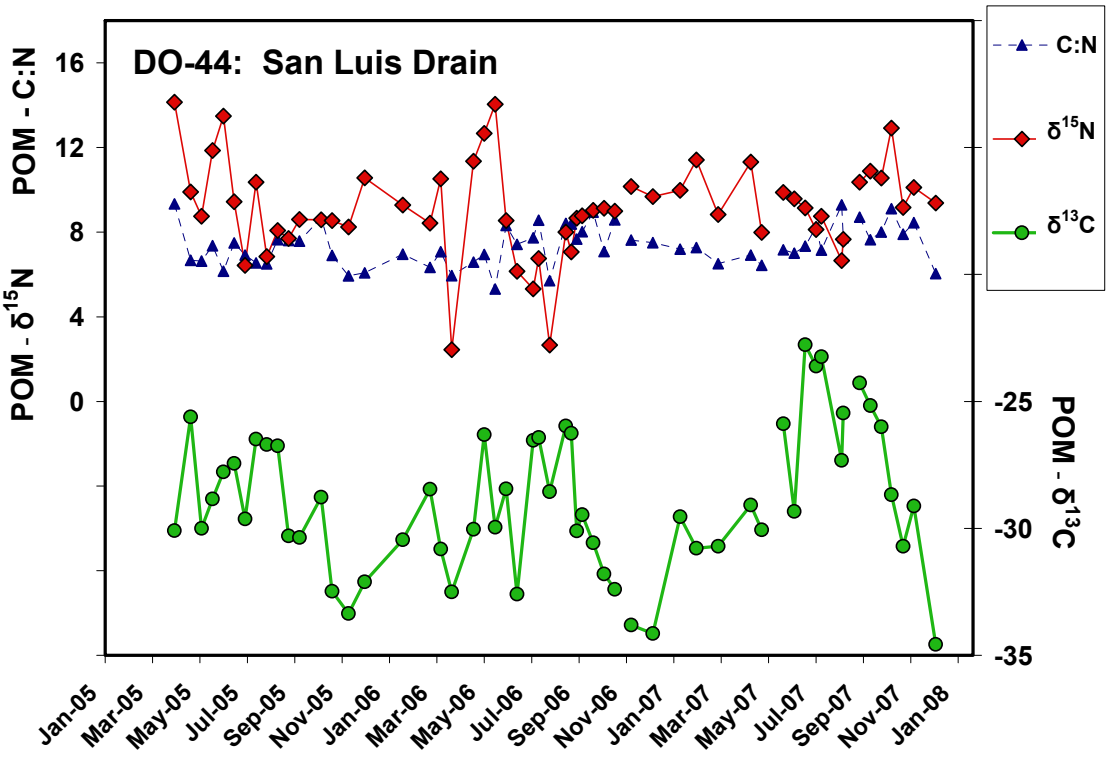

Figure 64. Temporal patterns in nitrate $\delta^{15}N$ and $\delta^{18}O$, NO_3 concentration, and water $\delta^{18}O$ water for two east-side drains at Westport (top) and Harding Drain (bottom).

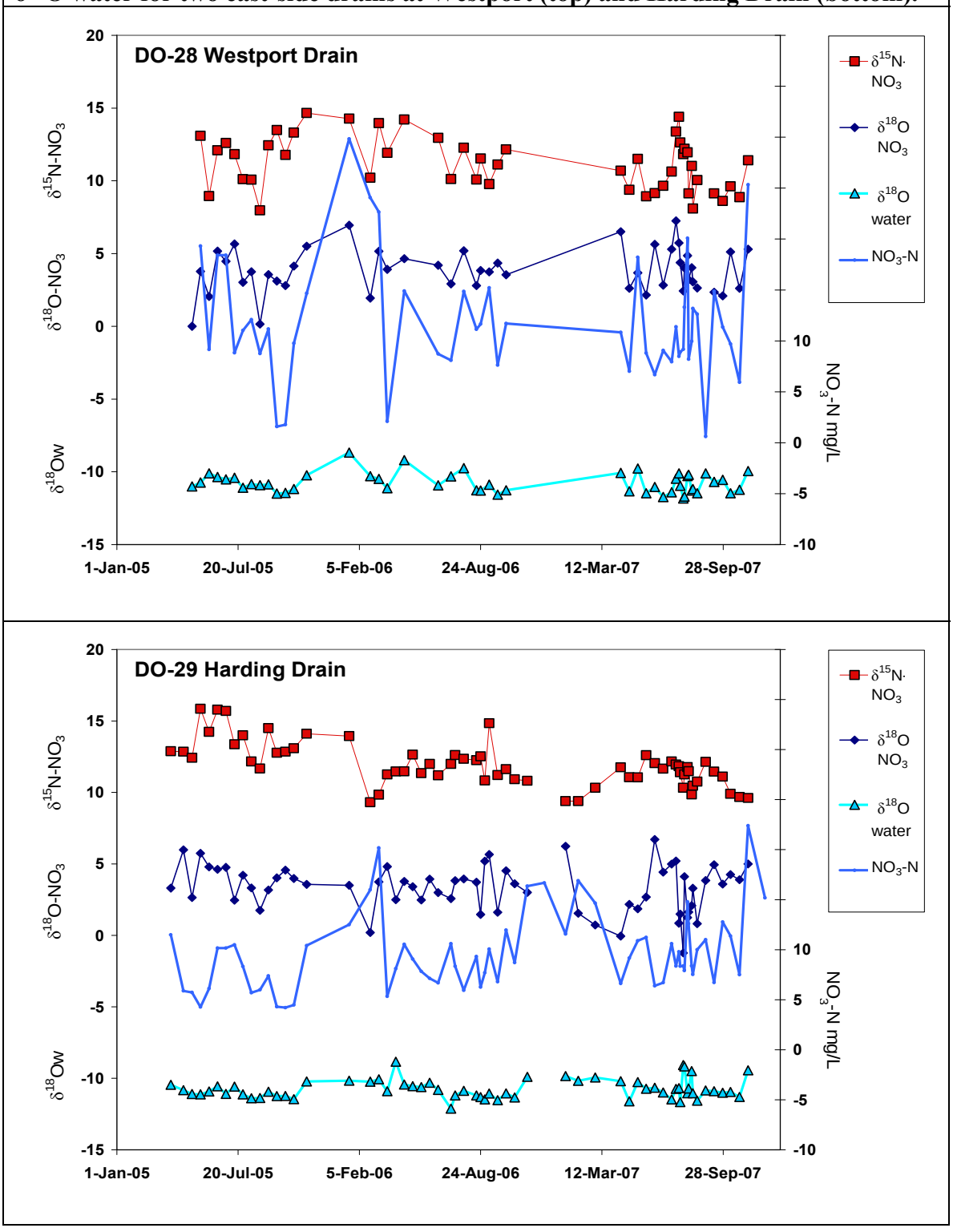

Figure 65. Nitrate isotope source diagram for selected upstream mixed wetland and agricultural sites. Mud Slough and San Luis Drain both show evidence of either denitrification or nitrate uptake, while Salt Slough shows a very different pattern.

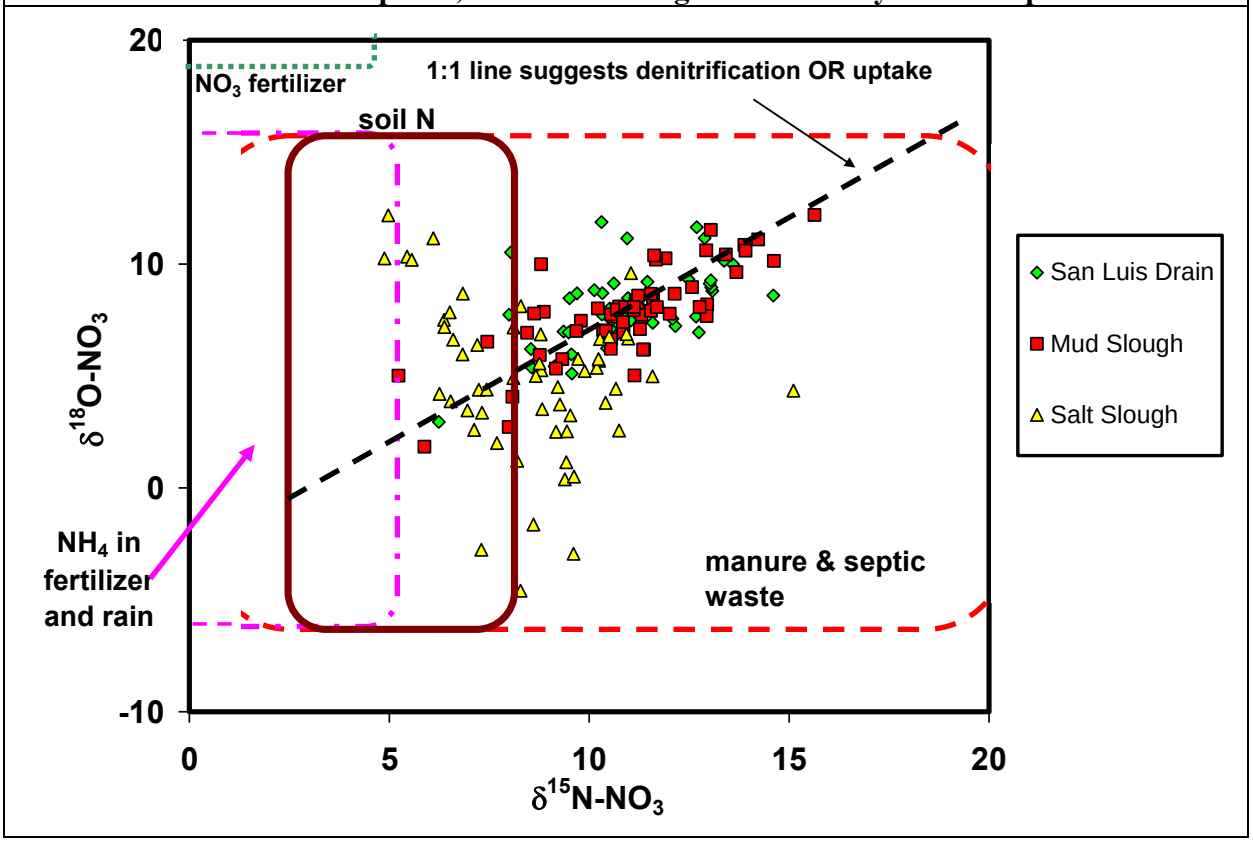

Figure 65. Nitrate isotope source diagram for the west-side tributary sites. Only nitrate in Hospital Creek falls close to the 1:1 line, while the other three sites show a decoupling between the two isotopes, with $\delta^{18}O\text{-}NO_3$ showing increased values not related to changes in $\delta^{15}N\text{-}NO_3$.

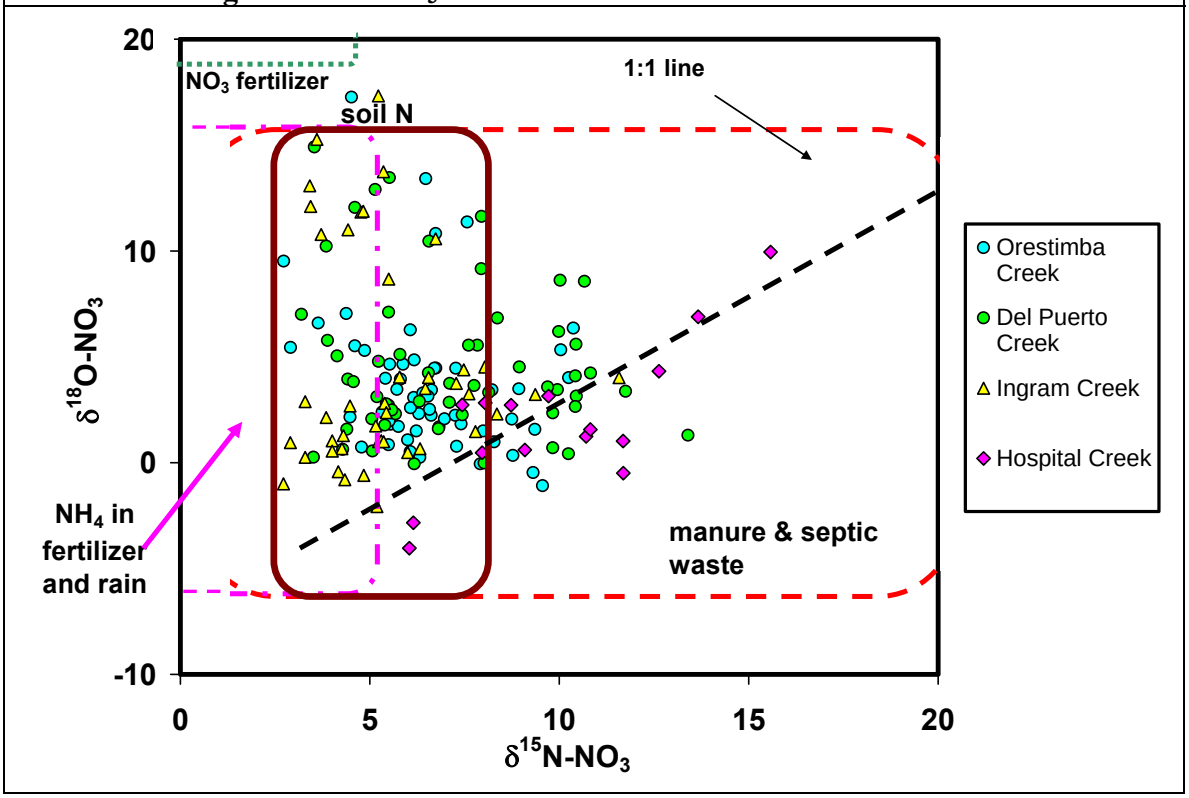

Figure 67. The $\delta^{18}O_p$-$\delta^{18}Ow$ as a function of temperature for water samples collected in the San Joaquin River watershed in November 2006. The use of $\delta^{18}O_p$-$\delta^{18}O_w$ for the y axis allows the equilibrium values to be plotted along a linear relationship with temperature. All except one of the samples fell outside of the expected equilibrium values.

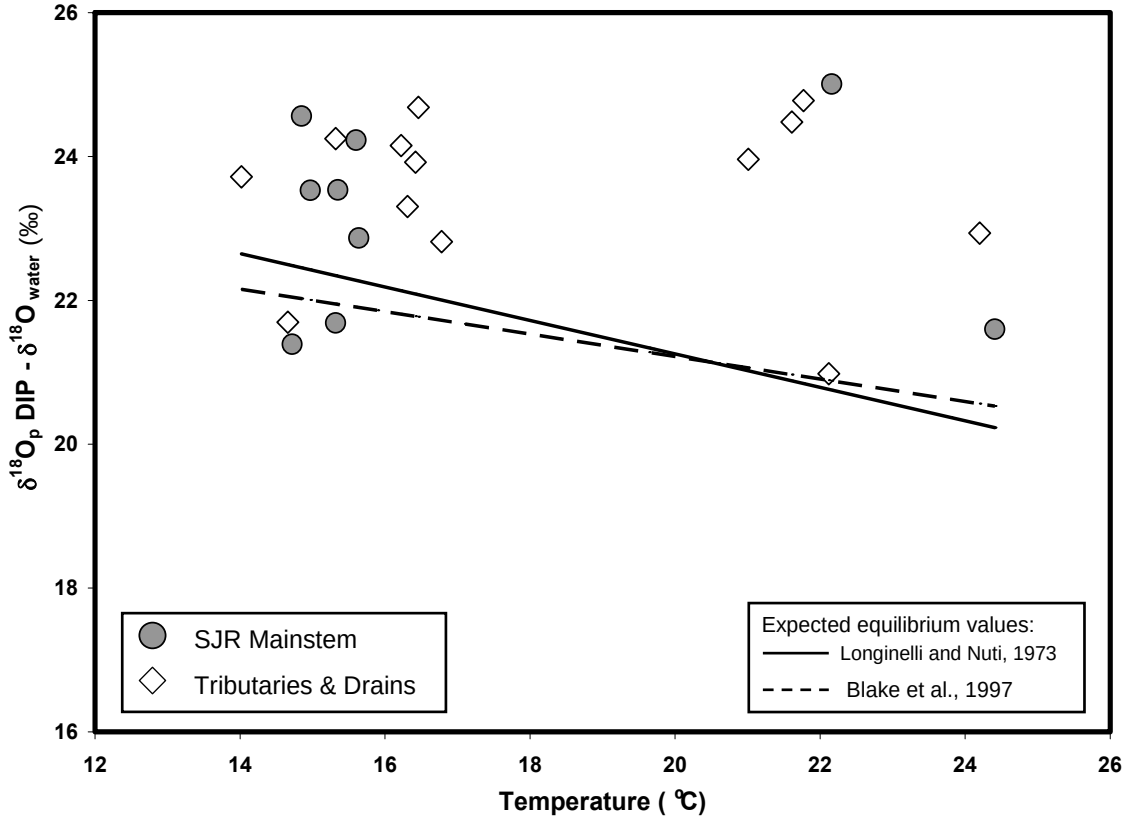

Appendix A: Methods

Sample Collection and Field Preparation

All samples used for Task 7 were collected as part of the existing monitoring program described in Task 4. At each site sampled for Task 4, two splits of water were collected for isotopic analysis; one split was filtered upon return to the laboratory and the other remained unfiltered. The unfiltered sample splits were collected in 250 mL HDPE Trace-Clean wide mouth plastic bottles, and the samples for filtration were collected in glass sampling bottles. All sample splits were stored in the dark at < 4º C until returned to the lab. The unfiltered samples were then placed in storage at -20º C prior to shipment.

The sample splits for filtration were filtered through precombusted Whatman GF/F 47mm filters (0.7 μm pore size) for POM collection within 24 hours of collection then stored at -20º C prior to shipment to the U.S. Geological Survey Isotope Tracers Laboratory in Menlo Park. The target volume filtered for POM analysis was either 1000 mL or less if four filters reached capacity prior to 1000mL. Total volume filtered was recorded for each sample, and all filters were kept at -20º C prior to shipment. All water and filter samples were shipped overnight on dry ice, and immediately placed in -20º C storage at the Isotope Tracers Lab until preparation for isotope analysis as described below.

POM Isotope and C:N Ratio Analysis

Sample filters with POM were kept frozen until preparation for analysis. The samples were prepared and analyzed following the method described in Kendall et al. (2001). Briefly, the surfaces of the filters were scraped while moist to remove the particulate organic matter. The scraped material was freeze-dried and ground in a ball grinder in order to homogenize the sample.

For analysis of $\delta^{13}C$, $\delta^{15}N$, and C:N ratio, between 10 and 20 mg of material was weighed out into silver capsules, depending upon the estimated amount of C and N in the sample. Any samples for which the initial analysis showed extremely high amounts of C and/or N were re-weighed and re-run using even less material (5-10mg). The material in the open capsules was moistened with a drop of organic-free deionized water, and then acidified under HCl fumes in a desiccator jar (without desiccant or vacuum grease) for up to 24 hours. The samples in the open capsules were then oven dried at 60 °C and folded closed. $\delta^{34}S$ analysis of POM requires a separate analysis, and samples are prepared in the same way except that since $\delta^{34}S$ analysis is not affected by the presence of carbonate material, and therefore the samples for $\delta^{34}S$ analysis do not need to be acidified and are weighed into tin boats instead.

Samples were analyzed by combustion to CO_2 and N_2 gas on a Carlo Erba 1500 or 2500 Elemental Analyzer (EA) interfaced with either an Optima or IsoPrime mass spectrometer. The resulting CO_2 and N_2 peaks were analyzed to produce values of %C, %N, $\delta^{13}C$, and $\delta^{15}N$. The raw data were corrected for instrument drift and sample size linearity using

internal standards. The $\delta^{13}C$ values are reported in ‰ relative to the VPDB standard, and the $\delta^{15}N$ values are reported in ‰ relative to the Air standard. Values of %C and %N are not reliable due to the incorporation of small amounts of the glass fiber filter. However, since the filter does not contain any C or N, the C:N ratio can be used since this reflects only the C:N ratio within the sample, and is independent of the incorporated filter mass. C:N ratios are reported as atomic ratios, not mass ratios. The analytical precision for standards is better than 0.2‰, but precisions are not as good for samples because of problems homogenizing the POM samples. Consequently, precision for $\delta^{13}C$ and $\delta^{15}N$ of POM samples prepared by this method is <0.5 ‰, and usually <0.3 ‰.

POM samples are analyzed for $\delta^{34}S$ on the same instruments as for $\delta^{13}C$ and $\delta^{15}N$, but using different reagents in the elemental analyzer and different mass spectrometer settings. The POM is combusted to produce SO_2 and the data are reported in ‰ relative to the CDT standard. Precision for $\delta^{34}S$ of this method based on repeated measurements is <0.5 ‰, and usually <0.3 ‰.

DOC Isotope Analysis

The $\delta^{13}C$ of dissolved organic carbon was determined on water samples filtered through a Polysulfone GD/X syringe filter, which includes graded density Multigrade GMF 150 (10:1 mm) and Grade GF/F (0.7 mm) prefilters. The samples were stored chilled in pre-combusted glass amber vials containing a droplet of 85% phosphoric acid. Samples were analyzed using an automated OI TOC analyzer interfaced with an IsoPrime IRMS (St. Jean, 2003). This method first acidifies water samples to remove dissolved inorganic carbon (DIC), and then analyzes the concentration and $\delta^{13}C$ value of CO_2 obtained from persulfate oxidation of DOC. Precision of $\delta^{13}C$ analyses is ±0.3‰.

Nitrate Isotope Analysis

$\delta^{15}N$ and $\delta^{18}O$ of nitrate were measured simultaneously for each sample using the microbial denitrifier method (Sigman et al., 2001, Casciotti et al., 2002) in which the nitrate is converted quantitatively to N_2O, which is then measured for $\delta^{15}N$ and $\delta^{18}O$ on an IsoPrime continuous flow mass spectrometer. Briefly, splits of the filtered sample water were thawed and aliquots were taken based upon the nitrate concentrations reported by UC Davis. The aliquots were injected into sealed vials containing prepared colonies of *Pseudomonas aureofaciens* denitrifying bacteria and triptic soy broth media. The vials were allowed to sit overnight to allow the bacteria to convert all of the nitrate into N_2O gas. The gas in the vials was then introduced via an autosampler into the continuous flow mass spectrometer. The N_2O was analyzed for both $\delta^{15}N$ and $\delta^{18}O$, and these values were used to calculate the $\delta^{15}N$ and $\delta^{18}O$ of the nitrate in the original sample. The raw data were corrected for instrument drift, size linearity, blank contribution, and fractionation effects by using repeated analyses of six different internal standards and blanks (vials with media but no added nitrate). All samples were prepared and analyzed in duplicate on the same day, and then analyzed a third or more times until the precisions were acceptable. The $\delta^{15}N$ and $\delta^{18}O$ values are reported in ‰ relative to the Air and VSMOW standards, respectively. The analytical precision was

generally 0.2% for $\delta^{15}N$ and 0.7% for $\delta^{18}O$.

Phosphate Isotope Analysis

The $\delta^{18}O_p$of dissolved inorganic phosphate (DIP) was collected and analyzed following the procedure detailed in McLaughlin et al. (2004). $\delta^{18}O_p$ samples require larger volumes of water (4 to 8 liters, depending upon PO_4 concentration) than most of the other isotope samples, therefore these samples were collected into separate containers at the same time than the standard water sampling was conducted. For each $\delta^{18}O_p$ sample, water was collected into either 1 or 2 4 liter HDPE Nalgene bottles that were prewashed with nitric acid and Milli-Q water. The sample bottles were rinsed three times with sample water prior to filling. Samples were kept chilled in the dark until returned to the laboratory. The samples were filtered through 0.45 µm capsule filters within 24 hours of collection. Immediately after filtration, $MgCl_2$ and 10M NaOH were added in order to strip all of the DIP from the water and bind it into a magnesium hydroxide ($Mg(OH)_2$)) flocculent (Karl and Tien, 1992; Thomson-Bulldis and Karl, 1998). The flocculent was allowed to settle for several hours, and the overlying water was siphoned off. The flocculent was then transferred into 250mL containers by successive centrifugation and removal of overlying water. Once all of the flocculent was transferred into the smaller containers, it was dissolved in concentrated acetic acid and 10M nitric acid, releasing the DIP back into solution. The DIP was then purified and precipitated as silver nitrate following the McLaughlin et al. (2006) procedure.

Isotopic analyses were conducted on a Eurovector elemental analyzer coupled to an Optima mass spectrometer. The silver phosphate was thermally decomposed in the presence of carbon to form carbon monoxide, which was then analyzed by isotope ratio mass spectrometry (IRMS) for masses 28, 29 and 30. Results were calibrated and precision monitored using calibrated standards. All oxygen isotopic measurements are reported in the standard delta notation in per mil units (‰) with respect to Vienna Standard Mean Ocean Water (VSMOW); the precision of $\delta^{18}O_p$is approximately ± 0.3 ‰.

Water Isotope Analysis

Sample splits of the filtered water for water isotope analysis were thawed and poured off into 20mL glass vials with polyseal caps at the Isotope Tracers Laboratory. $\delta^{18}O$-water was measured using two different methods: a standard CO_2 equilibration method and a laser spectroscopy method, while $\delta^{2}H$-water was measured solely by laser spectroscopy. $\delta^{18}O$-water was first measured by equilibrating a 2mL sample aliquot with CO_2 gas under controlled temperature conditions using the method of Epstein and Mayeda (1953), and the resulting CO_2 was analyzed for isotopic composition using a Finnigan MAT 251 mass spectrometer. Raw data were corrected for instrument drift and temperature-dependent isotope fractionation before reporting the final data. The $\delta^{18}O$ values are reported in ‰ relative to the VSMOW standard. Precision of this method based on repeated standard measurements is <0.2 ‰.

Both $\delta^{18}O$ and $\delta^{2}H$ of water were measured using laser spectroscopy on a Los Gatos Research DLT-100 Liquid-Water Isotope Analyzer, using a modification of the method

described in Lis et al. (2008). This instrument uses near infrared absorption spectroscopy to determine the isotopic composition of water samples. 2mL aliquots of sample were loaded into 2mL glass vials with split-cap septa and placed into the auto-sampler. For each sample, 4 to 6 sequential 1.2 μL aliquots of sample were injected into the instrument through the auto-sampler. Two internal water standards were measured after every 5th sample. The results for the first aliquot were discarded to eliminate any memory effect, the remaining aliquots were examined for additional outliers, and the acceptable aliquots were averaged and corrected for per mil scale linearity. Precision of this method based on repeated standard measurements is <1 ‰.

The two methods used for water isotope analysis provide different advantages. The CO_2 equilibration method for $\delta^{18}O$-water has higher precision (<0.2 ‰) than the laser spectroscopy method (<1 ‰). However, the laser spectroscopy method allows for the simultaneous measurement of both $\delta^{18}O$ and $\delta^{2}H$-water, and has higher sample throughput. For both methods, the data are normalized to the same two standards. A total of 786 (55% of all samples) water samples were analyzed for $\delta^{18}O$-water using both the CO_2 equilibration method and laser spectroscopy. The average difference between the two results was 0.3 ‰, which is within the analytical precision of the laser spectroscopy method. All water samples collected in 2007 were analyzed for $\delta^{18}O$-water using only laser spectroscopy due to a combination of instrument problems with the Finnigan MAT 251, and the large number of samples, which required a method with higher throughput than the CO_2 equilibration method. Use of the laser spectroscopy method allowed us to analyze all the collected water samples, rather than just the minimum number of samples required by the contract.

Sulfate Isotope Analysis

250 to 500mL of frozen filtered archived water samples were used for sulfate isotope analysis. Samples were prepared according to the method described in Shanley et al. (2005). Samples were adjusted to a pH of approximately 3 with hydrochloric acid, and 5 ml of 1M barium chloride solution was added to each sample in order to precipitate barium sulfate. Samples were then boiled for approximately 10 minutes to enhance barium sulfate crystal growth in order to easily extract the crystals during filtration. The barium sulfate precipitate was filtered onto pre-combusted glass fiber filters and then oven dried overnight at about 100ºC.

For sulfur analysis, approximately 0.8 mg of barium sulfate was weighed into silver boats. Vanadium pentoxide was added to the boat to enhance sample combustion. The samples were combusted on a Carlo Erba elemental analyzer, which converts the sample to SO_2, which is analyzed for sulfur isotopic composition on an Optima mass spectrometer. Samples were corrected to CDT using standard material NBS-127 (at +21.3‰), along with two in-house standards. The raw data were corrected for instrument drift and sample size linearity using multiple weights of the NBS-127 standard. A detailed description of the analytical procedure is given in Fry et al. (2002).

For sulfate oxygen isotope analysis, approximately 0.1 mg of barium sulfate was weighed into silver boats. Nickelized carbon was added to enhance sample combustion. The samples were combusted on a Eurovector elemental analyzer, which converted the sample to CO,

which is analyzed for oxygen isotopic composition on a GVI Optima Mass Spectrometer. Samples were corrected to standard NBS-127 using a value of +8.6‰. The raw data were corrected for instrument drift and sample size linearity using multiple weights of the NBS-127 standard

Quality Control and Analytical Precision

Replicate laboratory analyses were performed to determine the analytical precision for this data set associated with each type of isotope analysis (Table A1). Since additional samples and analyses will be included in the PIN700 report, the statistics reported here may be slightly different than the final statistics included in the PIN700 report. For POM and water isotope analyses, replicate samples were run approximately every 20 samples. The majority of nitrate isotope samples were run as replicate samples due to greater potential variability introduced by the sample preparation steps (processing through microbial cultures) and instrument performance.

At least one field duplicate sample was collected during each sampling event. A total of 1448 samples were collected between 2005 and 2007 for isotope analysis (not including Trip Blanks), and out of these samples, 74 were field duplicates, approximately 5% of the total samples. The site selected for the field duplicate was rotated every sampling event in order to make sure that duplicate variations were representative of the entire range of sampling sites. The absolute difference between data values was calculated to assess the variability found in field duplicates. A summary of the results of the duplicate isotope analyses is shown in Table A2. The number of field duplicates is different for each analysis because variations in concentration of each constituent (i.e., DOC, POM, NO_3) meant that some samples did not contain concentrations sufficient for specific isotope analyses.

Although the mean differences between field duplicates are typically higher than those found between laboratory replicates, the mean differences are all within acceptable ranges for each analysis. It is common for laboratory replicates to yield better agreement than field duplicates due to the combined variability of sample collection and sample processing in addition to analytical variability.

Table A1. Summary of current analytical precision of replicate isotope analysis for 2005-2007 samples (in ‰).

	$\delta^{13}C$-POM	$\delta^{15}N$-POM	$\delta^{15}N$-NO_3	$\delta^{18}O$-NO_3	$\delta^{18}O$-water	$\delta^{2}H$-water
Total replicates	247	236	941	933	305	305
Mean std. dev.	0.26	0.45	0.36	0.67	0.18	0.57

Table A2. Summary of current statistics for field duplicate samples from 2005 through 2007 (in ‰, except for C:N ratios which are unitless)

Analysis	$\delta^{13}C$-POM	$\delta^{15}N$-POM	C:N-POM	$\delta^{13}C$-DOC	$\delta^{15}N$-NO_3	$\delta^{18}O$-NO_3	$\delta^{18}O$-H_2O	$\delta^{2}H$-H_2O	$\delta^{34}S$-SO_4	$\delta^{18}O$-SO_4
Total N	74	72	73	10	64	62	69	66	10	8
MIN	0.0	0.0	0.0	0.0	0.0	0.0	0.0	0.0	0.0	0.0
MEDIAN	0.2	0.4	0.4	0.3	0.2	0.4	0.2	0.6	0.2	0.0
MEAN	0.3	0.5	0.6	0.5	0.3	0.6	0.3	1.0	0.2	0.9
MAX	1.6	1.7	2.6	1.1	2.3	1.9	1.6	2.9	0.5	3.7

Appendix B: Spatial Variation in POM-$\delta^{13}C$ and POM-$\delta^{15}N$

Different types of sites have moderately distinctive $\delta^{13}C$ and $\delta^{15}N$ values (Figure B1a), with upstream mixed wetlands and mainstem sites generally showing high $\delta^{15}N$ and low $\delta^{13}C$ values, and tributary, drain, and creek samples generally showing low $\delta^{15}N$ and high $\delta^{13}C$ values. Most of the "outlier" values for the mainstem sites are from Landers (Figure B1b). Comparison of these plots with the ranges of values Figure 3 (top panel) suggests that terrestrial derived organic matter is the dominant source of POM to major tributaries, drains, and creeks, whereas POM from the mainstem and wetlands sites appears to be dominated by algae.

There is little variation among sites in the mainstem SJR (Figure B2a), with overlapping $\delta^{15}N$ and $\delta^{13}C$ values for all sites except Lander, where POM samples often have lower $\delta^{13}C$ values than at the other sites. The major tributary sites also show overlapping $\delta^{15}N$ and $\delta^{13}C$ values (Figure B2b), but generally with higher $\delta^{13}C$ and lower $\delta^{15}N$ than the mainstem sites.

Figure B3, and especially the bottom panel, clearly shows that the $\delta^{15}N$ and $\delta^{13}C$ values of POM from wetlands sites overlap almost the entire range of values for mainstem sites. If we exclude the Landers site, the mainstem sites show a more limited range of values. Samples from small creeks and drains (e.g., Harding and Westport Drains; Orestimba, Del Puerto, and Ingram Creeks) have relatively narrow ranges of compositions, with lower $\delta^{15}N$ and higher $\delta^{13}C$ than mainstem or wetlands sites. Hence, the mainstem isotope values "could" be explained simply as wetlands-derived POM but could not be explained simply as drain, creek, or tributary-derived POM. However, the $\delta^{15}N$ and $\delta^{13}C$ values at mainstem sites "could" also be explained by various mixtures of wetlands-derived POM and POM derived from the other sites. None of these sites have statistically distinctive $\delta^{13}C$-$\delta^{15}N$ isotopic compositions.

The combination of C:N and $\delta^{13}C$ is usually more useful in distinguishing between algal and terrestrial sources of POM (Figure 3b, bottom panel) than the combination of $\delta^{15}N$ and $\delta^{13}C$ discussed above. Figure B4 shows the ranges of C:N and $\delta^{13}C$ values for different types of sites, again with Landers (which does not behave as a "normal" SJR site) plotted separately from other mainstem sites (as was done on Figure B1a). Different types of sites show moderately distinctive data "clusters", with samples from major tributaries showing a curving band of values ranging from very high C:N and mid-range $\delta^{13}C$ values to very low C:N and slightly higher $\delta^{13}C$. Most wetlands samples cluster within the range of "normal" (e.g., non-Lander) mainstem sites (with mid-range $\delta^{13}C$ values and mid-range C:N values); however, there are a fair number of samples with low $\delta^{13}C$ values that overlap the values for Lander samples and other samples that have high $\delta^{13}C$ values. Drain and creek samples fall within a roughly triangular area that is centered on the middle of the tributary "cluster" but has "arms" extending toward the high-C:N values of tributary sites, the low-$\delta^{13}C$ values of wetlands sites, and then toward very high $\delta^{13}C$ values. Normal mainstem sites generally cluster within the area of wetlands sites except for a fair number of samples with mid-range $\delta^{13}C$ values that have substantially higher C:N values than wetlands samples and plot within the range of typical tributary samples.

Comparison of the ranges of values on Figure B4a with those on Figure 3b suggests that most samples from the major tributaries and many samples from the drains and creeks are dominated by terrestrial organic matter or macrophytes. In contrast, most of the wetlands and mainstem samples are dominated by algae, and a fair number of samples can be explained solely by algae. Few mainstem samples show the very high $\delta^{13}C$ values seen in some drain sites; the mainstem sites with the highest $\delta^{13}C$ values are both from the Lander site. Except for Lander, the clusters of $\delta^{13}C$-C:N values for the other mainstem sites are indistinguishable (Figure B4b). The $\delta^{13}C$-C:N data clusters for the three tributaries (Figure B5a) are also indistinguishable. The $\delta^{13}C$-C:N data clusters for drain and creek sites are mostly indistinguishable except that Harding Drain has a band of samples with higher $\delta^{13}C$ and C:N values than usually seen at other sites (Figure B5b). The $\delta^{13}C$-C:N data clusters for the Mud Slough, Salt Slough, and Los Banos wetlands sites are indistinguishable; however, the San Luis Drain samples are moderately distinguishable from the other wetlands sites because of the lower $\delta^{13}C$ and higher $\delta^{15}N$ values (FigureB5b).

While the amount of POM in each sample was not directly measured, this can be estimated based on the total suspended sediment and total mineral solid measurements (e.g., POM = TSS – minerals). These POM concentrations were plotted against C:N in Figure B6 for tributary sites (top) and wetlands, drain, and creek sites (bottom), with the compositions of mainstem sites included for reference. Tributary sites show low POM concentrations (0-5 mg/L) with no correlation of C:N and POM concentration. Mainstem sites showed much higher POM concentrations, with an average of 7 but values ranging to >20. Wetlands, drain, and creek samples had much higher POM concentrations, with wetlands sites (especially San Luis Drain and Los Banos Creek) generally showing higher concentrations (8.7) versus 7.9 for the other sites. Westport Drain tended to have low POM concentrations whereas Ingram and Orestimba Creeks tended to have higher values. Sites with lower C:N values (which tended to be drain/creek sites) tended to have lower POM values.

Appendix B- Figures

Figure B1. Correlation of $\delta^{13}C$ and $\delta^{15}N$ values for POM samples from different types of sites (top), with the SJR site at Lander plotted separately from the other mainstem sites (bottom) because the Lander site has significantly lower $\delta^{13}C$ values and higher $\delta^{15}N$ values than other mainstem sites.

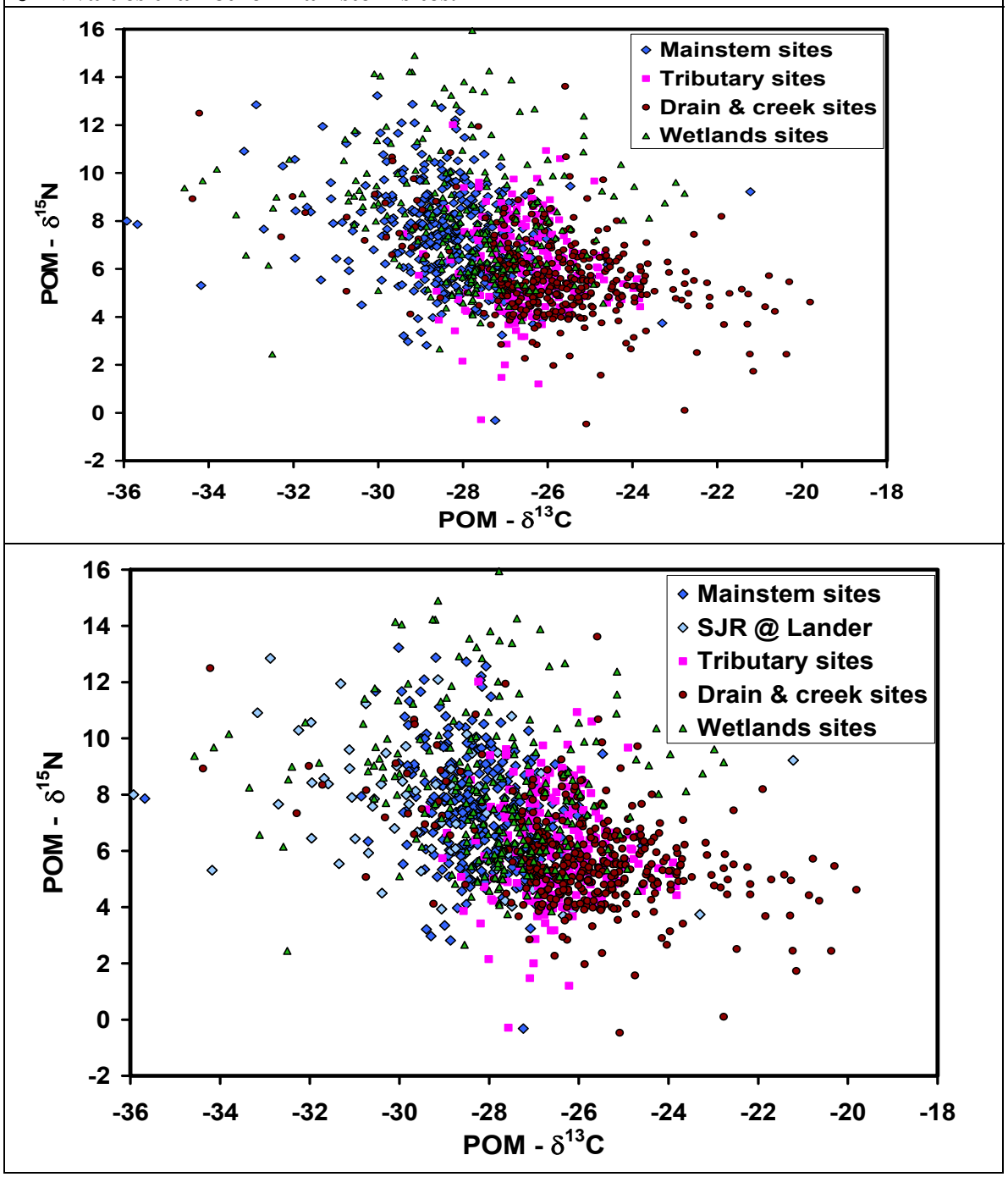

Figure B2. Correlation of $\delta^{13}C$ and $\delta^{15}N$ values for POM samples from different SJR mainstem sites (top), and major tributaries (bottom). The tributaries have similar ranges of $\delta^{15}N$ and $\delta^{13}C$ values, with lower $\delta^{15}N$ and higher $\delta^{13}C$ values than most of the mainstem sites.

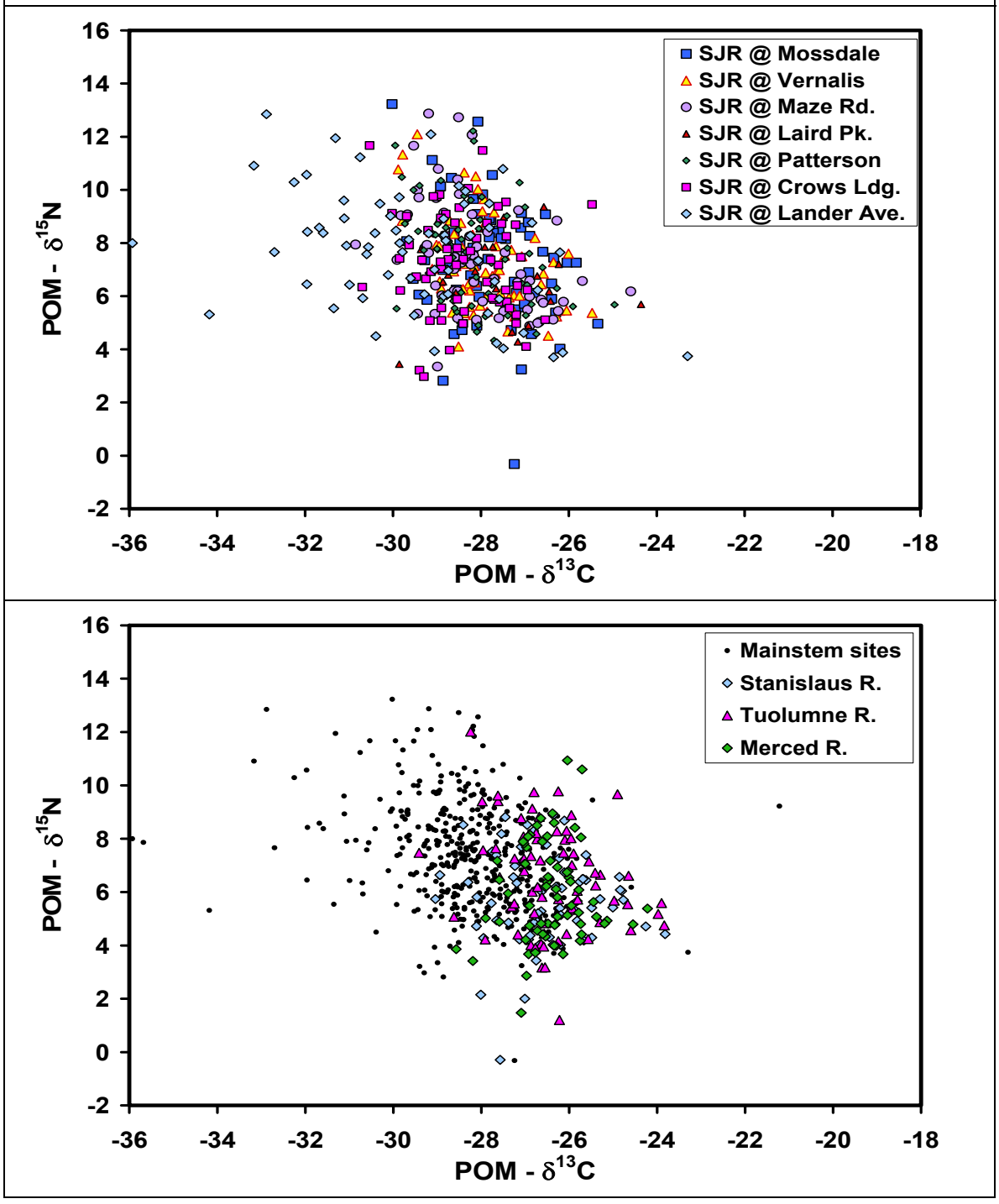

Figure B3. Correlation of $\delta^{13}C$ and $\delta^{15}N$ values for POM samples from selected drain, creek, and wetlands sites (top), plotted with the same scales as the plots above. To make it easier to see the symbols for the different sites, an expanded-scale version of this plot is shown below (bottom).

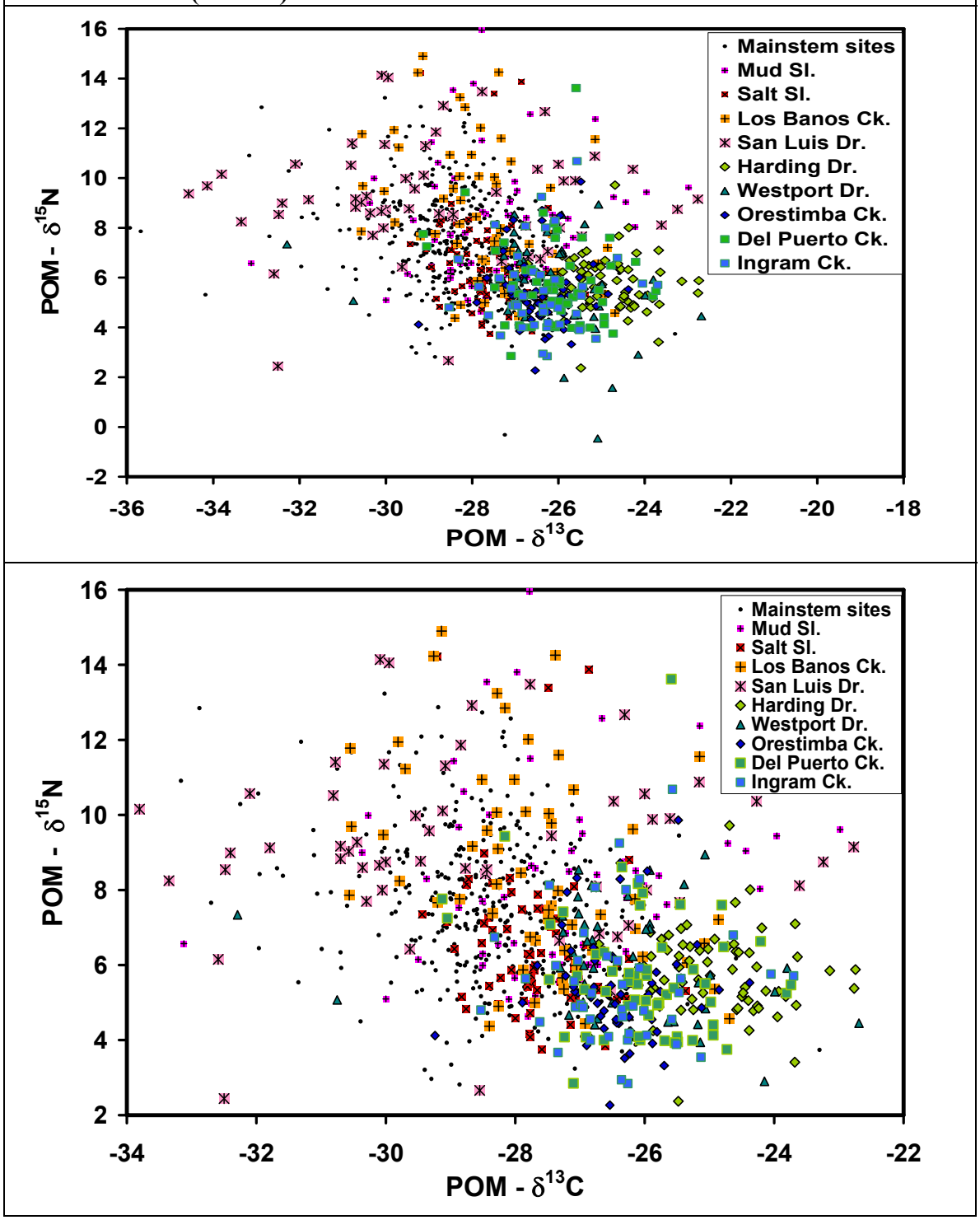

Figure B4. Correlation of $\delta^{13}C$ and C:N values for POM samples from different site types (top), and SJR mainstem sites (bottom) with data for the Lander site plotted separately. Mainstem sites generally have lower $\delta^{13}C$ and C:N values than tributary, drain, and wetlands sites.

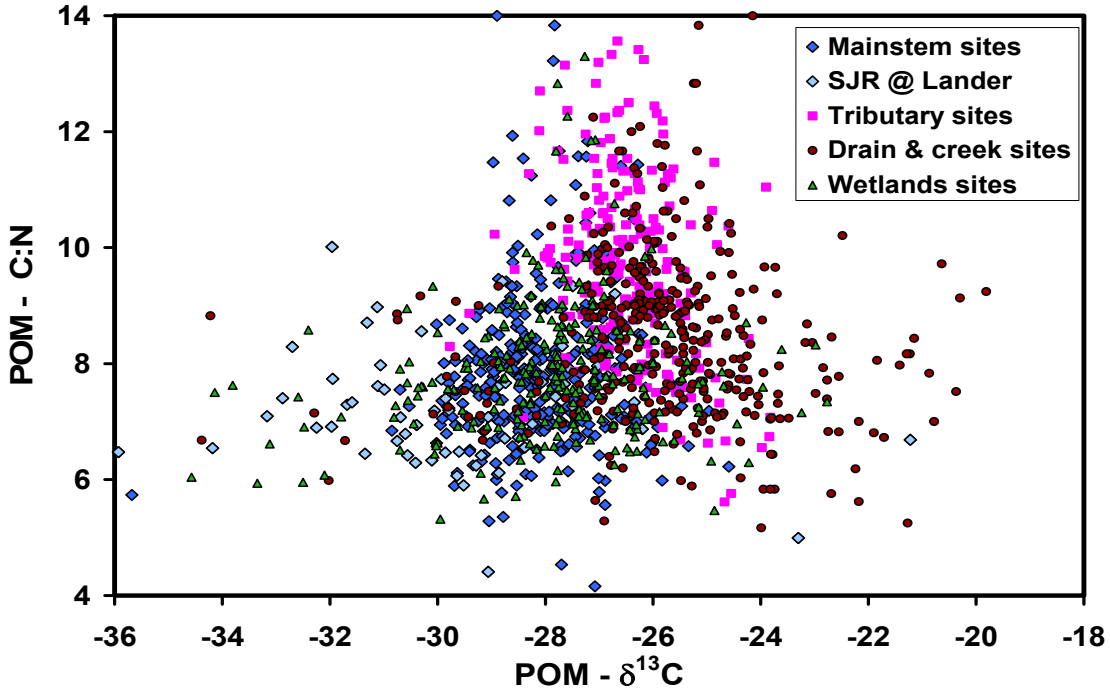

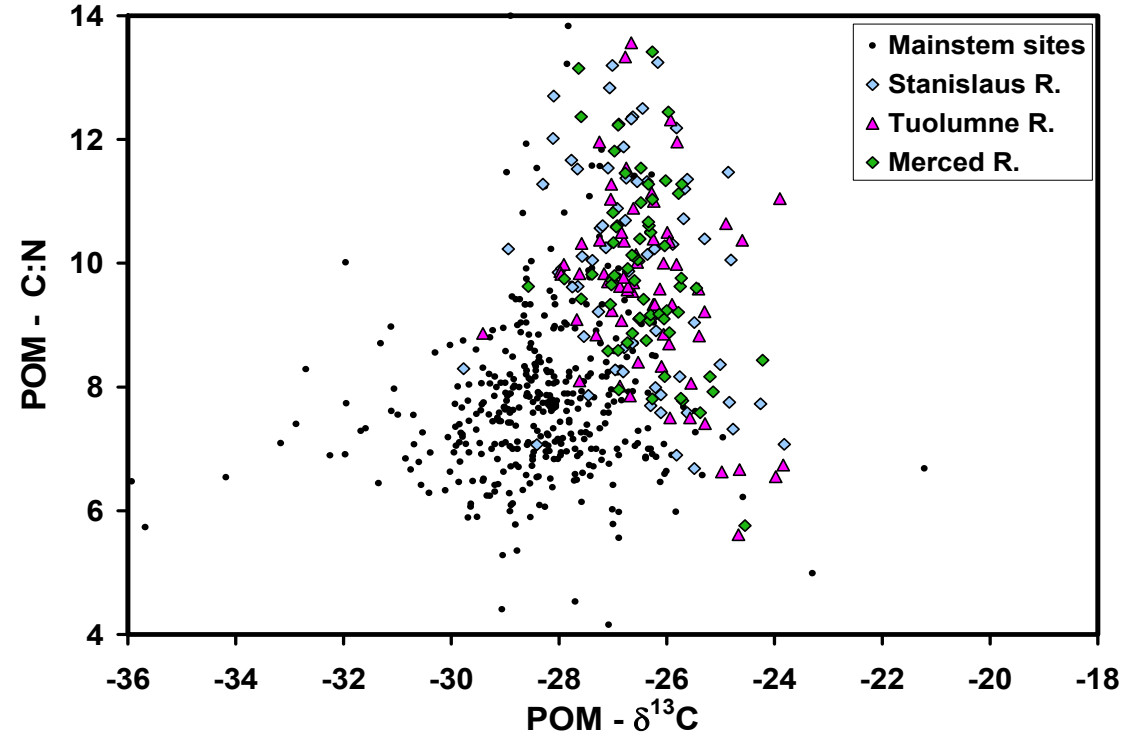

Figure B5. Correlation of $\delta^{13}C$ and C:N values for POM samples from the major tributaries (top), and selected drain, creek, and wetlands sites (bottom). Samples from the tributaries generally have higher $\delta^{13}C$ and $\delta^{15}N$ values than mainstem sites (top). The wetlands sites (Mud and Salt Slough, Los Banos Creek, and San Luis Drain) generally have lower $\delta^{13}C$ and $\delta^{15}N$ values than other drain sites (bottom).

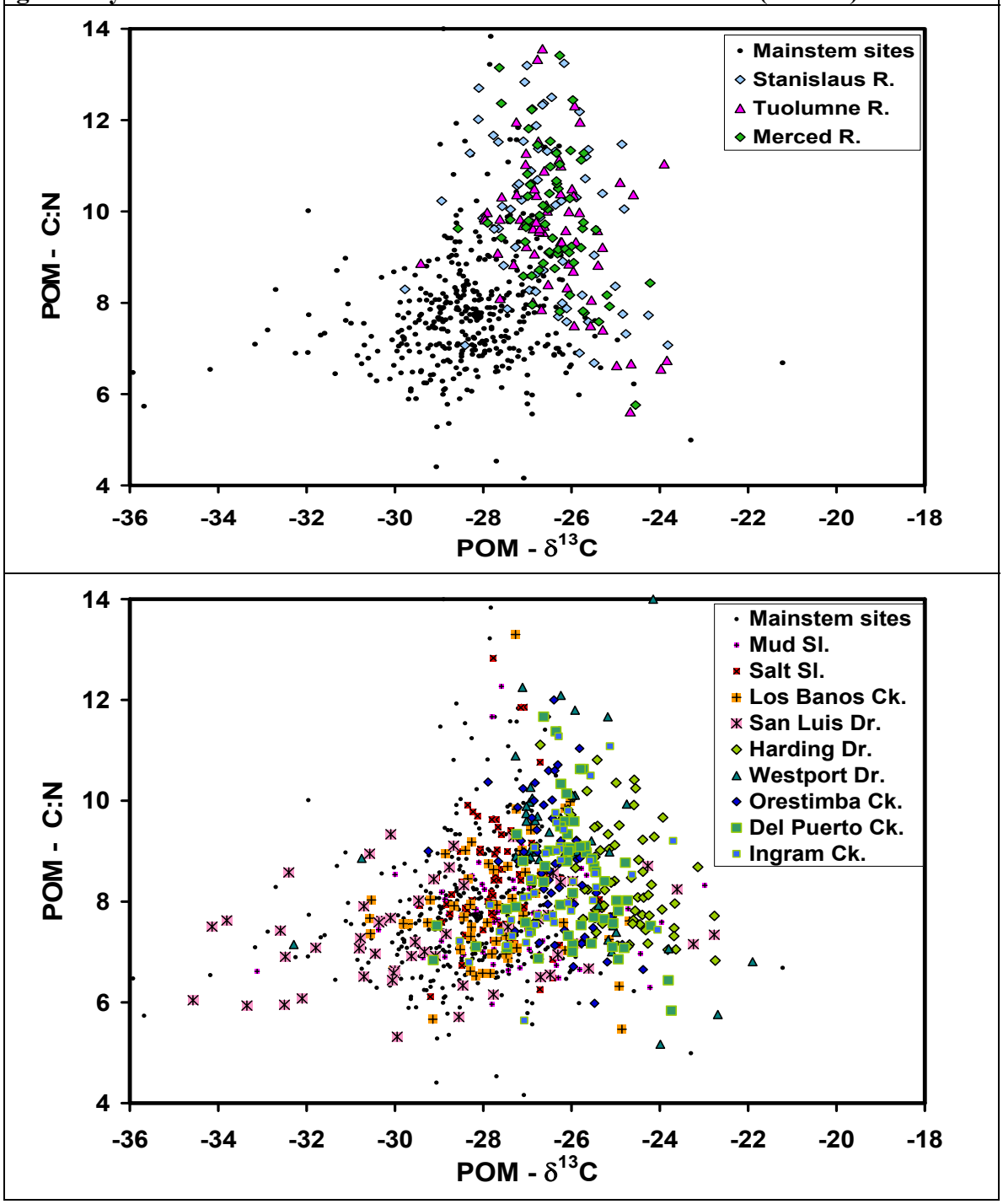

Figure B6. Correlation of C:N and calculated POM concentration in major tributaries sites (top) and selected drain, creek, and wetlands sites (bottom), with the compositions of mainstem sites included for reference. Note the difference in POM scales. Mainstem sites have much higher POM concentrations than tributaries, and much lower POM concentrations than most drain, creek, and wetlands sites. There is no obvious correlation of POM and C:N values.

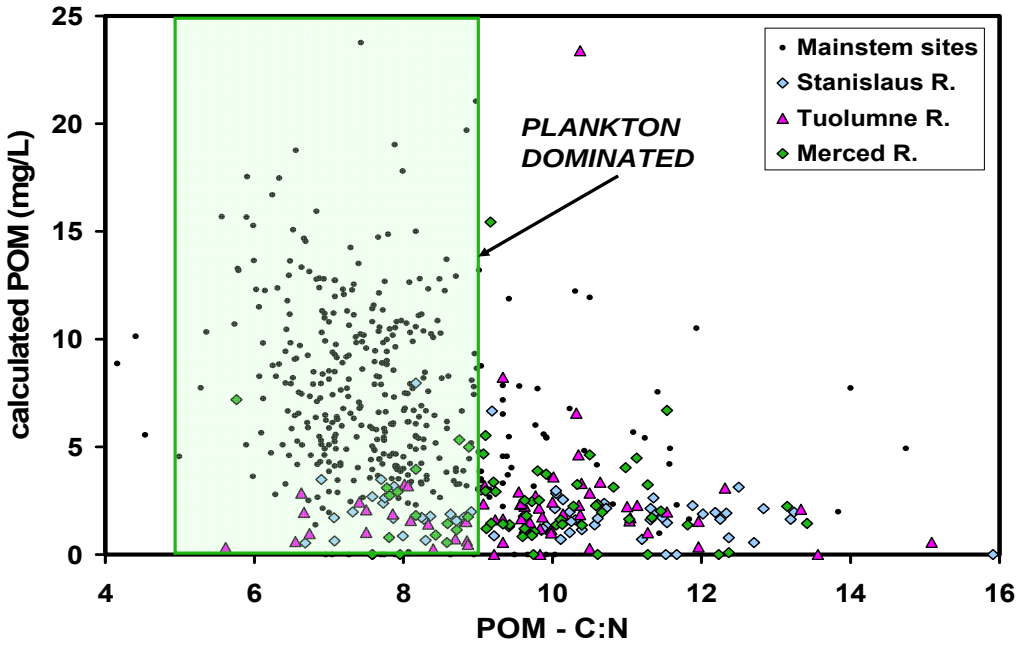

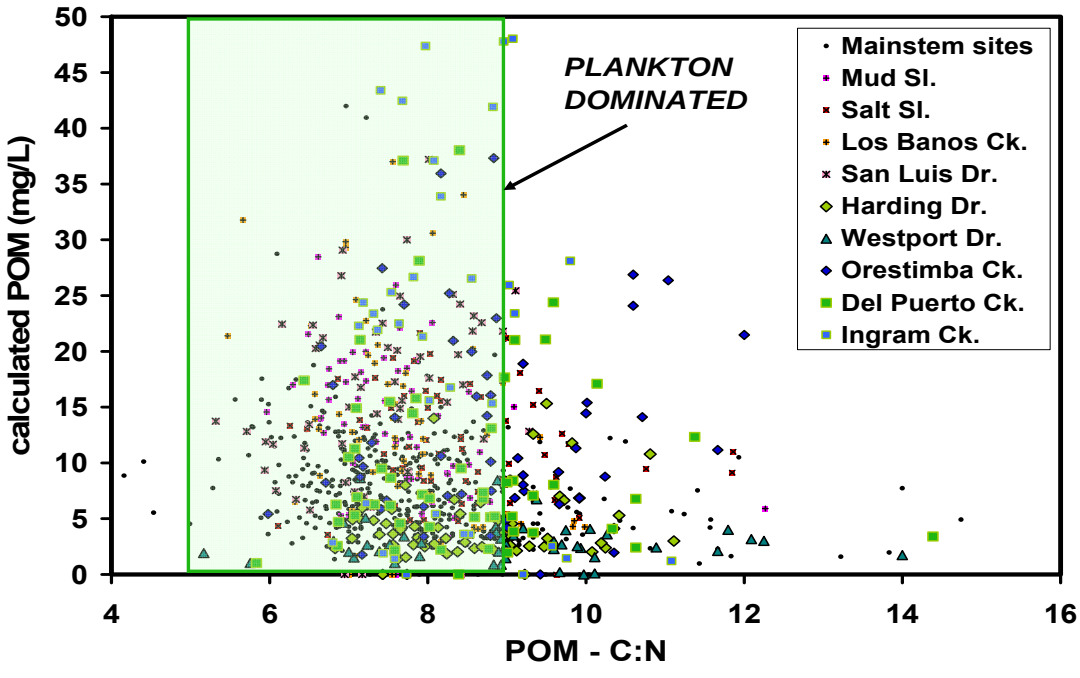

Appendix C: Temporal Variations in POM Isotopes

Introduction

Most sites showed considerable temporal variation in $\delta^{15}N$, $\delta^{13}C$, and C:N, with much of the variability apparently caused by changes in flow. Not surprisingly, during high discharge periods, larger amounts of terrestrial-derived POM are transported into the river. This POM is "isotopically" and "elementally" labeled -- with higher $\delta^{13}C$ values, lower $\delta^{15}N$ values, and most importantly, higher C:N values than algal-derived POM (Figure 3). Depending on the hydrological conditions at each site, and the sources of organic matter in the watershed, different sites often show similar temporal oscillations in the N, $\delta^{13}C$, and C:N of the POM (and other isotope tracers, as discussed in other sections). Since different sources of POM tend to have distinctive ranges of $\delta^{15}N$, $\delta^{13}C$, and C:N values, the compositions of these parameters often show similar temporal oscillations. To explore the temporal corrections between/among sites and between/among POM parameters, two suites of plots have been made.

The first suite of plots (Figures C1-C9) compares responses between sites and among groups of sites, with separate sets of plots for temporal variations in $\delta^{15}N$, $\delta^{13}C$, and C:N (respectively) of different sites and groups of sites, with a few plots for each parameter. To make comparisons among and between figures easier, whenever possible the same $\delta^{13}C$, $\delta^{15}N$, and C:N scales are used on these plots as above. Note that the isotope scales were sometimes shifted (but not expanded or decreased) to make space for the flow information at the bottom of some figures or to adjust for different mean values of different site groups. The second suite of plots (Figures C10-C21) compares responses between/among POM parameters for individual sites, with the data from each site on a separate plot, listed in order of the site number (e.g., DO-#). All these plots have the same scales to make intercomparisons easier.

Temporal Variation in POM-$\delta^{15}N$.

Figure C1 shows the temporal changes in $\delta^{15}N$ for major tributaries (top) and mainstem SJR sites (bottom), with the flow at Vernalis at the bottom of the panels. The $\delta^{15}N$ values show larger oscillations during high flow periods than during low flow periods. In many instances, the tributaries show similar oscillations to each other and to mainstem sites. For example, all three tributaries show increases in $\delta^{15}N$ as flow increases in March 2005, then remain relatively constant during the summer and fall of 2005 until all show a decrease in $\delta^{15}N$ as flow increases in early January 2006, and then they oscillate up and down during 2007. The $\delta^{15}N$ values during the dry season in 2005 are much lower than seen during the dry season in 2007. There does not seem to be a comparable dry season/low flow pattern in 2006, perhaps because this was an unusually wet year.

Figure C1b shows the temporal changes in $\delta^{15}N$ for all the mainstem sites. In general, the mainstem sites show less temporal variability than the major tributaries. Landers, as expected, shows more oscillations, and with a wider range of $\delta^{15}N$ values, than other sites. The mainstem sites show only small temporal oscillations, with a similar range of $\delta^{15}N$

values for different sites, except for the high flow period from January 2006 through about May 2007. This was the same period when the tributaries also showed the most variation in $\delta^{15}N$. Mainstem $\delta^{15}N$ values during the summer of 2005 are significantly lower than for summer of 2007, with gradually decreasing values as flow declined. This plot is rather complicated so the downstream (top-a) and upstream (bottom-b) data are plotted separately on Figure C2.

In general, there is more seasonal variability in $\delta^{15}N$ at downstream sites than upstream ones, with the sites at Mossdale and Lander showing particularly rapid oscillations of high and low $\delta^{15}N$ values. The close correspondence of many of the oscillations is intriguing, as are the times when one site is showing a different pattern than the sites upstream and downstream of it. The most important point to be taken from an inspection of these plots is that the $\delta^{15}N$ values are not showing random noise but instead represent a "signal" of changes in POM sources. Comparison of these patterns with $\delta^{13}C$ and C:N values (and other parameters) will indicate whether the rapid changes can best be explained by inputs of terrestrial organic material, perhaps releases of irrigation waters containing algae, or other processes in the water column (Figure 4).

Temporal changes in $\delta^{15}N$ for minor creek and drain sites (top) and wetlands sites (bottom) are shown in Figure C3. Upstream wetlands sites, except for Mud Slough, show considerably more temporal variation in $\delta^{15}N$ values than seen in the creek and drain sites. As was seen in mainstem and major tributary sites, oscillations are greater during high flow periods than during low flow periods. Fewer of the oscillations for different creek and drain sites are in phase than seen at sites with higher flow; the correspondence among sites is best during major hydrological events (e.g., the rainy season during the winter of 2005-6 and 2006-7). There is even less correspondence between oscillations at wetlands sites than drain/creek sites, but many of these sites also show and relatively steady $\delta^{15}N$ values during the rainy season. Mud Slough, Salt Slough, and Los Banos Creek generally have lower $\delta^{15}N$ values during the rainy season.

Temporal Variation in POM-$\delta^{13}C$.

Figure C4 shows the temporal changes in $\delta^{13}C$ for major tributaries (top) and mainstem SJR sites (bottom), with the flow at Vernalis at the bottom of the panels. There is considerably less variation in $\delta^{13}C$ in the tributaries than was seen with $\delta^{15}N$ (Figure C1). At the scale of these plots, it is not obvious but there is good correspondence between the oscillations in $\delta^{13}C$ for the different tributaries, especially during high flow periods where the $\delta^{13}C$ values usually decrease and then increase a week or so later. During dry spells, the $\delta^{13}C$ values slowly increase. All tributaries show a general trend of decreasing $\delta^{13}C$, with changes of about 1.5‰ in 2.7 years; however, the r^2 values are unimpressive (~0.1). Most of the mainstem sites also show a decrease of ~1.5‰ over the sampling period; the r^2 values for Patterson and Vernalis are both about 0.2.

The temporal oscillations in $\delta^{13}C$ at the mainstem sites have slightly greater amplitudes than the tributaries, but again the variability is small compared to the variability in $\delta^{15}N$. To better see the patterns at the different mainstem sites, the downstream (top) and downstream

(bottom) sites are plotted separately in Figure C5. The upstream sites, Lander in particular, show more variability than the downstream sites. Except for Lander, there is very close correspondence between the patterns for the different sites (e.g., the smoothly rising $\delta^{13}C$ values during the summers and fall of 2005 and 2006 as flow declined). The temporal changes in $\delta^{13}C$ at Lander seem almost totally unrelated to changes at other sites. One of the wetlands sites (San Luis Drain) that drains into the SJR near Lander also shows high amplitude oscillations (Figure C6b). To aid in comparison of the sites, the data for the San Luis Drain site are also plotted on Figure C5b, along with the upstream SJR sites. A closer examination of the temporal trends of these two sites shows fair correspondence in oscillation times, whereas the magnitudes of the changes in $\delta^{13}C$ are usually different..

Except for the San Luis Drain, the wetlands, drain, and creek sites – like the major tributaries and most of the mainstem sites -- show little seasonal variation in $\delta^{13}C$ (Figure C6) compared to their changes in $\delta^{15}N$ (Figure C3). There is generally very little correspondence of oscillations in the wetlands, creek, and drain sites. One notable exception is the close match of $\delta^{13}C$ values at the Mud Slough and Los Banos Creek sites in late summer and fall 2007, probably related to the management of the wetlands sites. Some of the sites show a hint of the kind of general decrease in $\delta^{13}C$ over time seen in tributary and mainstem sites (e.g., Los Banos Creek, Salt Slough, Del Puerto Creek).

Temporal Variation in POM-C:N.

Figure C7 shows the temporal changes in $\delta^{13}C$ for major tributaries (top) and mainstem SJR sites (bottom), with the flow at Vernalis at the bottom of the panels. There is a tremendous amount of seasonal variability in C:N at tributary sites. If the data points were not connected by lines, this variability might seem like noise. However, with the lines connecting the data points, it is clear that the oscillations in one tributary usually occur at about the same time in one or both of the other tributaries, although perhaps the amplitudes of the oscillations are different. The Merced oscillations seem to have the highest amplitudes and the Tuolumne the lowest. The highest C:N values (of ~25) occurred at all sites in December 2005-January 2006, associated with a sudden increase in flow. These high C:N values indicated that very refractory organic matter was washed into these tributaries during this period, not just normal living terrestrial vegetation. While the trend is difficult to see amidst the oscillations, C:N values increase by >1 during the 2.7 years of this study.

Mainstem SJR sites also show considerable temporal variation in C:N (Figure C7b), but with lower amplitudes than the tributaries. Note that all of the mainstem sites also show a large increase in C:N in January 2006, but C:N values do not rise above 14. To better see the patterns at the different mainstem sites, the downstream (top) and downstream (bottom) SJR mainstem sites are plotted separately in Figure C8. Surprisingly, Mossdale shows more variation in C:N than upstream sites. This could be interpreted as additional inputs between Mossdale and Vernalis, but could also reflect problems with the sampling site. USGS protocols for large river sampling require depth and width-integrated samples. This type of expensive sampling is more critical for constituents that can settle out of solution or are particle-attractive, like suspended sediments. The spatial and temporal patterns of C:N may be useful for improving the interpretation of other water quality data collected at these sites.

There is very good correspondence of the oscillations in C:N at the various mainstem sites, and most of the oscillations can be correlated with similar oscillations in the tributaries, which clearly indicates the dominant source of this POM. Excluding the Lander site, the average C:N of the mainstem sites is 7.9, which according to Figure 3, indicates that the POM is highly dominated by phytoplankton. This compares with an average C:N of 10.1 for the major tributaries, which is consistent with a large amount of terrigenous material in these rivers. Oscillations at upstream sites have higher C:N values than at downstream sites, except for the high values seen at Vernalis in summer 2005. However, there is no trend of gradually decreasing amplitude downstream. Proximity of the site to one of the tributaries, and its inputs of POM with highly variable C:N, appears to be responsible for most of the differences in amplitudes. For example, the Patterson site shows much higher C:N values during flow events than Crows Landing or Laird Park.

Mainstem sites show rapid increases during major flow events, but then return to "normal" baseline C:N values of 6-7, indicative of an algal source of almost all of the POM. C:N values drop substantially below 6 only a few times, most notably late July 2006 at several sites including Lander. There is no similar low C:N value at this time in any of the upstream wetlands or other sites, so it remains an interesting puzzle. Very low C:N values like these are typical of bacteria. All sites show a general pattern of slowly decreasing C:N values as flows slowly decline during the late summer and fall.

The wetlands, drain, and creek sites generally show smaller oscillations in C:N than the mainstem or tributary sites, except for a few times at Del Puerto Creek, Los Banos Creek, and Salt Slough (Figure C9). Many of these periods of high C:N occur in the winter, as is seen in the tributaries, for probably the same reason – runoff of terrestrial POM into the waterways during storm events. Other sites (e.g., the San Luis Drain) show less variability at this time of the year. In the summer and fall, the C:N values are generally lower, with frequent small oscillations in C:N probably related to irrigation needs. There is little correspondence among sites for these small oscillations. The San Luis Drain site had slightly lower C:N values than the other wetlands sites, with occasional values in the unusual range of 5-6. In general, the wetland sites had lower C:N values (average = 7.9) than the creek and drain sites (8.7), suggesting a greater dominance of algae in POM from the wetlands sites.

Temporal patterns in the δ^{13}C-POM and δ^{15}N-POM were not tightly coupled and showed considerable variation between sites, both within the mainstem SJR and tributaries. In general, the δ^{13}C-POM values in the SJR mainstem dropped when δ^{15}N-POM values increased. POM isotopes in the San Luis Drain showed the opposite trend for parts of the year, where both isotope values rose and fell at the same times; however, this pattern does not appear to hold true during the fall and winter months.

Correlations between Temporal Variations in δ^{15}N, δ^{13}C and C:N for Individual Sites.

Figures C10-C21 compare responses between/among POM parameters for individual sites,

with the data from each site on a separate plot, listed in order of the site number (e.g., DO-#). All these plots have the same scales to make intercomparisons easier.

Appendix C- Figures

Figure C1. Temporal changes in flow and POM-δ^{15}N values for major tributaries (top) and for mainstem SJR sites (bottom). δ^{15}N values show larger oscillations during high flow periods than during low flow periods; in many instances, the tributaries show similar oscillations to each other and to mainstem sites.

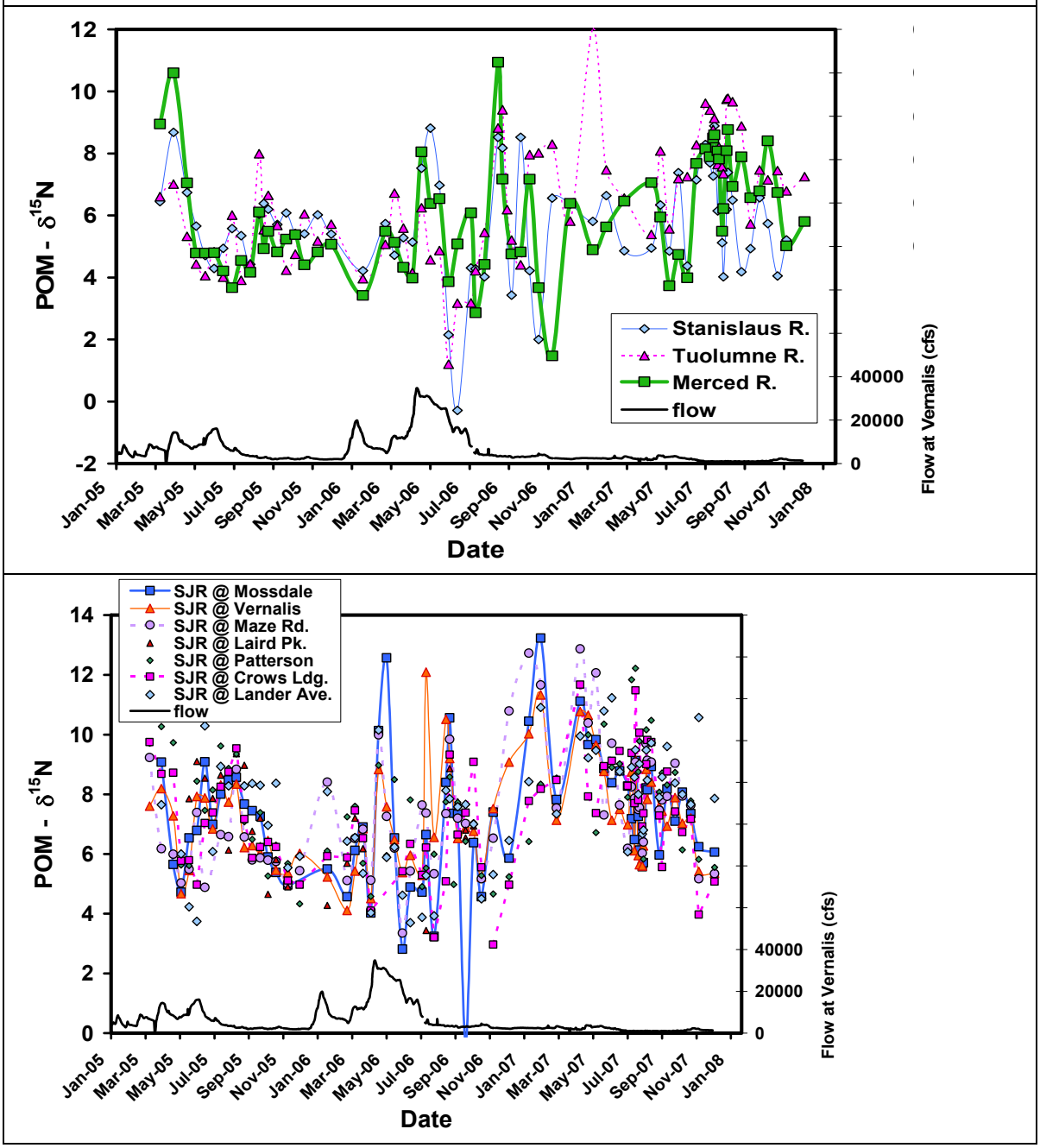

Figure C2. Temporal changes in flow and POM-$\delta^{15}N$ values for downstream (top) and upstream (bottom) mainstem SJR sites. In general, there is more seasonal variability in $\delta^{15}N$ values at downstream sites than upstream sites, with the sites at Mossdale and Lander showing particularly rapid oscillations of high and low $\delta^{15}N$ values.

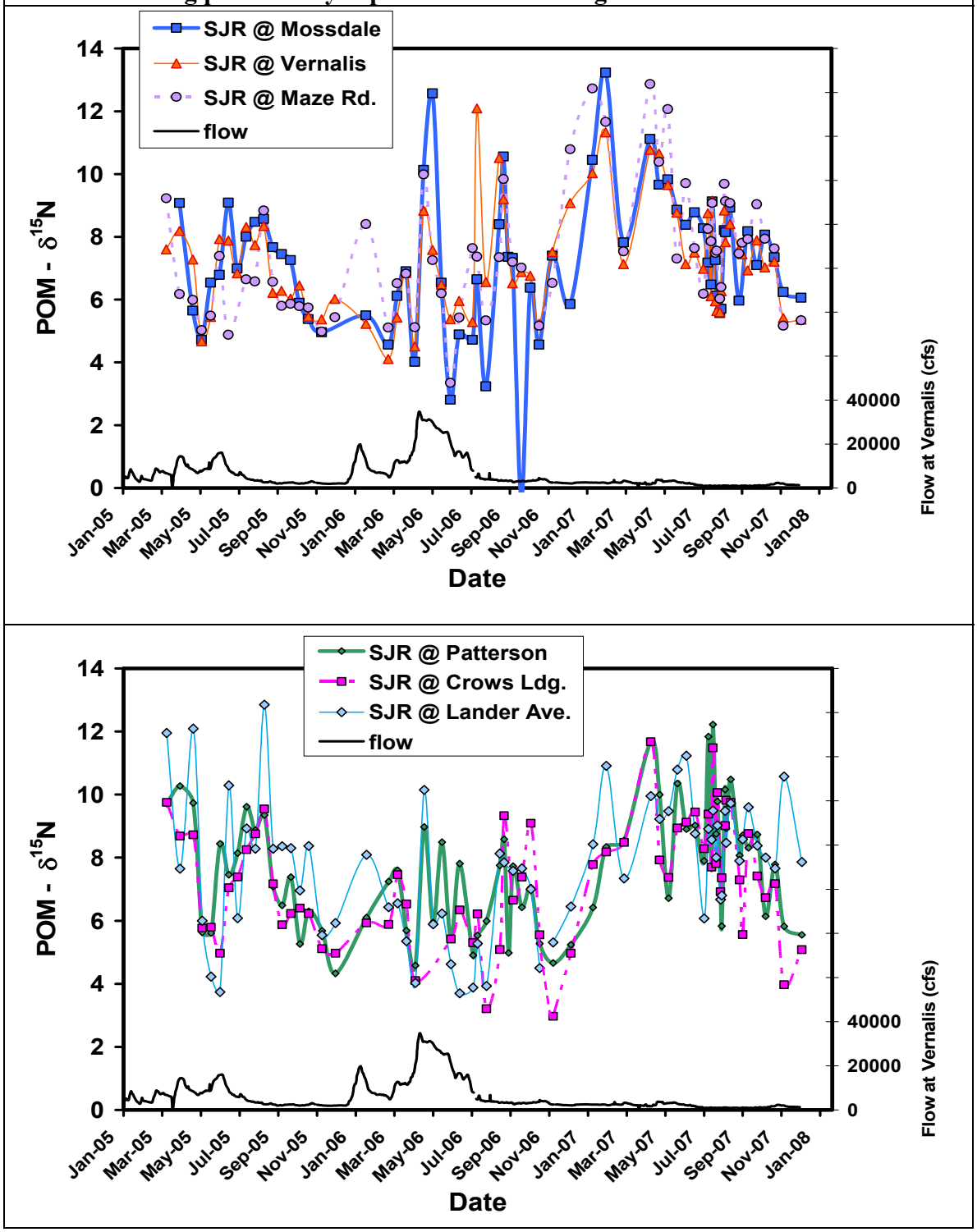

Figure C3. Temporal changes in POM-$\delta^{15}N$ values for downstream drain and creek sites (top) and upstream wetlands sites (bottom). Wetlands sites, except for Mud Slough, show considerably more temporal variation than other minor sites. Oscillations are greatest during higher flow periods than during low flow periods.

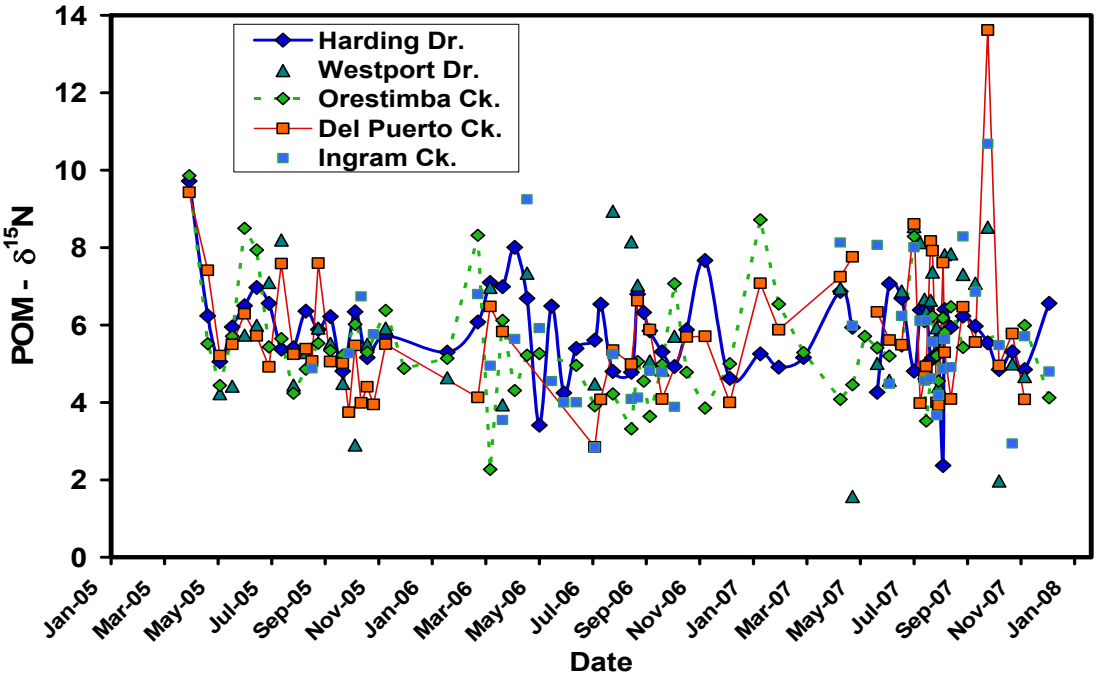

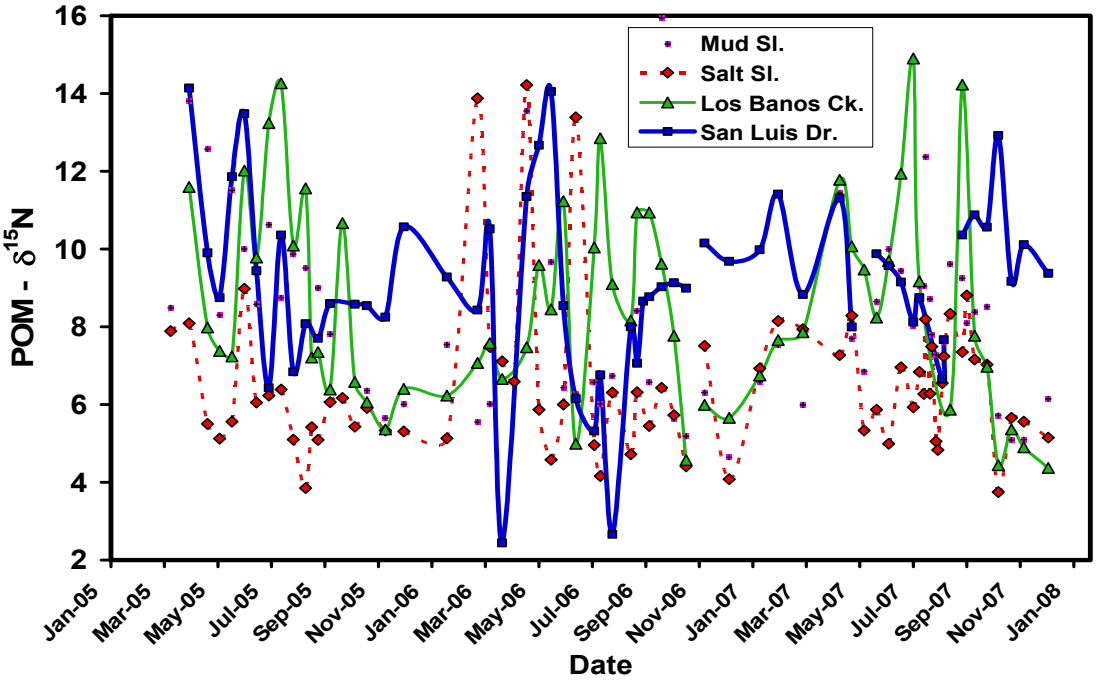

Figure C4. Temporal changes in flow and POM-$\delta^{13}C$ values for major tributaries (top) and for mainstem SJR sites (bottom). $\delta^{13}C$ values show slightly larger oscillations during high flow periods than during low flow periods; in some instances, the tributaries show similar oscillations to each other and to mainstem sites.

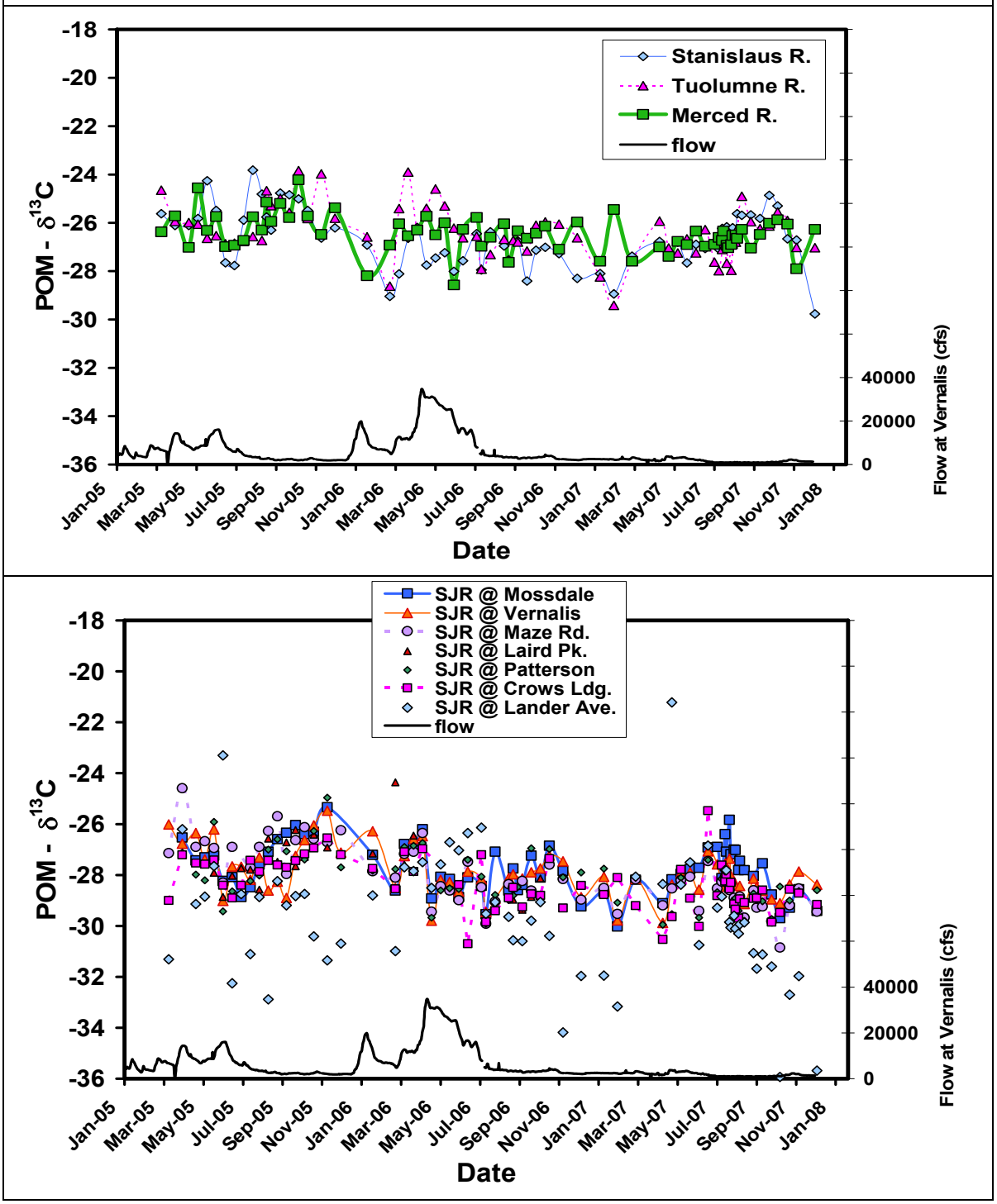

Figure C5. Temporal changes in flow and POM-$\delta^{13}C$ values for downstream (top) and upstream (bottom) mainstem SJR sites. There is substantially more seasonal variability in $\delta^{13}C$ values at upstream sites than downstream sites, with the site at Lander showing particularly rapid oscillations of high and low $\delta^{13}C$ values. Data for the San Luis Drain are plotted on the bottom plot to aid in comparison of it's the seasonal changes with those at Lander.

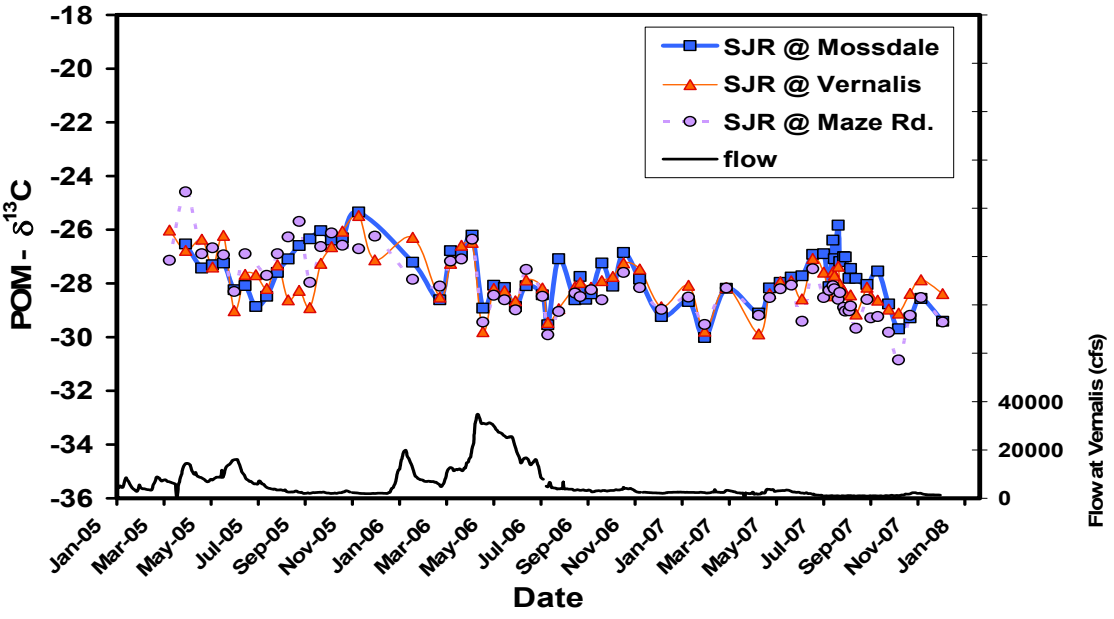

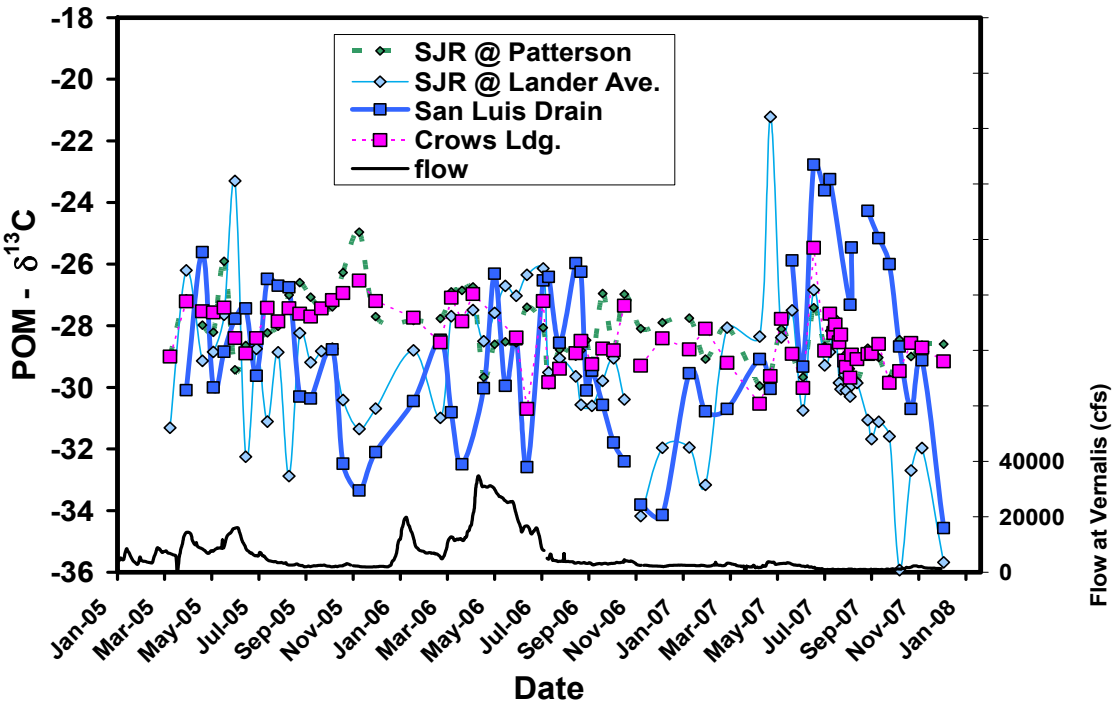

Figure C6. Temporal changes in POM-$\delta^{13}C$ values for downstream drain and creek sites (top) and upstream wetlands sites (bottom). The San Luis Drain site shows much more variability than other wetlands, drain, or creek sites.

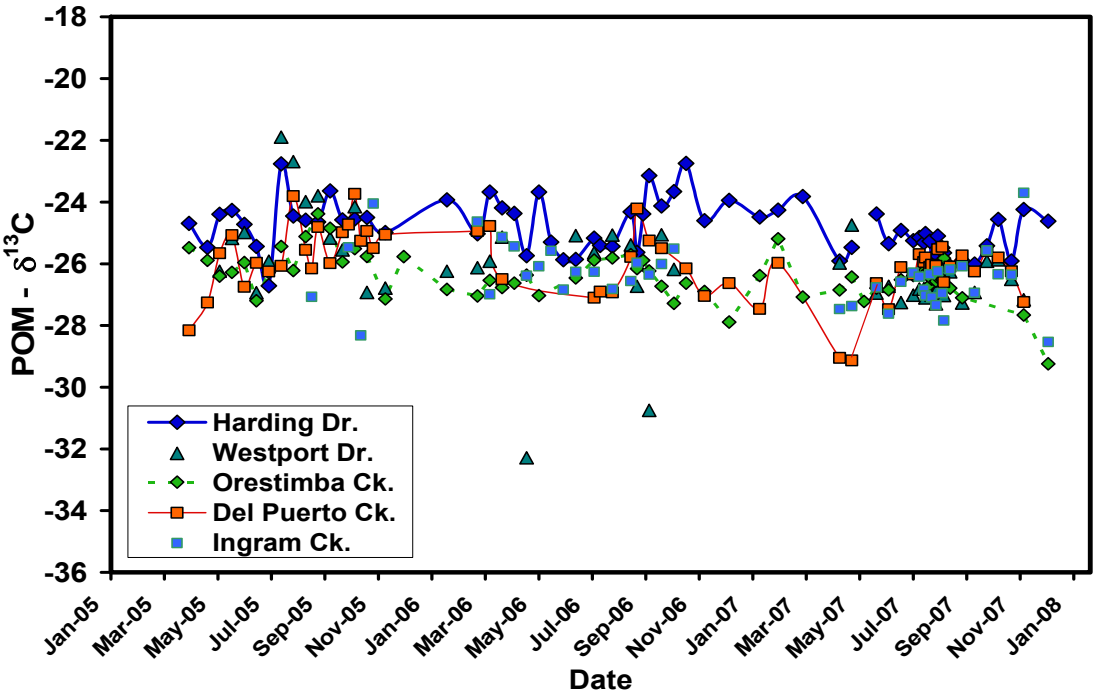

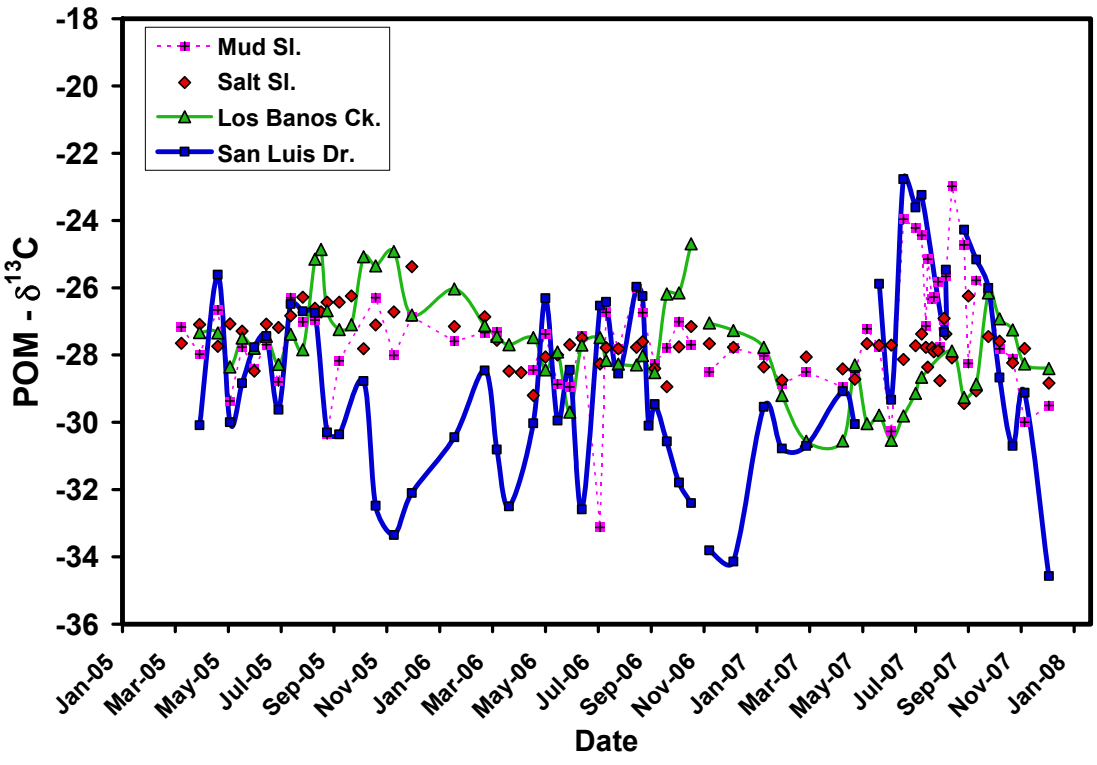

Figure C7. Temporal changes in flow and POM-C:N values for major tributaries (top) and for mainstem SJR sites (bottom). C:N values show larger oscillations during high flow periods than during low flow periods; in many instances, the tributaries show similar oscillations to each other and to mainstem sites. Mainstem sites show less variability than the tributary sites.

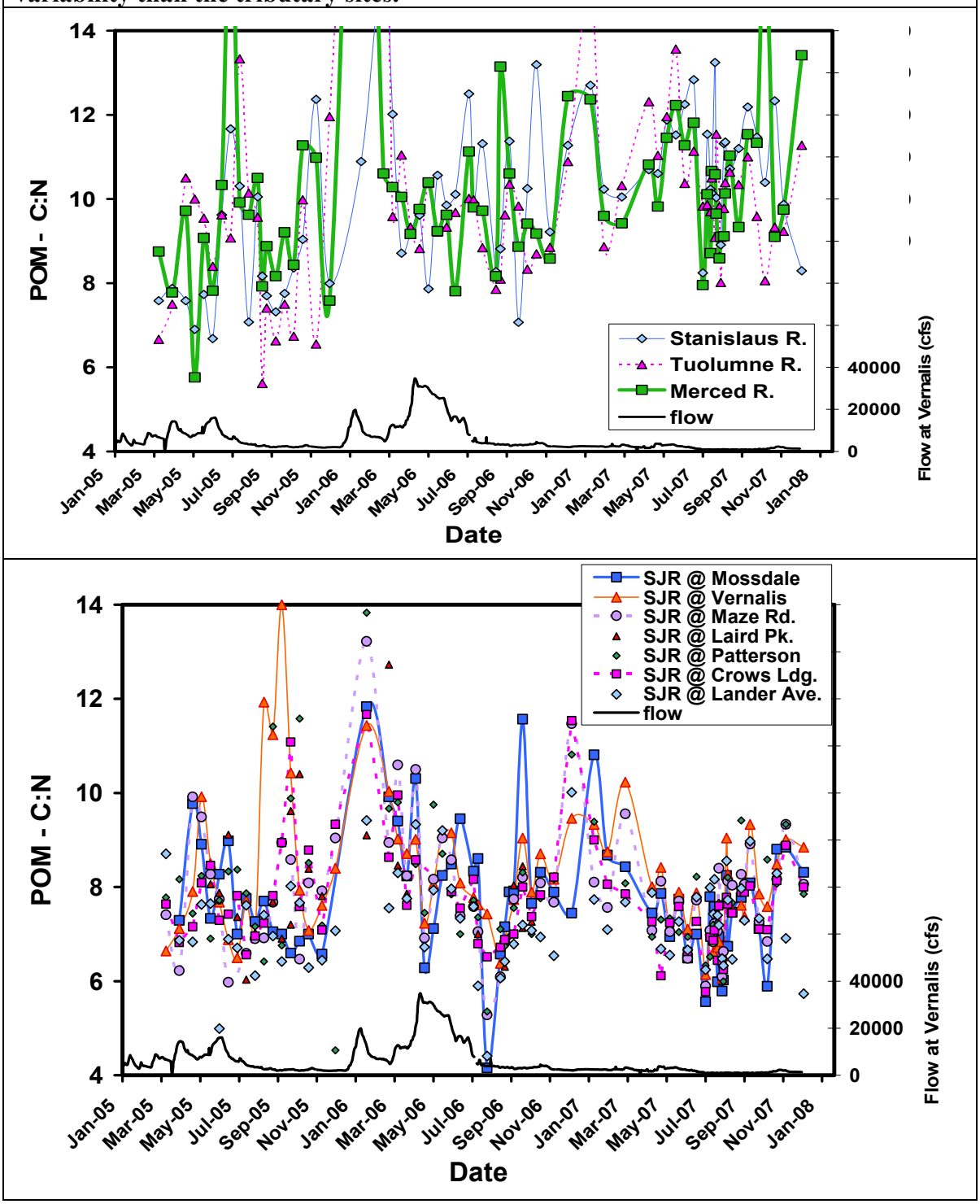

Figure C8. Temporal changes in flow and POM-C:N values for downstream (top) and upstream (bottom) mainstem SJR sites. Upstream sites show more variability than downstream sites. In general, there is more seasonal variability in C:N values during high flow times than during the summer.

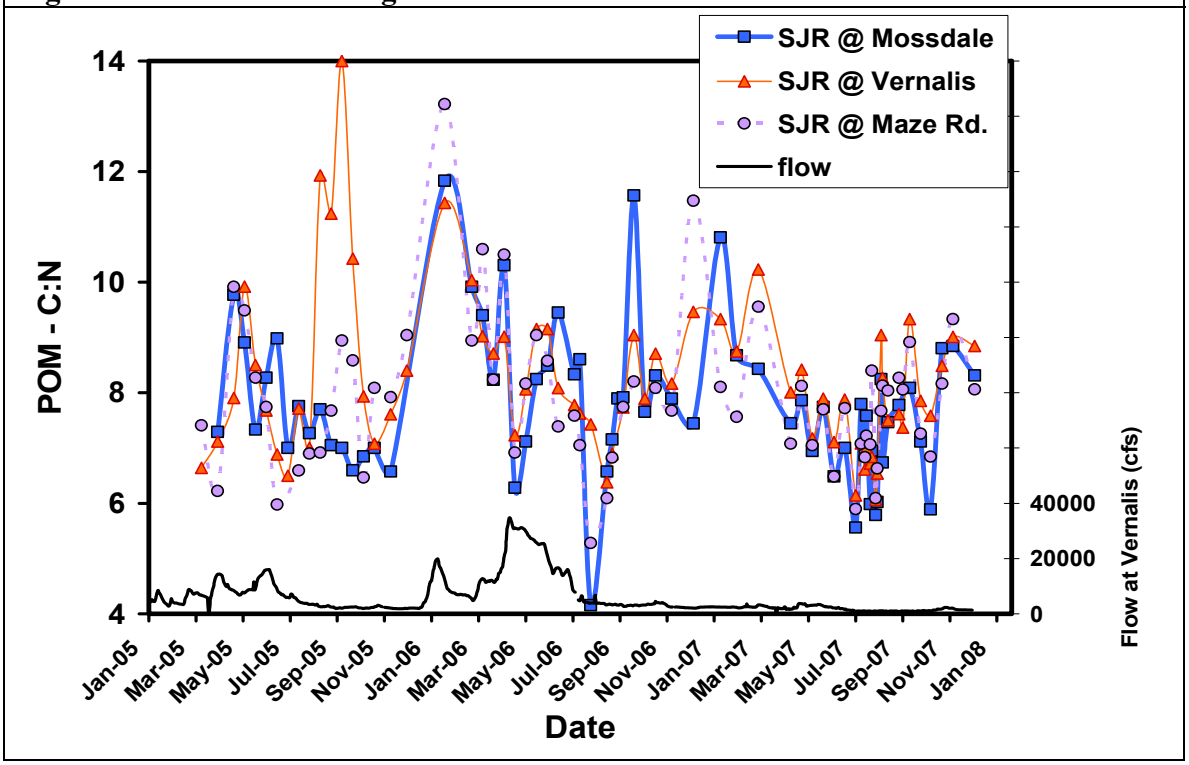

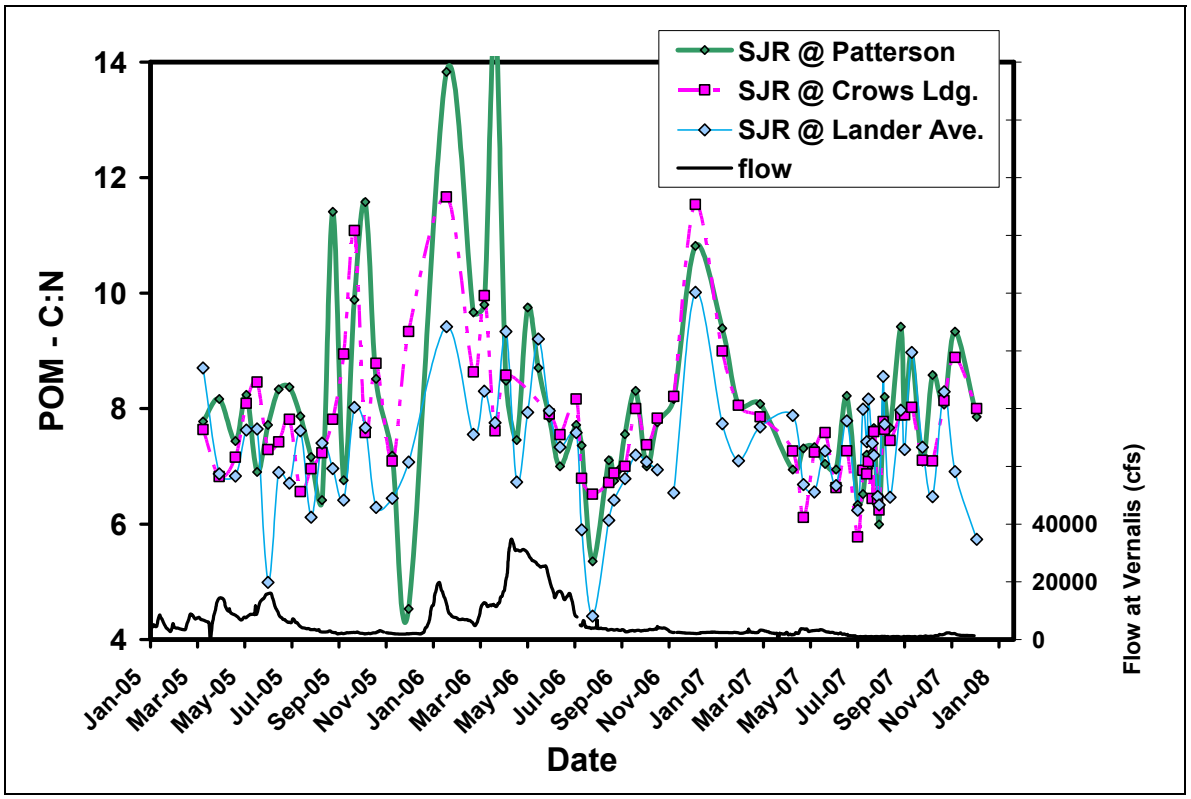
SJR @ Patterson
SJR @ Crows Ldg.
SJR @ Lander Ave.
flow
POM - C:N
14
12
10
8
6
4
40000
20000
0
Flow at Vernalis (cfs)
Jan-05
Mar-05
May-05
Jul-05
Sep-05
Nov-05
Jan-06
Mar-06
May-06
Jul-06
Sep-06
Nov-06
Jan-07
Mar-07
May-07
Jul-07
Sep-07
Nov-07
Jan-08
Date

Figure C9. Temporal changes in POM-C:N values for downstream drain and creek sites (top) and upstream wetlands sites (bottom). Wetlands sites, except for Mud Slough, show considerably more temporal variation than other minor sites. Oscillations are greatest during higher flow periods than during low flow periods.

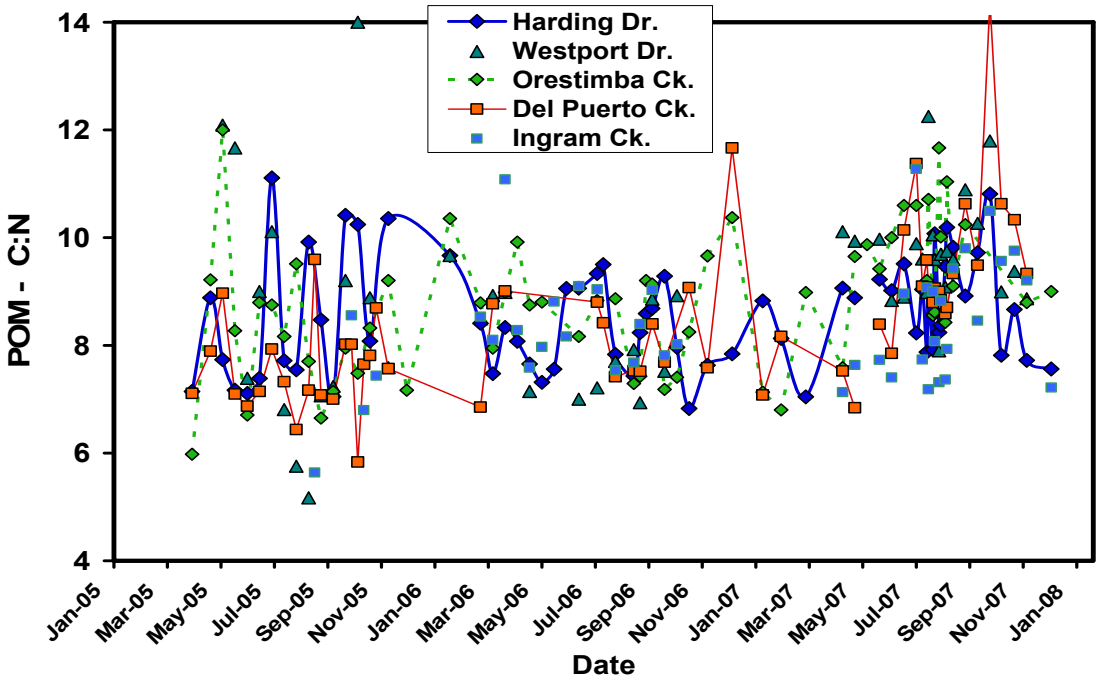

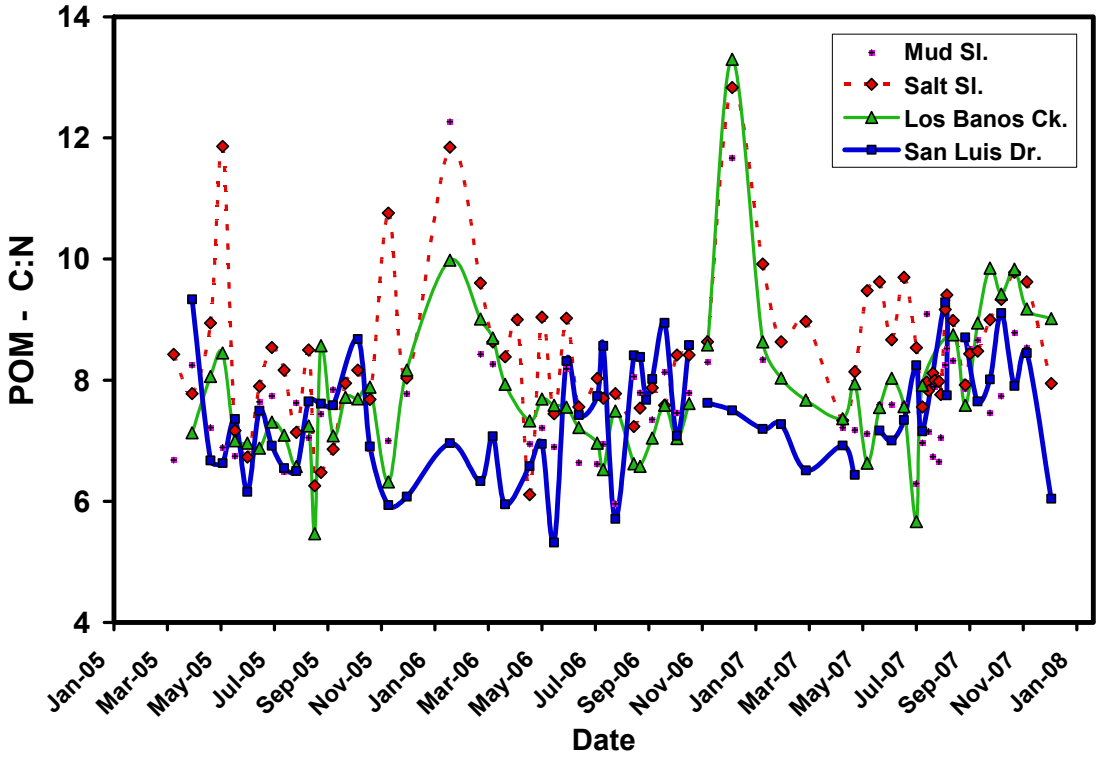

Figure C10. Temporal variation in the C:N, $\delta^{15}N$, and $\delta^{13}C$ of POM at the SJR @ Mossdale (top) and Vernalis (bottom).

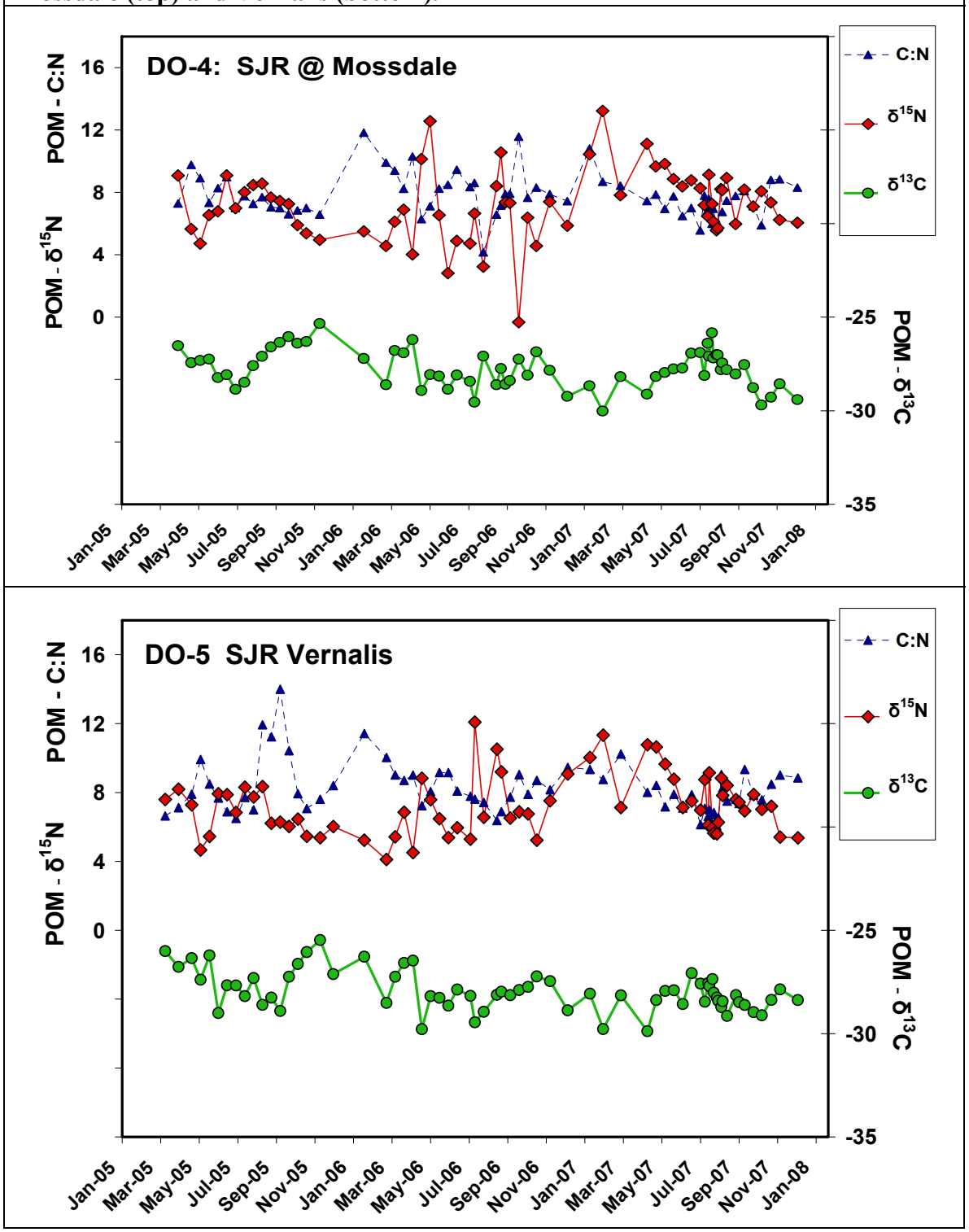

Figure C11. Temporal variation in the C:N, $\delta^{15}N$, and $\delta^{13}C$ of POM at the SJR @ Maze (top) and Laird Park (bottom).

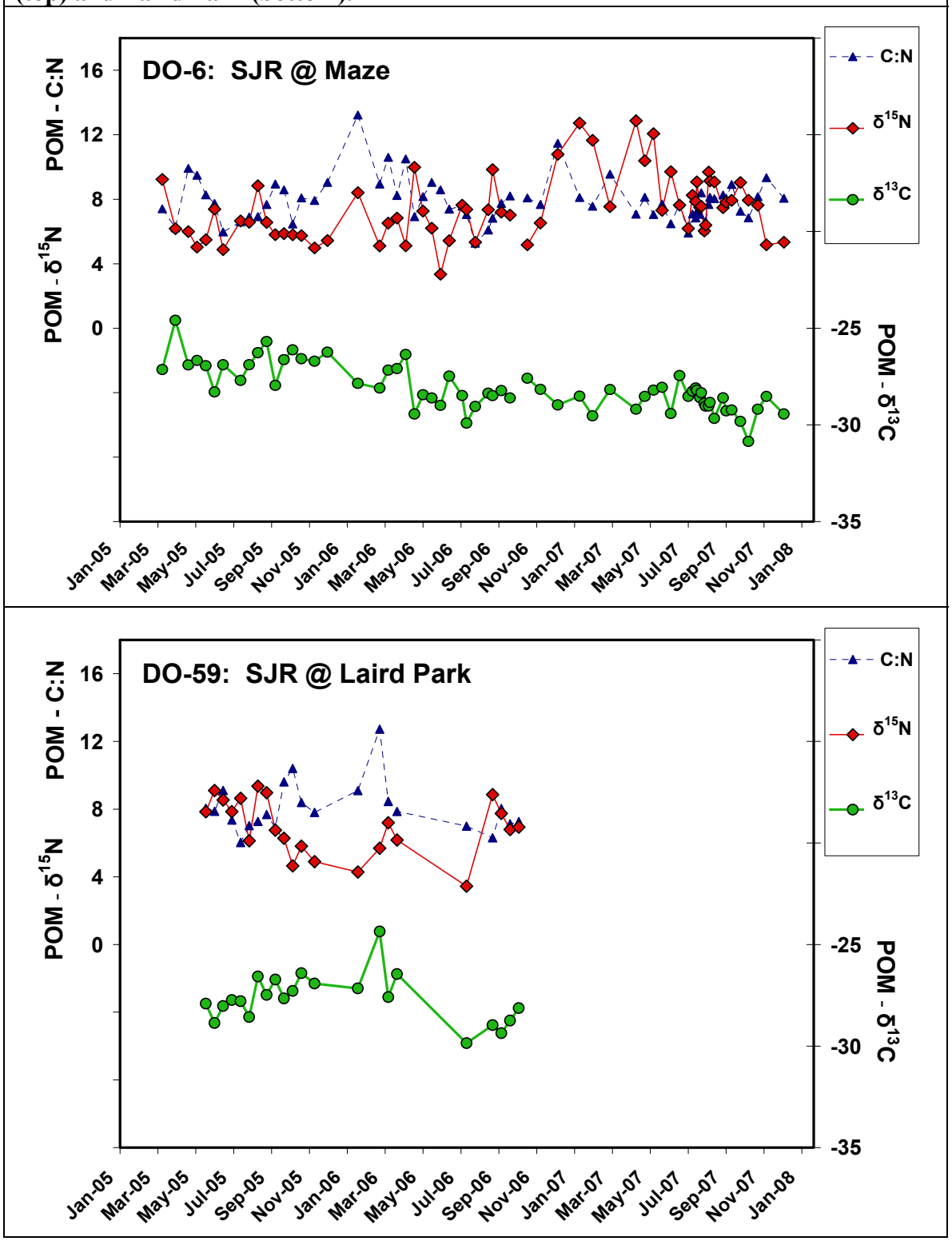

Figure C12. Temporal variation in the C :N, $\delta^{15}N$, and $\delta^{13}C$ of POM at the SJR @ Patterson (top) and Crows Landing (bottom).

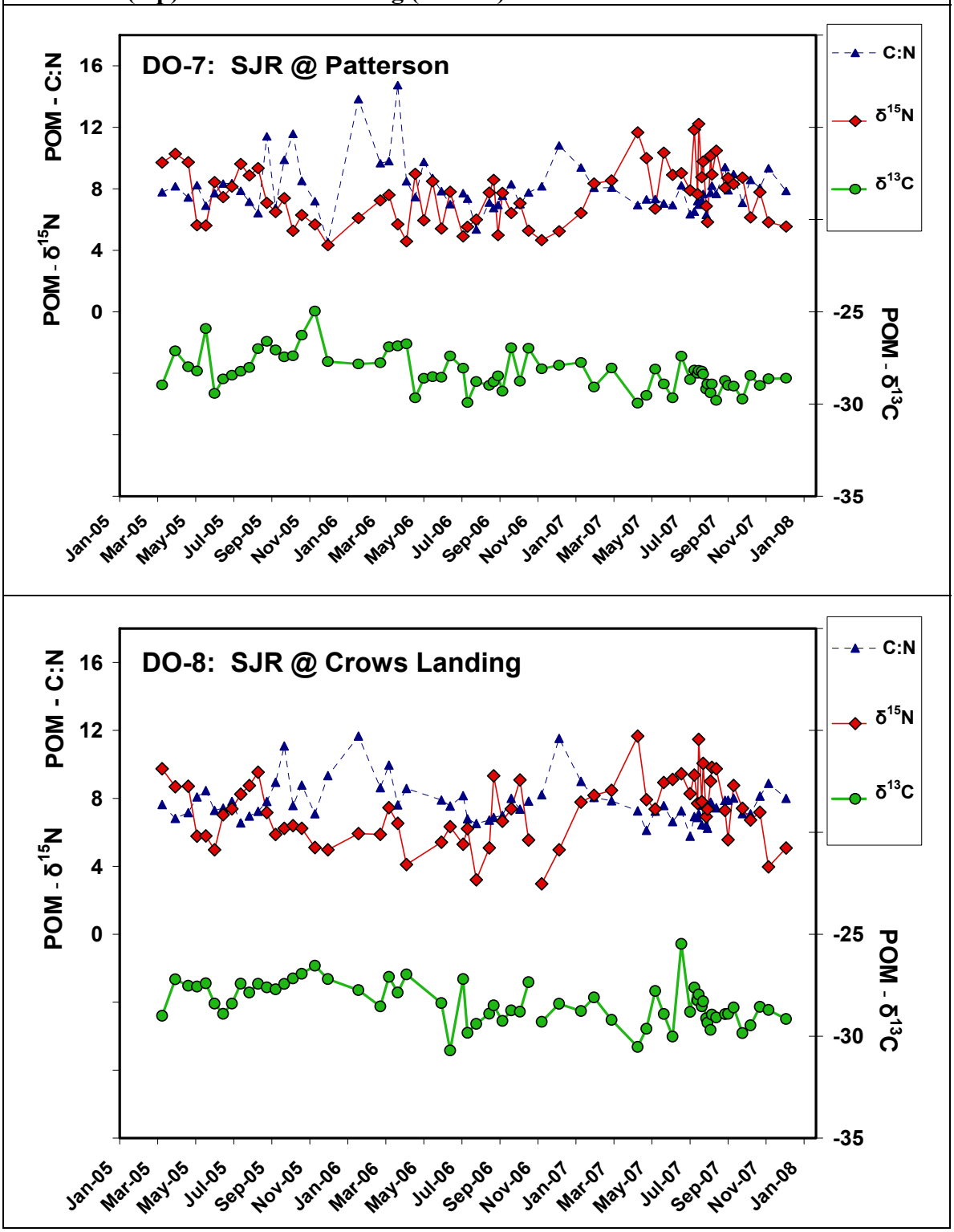

Figure C13. Temporal variation in the C:N, $\delta^{15}N$, and $\delta^{13}C$ of POM at the SJR @ Lander Ave. (top) and the Stanislaus River (bottom).

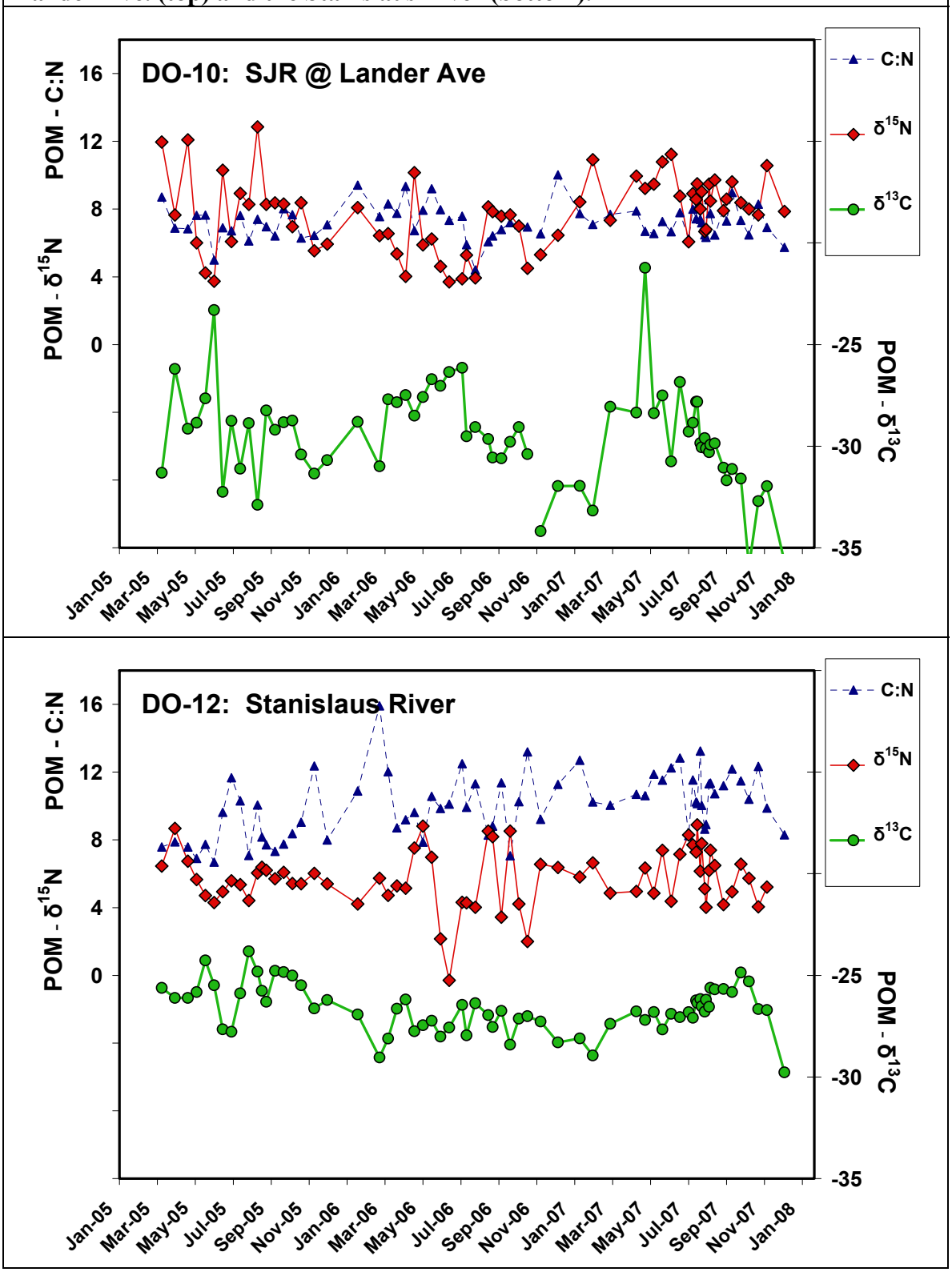

Figure C14. Temporal variation in the C:N, $\delta^{15}N$, and $\delta^{13}C$ of POM at the Tuolumne River (top) and the Merced River (bottom).

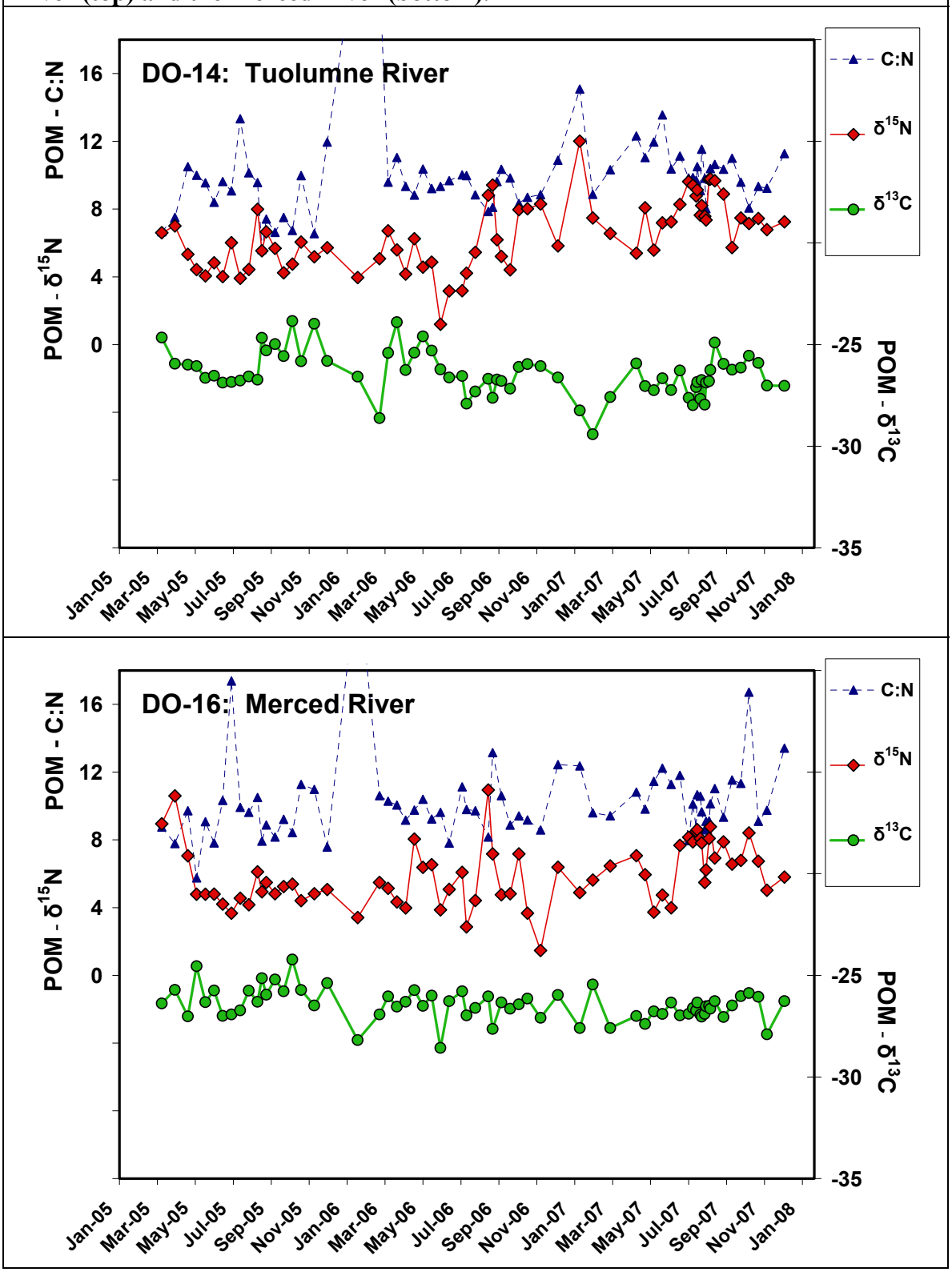

Figure C15. Temporal variation in the C:N, $\delta^{15}N$, and $\delta^{13}C$ of POM at Modesto ID Lat 5 (top) and MID Miller Lake to Stanislaus (bottom).

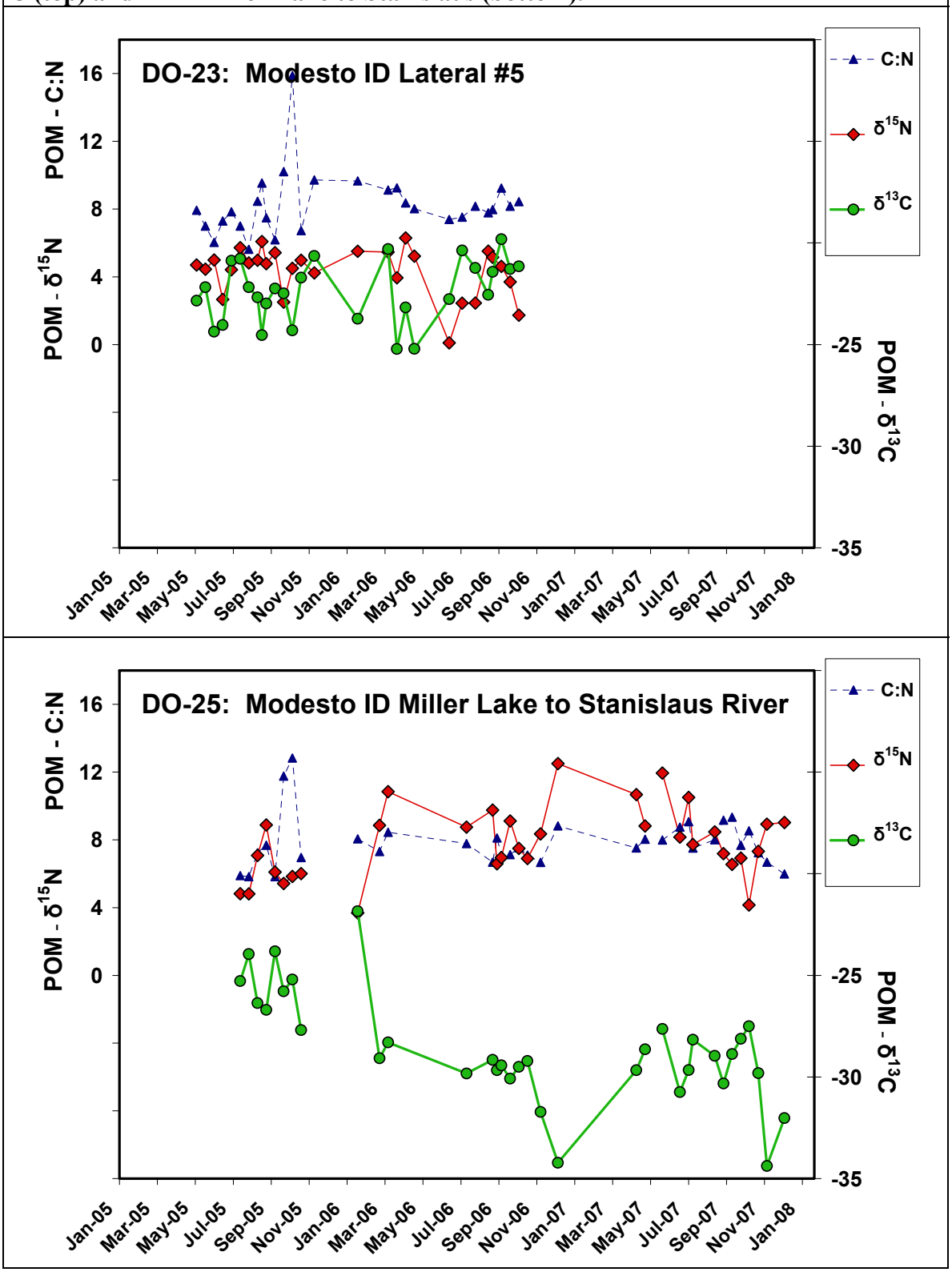

Figure C16. Temporal variation in the C:N, $\delta^{15}N$, and $\delta^{13}C$ of POM at Westport Drain (top) and Harding Drain (bottom).

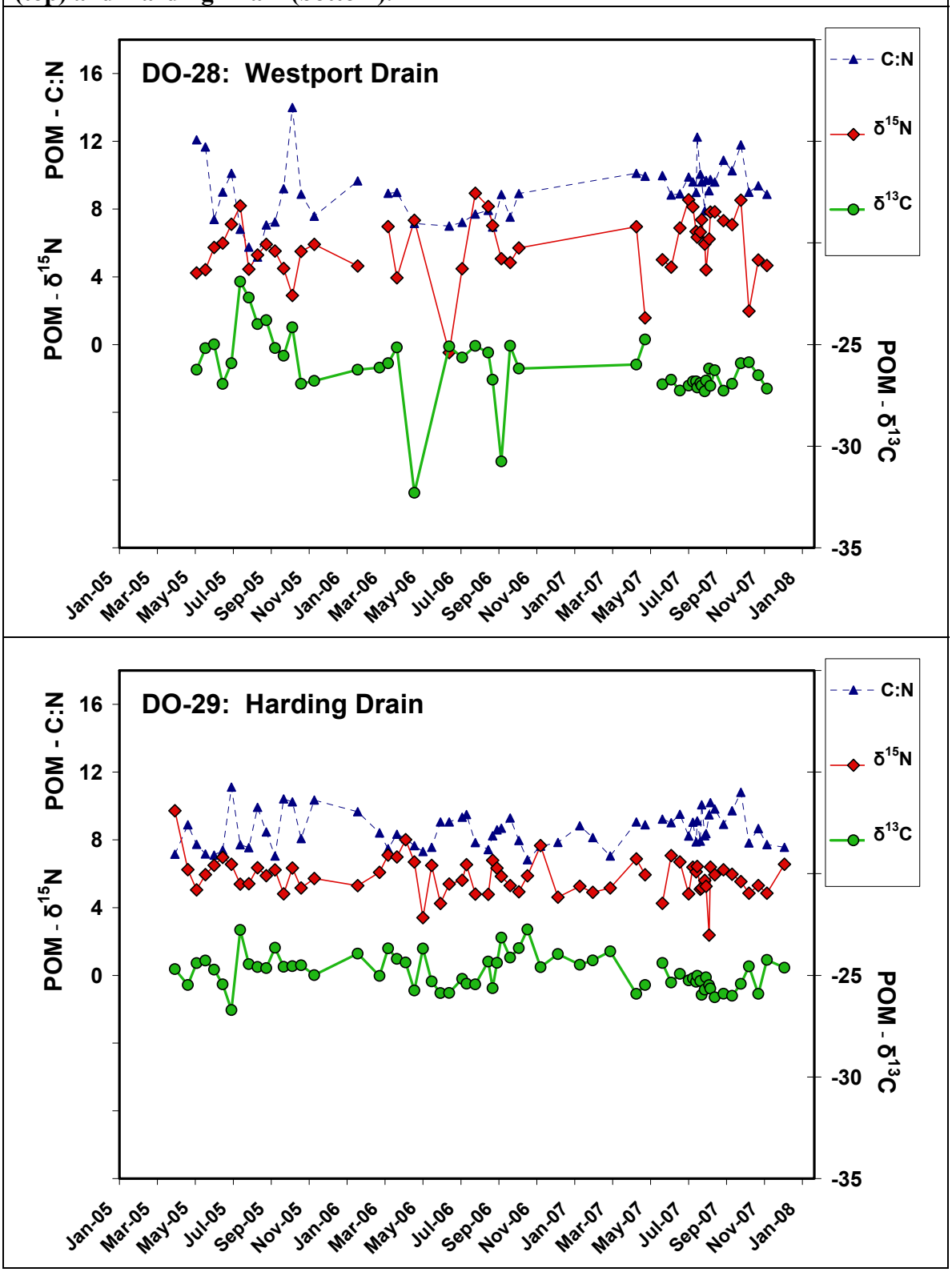

Figure C17. Temporal variation in the C:N, $\delta^{15}N$, and $\delta^{13}C$ of POM at TID Lat 6&7 (top) and Hospital Creek (bottom).

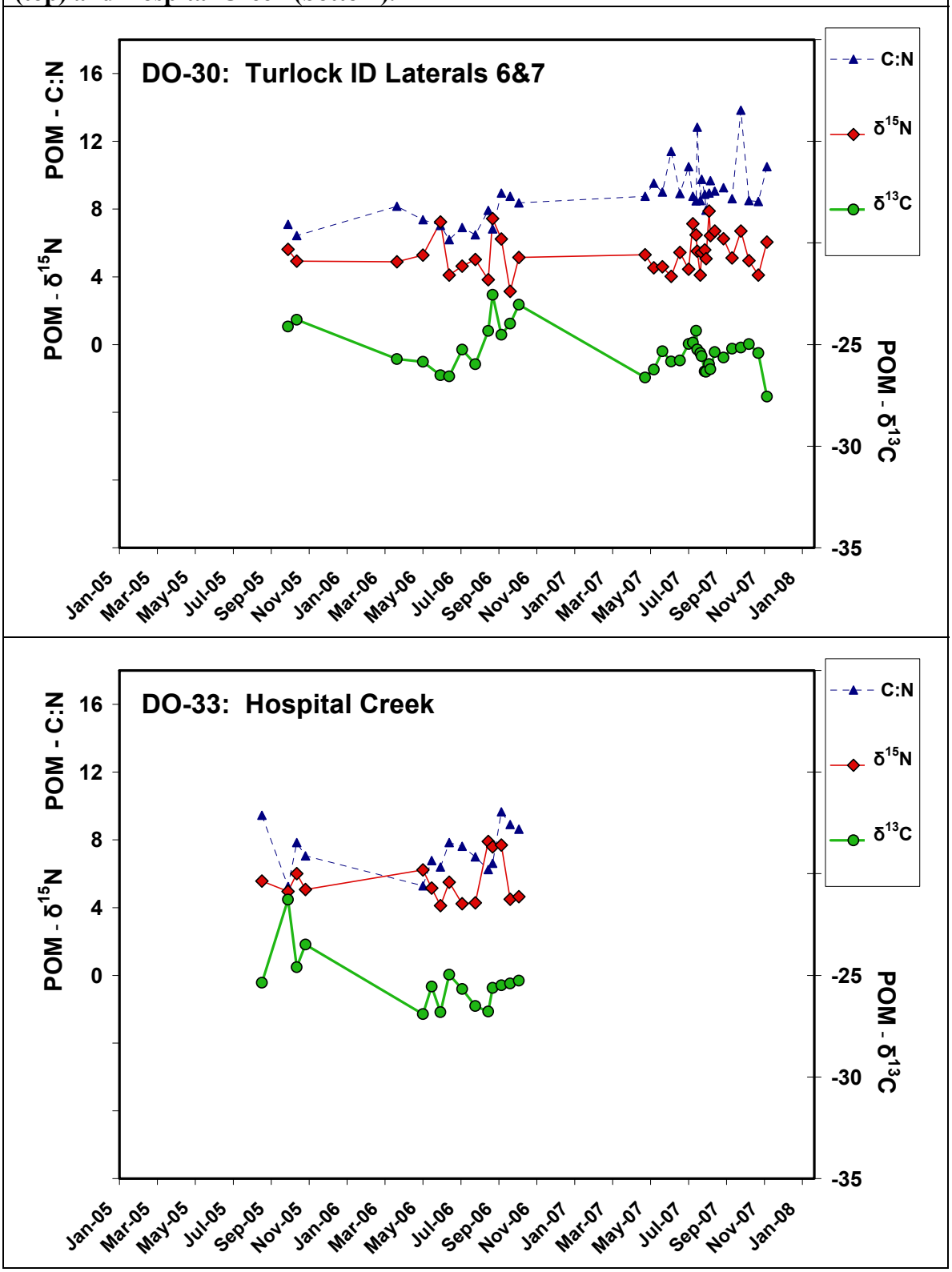

Figure C18. Temporal variation in the C:N, $\delta^{15}N$, and $\delta^{13}C$ of POM at Ingram Creek (top) and Del Puerto Creek (bottom).

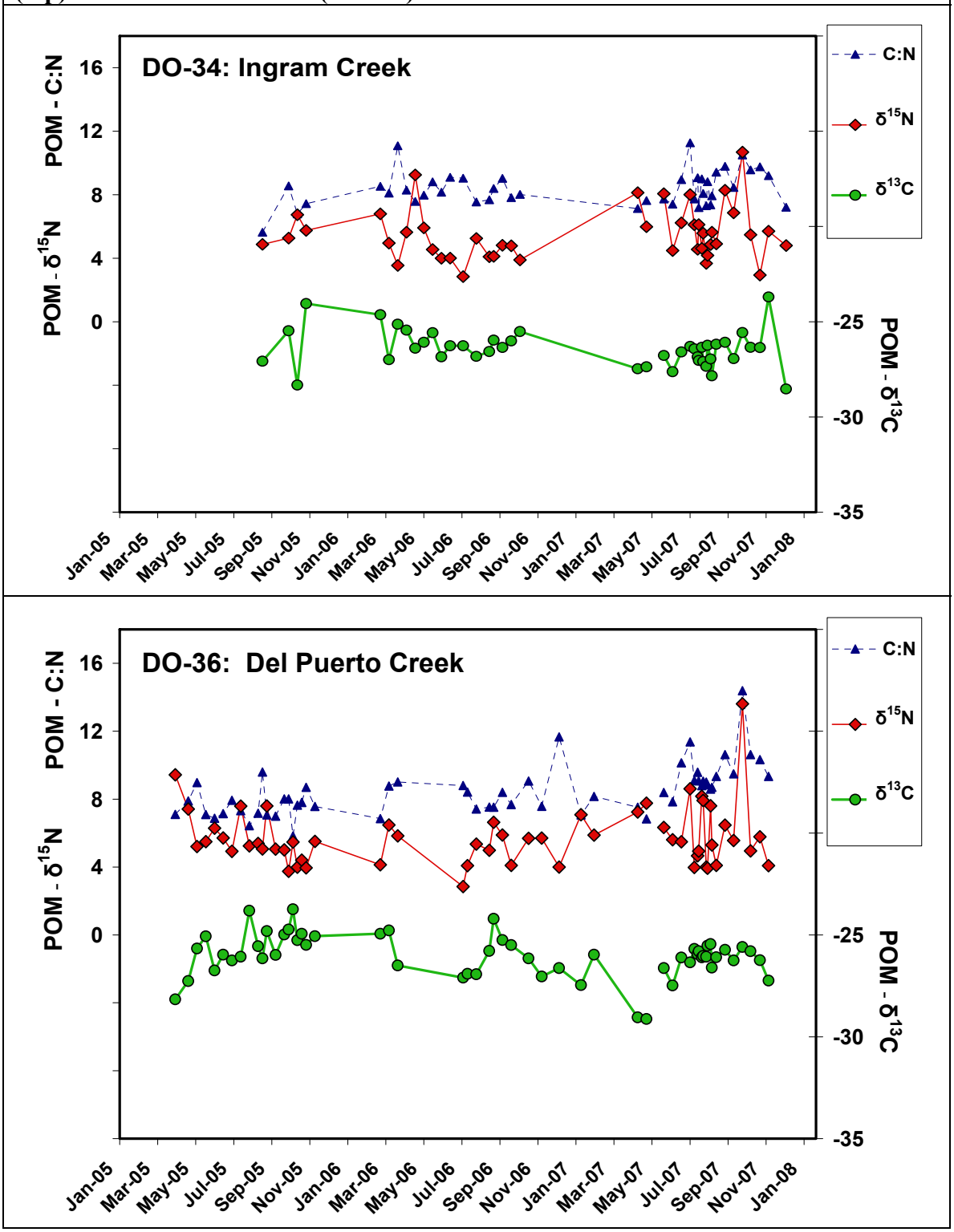

Figure C19. Temporal variation in the C:N, $\delta^{15}N$, and $\delta^{13}C$ of POM at Orestimba Creek (top) and Los Banos Creek (bottom).

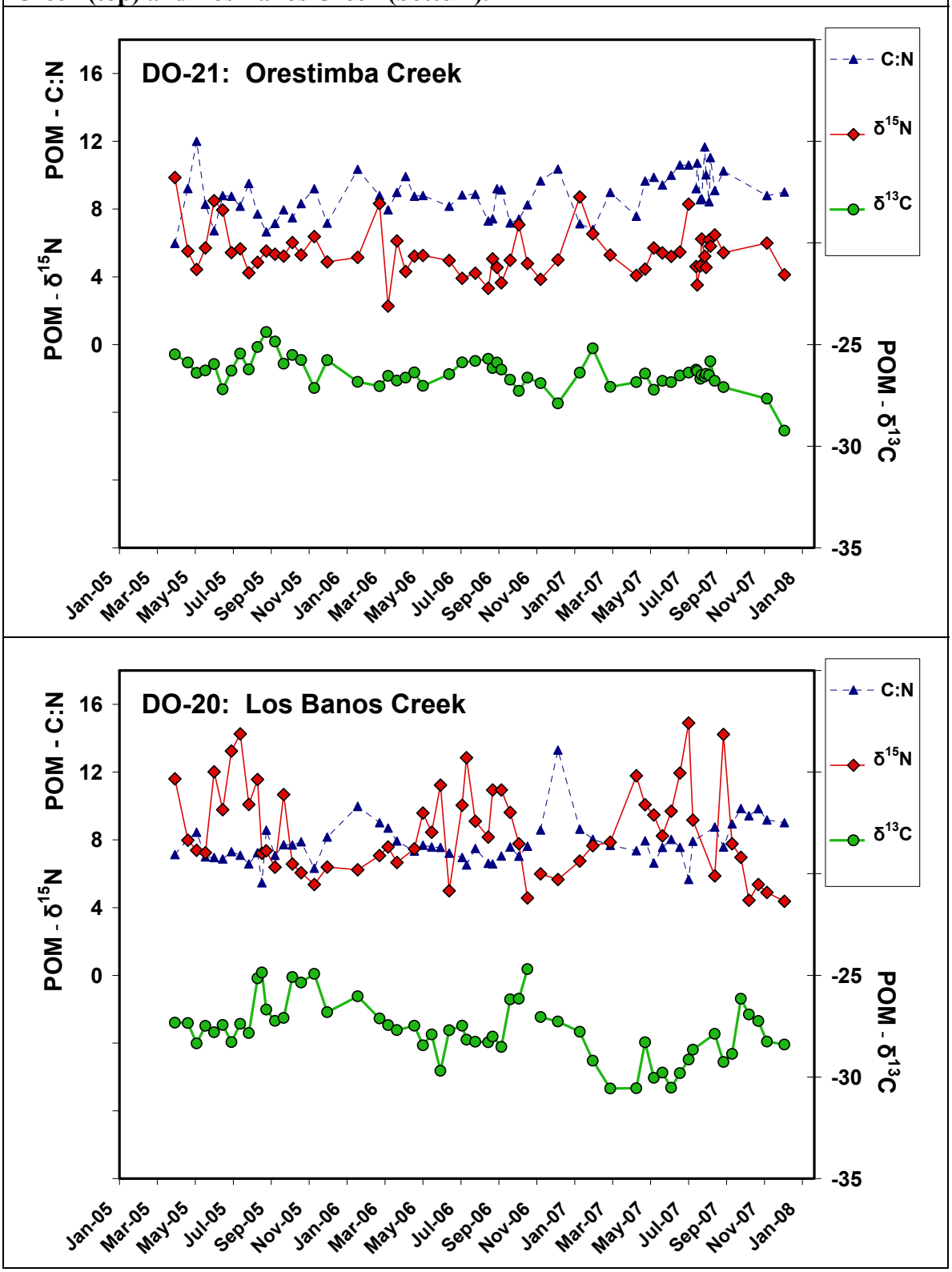

Figure C20. Temporal variation in the C:N, $\delta^{15}N$, and $\delta^{13}C$ of POM at Mud Slough (top) and San Luis Drain (bottom).

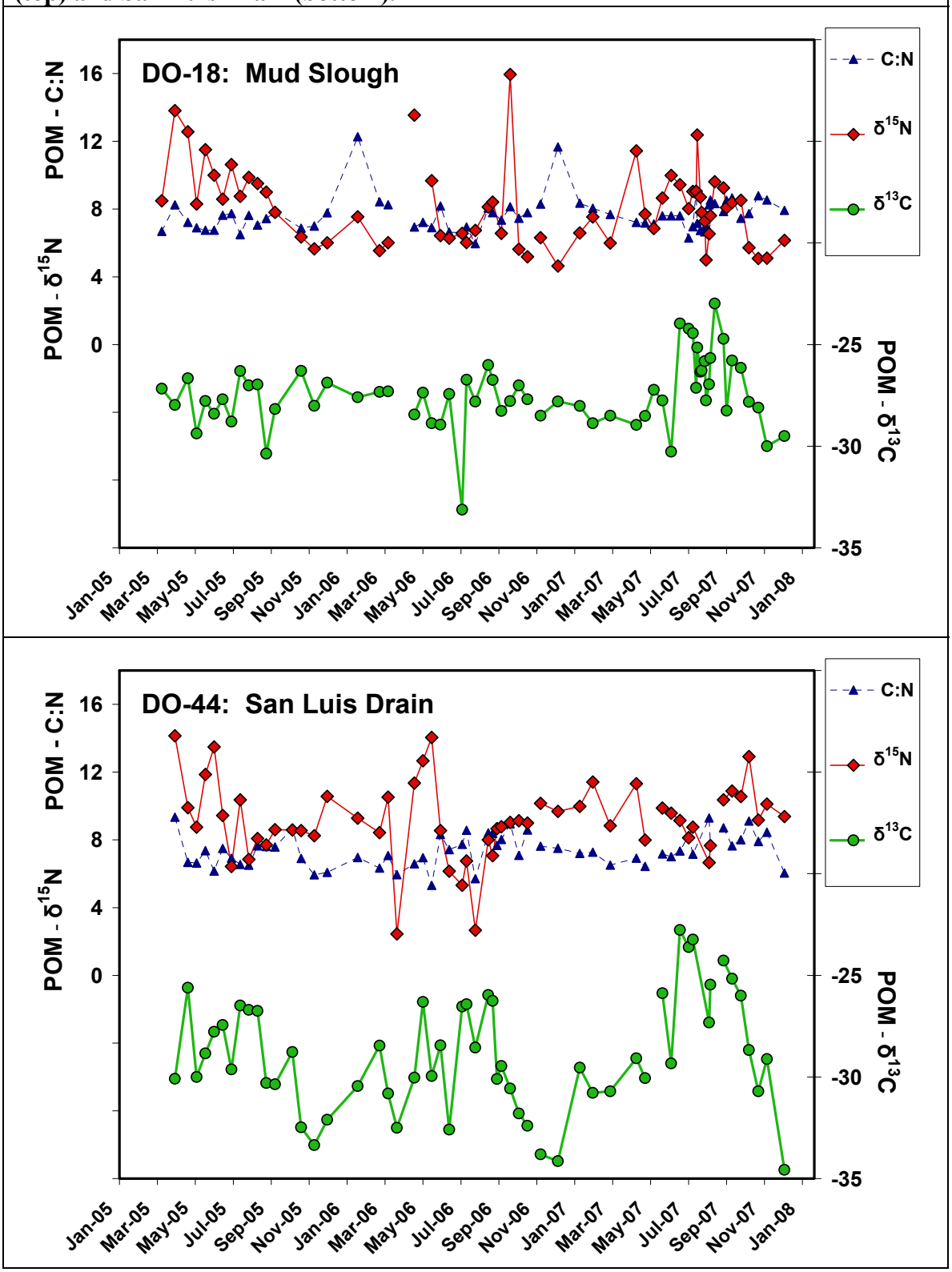

Figure C21. Temporal variation in the C:N, $\delta^{15}N$, and $\delta^{13}C$ of POM at Salt Slough.

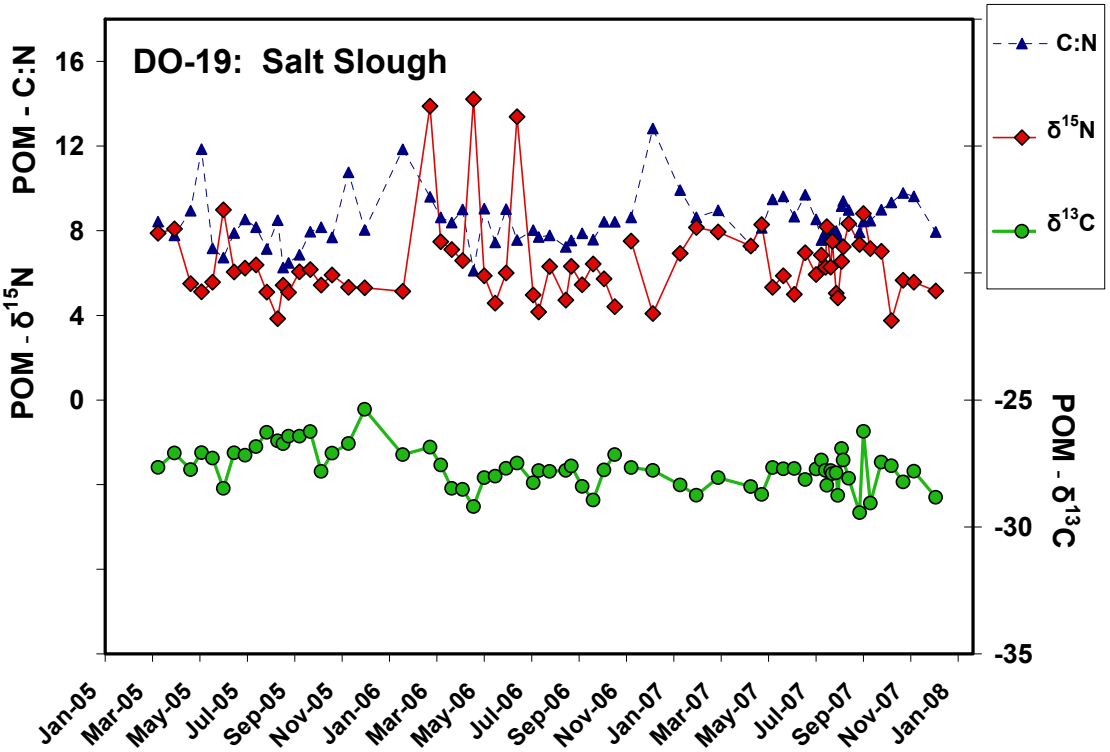

Appendix D: Relations between Algal Pigments, BOD, and the $\delta^{15}N$ and $\delta^{13}C$ of POM

Introduction

The measurement of algal pigments (chlorophyll-A plus pheophytin) provides a means for identifying "relatively" fresh organic matter produced by phytoplankton. There is a very close correlation of chlorophyll with algal pigments, with an r^2 of 0.96 for the set of samples analyzed for POM isotopes. One way to determine the "freshness" or bioavailability of algal and other organic matter is to analyze the samples for Biological Oxygen Demand (BOD). BOD can also be further separated into nitrogenous BOD (NBOD) and carbonaceous BOD (CBOD), depending on how much nitrate and carbon dioxide, respectively, are produced by microbial respiration (oxidation) during laboratory incubations. Hence, the measurement of BOD provides an independent measure of the bioavailability of organic matter. There is a good positive correlation of BOD and algal pigments (r^2 of 0.57 for the samples analyzed for POM isotopes) because most of the bioavailable organic matter is of algal origin. The higher C:N values and chemical composition of terrestrial organic matter make it generally less useful for bacterial respiration than algal material with an average C:N of 6.7 (the so-called Redfield Ratio).

We have already discussed the correlation of C:N with algal pigment and BOD in the body of the report. In this appendix, we will now compare algal pigment and BOD concentrations with $\delta^{15}N$ and $\delta^{13}C$, to explore how the isotope data allow enhanced discrimination among sources of POM. This discussion will be divided into 2 sections, each aimed at discussing the usefulness of one of the new parameters measured.

Correlation of POM-$\delta^{15}N$ and Algal Pigment and BOD Concentrations.

Figures D1-D3 show the correlations of $\delta^{15}N$ and BOD, CBOD, NBOD, and algal pigments for the various site types. Figure D1 shows the C:N and BOD values for mainstem and tributary sites. Almost all tributary samples had low BOD values, as expected for samples with the high C:N values of mainly terrestrial organic matter. These samples had a range of $\delta^{15}N$ values with absolutely no correlation of $\delta^{15}N$ and BOD. Mainstem samples showed no simple linear correlation with BOD but instead formed a vaguely triangular cluster with increasing BOD values with increasing $\delta^{15}N$ values. This makes a bit of sense in that high $\delta^{15}N$ values often indicate either manure/waste inputs, both of which are often associated with algal production, or intense N cycling, which is also often associated with increased algal production. Samples from Lander constitute a large percent of the high-$\delta^{15}N$, high-BOD samples.

Figures D2 and D3 compare the correlations of $\delta^{15}N$ with BOD, CBOD, NBOD, and algal pigments for wetlands, drain, and creek sites, with the values of mainstem sites added for reference. Sites with higher $\delta^{15}N$ (which are predominately wetlands sites) tend to have higher BOD on average than sites with lower $\delta^{15}N$ (which tend to be creeks and drains). A higher proportion of the BOD at wetlands sites is CBOD than at other sites (Figure D2). In other words, the wetlands sites tend to have a low proportion of NBOD than the creek/drain

sites. Drain/creek sites usually have relatively low pigment concentrations and $\delta^{15}N$ values; in contrast, wetlands sites have higher $\delta^{15}N$ values and a wide range of pigment concentrations.

Interestingly, examination of Figure D3 shows that the wetlands samples with high $\delta^{15}N$ and low NBOD (San Luis Drain, Los Banos Creek, and Mud Slough), have high algal pigment concentrations, much higher than seen at the creek/drain sites or Salt Slough. Hence, here we see a good example where high $\delta^{15}N$ values distinguish between lower BOD sources of organic matter (creeks/drains) and higher BOD sources of organic matter (upstream wetlands sites) where the organic matter is clearly dominated by fresh algae. The high $\delta^{15}N$ values could have been the result of intense N cycling in the marshes, which reduced the ammonium concentrations, thus explaining the relatively low NBOD at these sites. In contrast, Del Puerto and Ingram Creeks tend to have higher NBOD than other sites.

Correlation of POM-$\delta^{13}C$ and Algal Pigment and BOD Concentrations.

Figures D4-D8 show the correlations of $\delta^{13}C$ and BOD, CBOD, NBOD, and algal pigments for the various site types. As shown before, tributary sites have higher $\delta^{13}C$ values and substantially lower algal pigment concentrations than mainstem sites (Figure D4). Samples with $\delta^{13}C$ values > -27‰ tend to have low algal concentrations and high C:N values (meaning that the POM is largely terrestrial) versus samples with $\delta^{13}C$ values < -27‰, which tend to have low C:N and high pigment concentrations, indicating an algal origin. Hence, here the combination of $\delta^{13}C$ and C:N can be used to distinguish between fresh algae and terrestrial sources of POM to the SJR. Comparison of these observations with Figure D5 confirms that the POM with the low C:N and low $\delta^{13}C$ values has high BOD concentrations, meaning it is more bioavailable.

Figure D6 shows that there is little correlation of $\delta^{13}C$ with BOD or NBOD for mainstem sites. However, the triangular distributions of BOD and NBOD values indicates that samples with "mid-range" $\delta^{13}C$ values then to have higher BOD and NBOD than samples with "outlier" $\delta^{15}N$ values. It is important to note that most of the samples with low $\delta^{13}C$ values and low NBOD are from the Lander site, as are the samples with mid-range $\delta^{13}C$ values and high BOD. Besides the Landers samples, the site that shows the highest BOD and NBOD values is Mossdale, which is curious; where is this bioavailable organic matter coming from?

Figures D7 and D8 compare the $\delta^{13}C$ and BOD, CBOD, NBOD, and algal pigments for selected wetlands, drain, and creek sites. The creek/drain sites have higher $\delta^{13}C$ values and lower pigment concentrations than wetlands sites; it is interesting how little overlap there is in $\delta^{13}C$ values between these two site types. The drain/creek sites have $\delta^{13}C$ values similar to the major tributaries, perhaps largely for the same reason: because a large proportion of the POM is derived from terrestrial organic matter, which typically has a narrow range of $\delta^{13}C$ values. However, the BOD concentrations (Figure D8) of the creek/drain sites (especially Del Puerto Creek, and to some extent Harding Drain and Ingram Creek) are higher than for tributary sites, indicating that these sites contain a higher percentage of algal material than tributary sites. Westport Drain and Orestimba Creek appear to have lower percentages of algal material than other drain/creek sites, and Salt Slough tends to have

lower pigment concentrations and BOD than other wetlands sites.

For San Luis Drain samples, there is an interesting positive correlation of $\delta^{13}C$ values and NBOD (Figure D8b), with samples with low NBOD having very low $\delta^{13}C$ values. One explanation is that uptake of ammonium by algae is causing the low NBOD. Algae preferentially uptake DIC with low $\delta^{13}C$ values, which, if the pool of DIC is large, can result in POM with low $\delta^{13}C$ values. Alternatively, the low $\delta^{13}C$ values could reflect methane formation and oxidation in anoxic sediments (Figure 4).

Relations among POM-Related Measurements.

Figure D9 is an attempt to combine the correlations between $\delta^{13}C$, $\delta^{15}N$, and C:N for the entire dataset onto a single plot. The plot was constructed by sorting the samples by C:N value, and then plotting the C:N values as a thick red line, the $\delta^{15}N$ values as pink diamonds, and the $\delta^{13}C$ values as blue dashes. The $\delta^{13}C$ values generally increase as C:N increases, reflecting increasing inputs of terrestrial sources of POM. Note that the variability in $\delta^{13}C$ decreases as the $\delta^{13}C$ and C:N increase. These trends can be explained by the much narrower range of $\delta^{13}C$ values of C3 terrestrial vs aquatic sources of POM. In contrast, the $\delta^{15}N$ values decrease as C:N increases, and the variability in $\delta^{15}N$ decreases as C:N increases. These trends can be explained in the same way as for $\delta^{13}C$: there is a narrower range of $\delta^{15}N$ values for terrestrial vs aquatic sources of POM, and typical $\delta^{15}N$ values for terrestrial organic matter are usually lower than the ranges possible for aquatic plants (Figure 3). The r^2 values for the trends of $\delta^{13}C$ and $\delta^{15}N$ values are low (<0.1), but the relationships with C:N are very clear anyway, despite the high degree of variability in values.

Figure D10 takes a similar approach, but in this case attempts to combine the correlations with C:N, BOD, algal pigments, and POM concentrations into a single plot. This plot was constructed by sorting the samples by BOD concentration, and then plotting the BOD concentrations as a thick green line, the C:N ratios as small symbols as red dashes, the pigments as larger brown squares, and the calculated POM concentrations as small purple crosses. The C:N values decrease as BOD increases, and show less variability as the C:N values decrease. POM concentrations increase as BOD increases, and show that high BOD samples necessarily have high POM concentrations (i.e., there are no low-POM samples that have high BOD), clearly showing the fact that POM is a much more significant source of BOD than DOC or ammonium).

Algal pigments increase as BOD decreases, but the pigments do not show the type of well-defined linear patterns shown by C:N and POM. Instead, the algal pigment concentrations show a wide range of concentrations (i.e., extending down to almost 0) for all BOD concentrations; the pigment concentrations at each BOD value appear to be evenly distributed. The vague line defined by the maximum pigment values at each BOD concentration shows an interesting pattern: the increase in pigments with BOD has an abrupt increase in slope at about where mean C:N values fall below about 8 (at about sort # 800). It is unclear whether this abrupt change in maximum pigment values represents a change in quality of the pigments, reflects the exponential change in BOD, or is a step function (i.e., above this BOD concentration, the correlations between BOD and pigments become more

tenuous). But the most intriguing aspect of this plot is the high degree of "noise" in the concentration of algal pigments compared to C:N and POM, suggesting that the combination of C:N and POM may be superior predictors of BOD than the more difficult to measure algal pigments. This notion is worth further investigation.

Appendix D- Figures

Figure D1. Correlation of $\delta^{15}N$ of POM and BOD for mainstem SJR sites (top) and major tributaries (bottom). Mainstem sites with low $\delta^{15}N$ values have lower BOD than sites with high $\delta^{15}N$; however tributary samples show a narrower range of BOD values, significantly lower than values at mainstem sites, with no correlation with $\delta^{15}N$ values.

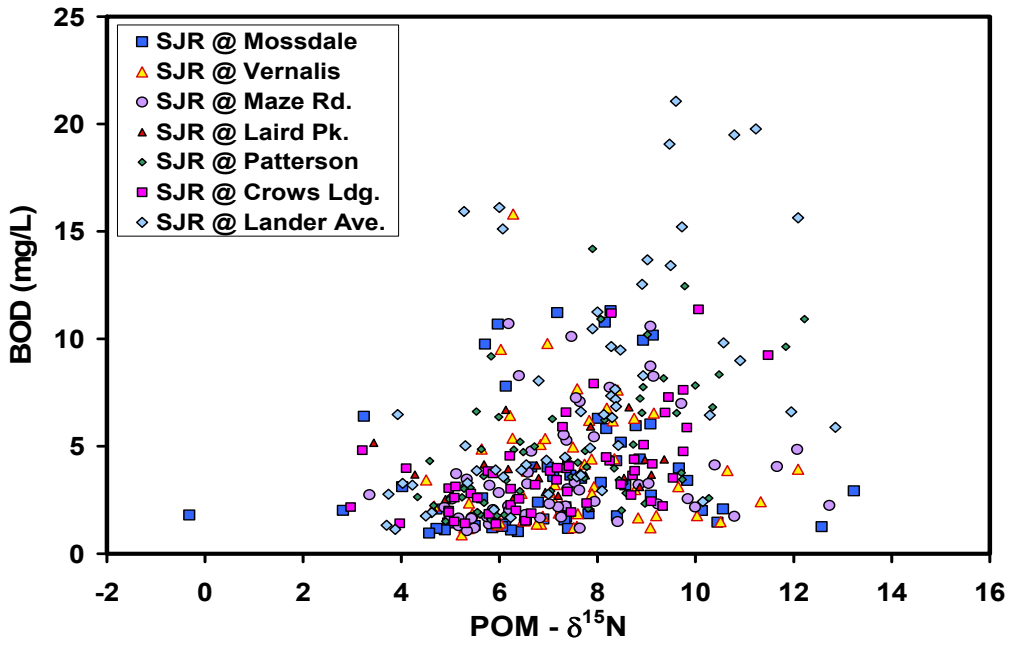

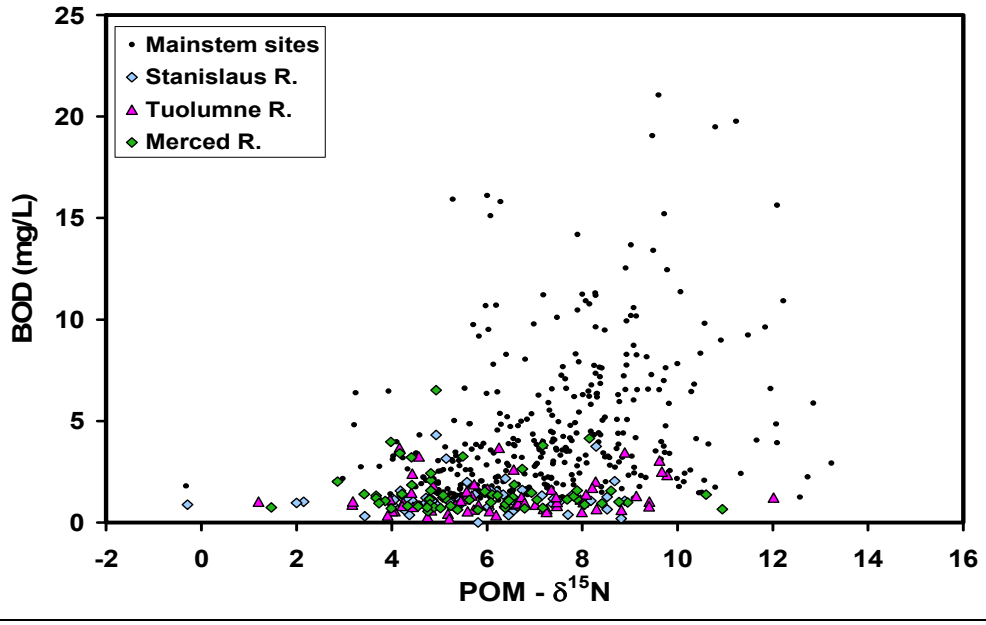

Figure D2. Correlation of $\delta^{15}N$ of POM and BOD (top) and CBOD (bottom) for selected drain, creek, and wetlands sites, with the compositions of mainstem sites included for reference. Sites with higher $\delta^{15}N$ (which are predominately wetlands sites) tend to have higher BOD on average than sites with lower $\delta^{15}N$ (which tend to be creeks and drains. A higher proportion of the BOD at wetlands sites is CBOD than at other sites.

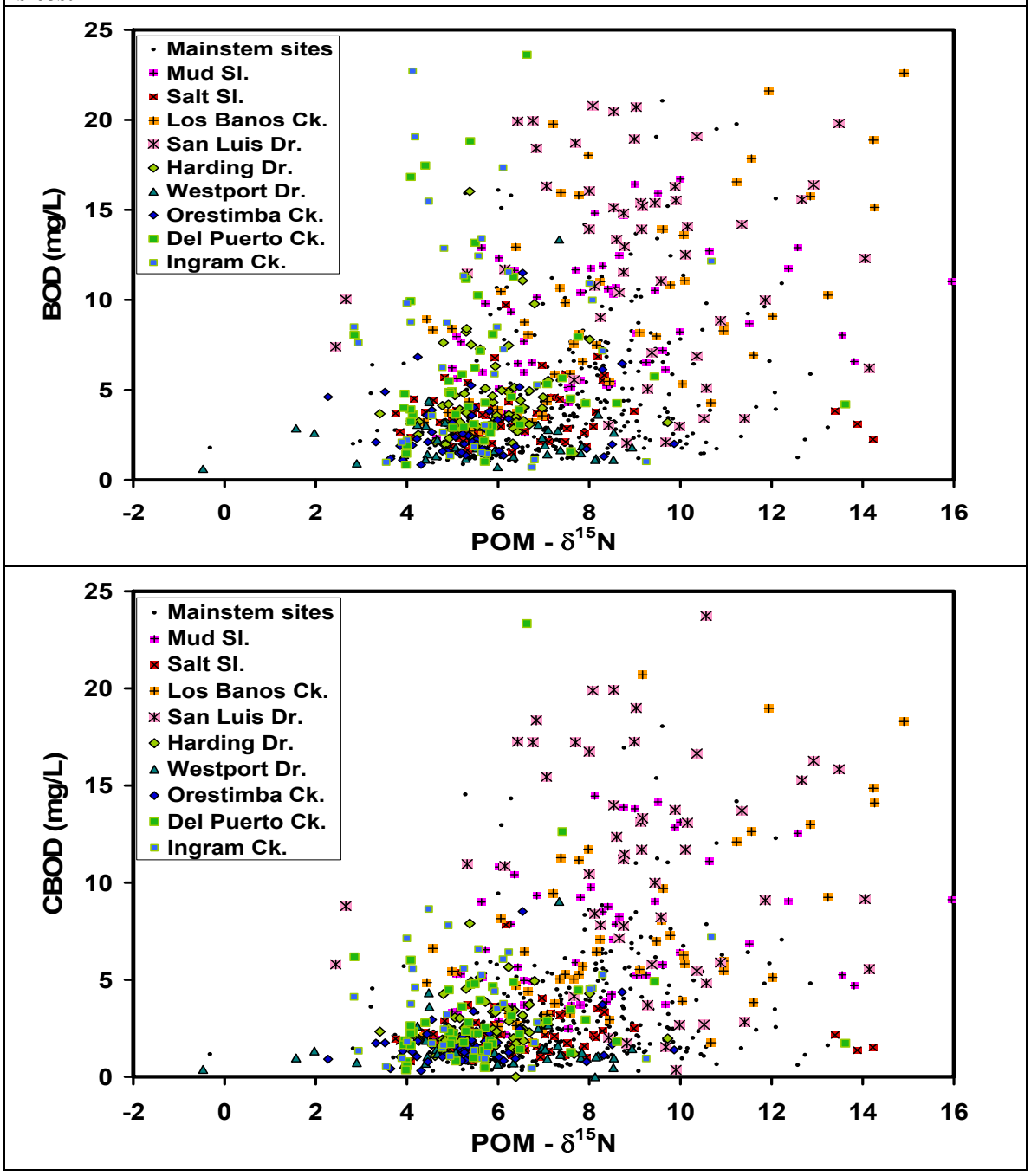

Figure D3. Correlation of $\delta^{15}N$ of POM and NBOD (top) and algal pigments (bottom) at selected drain, creek, and wetlands sites, with the values for mainstem sites included for reference. Wetlands sites have higher $\delta^{15}N$ values and generally lower NBOD than drains and creeks. The samples with the highest NBOD had the highest algal pigment concentrations.

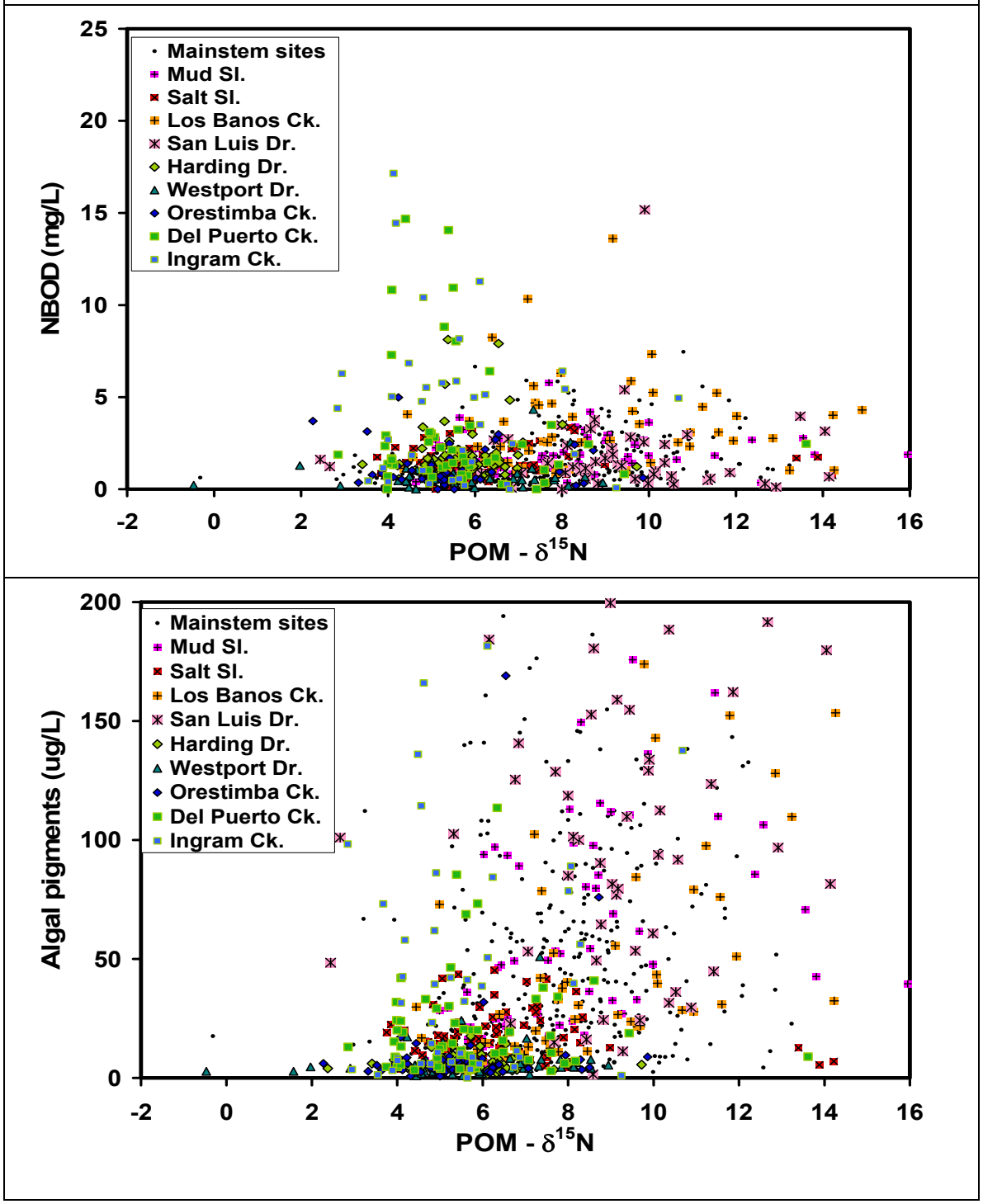

Figure D4. Correlation of $\delta^{13}C$ values of POM and algal pigment concentrations for mainstem SJR sites and major tributaries (top), with the data presented with an expanded algal pigment scale below (bottom). Tributaries samples show a narrow range of pigment values, significantly lower than values at mainstem sites, and generally higher $\delta^{13}C$ values.

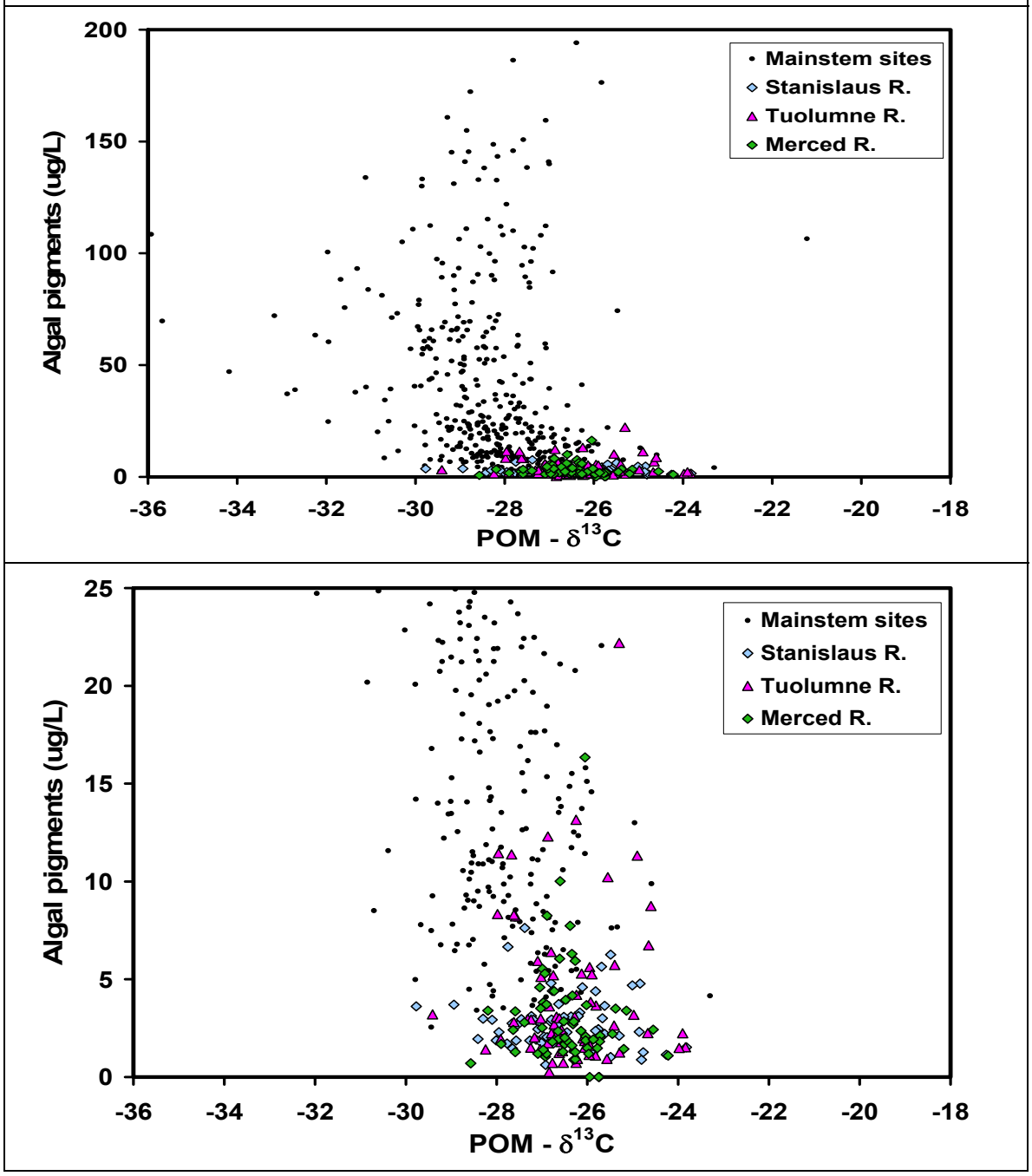

Figure D5. Correlation of $\delta^{13}C$ of POM and BOD for mainstem SJR sites and major tributaries. Tributaries samples show a narrow range of BOD values, significantly lower than values at mainstem sites, and generally higher $\delta^{13}C$ values.

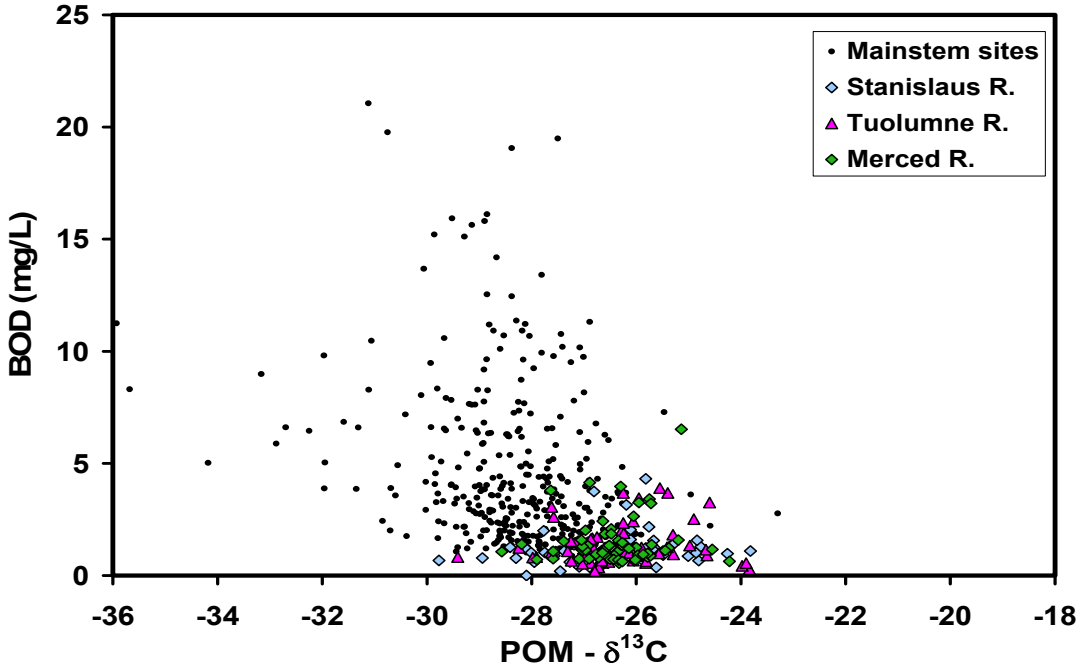

Figure D6. Correlation of $\delta^{13}C$ of POM and BOD (top) and NBOD (bottom) for mainstem SJR sites. Mainstem sites show a narrow range of $\delta^{13}C$ values but no obvious correlation with BOD or NBOD except that both are higher for samples with mid-range $\delta^{13}C$ values.

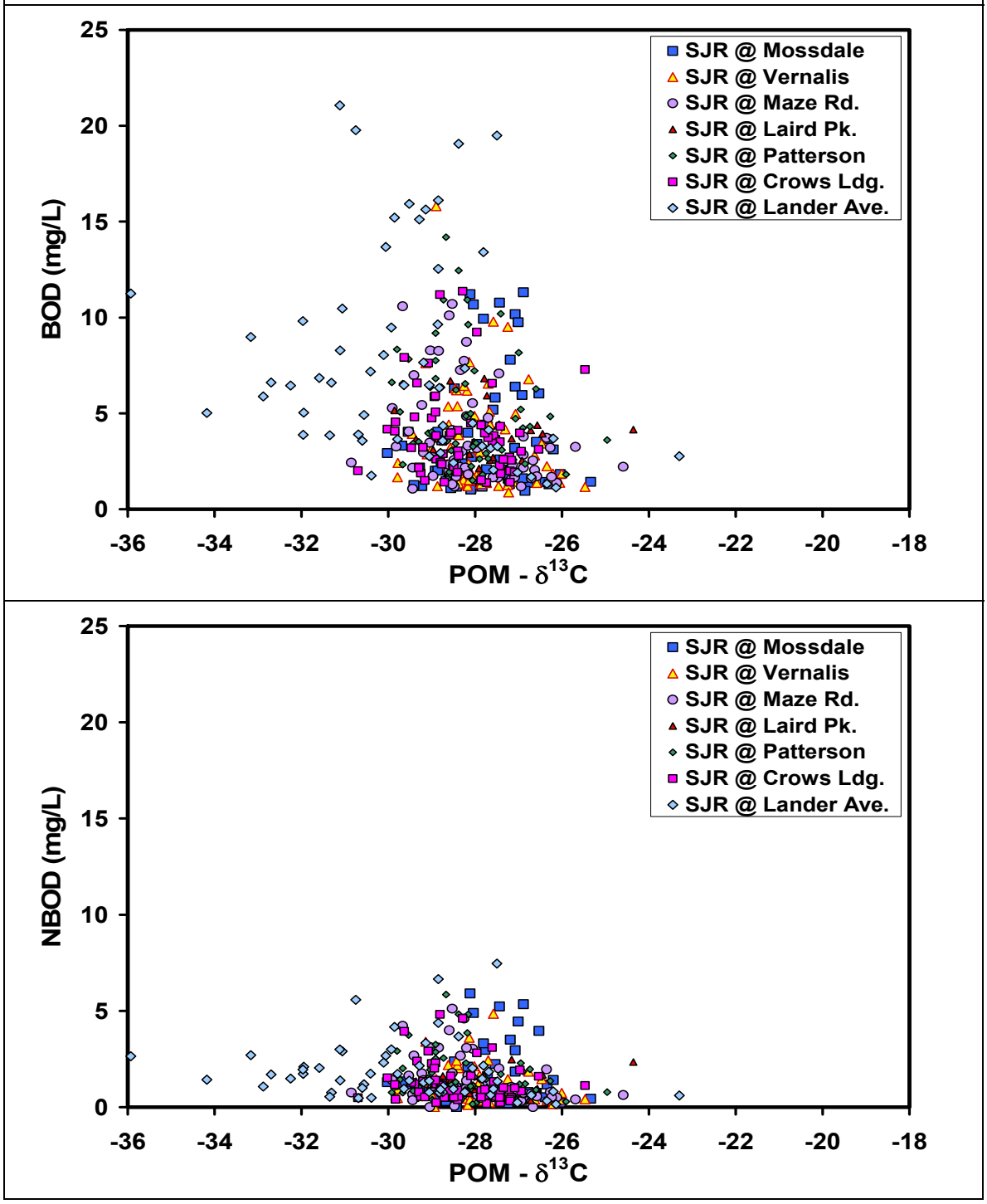

Figure D7. Correlation of $\delta^{13}C$ values of POM and algal pigment concentrations for selected drain, creek, and wetlands sites (top), with the data presented with an expanded algal pigment scale below (bottom). Wetlands sites generally have lower $\delta^{13}C$ values than other sites. Different site types all show wide ranges of pigment values; however, average wetlands pigments values are generally higher than for other sites.

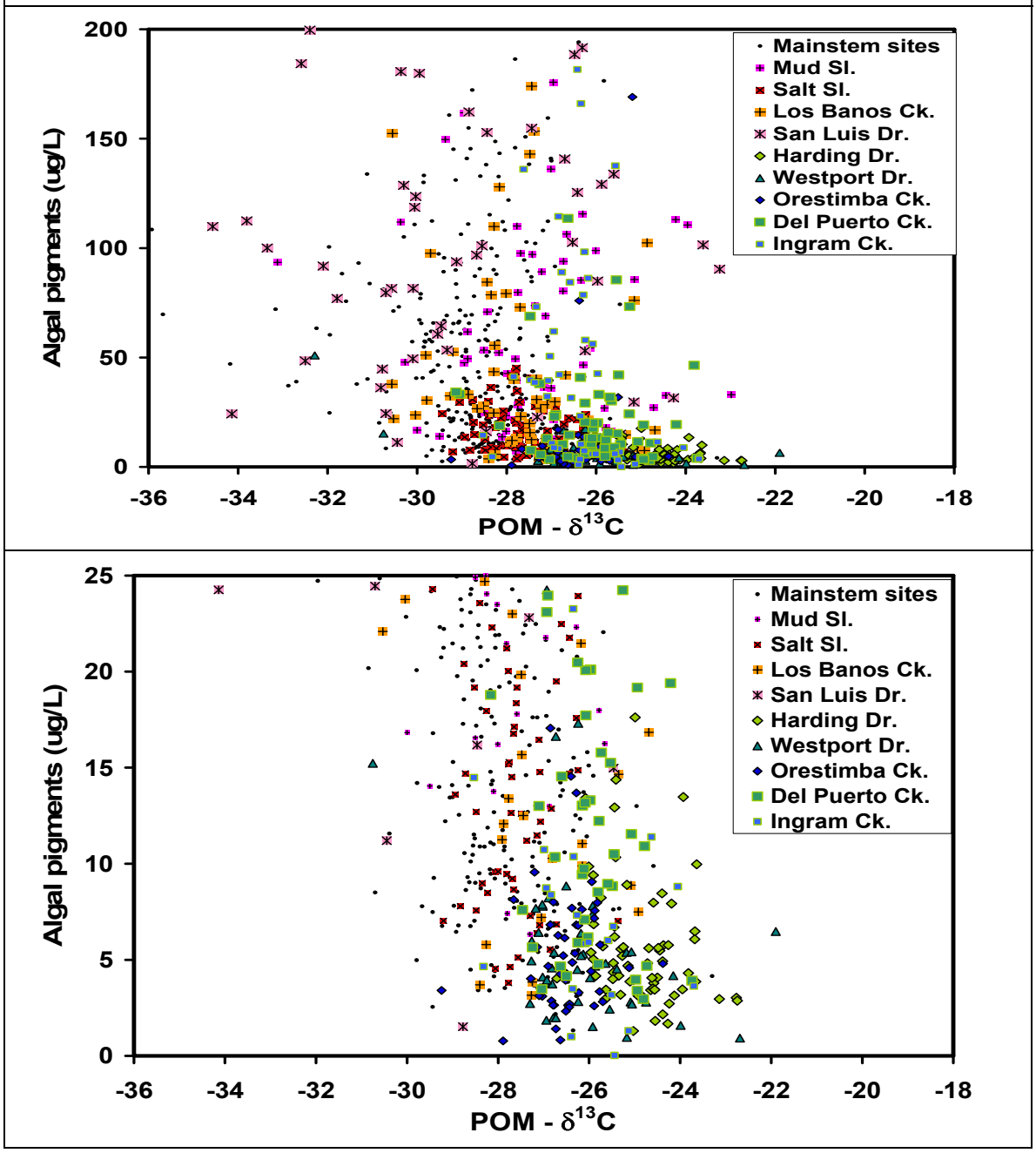

Figure D8. Correlation of $\delta^{13}C$ values of POM from selected drain, creek, and wetlands sites with BOD (top) and NBOD (bottom) values. BOD values are similar for wetlands, creeks, and drain sites. However, wetlands sites (Mud and Salt Slough, Los Banos, and San Luis Drain) have a narrower and lower range of NBOD values than other drain and creek sites.

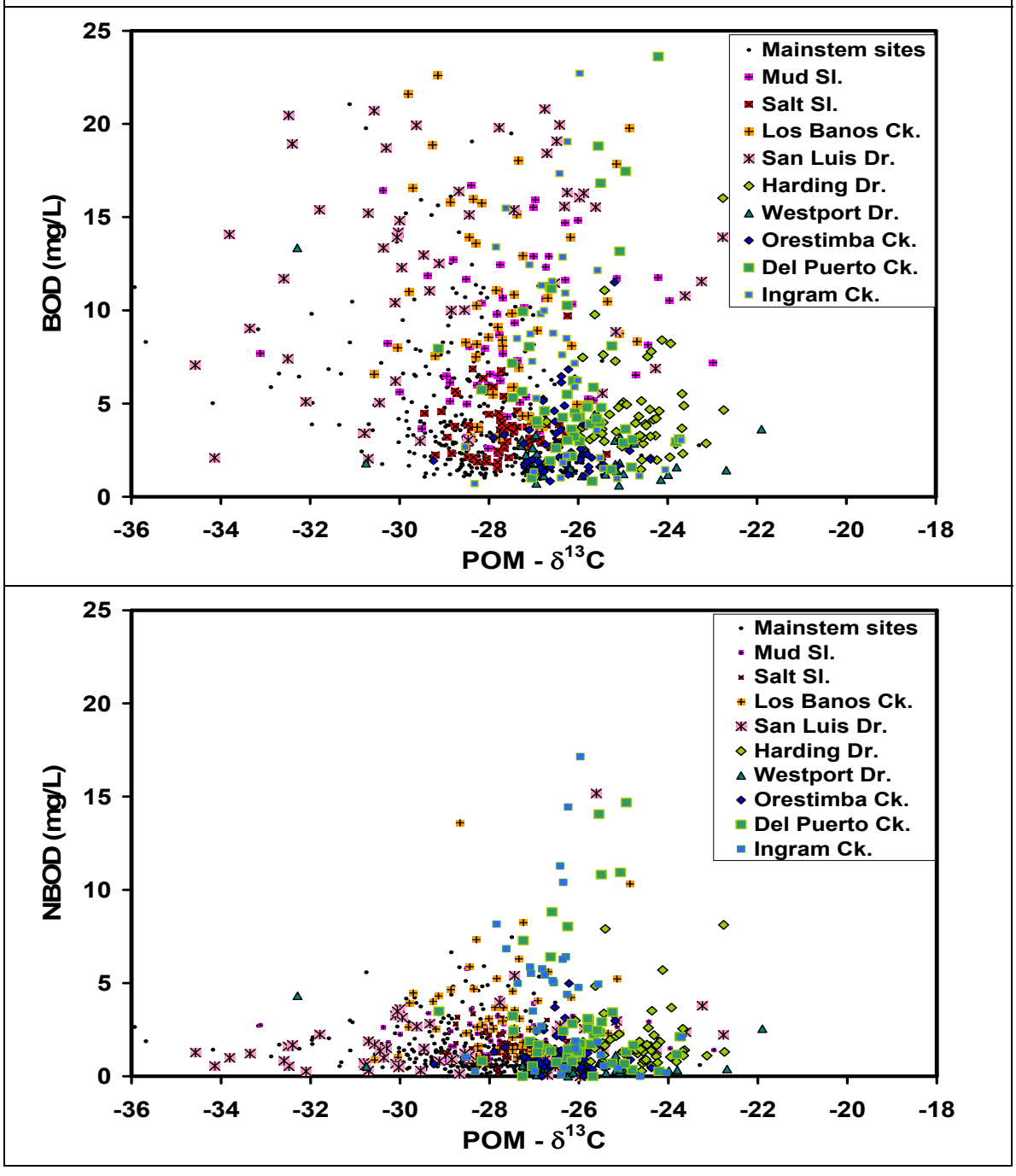

Figure D9. Variability in the POM-$\delta^{15}N$, and POM-$\delta^{13}C$ values with increasing POM-C:N value for the ~1400 samples analyzed. Linear trend lines for $\delta^{13}C$ and $\delta^{15}N$ have r^2 values of 0.02 and 0.07, respectively. Vertical bars show the C:N values.

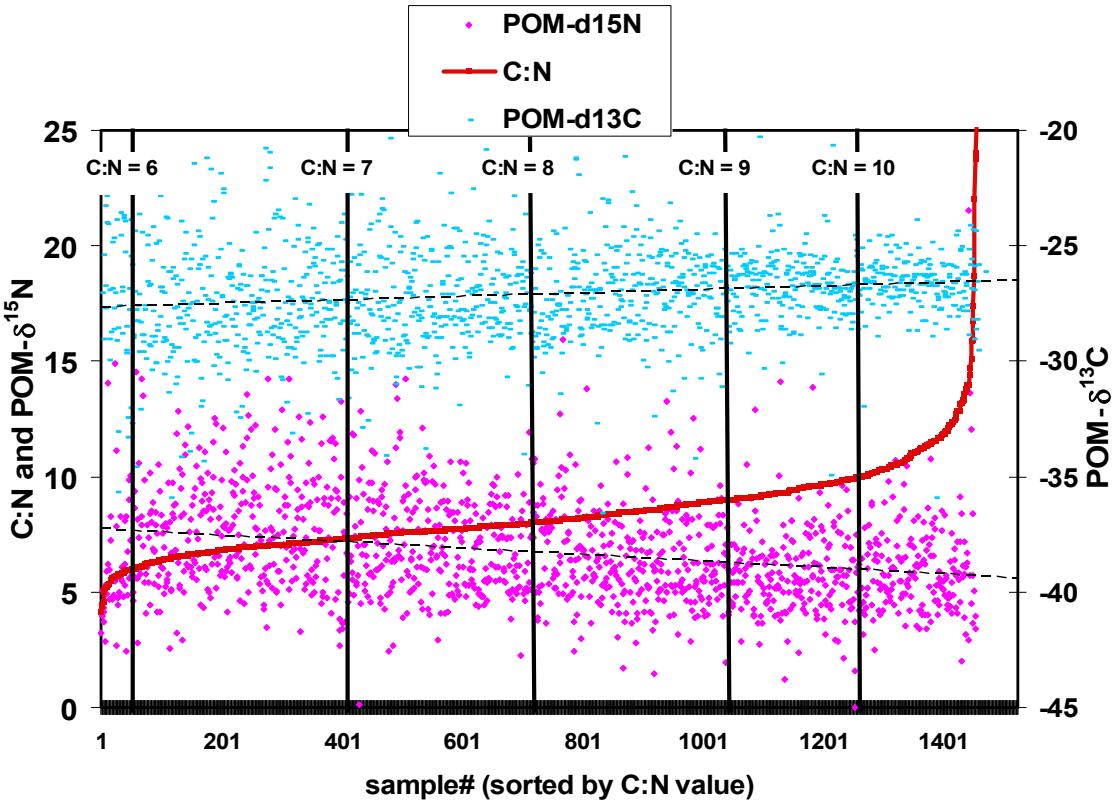

Figure D10. Variability in the C:N, BOD, algal pigments, and calculated POM with increasing BOD value for the ~1200 samples analyzed for C:N that had measured algal pigment concentrations <200 ug/L. The linear trend lines for C:N and POM have r^2 values of 0.15, and linear and polynomial trend lines for algal pigments have r^2 values of 0.33 and 0.43, respectively.

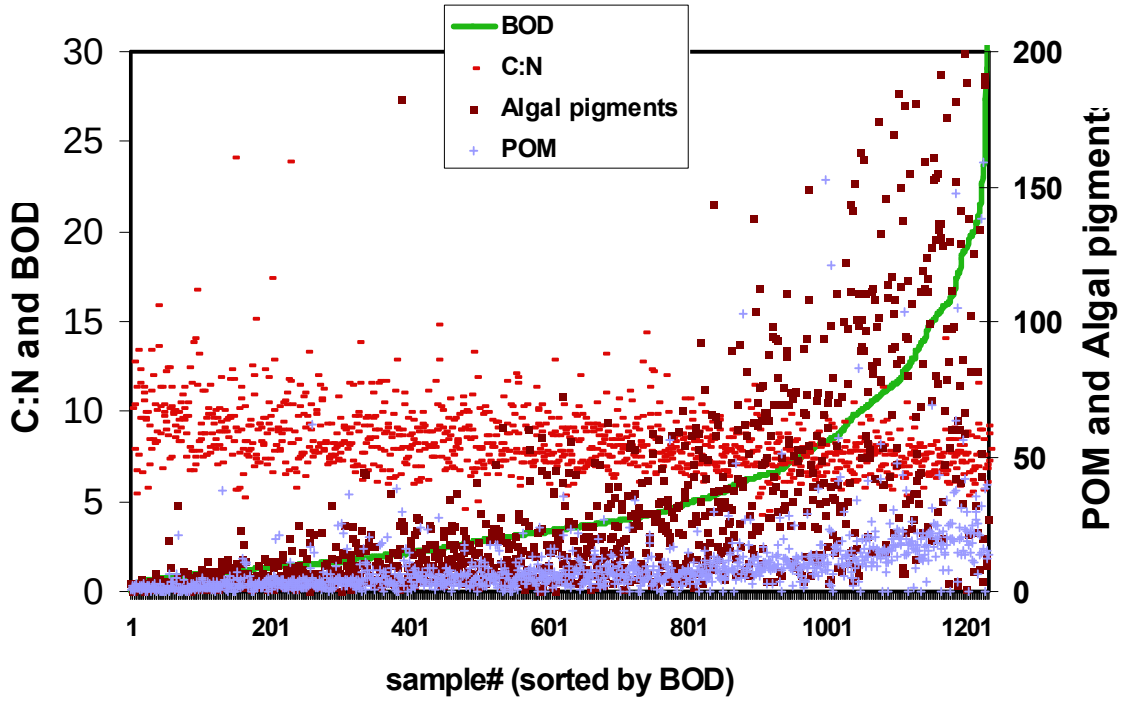

Appendix E: Temporal Variation in Nitrate-$\delta^{15}N$ and $\delta^{18}O$, Water-$\delta^{18}O$, and Nitrate Concentrations at Individual Sites

This section contains a set of plots (Figures E1-E11) showing the temporal variations in $\delta^{15}N$ and $\delta^{18}O$ of nitrate, the $\delta^{18}O$ of water, and nitrate concentrations for all the core sites, with separate plots for each site. Differences between many of the individual sites are discussed in the main section of the report.

Appendix E- Figures

Figure E1. Temporal patterns in $\delta^{15}N$ and $\delta^{18}O$ of NO_3, NO_3 concentration, and $\delta^{18}O$ of water for SJR mainstem sites at Mossdale (top) and Vernalis (bottom).

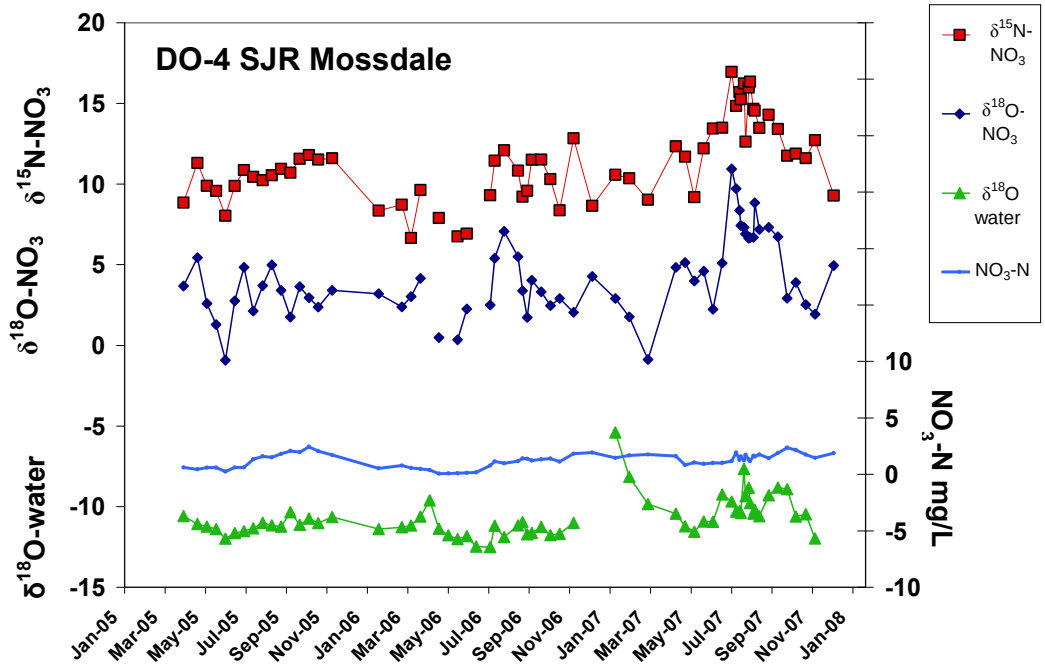

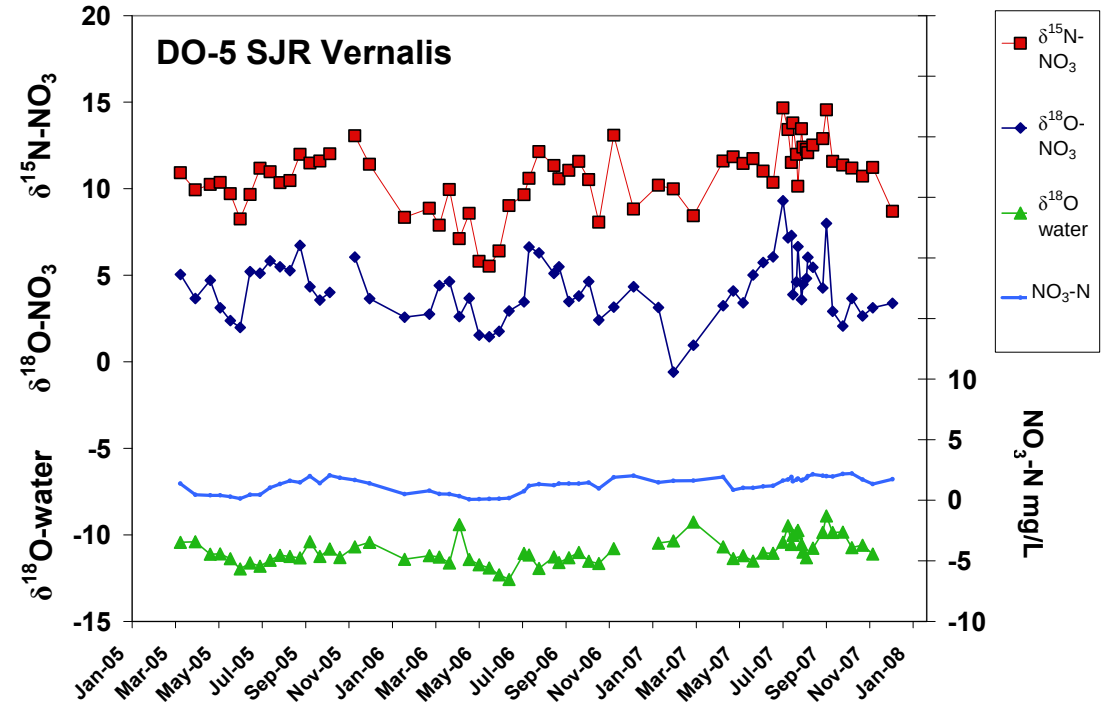

Figure E2. Temporal patterns in $\delta^{15}N$ and $\delta^{18}O$ of NO_3, NO_3 concentration, and $\delta^{18}O$ of water for SJR mainstem sites at Maze (top) and Laird Park (bottom).

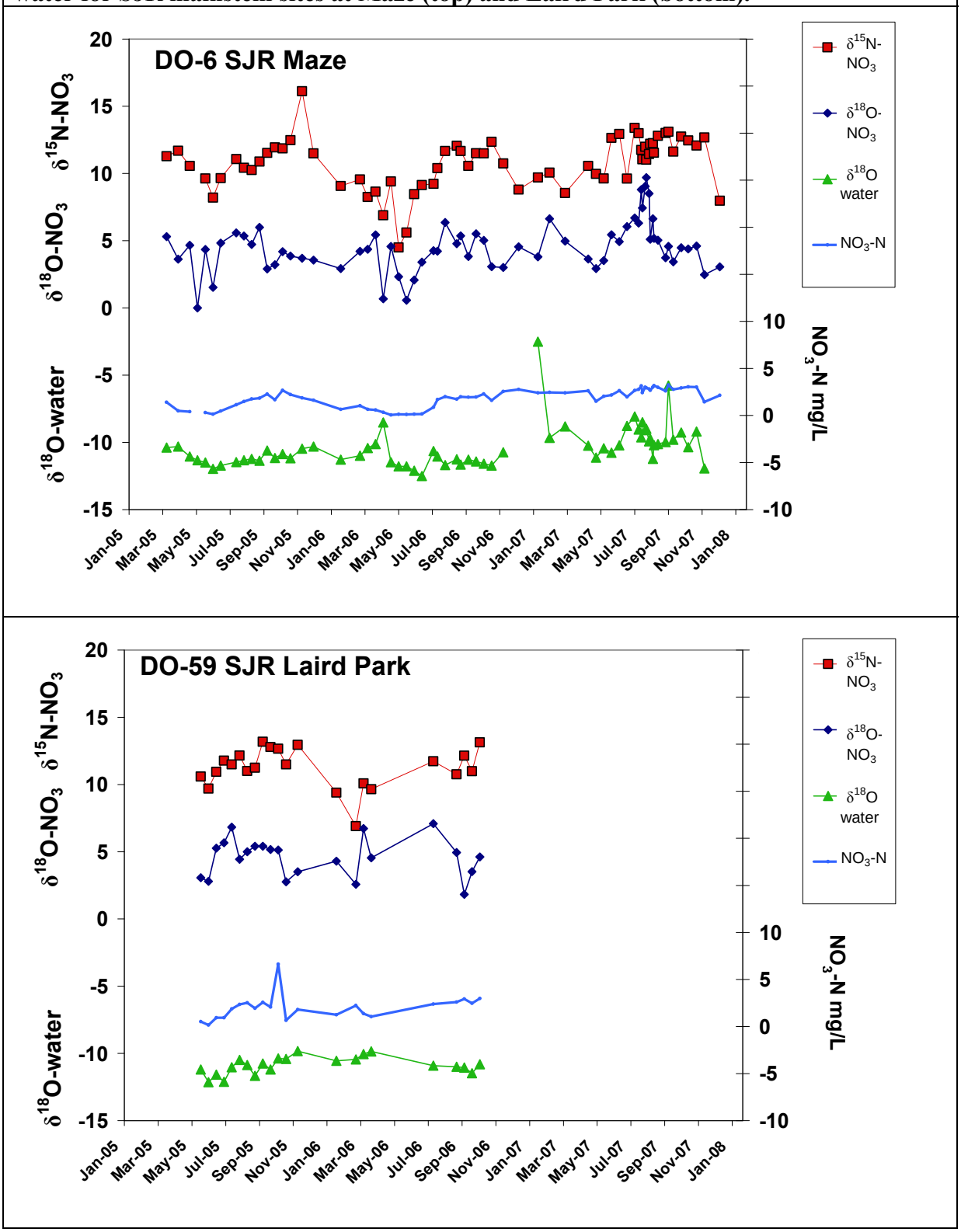

Figure E3. Temporal patterns in $\delta^{15}N$ and $\delta^{18}O$ of NO_3, NO_3 concentration, and $\delta^{18}O$ of water for SJR mainstem sites at Patterson (top) and Crows Landing (bottom).

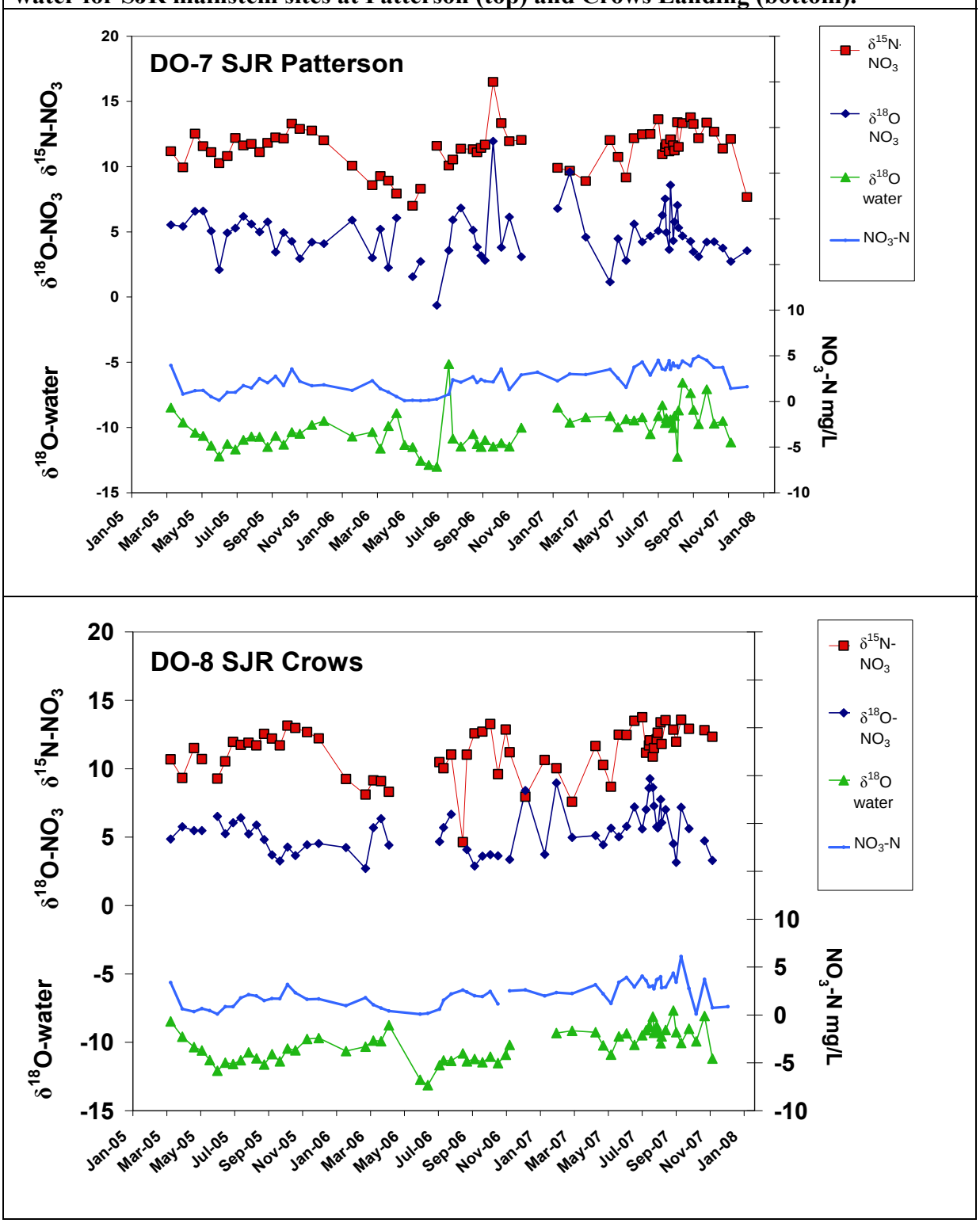

Figure E4. Temporal patterns in $\delta^{15}N$ and $\delta^{18}O$ of NO_3, NO_3 concentration, and $\delta^{18}O$ of water for the SJR mainstem site at Lander Avenue and the Stanislaus River.

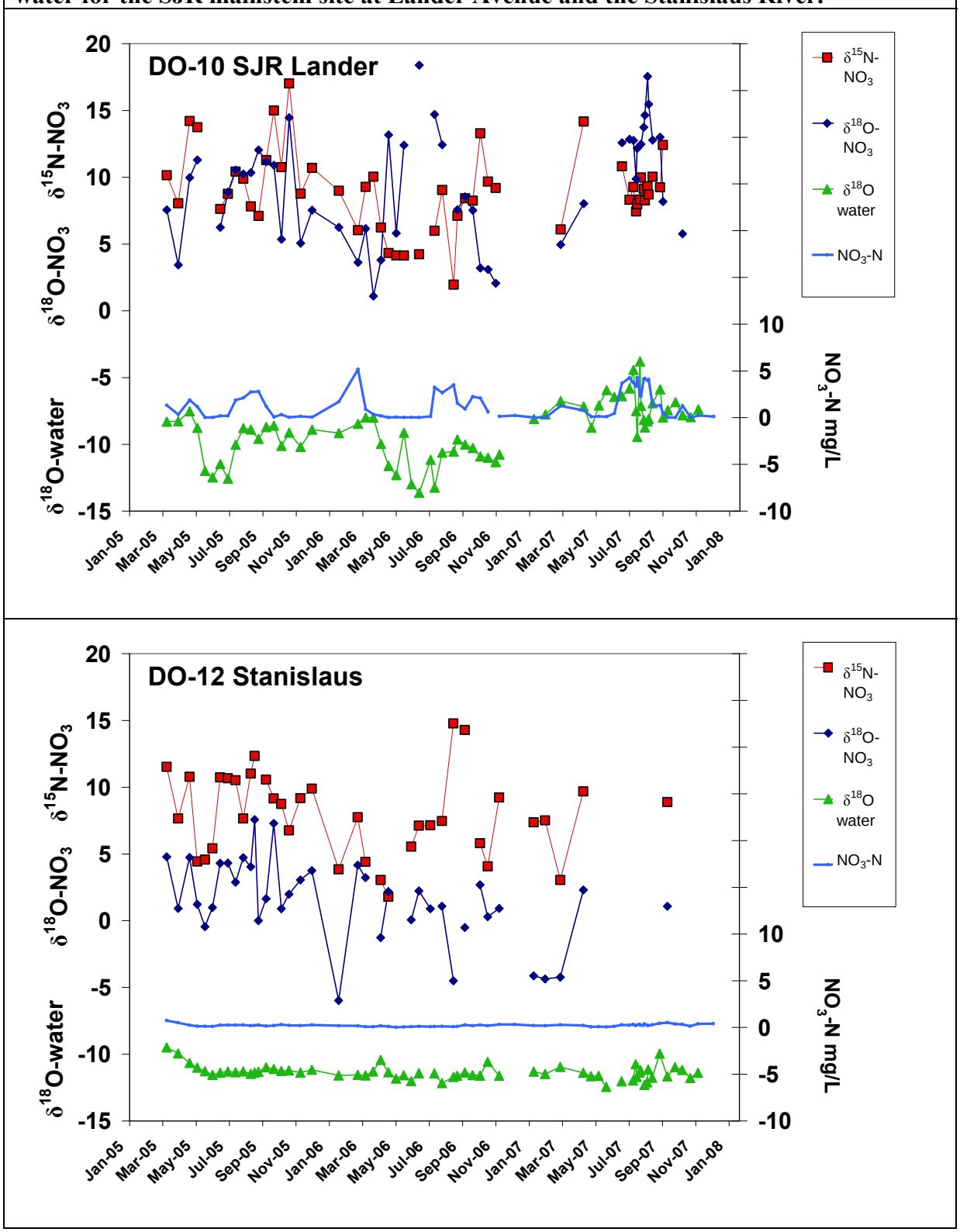

Figure E5. Temporal patterns in $\delta^{15}N$ and $\delta^{18}O$ of NO_3, NO_3 concentration, and $\delta^{18}O$ of water for the Tuolumne River and Merced River.

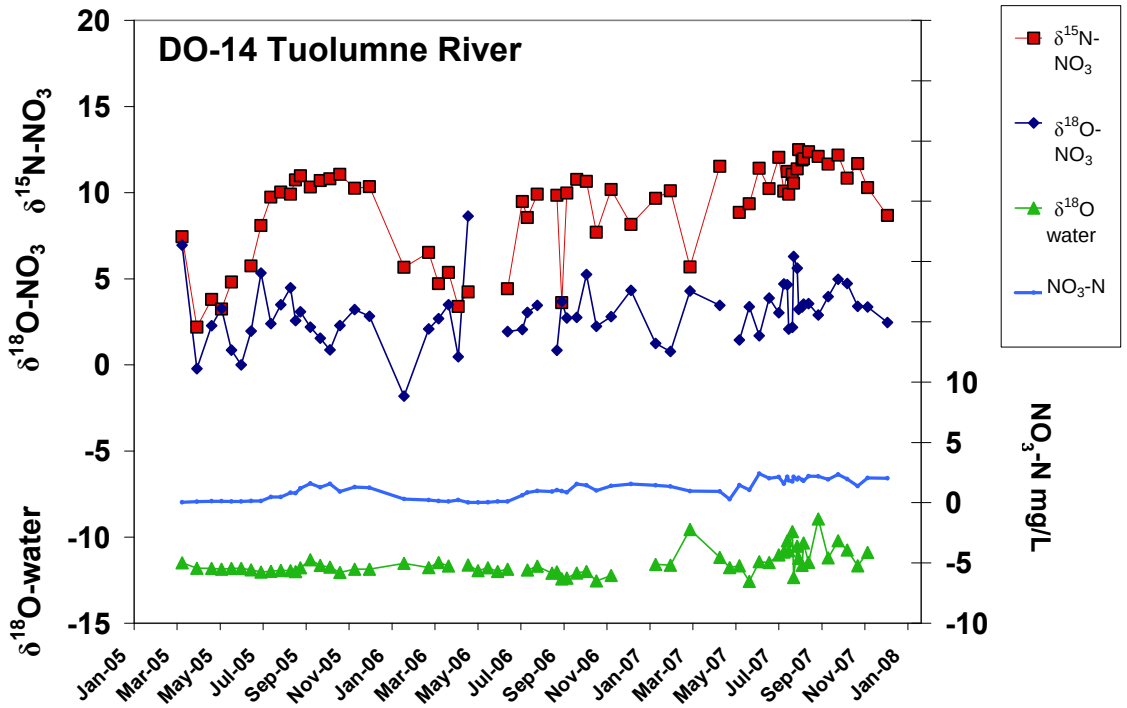

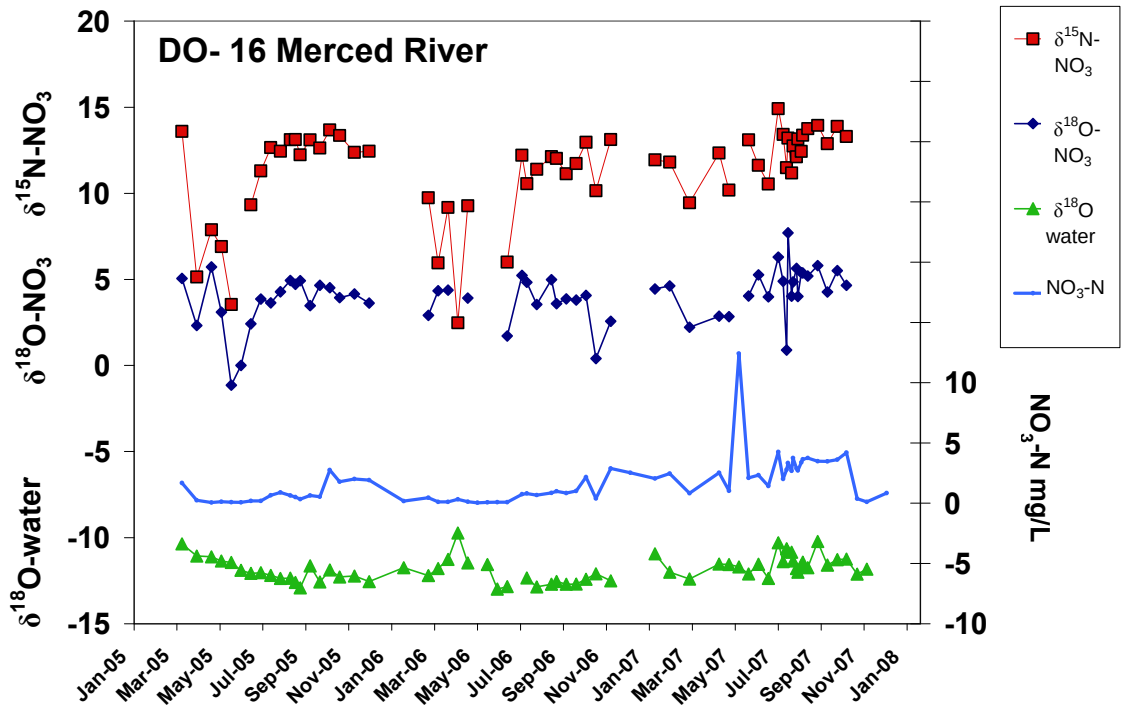

Figure E6. Temporal patterns in $\delta^{15}N$ and $\delta^{18}O$ of NO_3, NO_3 concentration, and $\delta^{18}O$ of water for Los Banos Creek and Orestimba Creek.

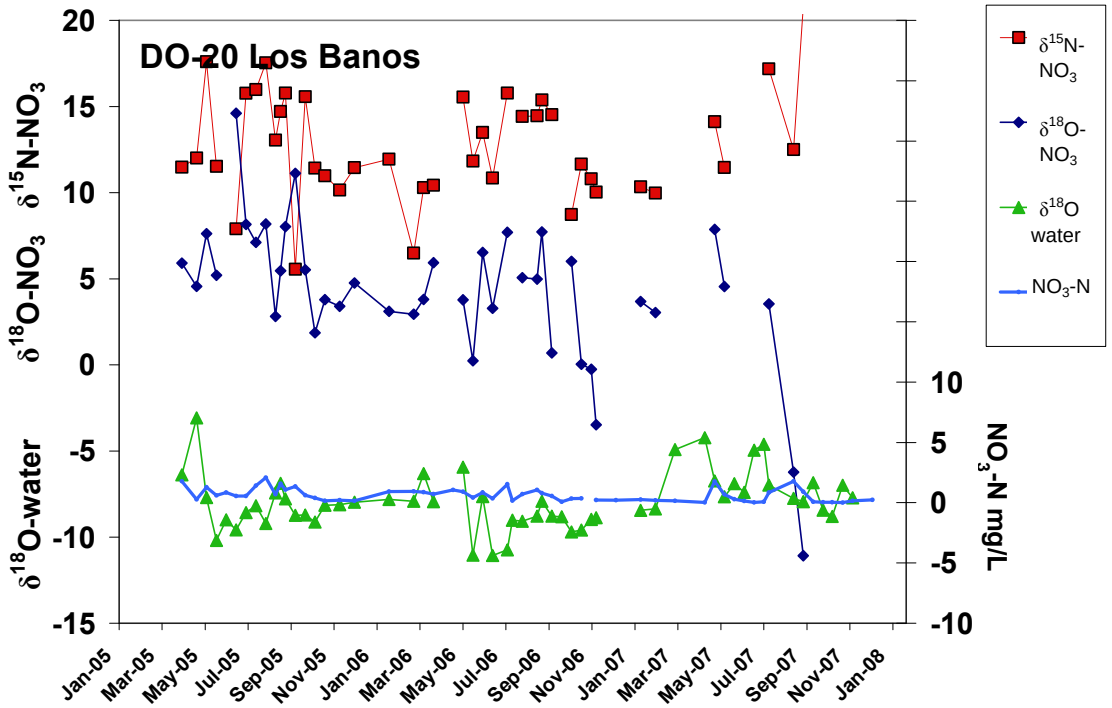

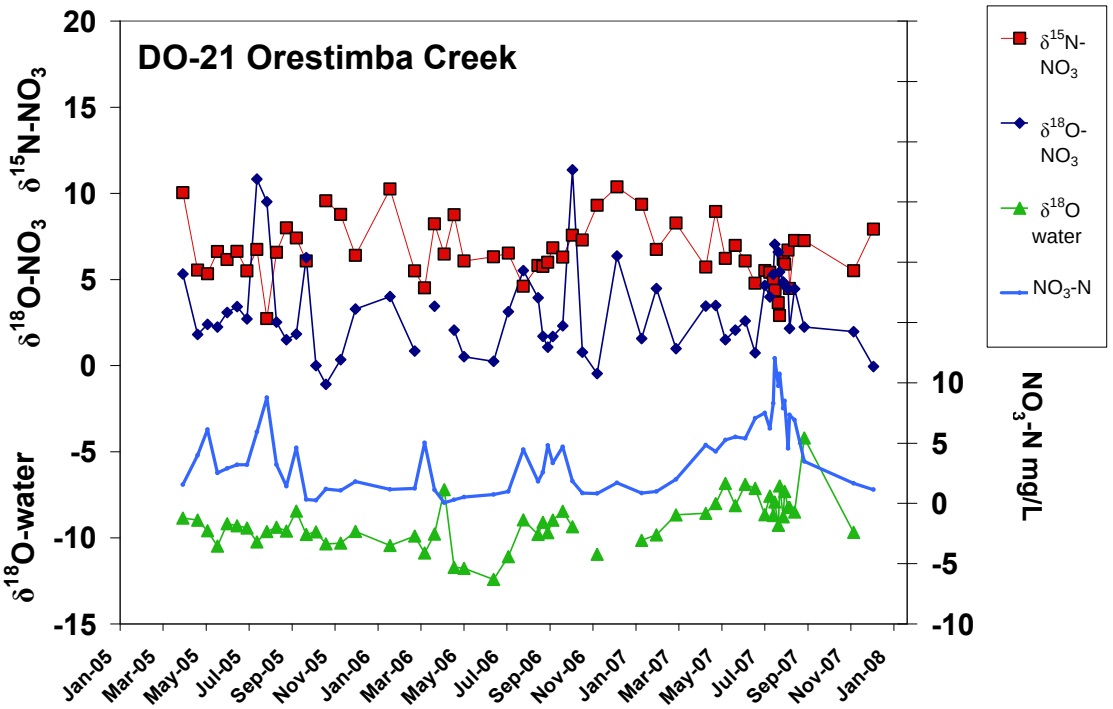

Figure E7. Temporal patterns in $\delta^{15}N$ and $\delta^{18}O$ of NO_3, NO_3 concentration, and $\delta^{18}O$ of water for MID Lat 5 to the Tuolumne River and MID to Miller Lake.

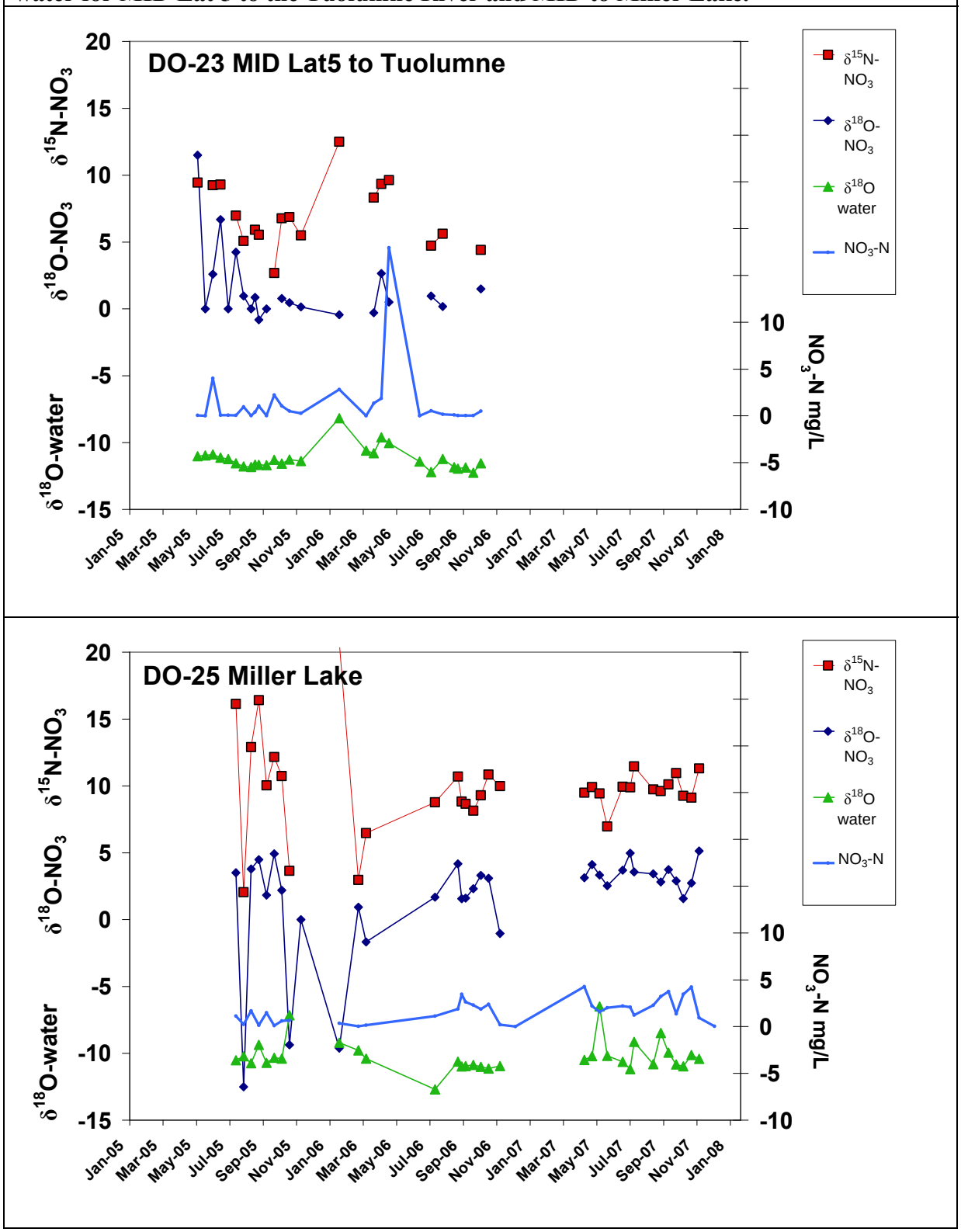

Figure E8. Temporal patterns in $\delta^{15}N$ and $\delta^{18}O$ of NO_3, NO_3 concentration, and $\delta^{18}O$ of water for MID to Westport Drain and Harding Drain.

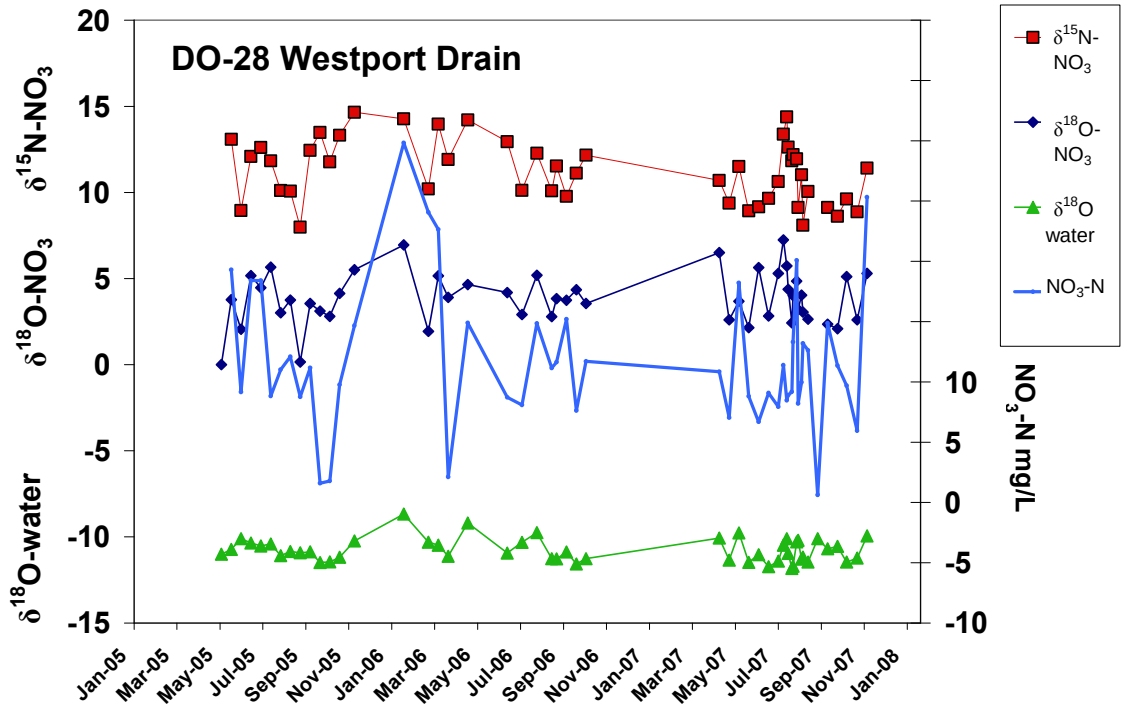

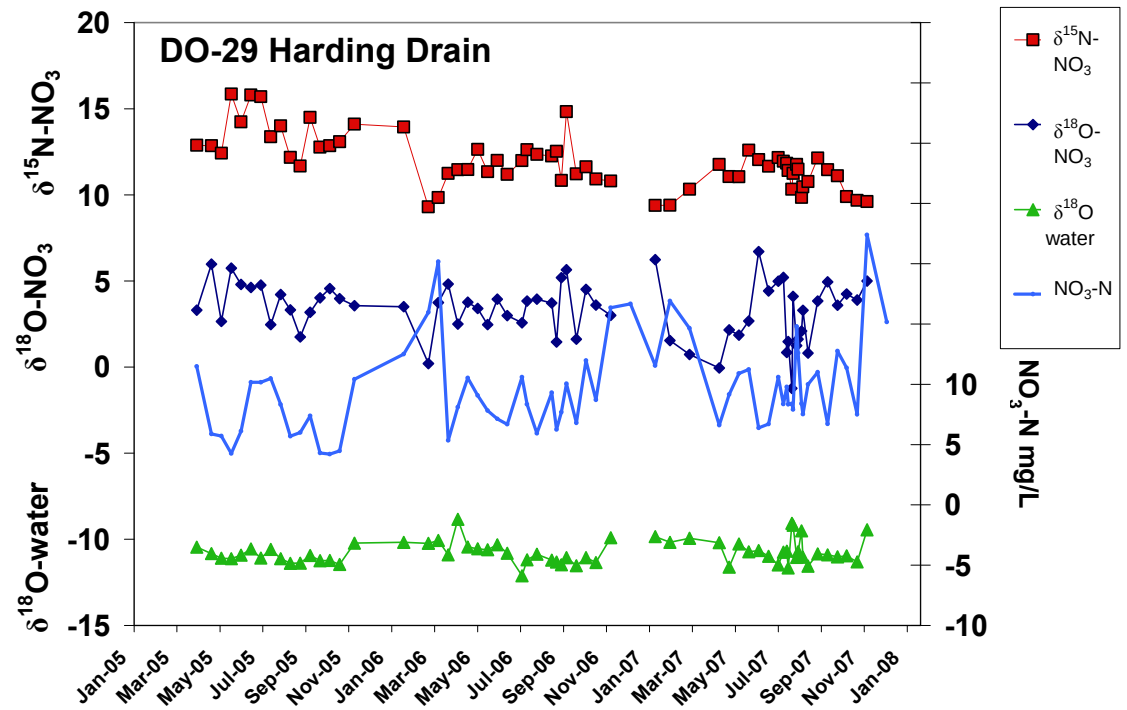

Figure E9. Temporal patterns in $\delta^{15}N$ and $\delta^{18}O$ of NO_3, NO_3 concentration, and $\delta^{18}O$ of water for TID Lat 6/7 and Hospital Creek.

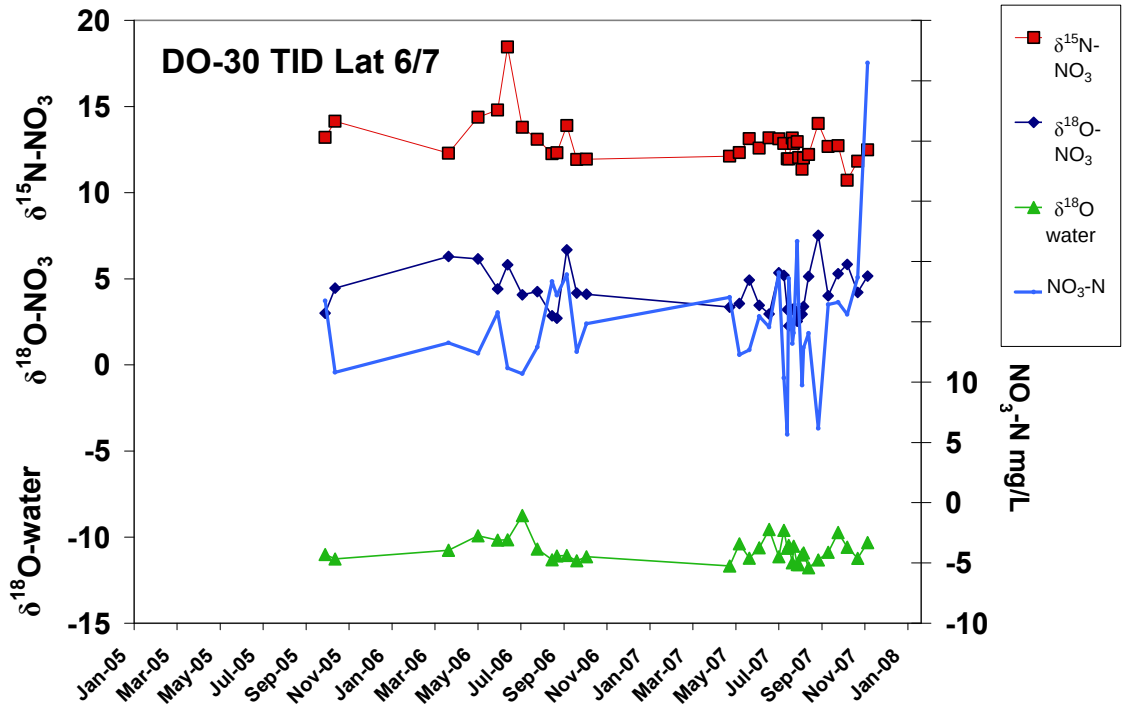

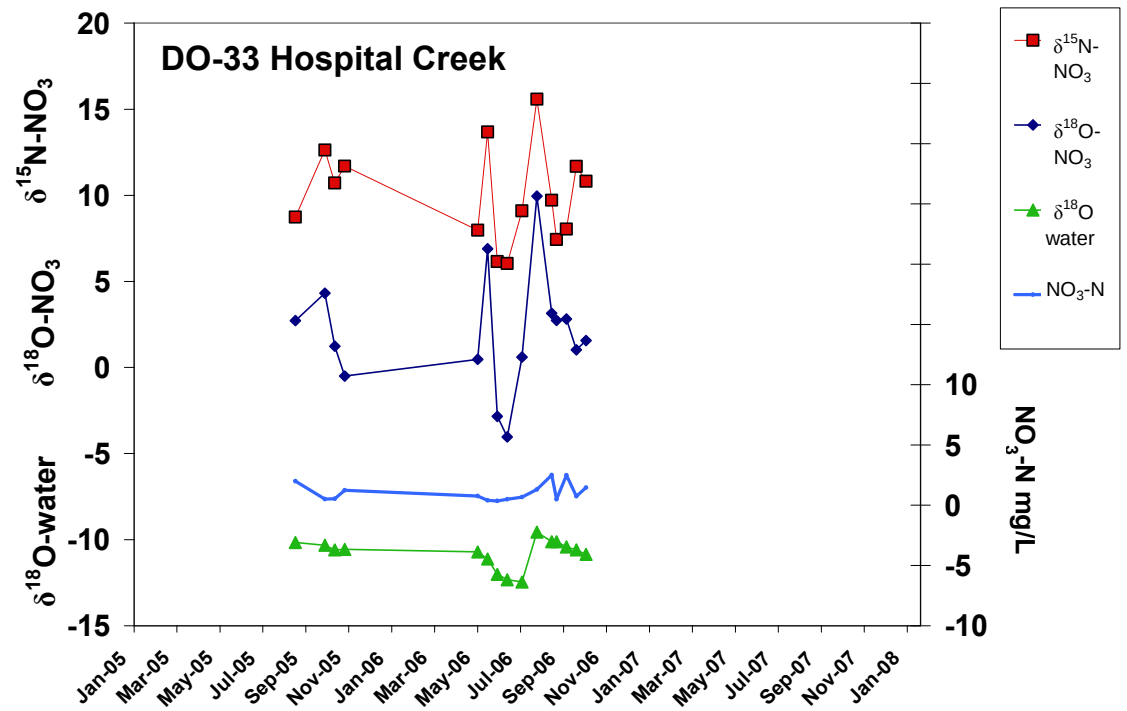

Figure E10. Temporal patterns in $\delta^{15}N$ and $\delta^{18}O$ of NO_3, NO_3 concentration, and $\delta^{18}O$ of water for Ingram Creek and Del Puerto Creek.

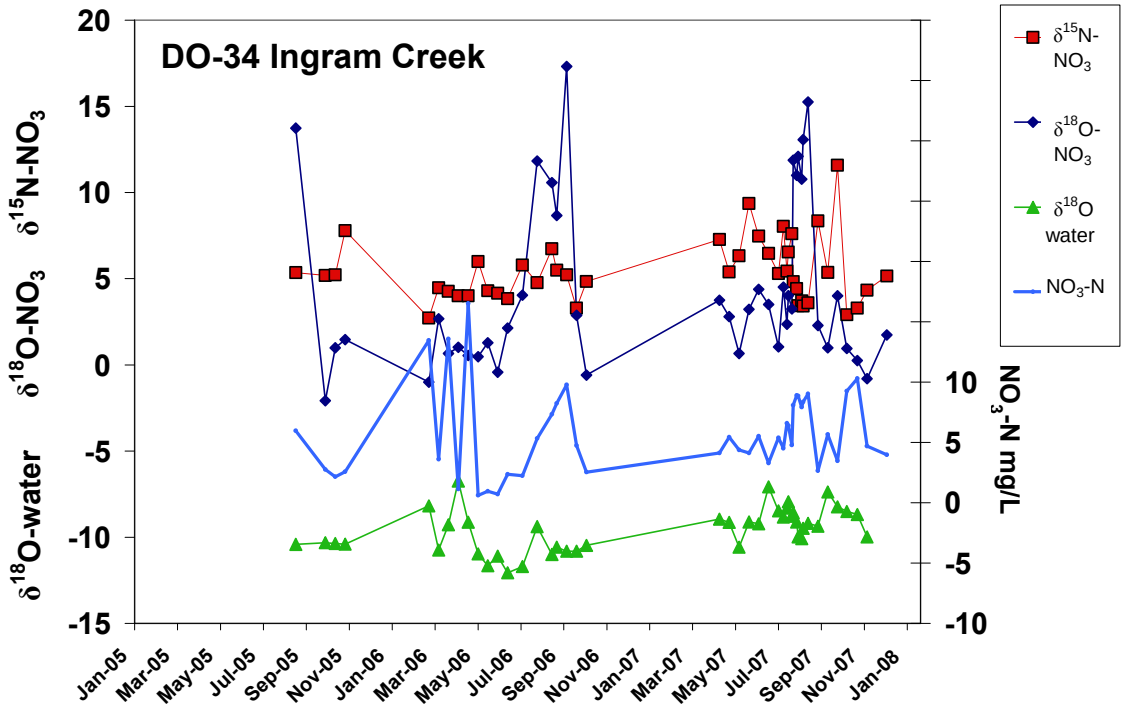

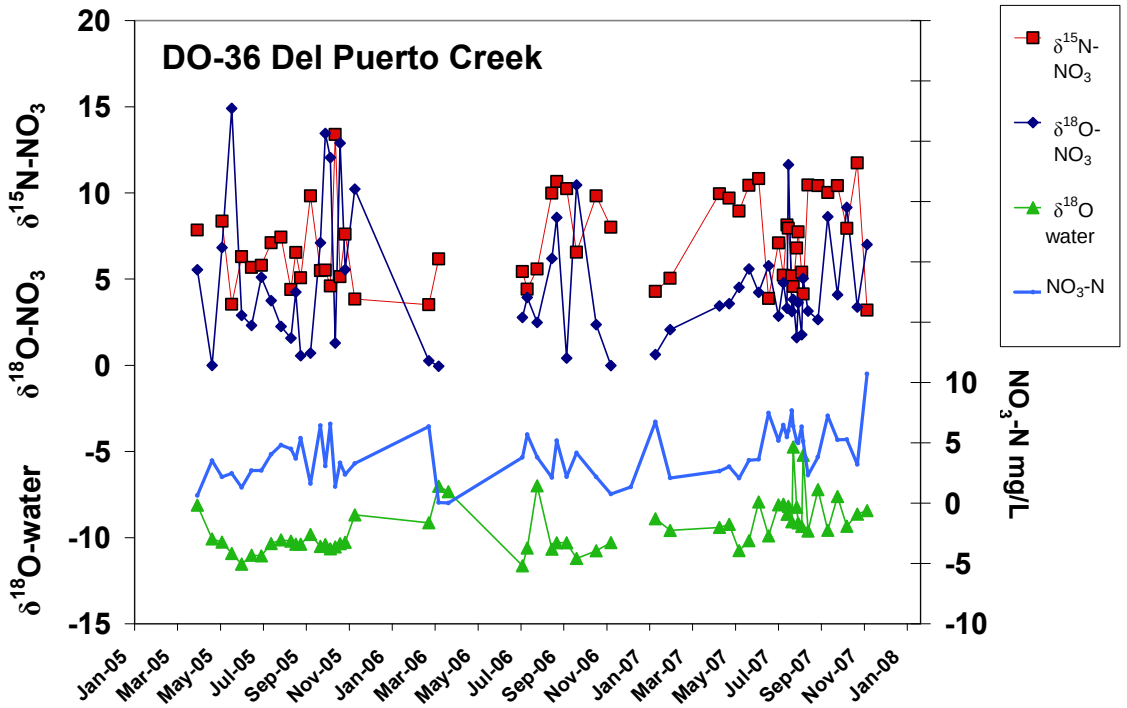

Figure E11. Temporal patterns in $\delta^{15}N$ and $\delta^{18}O$ of NO_3, NO_3 concentration, and $\delta^{18}O$ of water for San Luis Drain.

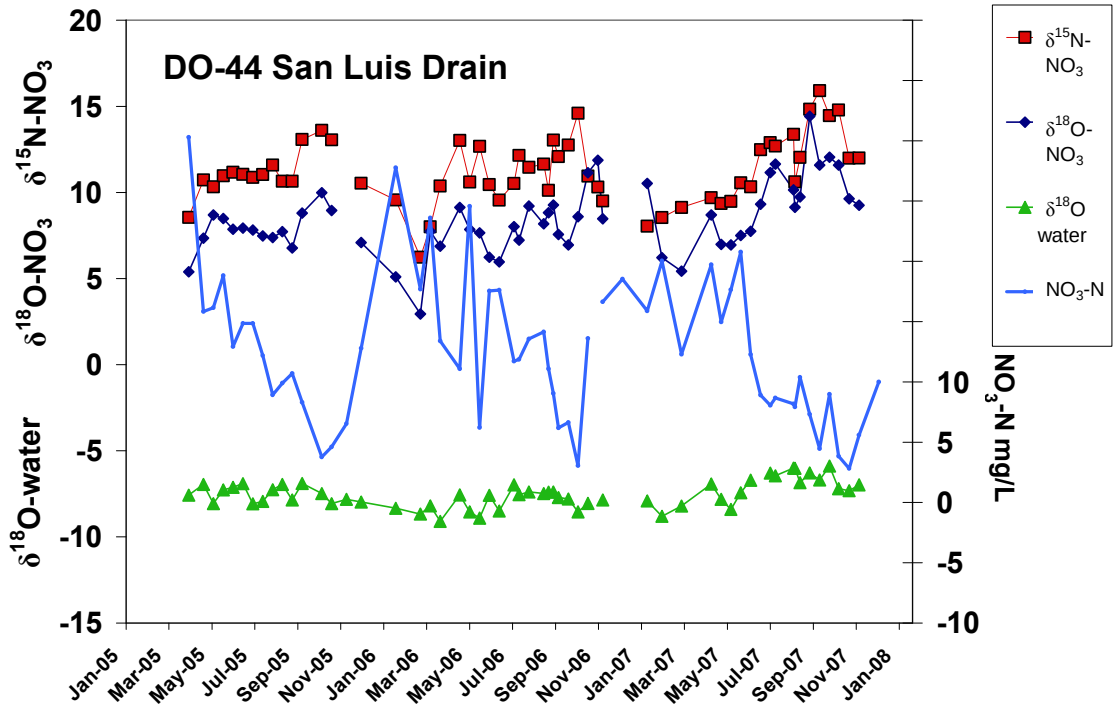

Appendix F: Water Isotope Plots

This section contains two tables with the calculated local meteoric water lines for different sites, and a set of plots showing the temporal variations in $\delta^{18}O$ and $\delta^{2}H$ of water for the most frequently sampled sites (Figures F1-F4).

Appendix F- Tables

Table F1. Local water lines calculated for all of the mainstem SJR sites

Site	# samples	Water line equation	R^2
All SJR Mainstem Sites	423	$\delta^{2}H = 4.7\delta^{18}O-29.0$	0.8
DO-4 SJR Mossdale	65	$\delta^{2}H = 3.9\ \delta^{18}O -38.5$	0.7
DO-5 SJR Vernalis	67	$\delta^{2}H = 4.7\ \delta^{18}O -29.4$	0.7
DO-6 SJR Maze	66	$\delta^{2}H = 4.4\ \delta^{18}O -32.6$	0.8
DO-59 SJR Laird Park	24	$\delta^{2}H = 5.6\ \delta^{18}O -18.5$	0.8
DO-7 SJR Patterson	68	$\delta^{2}H = 4.9\ \delta^{18}O -27.6$	0.8
DO-8 SJR Crows Landing	65	$\delta^{2}H = 5.5\ \delta^{18}O -20.9$	0.9
DO-10 SJR Lander Avenue	68	$\delta^{2}H = 5.2\ \delta^{18}O -23.9$	0.9

Table F2. Local water lines calculated for selected drains and tributaries

Site	# samples	Water line equation	R^2
DO-12 Stanislaus R	67	$\delta^{2}H = 3.\ \delta^{18}O\ 8-39.8$	0.6
DO-14 Tuolumne R	68	$\delta^{2}H = 4.4\ \delta^{18}O -34.1$	0.6
DO-16 Merced R	67	$\delta^{2}H = 4.4\ \delta^{18}O -34.6$	0.5
DO-18 Mud Slough	65	$\delta^{2}H = 5.1\ \delta^{18}O -24.3$	0.8
DO-19 Salt Slough	69	$\delta^{2}H = 5.4\ \delta^{18}O -23.0$	0.8
DO-20 Los Banos	58	$\delta^{2}H = 5.5\ \delta^{18}O -20.8$	0.9
DO-21 Orestimba Creek	59	$\delta^{2}H = 5.4\ \delta^{18}O -19.6$	0.8
DO-28 Westport Drain	50	$\delta^{2}H = 5.3\ \delta^{18}O -24.2$	0.7
DO-29 Harding Drain	65	$\delta^{2}H = 5.4\ \delta^{18}O -22.2$	0.7
DO-30 TID 6/7	35	$\delta^{2}H = 4.2\ \delta^{18}O -36.0$	0.7
DO-33 Hospital Creek	15	$\delta^{2}H = 4.7\ \delta^{18}O -28.7$	0.9
DO-34 Ingram	44	$\delta^{2}H=4.9\ \delta^{18}O -26.0$	0.8
DO-36 Del Puerto	58	$\delta^{2}H=5.0\ \delta^{18}O -25.0$	0.8
DO-44 San Luis Drain	59	$\delta^{2}H=3.5\ \delta^{18}O -36.1$	0.6

Appendix F- Figures

Figure F1. Water isotope plot showing $\delta^{18}O$ vs $\delta^{2}H$ for all water samples collected in the SJR mainstem (top), and for just the water samples collected in the downstream SJR sites (bottom).

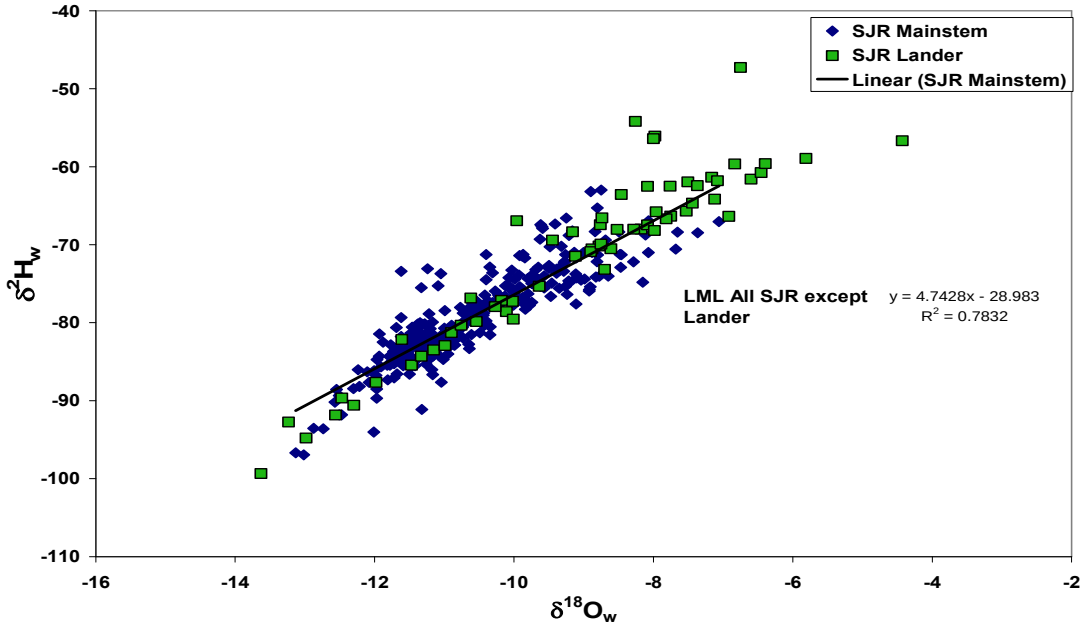

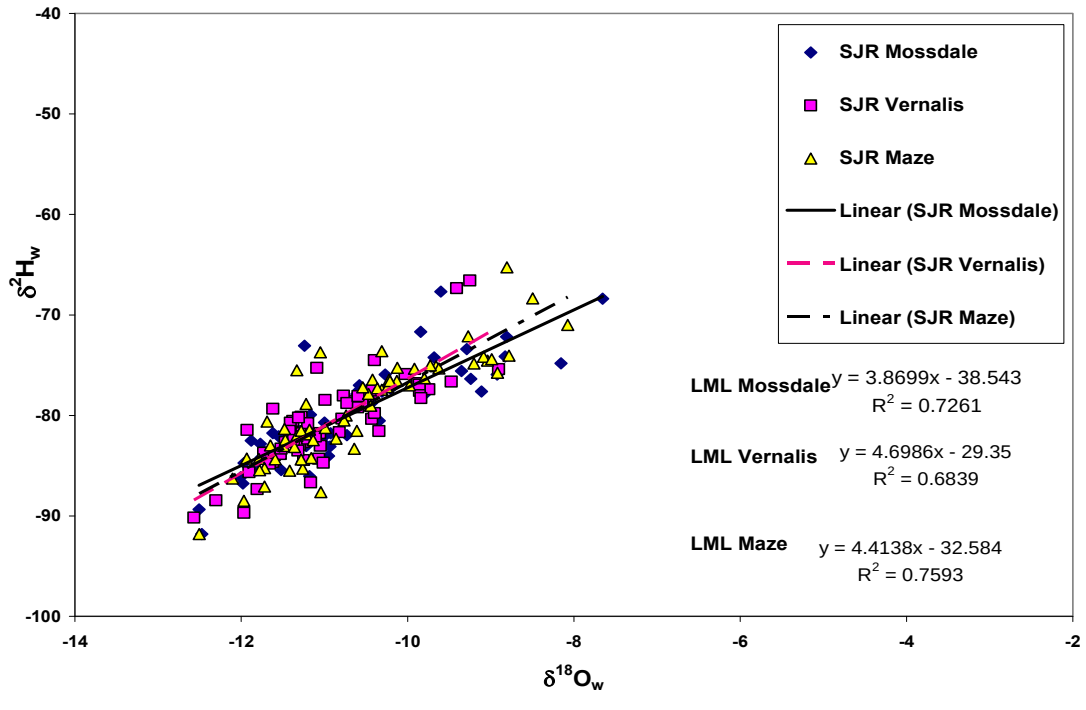

Figure F2. Water isotope plot showing $\delta^{18}O$ vs $\delta^{2}H$ for water samples from various sites in the mainstem SJR and the major east-side tributaries.

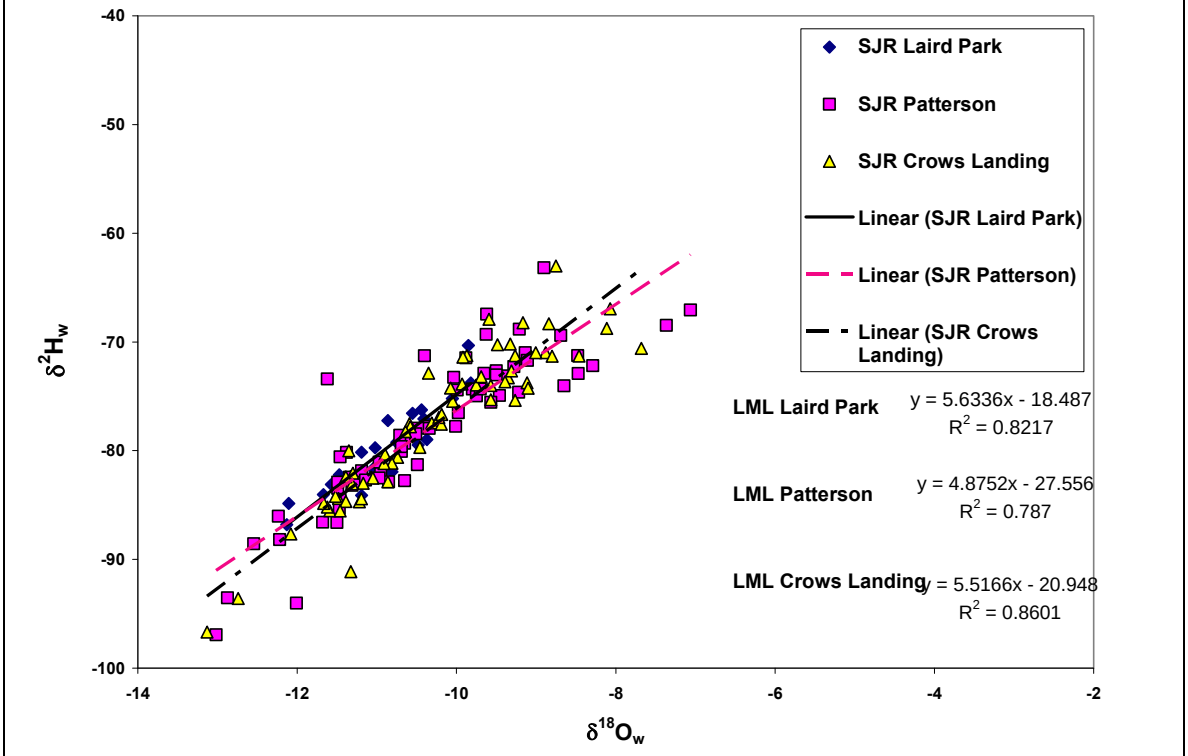

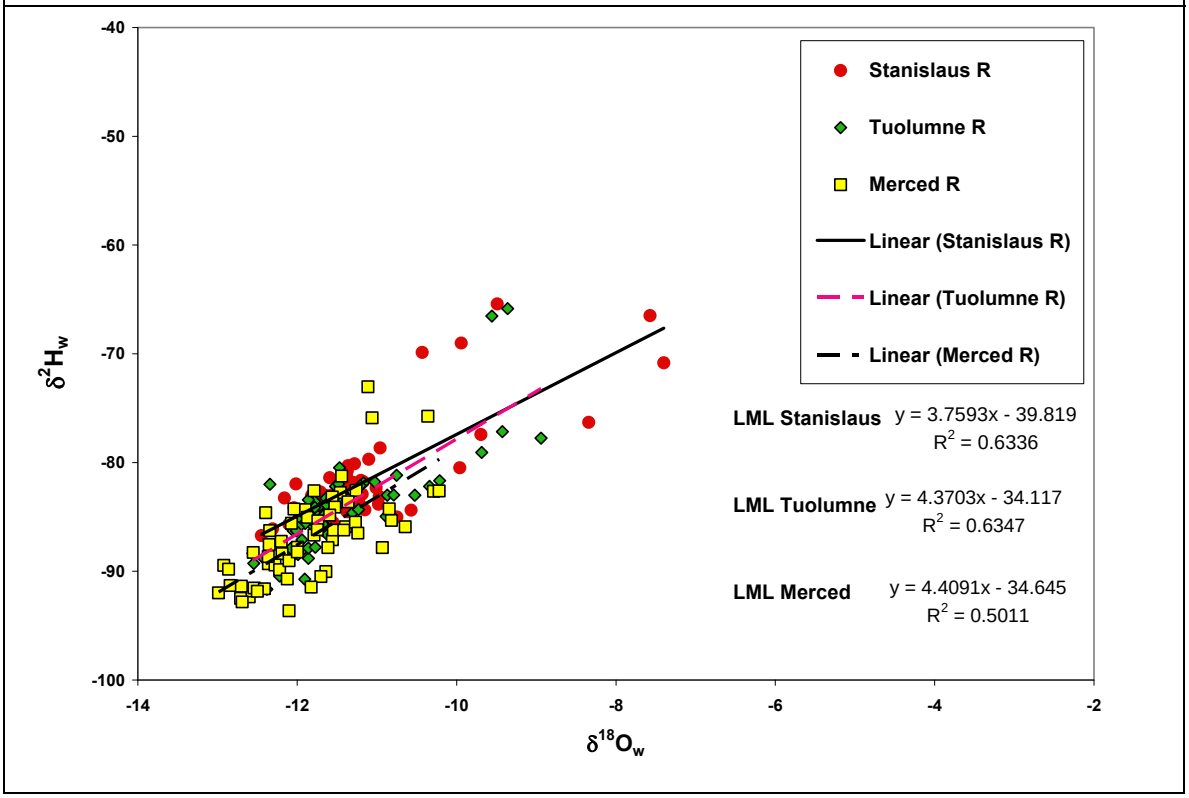

Figure F3. Water isotope plot showing $\delta^{18}O$ vs $\delta^{2}H$ for water samples from various selected tributaries. Upstream tributaries which drain agriculture and wetlands are shown in the top panel, and three drains are shown in the bottom panel.

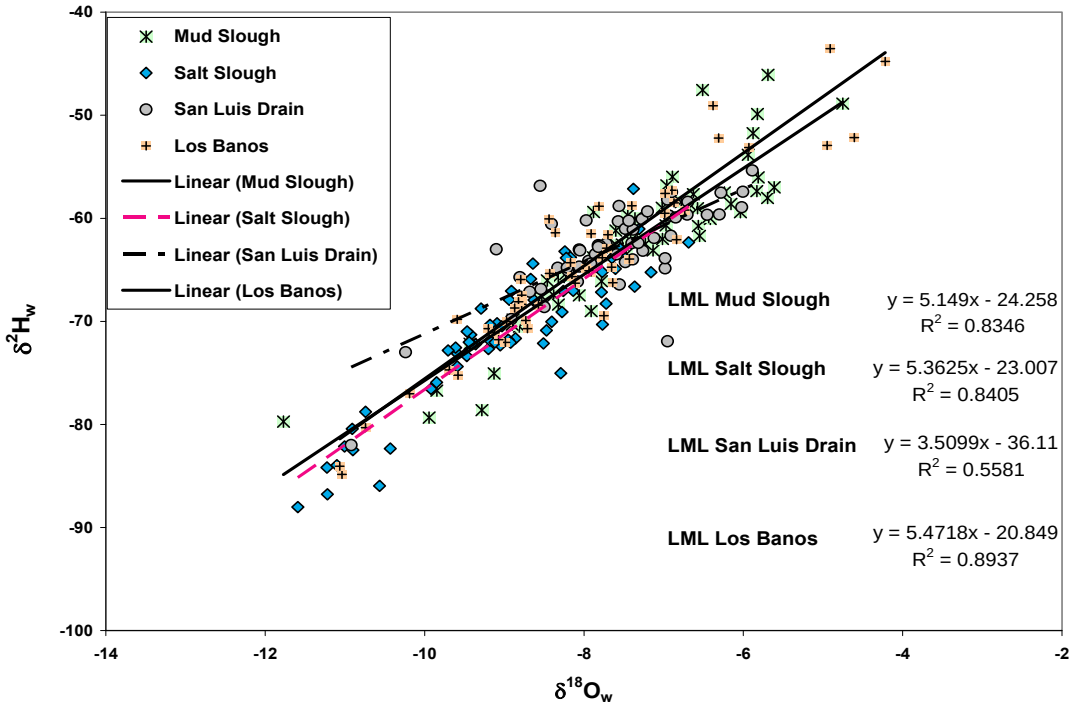

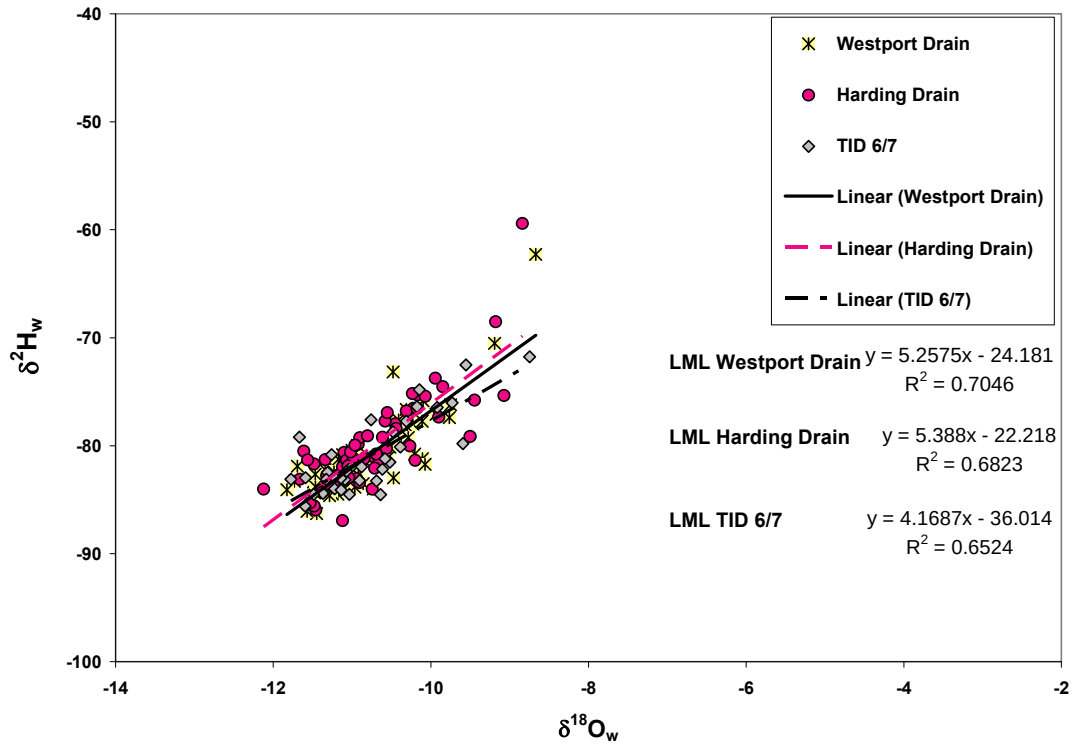

Figure F4. Water isotope plot showing $\delta^{18}O$ vs $\delta^{2}H$ for water samples from various selected tributaries.

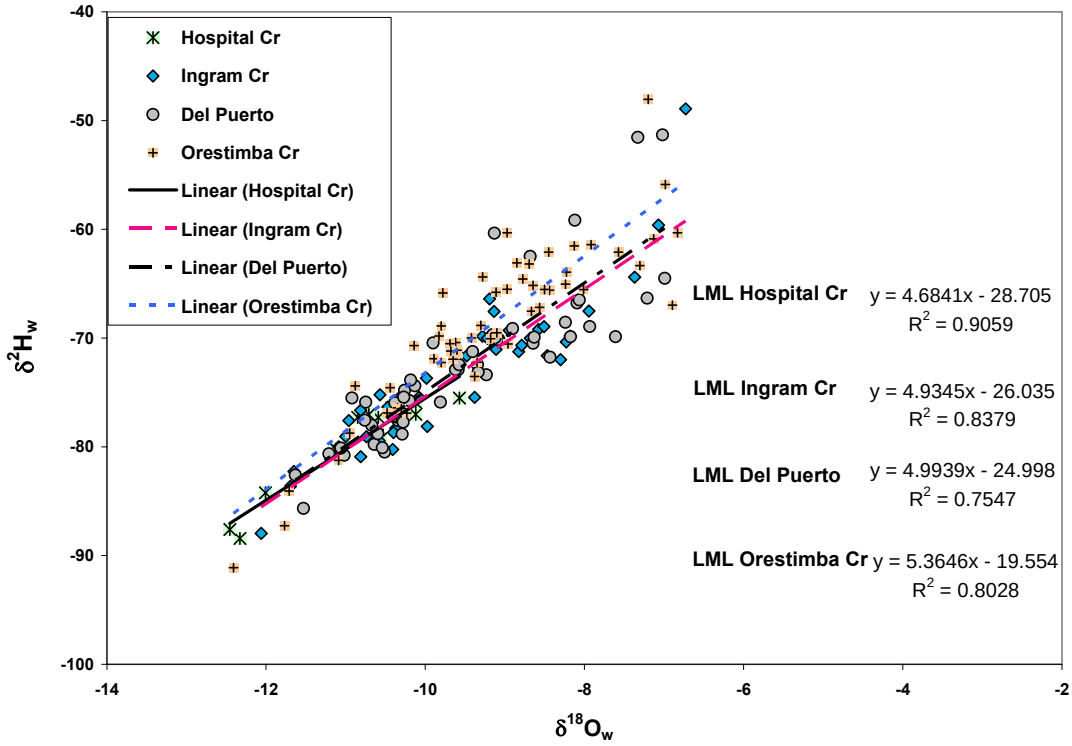

Task #7 Report

List of Tables

List of Figures

$\delta^{18}O$ slope, this strongly suggests that one of these processes is controlling the nitrate isotope values.

Figure 6. Schematic showing the $\delta^{18}O$ and $\delta^{2}H$ of precipitation and evaporated waters.

Figure 7. Typical $\delta^{34}S$ and $\delta^{18}O$ SO_4 values for various potential sulfate sources. The values shown are for unaltered dissolved SO_4 from each source. Biological sulfate cycling processes such as sulfate reduction will alter the isotopic composition of the sulfate.

Figure 8. Distribution of POM $\delta^{13}C$ values for San Joaquin River mainstem sites (top) and major tributaries and drains (bottom) from March 2005 through December 2007. The median (line), 25^{th} and 75^{th} percentile (box), 10^{th} and 90^{th} percentile (whisker), and outlier points (circles) are shown.

Figure 9. Distribution of POM $\delta^{15}N$ values for San Joaquin River mainstem sites (top) and major tributaries and drains (bottom) from March 2005 through December 2007.

Figure 10. Distribution of POM C:N atomic ratios for San Joaquin River mainstem sites (top) and major tributaries and drains (bottom) from March 2005 through December 2007.

Figure 11. Distribution of $\delta^{15}N$ vs $\delta^{13}C$ (top) and C:N vs $\delta^{13}C$ (bottom) values of POM from mainstem SJR and major tributary sites, with the expected ranges of values for major sources of POM.

Figure 12. Distribution of $\delta^{15}N$ vs $\delta^{13}C$ (top) and C:N vs $\delta^{13}C$ (bottom) values of POM from mainstem SJR, minor tributaries, and upstream wetlands sites, with the expected ranges of values for major sources of POM.

Figure 13. Distribution of DOC $\delta^{13}C$ values for San Joaquin River mainstem sites (top) and major tributaries and drains (bottom) from March 2005 through December 2006.

Figure 14. Comparison of $\delta^{13}C$ values of DOC and POM for all samples collected 2005-2006. A diagonal 1:1 line is provided for reference.

Figure 15. Correlation of DOC-$\delta^{13}C$ with DOC concentration (top) and algal pigments concentration (bottom) for different site types.

Figure 16. Nitrate $\delta^{15}N$ and $\delta^{18}O$ values for all core sampling sites from March 2005 to December 2007.

Figure 17. Distribution of nitrate $\delta^{15}N$ values for San Joaquin River mainstem sites (top) and major tributaries and drains (bottom) from March 2005 through December 2007.

Figure 18. Distribution of nitrate $\delta^{18}O$ values for San Joaquin River mainstem sites (top) and major tributaries and drains (bottom) from March 2005 through December 2007.

Figure 19. Nitrate concentration vs $\delta^{15}N$ for the SJR mainstem and Merced, Tuolumne, and Stanislaus Rivers. The top panel shows all of the data, while the bottom panel shows the distribution of samples from the three major tributaries, with one mainstem SJR site for reference.

Figure 20. Nitrate concentration vs $\delta^{15}N$ for all of the core sampling sites (including drains & tributaries) from March 2005- December 2007.

Figure 21. Nitrate concentration, $\delta^{15}N$, and flow data (from SJR Vernalis) for the entire study period at one upstream (Crows Landing) and one downstream (Vernalis site).

Figure 22. $\delta^{15}N$ in the Merced River and the SJR at Crows Landing (downstream of the confluence with the Merced). During low flow periods, the Merced River tends to carry nitrate with a high $\delta^{15}N$ signature.

Figure 23. Nitrate concentration and $\delta^{15}N$ in the SJR at Lander Avenue, upstream of the confluence with the Merced River.

Figure 24. Comparison of nitrate concentration, $\delta^{15}N$, and $\delta^{18}O$ of the mainstem SJR sites, upstream tributaries, and major east-sideside tributaries under high flow (top panel) and low flow (bottom panel) conditions.

Figure 25. Mean nitrate $\delta^{15}N$ and $\delta^{18}O$ for all core sampling sites between March 2005 and December 2007. Error bars show one standard deviation.

Figure 26. The $\delta^{18}O$ of dissolved inorganic phosphate in the San Joaquin River and tributaries. The differences between sites are much larger than analytical error. Error bars represent replicate analyses.

Figure 27. $\delta^{18}O$ and $\delta^{2}H$ of water for all of the mainstem SJR sites (top) and all core sites (bottom) sampled between March 2005 and December 2007.

Figure 28. Distribution of water $\delta^{18}O$ values for San Joaquin River mainstem sites (top) and major tributaries and drains (bottom) from March 2005 through December 2007.

Figure 29. Distribution of water δ^2H values for San Joaquin River mainstem sites (top) and major tributaries and drains (bottom) from March 2005 through December 2007.

Figure 30. Temporal variability in the $\delta^{18}O$ of water for the major east-sideside tributaries and Salt Slough. SJR at Crows Landing is included for reference.
Figure 31. Spatial variability in $\delta^{18}O$ of water in the mainstem SJR, major east-sideside tributaries, and upstream wetlands sites during a high flow period (top) and a low flow period (bottom).

Figure 32. Distribution of sulfate $\delta^{34}S$ values for San Joaquin River mainstem sites (top) and major tributaries and drains (bottom) from March 2005 through December 2007.

Figure 33. Distribution of sulfate $\delta^{18}O$ values for San Joaquin River mainstem sites (top) and major tributaries and drains (bottom) from March 2005 through December 2007.

Figure 34. Sulfate $\delta^{34}S$ and $\delta^{18}O$ for all SJR mainstem, tributary, and drain sites, with expected ranges shown for major potential sulfate sources.

Figure 35. Sulfate $\delta^{34}S$ values over time for mainstem SJR sites. The three sites upstream of the confluence with the Tuolumne River have $\delta^{34}S$ values that are distinct from the downstream sites.

Figure 36. Sulfate $\delta^{34}S$ values over time for selected mainstem SJR and tributary sites (top), and $\delta^{18}O$ values for mainstem SJR sites (bottom).

Figure 37. Relationship between sulfate $\delta^{34}S$ and electrical conductivity for selected mainstem SJR, tributary, and drain sites.

Figure 38. General predictions of relative contribution of terrestrial and autotrophic organic matter to rivers, as inferred from the River Continuum Model of Vannote et al. (1980).

Figure 39. Correlation of algal pigments (the sum of chlorophyll-*A* and pheophytin) with C:N of POM samples from various groups of sites (top) with an expanded pigments scale (bottom).

Figure 40. Correlation of C:N values of POM and algal pigment concentrations for mainstem SJR sites (top), with the data presented with an expanded algal pigment scale below (bottom).

Figure 41. Correlation of C:N values of POM and algal pigment concentrations for selected drain, creek, and wetlands sites (top), with the data presented with an expanded algal pigment scale below (bottom). Wetlands sites generally have lower

C:N values than other sites. Different site types all show wide ranges of pigment values; however, average wetlands pigments values are generally higher than for other sites. At low pigment concentrations (bottom) there is little correlation of pigments and C:N whereas at higher pigment concentrations, the C:N values are significantly lower.

Figure 42. Distribution of BOD vs C:N from various groups of sites (top) with an expanded scales (bottom) so the symbols are more readable.

Figure 43. Correlation of C:N of POM and BOD for mainstem SJR sites (top) and major tributaries (bottom). Tributary sites have much lower BOD concentrations than mainstem sites. Samples with low C:N values have a wide range of BOD values, whereas samples with high C:N have low BOD values.

Figure 44. Correlation of C:N values of POM and CBOD (top) and NBOD (bottom) for major tributaries and mainstem SJR sites. Mainstem sites have a larger range of CBOD and NBOD values than tributaries. A higher proportion of the BOD is NBOD in the tributaries than the mainstem sites.

Figure 45. Correlation of C:N values of POM and CBOD (top) and NBOD (bottom) for the different mainstem SJR sites.

Figure 46. Correlation of C:N of POM and BOD for selected drain, creek, and wetlands sites. Different site types have similar ranges of BOD values. However, samples with high C:N have lower BOD values than samples with low C:N. Mud Slough, Los Banos Creek, and San Luis Drain have higher BOD concentrations than Salt Slough.

Figure 47. Relative contributions of different kinds of POM to the different sites, based on the criteria listed in the legend. Within each group of sites, sites are listed in order of upstream (right) to downstream (left). Each bar reflects an average of 53 samples, with a range of 14 to 69 samples for each site. Note that about 10% of the samples did not have BOD measurements, resulting in "unclassified" POM samples.

Figure 48. Relative contributions of different kinds of POM to various infrequently sampled sites, based on the criteria listed in the legend. Each bar reflects an average of 3 samples, with a range of 1-9 samples for each site. Within each group of sites, sites are listed in order of DO#. Note that 10-50% of the samples did not have BOD measurements, resulting in "unclassified" POM samples.

Figure 49. Downstream changes in nitrate concentration and $\delta^{15}N$ of NO3 and POM for mainsteam, major tributary, and wetlands sites for high flow periods in March 31, 2005 (top) and April 21, 2005 (bottom). $\delta^{15}N$ values for wetlands sites are circled in green, and $\delta^{15}N$ values of POM and NO3 for tributary sites are connected with yellow vertical bands. The X axis is latitude of the site.

Figure 50. Downstream changes in nitrate concentration and $\delta^{15}N$ of NO3 and POM for mainsteam, major tributary, and wetlands sites for high flow periods in May 5, 2005 (top) and May 18, 2005 (bottom). $\delta^{15}N$ values for wetlands sites are circled in green, and $\delta^{15}N$ values of POM and NO3 for tributary sites are connected with yellow vertical bands. The X axis is latitude of the site.

Figure 51. Downstream changes in nitrate concentration and $\delta^{15}N$ of NO3 and POM for mainsteam, major tributary, and wetlands sites for low flow periods in August 25, 2006 (top) and February 1, 2007 (bottom). $\delta^{15}N$ values for wetlands sites are circled in green, and $\delta^{15}N$ values of POM and NO3 for tributary sites are connected with yellow vertical bands. The X axis is latitude of the site.

Figure 52. Distribution of nitrate isotope values for selected sites, with expected ranges shown for various potential nitrate sources.

Figure 53. Detail of the nitrate isotope composition of samples from the mainstem SJR.

Figure 54. $\delta^{15}N$-NO_3 upstream (Crows Landing) and downstream (Mossdale) in the SJR. Values for the Stanislaus River are also shown, since this is a major water source upstream of Mossdale and Vernalis.

Figure 55. Downstream nitrate isotope dynamics in the SJR mainstem and tributaries between June 7 and September 27. During this period, $\delta^{15}N$-NO_3 values at the downstream SJR sites increase in relation to the upstream sites, and none of the measured tributaries have high $\delta^{15}N$-NO_3 values that could account for the increase.

Figure 56. Downstream nitrate isotope dynamics in the SJR mainstem and tributaries between June 7 and September 27. During this period, $\delta^{15}N$ values at the downstream SJR sites increase in relation to the upstream sites, and none of the measured tributaries have high $\delta^{15}N$ values that could account for the increase.

Figure 57. Downstream nitrate isotope dynamics in the SJR mainstem and tributaries between June 7 and September 27. During this period, $\delta^{15}N$ values at the downstream SJR sites increase in relation to the upstream sites, and none of the measured tributaries have high $\delta^{15}N$ values that could account for the increase.

Figure 58. The curves on a plot of $\delta^{15}N$ vs NO_3 (a), resulting from mixing of two sources of nitrate with different concentrations can be distinguished from the curves resulting from denitrification with two different fractionations by plotting $\delta^{15}N$ vs ln NO_3 (b) where different denitrification fractionations yield straight lines whereas mixing yields a curve, and by plotting $\delta^{15}N$ vs $1/NO_3$ (c) where different

denitrification fractionations yield curves whereas mixing yields a straight line. From Kendall et al. (2007).

Figure 59. Relationship between $\delta^{15}N\text{-}NO_3$ and the inverse of nitrate concentration (top). The lack of linear trends suggest that the observed $\delta^{15}N\text{-}NO_3$ in the SJR mainstem cannot be explained by simple mixing between two nitrate sources. Relationship between $\delta^{15}N\text{-}NO_3$ and ln $[NO_3]$ (bottom). The lack of linear trends indicates that the $\delta^{15}N\text{-}NO_3$ in the SJR mainstem cannot be explained only by uptake or denitrification, but the data do not rule out nitrification or input of multiple nitrate sources with high $\delta^{15}N$ values.

Figure 60. Temporal patterns in the $\delta^{15}N$, $\delta^{13}C$, and C:N of POM for the mainstem SJR at Mossdale (top) and Vernalis (bottom).

Figure 61. Temporal patterns in the $\delta^{15}N$, $\delta^{13}C$, and C:N of POM for the mainstem SJR at Crows Landing (top) and Lander (bottom).

Figure 62. Temporal patterns in the $\delta^{15}N$, $\delta^{13}C$, and C:N of POM for upstream wetlands sites at Mud Slough (top) and Salt Slough (bottom).

Figure 63. Temporal patterns in the $\delta^{15}N$, $\delta^{13}C$, and C:N of POM for the San Luis Drain.

Figure 64. Temporal patterns in nitrate $\delta^{15}N$ and $\delta^{18}O$, NO_3 concentration, and water $\delta^{18}O$ water for two east-side drains at Westport (top) and Harding Drain (bottom).

Figure 65. Nitrate isotope source diagram for selected upstream mixed wetland and agricultural sites. Mud Slough and San Luis Drain both show evidence of either denitrification or nitrate uptake, while Salt Slough shows a very different pattern.

Figure 65. Nitrate isotope source diagram for the west-sideside tributary sites. Only nitrate in Hospital Creek falls close to the 1:1 line, while the other three sites show a decoupling between the two isotopes, with $\delta^{18}O\text{-}NO_3$ showing increased values not related to changes in $\delta^{15}N\text{-}NO_3$.

Figure 67. The $\delta^{18}O_p$-δ^{18}Ow as a function of temperature for water samples collected in the San Joaquin River watershed in November 2006. The use of $\delta^{18}O_p$-$\delta^{18}O_w$ for the y axis allows the equilibrium values to be plotted along a linear relationship with temperature. All except one of the samples fell outside of the expected equilibrium values.

Appendix A: Methods

List of Tables-

Appendix B: Spatial Variation in POM-$\delta^{13}C$ and POM-$\delta^{15}N$

List of Figures

Figure B6. Correlation of C:N and calculated POM concentration in major tributaries sites (top) and selected drain, creek, and wetlands sites (bottom), with the compositions of mainstem sites included for reference. Note the difference in POM scales. Mainstem sites have much higher POM concentrations than tributaries, and much lower POM concentrations than most drain, creek, and wetlands sites. There is no obvious correlation of POM and C:N values.

Appendix C: Temporal Variations in POM Isotopes

List of Figures

Figure C1. Temporal changes in flow and POM-δ^{15}N values for major tributaries (top) and for mainstem SJR sites (bottom). δ^{15}N values show larger oscillations during high flow periods than during low flow periods; in many instances, the tributaries show similar oscillations to each other and to mainstem sites.

Figure C2. Temporal changes in flow and POM-δ^{15}N values for downstream (top) and upstream (bottom) mainstem SJR sites. In general, there is more seasonal variability in δ^{15}N values at downstream sites than upstream sites, with the sites at Mossdale and Lander showing particularly rapid oscillations of high and low δ^{15}N values.

Figure C3. Temporal changes in POM-δ^{15}N values for downstream drain and creek sites (top) and upstream wetlands sites (bottom). Wetlands sites, except for Mud Slough, show considerably more temporal variation than other minor sites. Oscillations are greatest during higher flow periods than during low flow periods.

Figure C4. Temporal changes in flow and POM-δ^{13}C values for major tributaries (top) and for mainstem SJR sites (bottom). δ^{13}C values show slightly larger oscillations during high flow periods than during low flow periods; in some instances, the tributaries show similar oscillations to each other and to mainstem sites.

Figure C5. Temporal changes in flow and POM-δ^{13}C values for downstream (top) and upstream (bottom) mainstem SJR sites. There is substantially more seasonal variability in δ^{13}C values at upstream sites than downstream sites, with the site at Lander showing particularly rapid oscillations of high and low δ^{13}C values. Data for the San Luis Drain are plotted on the bottom plot to aid in comparison of its the seasonal changes with those at Lander.

Figure C6. Temporal changes in POM-δ^{13}C values for downstream drain and creek sites (top) and upstream wetlands sites (bottom). The San Luis Drain site shows much more variability than other wetlands, drain, or creek sites.

Figure C7. Temporal changes in flow and POM-C:N values for major tributaries (top) and for mainstem SJR sites (bottom). C:N values show larger oscillations during high flow periods than during low flow periods; in many instances, the tributaries show similar oscillations to each other and to mainstem sites. Mainstem sites show less variability than the tributary sites.

Figure C8. Temporal changes in flow and POM-C:N values for downstream (top) and upstream (bottom) mainstem SJR sites. Upstream sites show more variability than downstream sites. In general, there is more seasonal variability in C:N values during high flow times than during the summer.

Figure C9. Temporal changes in POM-C:N values for downstream drain and creek sites (top) and upstream wetlands sites (bottom). Wetlands sites, except for Mud Slough, show considerably more temporal variation than other minor sites. Oscillations are greatest during higher flow periods than during low flow periods.

Figure C10. Temporal variation in the C:N, $\delta^{15}N$, and $\delta^{13}C$ of POM at the SJR @ Mossdale (top) and Vernalis (bottom).

Figure C11. Temporal variation in the C:N, $\delta^{15}N$, and $\delta^{13}C$ of POM at the SJR @ Maze (top) and Laird Park (bottom).

Figure C12. Temporal variation in the C :N, $\delta^{15}N$, and $\delta^{13}C$ of POM at the SJR @ Patterson (top) and Crows Landing (bottom).

Figure C13. Temporal variation in the C:N, $\delta^{15}N$, and $\delta^{13}C$ of POM at the SJR @ Lander Ave. (top) and the Stanislaus River (bottom).

Figure C14. Temporal variation in the C:N, $\delta^{15}N$, and $\delta^{13}C$ of POM at the Tuolumne River (top) and the Merced River (bottom).

Figure C15. Temporal variation in the C:N, $\delta^{15}N$, and $\delta^{13}C$ of POM at Modesto ID Lat 5 (top) and MID Miller Lake to Stanislaus (bottom).

Figure C16. Temporal variation in the C:N, $\delta^{15}N$, and $\delta^{13}C$ of POM at Westport Drain (top) and Harding Drain (bottom).

Figure C17. Temporal variation in the C:N, $\delta^{15}N$, and $\delta^{13}C$ of POM at TID Lat 6&7 (top) and Hospital Creek (bottom).

Figure C18. Temporal variation in the C:N, $\delta^{15}N$, and $\delta^{13}C$ of POM at Ingram Creek (top) and Del Puerto Creek (bottom).

Figure C19. Temporal variation in the C:N, $\delta^{15}N$, and $\delta^{13}C$ of POM at Orestimba Creek (top) and Los Banos Creek (bottom).

Figure C20. Temporal variation in the C:N, $\delta^{15}N$, and $\delta^{13}C$ of POM at Mud Slough (top) and San Luis Drain (bottom).

Figure C21. Temporal variation in the C:N, $\delta^{15}N$, and $\delta^{13}C$ of POM at Salt Slough (top).

Appendix D: Relations Between Algal Pigments, BOD, and the $\delta^{15}N$ and $\delta^{13}C$ of POM

List of Figures

Figure D1. Correlation of $\delta^{15}N$ of POM and BOD for mainstem SJR sites (top) and major tributaries (bottom). Mainstem sites with low $\delta^{15}N$ values have lower BOD than sites with high $\delta^{15}N$; however tributary samples show a narrower range of BOD values, significantly lower than values at mainstem sites, with no correlation with $\delta^{15}N$ values.

Figure D2. Correlation of $\delta^{15}N$ of POM and BOD (top) and CBOD (bottom) for selected drain, creek, and wetlands sites, with the compositions of mainstem sites included for reference. Sites with higher $\delta^{15}N$ (which are predominately wetlands sites) tend to have higher BOD on average than sites with lower $\delta^{15}N$ (which tend to be creeks and drains. A higher proportion of the BOD at wetlands sites is CBOD than at other sites.

Figure D3. Correlation of $\delta^{15}N$ of POM and NBOD (top) and algal pigments (bottom) at selected drain, creek, and wetlands sites, with the values for mainstem sites included for reference. Wetlands sites have higher $\delta^{15}N$ values and generally lower NBOD than drains and creeks. The samples with the highest NBOD had the highest algal pigment concentrations.

Figure D4. Correlation of $\delta^{13}C$ values of POM and algal pigment concentrations for mainstem SJR sites and major tributaries (top), with the data presented with an expanded algal pigment scale below (bottom). Tributaries samples show a narrow range of pigment values, significantly lower than values at mainstem sites, and generally higher $\delta^{13}C$ values.

Figure D5. Correlation of $\delta^{13}C$ of POM and BOD for mainstem SJR sites and major tributaries. Tributaries samples show a narrow range of BOD values, significantly lower than values at mainstem sites, and generally higher $\delta^{13}C$ values.

Figure D6. Correlation of $\delta^{13}C$ of POM and BOD (top) and NBOD (bottom) for mainstem SJR sites. Mainstem sites show a narrow range of $\delta^{13}C$ values but no

obvious correlation with BOD or NBOD except that both are higher for samples with mid-range $\delta^{13}C$ values.

Figure D7. Correlation of $\delta^{13}C$ values of POM and algal pigment concentrations for selected drain, creek, and wetlands sites (top), with the data presented with an expanded algal pigment scale below (bottom). Wetlands sites generally have lower $\delta^{13}C$ values than other sites. Different site types all show wide ranges of pigment values; however, average wetlands pigments values are generally higher than for other sites.

Figure D8. Correlation of $\delta^{13}C$ values of POM from selected drain, creek, and wetlands sites with BOD (top) and NBOD (bottom) values. BOD values are similar for wetlands, creeks, and drain sites. However, wetlands sites (Mud and Salt Slough, Los Banos, and San Luis Drain) have a narrower and lower range of NBOD values than other drain and creek sites.

Figure D9. Variability in the POM-$\delta^{15}N$, and POM-$\delta^{13}C$ values with increasing POM-C:N value for the ~1400 samples analyzed. Linear trend lines for $\delta^{13}C$ and $\delta^{15}N$ have r^2 values of 0.02 and 0.07, respectively. Vertical bars show the C:N values.

Figure D10. Variability in the C:N, BOD, algal pigments, and calculated POM with increasing BOD value for the ~1200 samples analyzed for C:N that had measured algal pigment concentrations <200 ug/L. The linear trend lines for C:N and POM have r^2 values of 0.15, and linear and polynomial trend lines for algal pigments have r^2 values of 0.33 and 0.43, respectively.

Appendix E: Temporal Variation in Nitrate-$\delta^{15}N$ and $\delta^{18}O$, Water-$\delta^{18}O$, and Nitrate Concentrations at Individual Sites

List of Figures

Figure E1. Temporal patterns in $\delta^{15}N$ and $\delta^{18}O$ of NO_3, NO_3 concentration, and $\delta^{18}O$ of water for SJR mainstem sites at Mossdale (top) and Vernalis (bottom).

Figure E2. Temporal patterns in $\delta^{15}N$ and $\delta^{18}O$ of NO_3, NO_3 concentration, and $\delta^{18}O$ of water for SJR mainstem sites at Maze (top) and Laird Park (bottom).

Figure E3. Temporal patterns in $\delta^{15}N$ and $\delta^{18}O$ of NO_3, NO_3 concentration, and $\delta^{18}O$ of water for SJR mainstem sites at Patterson (top) and Crows Landing (bottom).

Figure E4. Temporal patterns in $\delta^{15}N$ and $\delta^{18}O$ of NO_3, NO_3 concentration, and $\delta^{18}O$ of water for the SJR mainstem site at Lander Avenue and the Stanislaus River

Appendix F: Water Isotope Plots

List of Tables

List of Figures

Figure F4. Water isotope plot showing $\delta^{18}O$ vs $\delta^{2}H$ for water samples from various selected tributaries.